THE PHOTOCHEMICAL PROPERTIES OF ARENE METAL CARBONYL COMPLEXES OF GROUP 6 AND 7 ELEMENTS

DCU

THIS THESIS IS PRESENTED FOR THE DEGREE OF DOCTOR OF PHILOSOPHY
AT
DUBLIN CITY UNIVERSITY
BY

Peter Brennan B.Sc.

UNDER THE SUPERVISION OF DR. MARY PRYCE AND PROF. CONOR LONG

SCHOOL OF CHEMICAL SCIENCES

FEBRUARY-2003

DECLARATION

I hereby certify that this thesis, which I now submit for assessment on the programme of study leading to the award of Doctor of Philosophy is entirely my own work and has not been taken from the work of others save and to the extent that such work has been cited and acknowledged within the text of my work

Signed : _____

Date : _____

Peter Brennan

Student ID No. 97970646

Table of contents

Acknowledgements

I would like to say a most heartfelt thanks to all the following people; Prof. Conor Long and Dr. Mary Pryce for all their support, help and advice over the past few years. All members past and present of the research group, Bronagh, Carl, Ciaran, Davnat, Jennifer and Kevin. All members of the chemistry department, especially the technicians, who were always at hand to help when a problem arose. Finally I would like to thank my family for their infinite patience with the apparently everlasting endeavour I have undertaken.

Abstract

The aim of this work was to determine the photochemical properties of a number of compounds of the general type (η^X-arene)$M(CO)_3$ (M=Cr, Mn, X = 5,6). A range of techniques were used including ultraviolet/visible flash photolysis, time resolved infrared spectroscopy and matrix isolation.

The first chapter contains a literature survey of the group 6 and 7 metal carbonyl complexes, also presented is a brief description of the role of transition metal complexes in some important industrial processes. In addition, the metal carbonyl bond and the metal arene bond are described, while the nature of the absorption spectra of group 6 and 7 metal carbonyls are discussed, as are their known photochemical and thermal properties.

The second chapter describes the photochemistry of functionalised (η^6-C_6H_5X)$M(CO)_3$ Complexes (X = OCH_3, NH_2, CO_2CH_3 or C(O)H). The nature of the functionality on the arene ring has been shown to affect the photochemical properties of these complexes. The relative importance of CO loss versus arene loss is measured and these observations are explained in terms of electronic character of the arene substituent.

The third and fourth chapters deal with the photochemistry of a series of compounds which are used to model the hydrodesulphurisation reaction, namely (η^5-thiophene)$Cr(CO)_3$, (η^6-benzothiophene)$Cr(CO)_3$, (η^6-dibenzothiophene)$Cr(CO)_3$ and (η^5-selenophene)$Cr(CO)_3$. Both steady state photolysis and time-resolved techniques were used to investigate the photochemistry of these complexes. In addition to CO loss, evidence of a hapticity change from η^5 to η^4 is observed for (η^5-thiophene)$Cr(CO)_3$ and (η^5-selenophene)$Cr(CO)_3$ under photochemical conditions.

This research was also extended to group 7 metal carbonyls. The fifth chapter deals with the photochemistry of (η^5-pyrrollyl)$Mn(CO)_3$. While CO loss was observed as the dominant photoprocess, evidence for a ring-slip process was also obtained.

The sixth chapter details the different synthetic procedures used, as well as the experimental techniques of ultraviolet/visible flash photolysis, time resolved infrared spectroscopy and matrix isolation techniques.

Chapter 1

Literature survey

1.1 Introduction to the chemistry of organometallic complexes

The bulk of organic chemicals produced in the world today are either hydrocarbons such as ethene, propylene and butadiene or oxygenated compounds such as alcohols, ketones or carboxylic acids. These compounds are used as the starting materials for many other syntheses. In the case of hydrocarbons, olefins such as ethylene or propylene can be polymerised into useful polymers. The petroleum industry is the source of most of these chemical compounds. The drain on the worlds natural supplies of gas and oil coupled with events such as the middle east oil crisis of the 1970s led to the search for alternative sources to these strategically important materials.

Transition metal complexes are frequently used as catalysts in many industrial processes which convert simple molecules such as, methane, , water or hydrogen etc to industrially important organic molecules. Two types of catalysis maybe employed, homogeneous or heterogeneous. The catalyst is said to be heterogeneous if it is not in the same phase as the reaction mixture while for the homogeneous system, the catalysts are present in the same phase as the reactants. Heterogeneous catalysts are usually used because of their high economy and efficiency. Since not soluble in solution the heterogeneous catalyst is contained on a oxide or metal support. One of the advantages of using a heterogeneous catalyst is that they are easily separated from the reaction mixture, however they do tend to require elevated pressures and temperatures and in some cases can result in formation of a mixture of products, giving the reaction a low selectivity. Homogeneous catalytic reactions in solution are generally very complex and the exact mechanism of many such catalysts remains uncertain. The advantages of using a homogeneous system are two fold. They operate at low temperatures and pressure and offer a high selectivity. However they do have the disadvantage of the need to remove the catalyst after the reaction has been completed.

From a scientific and economic perspective one of the most important discoveries involving transition metal catalytic action is the Ziegler Natta low pressure polymerisation of ethylene or propylene, for which Ziegler and Natta jointly received the Nobel Prize in 1963. Over 15 million tonnes of polyethylene are made annually using the Ziegler Natta catalyst .[1] The Ziegler Natta catalyst is made by treating

titanium chloride with trietyl aluminium with $MgCl_2$ as a support. Titanium does not have a filled coordination sphere and acts like a lewis acid, accepting propylene or ethylene as the other ligand. The reaction is thought to proceed as shown below.

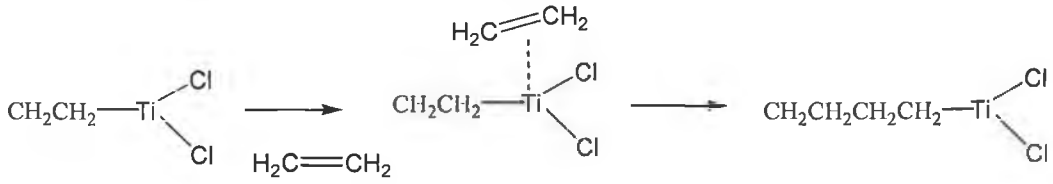

An alkyl titanium intermediate

Chain - extended alkyl titanium intermediate.

Scheme 1.1.1 The polymerisation of ethylene by treatment with the Ziegler Natta catalyst.

Syn gas, a mixture of CO and H_2 may be obtained by steam reforming of natural gas . This is the starting point for many industrial chemicals. Some examples are the hydroformylation process which is the addition of H_2 and CO to an alkene molecule producing aldehydes and alcohols. An example of this is the Monsanto process for the production of acetic acid from methanol. Metal carbonyl compounds are used in a number of such industrially important processes, for instance hydroformylation. Cobalt carbonyl compounds were used as catalysts at temperatures of 150 °C and greater than 200-atmospheres pressure. This process gave mixtures of straight and branched-chain products in the ratio of 3:1. Unfortunately the process employing cobalt catalysts also resulted in the reduction of the feedstock alkenes to alkanes. In 1956 Schiller demonstrated that rhodium catalysts were superior to cobalt catalysts for the hydroformylation of alkenes.[2] In the 1970s Union Carbide applied the catalyst in the synthesis of aldehydes. Wilkinson and co workers investigated the mechanism of hydroformylation of alkenes to aldehydes using rhodium triphenyl phosphine complexes and a simplified scheme is shown in scheme 1.1.2.[3]

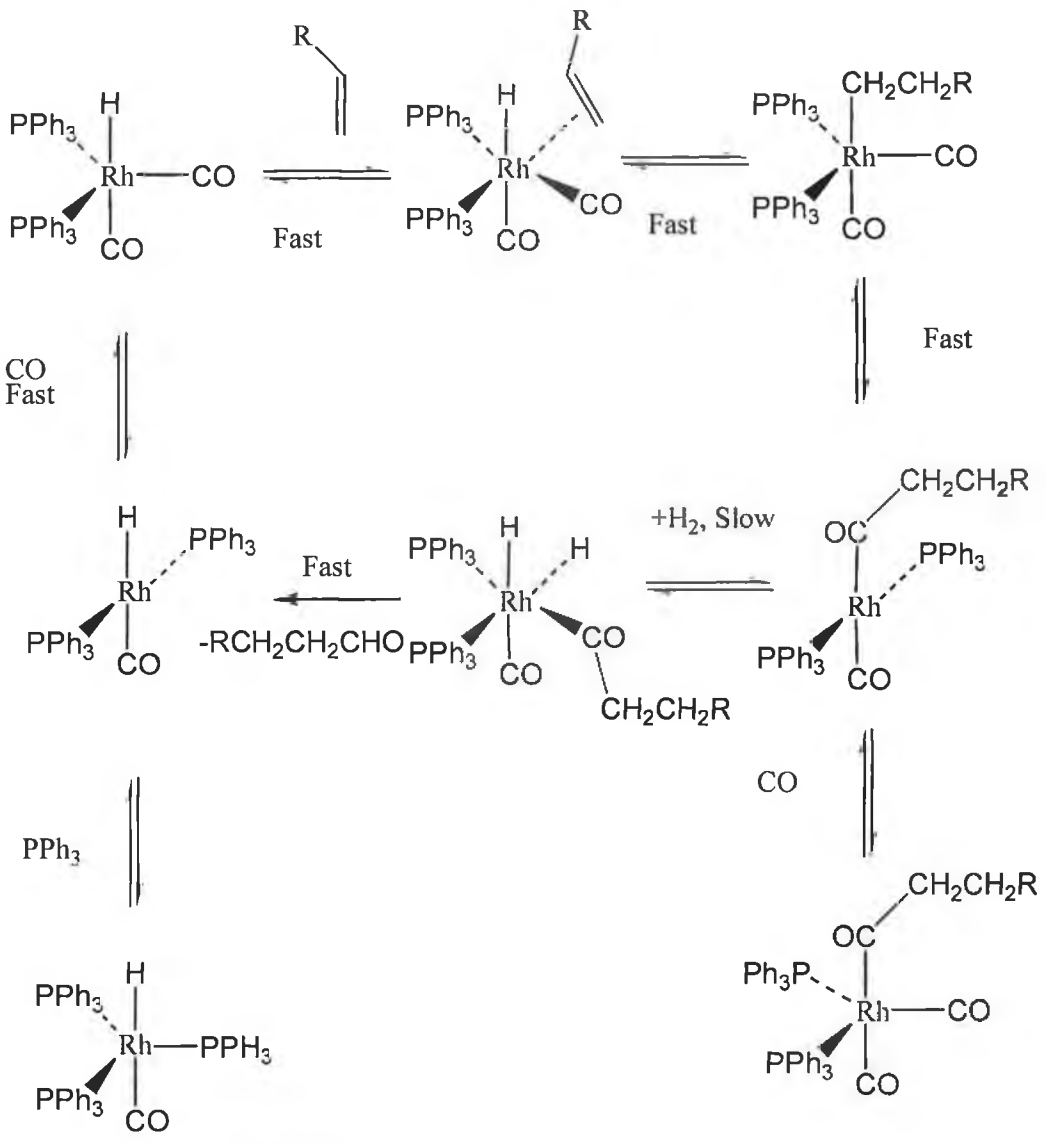

Scheme 1.1.2 The hydroformylation of alkenes by rhodium triphenyl phosphine complexes.

Under the reaction conditions the aldehyde may be further reduced to the alcohol analogue. The alcohol thus produced can be readily converted to gasoline in a process developed by the Mobil oil company using their ZSM-5 zeolite catalyst.[4] In the early 1970's Monsanto introduced a process for the manufacture of acetic acid by low pressure carbonylation of methanol.[5] The catalyst for the Monsanto process uses a rhodium catalyst and a source of iodine. Under the conditions of the reactions the iodide converts the methanol to methyl iodide which this adds oxidatively to the rhodium(I) species to give a Rh-CH_3 bond which undergoes migratory insertion of carbon monoxide. The overall reaction scheme is shown in scheme 1.1.3.

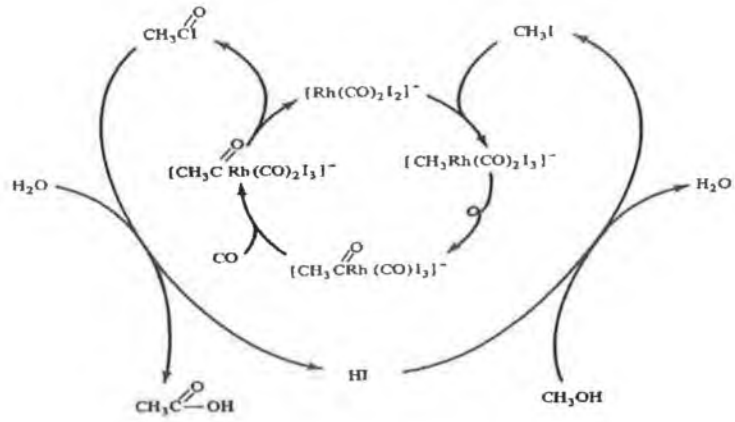

Scheme 1.1.3 The proposed mechanism for the Monsanto acetic acid process using a rhodium carbonyl mediated catalyst.

Roelen discovered the OXO process in 1938, the reaction of an alkene with carbon monoxide and hydrogen catalysed by cobalt carbonyl complex to form an aldehyde, and is the oldest and largest volume catalytic reaction of alkenes. Conversion of propylene to butyraldehyde is the most important with about 5 million tonnes annually being produced, it is by far the most important industrial synthesis involving metal carbonyls as a catalyst.[6] The most widely accepted reaction mechanism is that proposed by Heck and Breslow (Reaction 1.1.4.).[7]

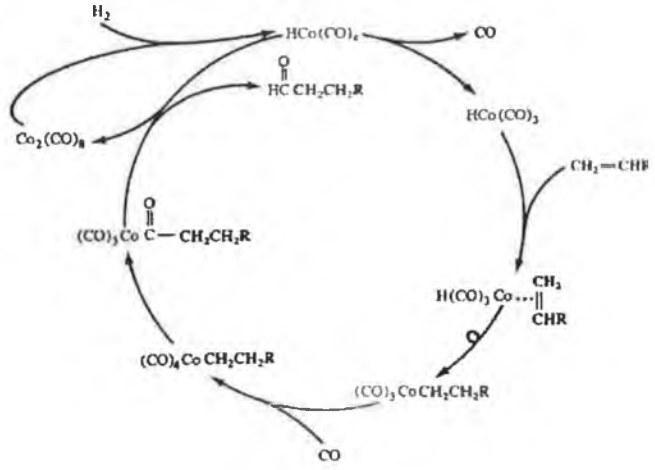

Scheme 1.1.4 The proposed mechanism of cobalt carbonyl mediated hydroformylation.

An important use of $Mo(CO)_6$ (in fact any Mo complex when heated with olefins on alumina gives a methathesis catalyst) and $W(CO)_6$ is in the metathesis or dismutation reaction of alkenes. This happens when the olefins are passed over the metal carbonyls deposited on Al_2O_3 at 150 °C to 500 °C.

For all catalytic reactions involving transition metal complexes there is one feature that is common to all of them. That is the initial steps would seem to be the generation of vacant coordinate sites on the metal, subsequently followed by reaction at these sites. It is generation of vacant sites on metal carbonyl complexes by photochemical means that forms the basis of the work in this thesis.

The generation of vacant sites on metal carbonyl complexes by photochemical means, followed by reaction at these sites has been exploited in the devolopment of the Pauson Khand reaction. The Pauson Khand reaction uses a dicobalt octacarbonyl in the co-cyclisation of alkynes with alkenes and carbon monoxide leading to formation of a cyclopentanone. It has become one of the most useful methodologies in the preparation of cyclopentanones. The Pauson Khand reaction can be highly regio and stereo selective, and as many natural products contain a cyclopentanone ring as one of their structural features, the Pauson Khand cycloaddition has seen extensive use in a variety of approaches to natural product synthesis. Most of the known Pauson Khand reactions are stoichiometric and slow. However elevating the temperature to increase rates of reaction of the Pauson Khand reaction is a severe disadvantage, as it may lead to thermally induced rearrangements of the olefin. Consequently techniques that reduce the thermal demand of this process will significantly expand its application.

The mechanism for the Pauson Khand reaction was originally proposed by Magnus (scheme 1.1.4.).[8] Livinghouse was the first to develop the photochemical Pauson Khand reaction.[9] Two groups demonstrated that the initial step after irradiation with ultraviolet photolysis to be the loss of the CO ligand, namely Gordon *et al.* who used low temperature matrix isolation techniques.[10] Draper, Long and Meyer used UV/vis laser flash photolysis and steady state IR and UV/vis monitored photolysis.[11] These workers found that pulsed excitation in cyclohexane solution with λ_{exc} = 355nm causes Co-CO bond homolysis while photolysing at λ_{exc} = 532nm results in CO loss.

It was also shown that steady state photolysis in the presence of a suitable trapping ligand (acetonitrile or triphenyl phosphine) resulted in formation of the monosubstitued complexes in high yields.

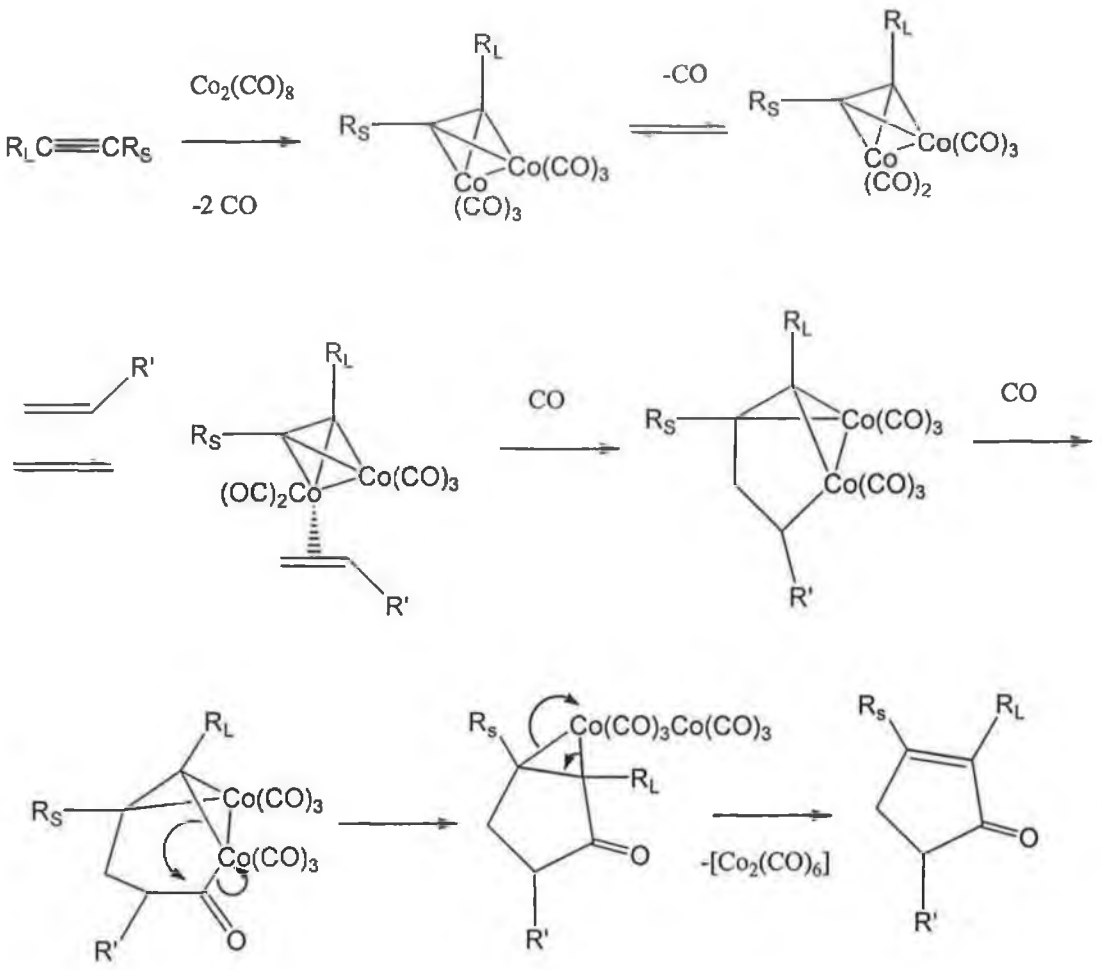

Scheme 1.1.5 The generally accepted mechanism pathway for the Pauson Khand reaction as developed by Magnus.

1.2 UV/vis monitored flash photolysis

Along with conventional IR, UV/vis and NMR spectroscopies more exotic experimental techniques were employed to probe the reaction pathways of metal carbonyl's. Norrish and Porter developed flash photolysis in the 1950s, as a technique for the study of extremely fast chemical reactions.[12] Flash spectroscopy works by producing an intense pulse of light in a very short time thereby producing a high concentration of the photo product. By very quickly analysing the time evolution of the system by absorbance or emission spectroscopy, the decay of concentration of the excited species with time may be measured. Also the rates of formation of the new species can be measured.

The light / pump source excites the sample, inducing a change in the electronic state and in some cases initiating a photochemical reaction. The changes induced in the sample are monitored by passing a beam of a second weaker light source through the sample. Flash lamps were at first used as the monitoring beam but by the 1960s they were replaced by lasers. The amount of monitoring light being transmitted through the solution before the laser flash, I_0 is initially recorded. This is the voltage corresponding to the amount of light detected by the photo-multiplier tube when the monitoring source (Xe arc lamp) shutter is open, less the voltage generated by stray light. When the monitoring source is opened, while simultaneously firing the laser, the laser pulse passes through the sample, and the amount of light transmitted through is I_t. Since $\log I_o/I_t$ = absorbance, the change in intensity of the probe beam transmitted through the sample is measured as a function of time and wavelength.

The excitation source used was a neodynium ytrium aluminium garnet (Nd YAG) laser which operates at 1064 nm. Nd atoms are implanted in the host YAG crystals of approximately one part per hundred. The YAG host material has the advantage of having a relatively high thermal conductivity to remove heat, thus allowing these crystals to be operated at high repetition rates of many pulses per second. By use of non-linear optics it is possible to double, triple or quadruple the frequency of the laser, thus generating a second, third and fourth harmonic lines at 532 nm, 355 nm and 266 nm. The power of the laser can also be amplified by varying the applied voltage across the amplifier flash tube. The pulse time is approximately 10 ns. By recording transient

signals sequentially over a range of wavelengths, absorbance readings can be calculated at any time after the flash, to generate a difference spectrum of the transient species. Spectra are obtained as a result of point by point detection built up by changing the wavelength of the monochromator and recording the respective signal. A xenon arc lamp is arranged at right angles to the laser beam emitting a beam that passes through the sample cell and is focussed onto the monochromator slit. The light is detected by the photo-multiplier which is linked to the digital storage oscilloscope. The digital oscilloscope is interface to a PC. Metal carbonyl compounds are well suited to laser flash photolysis studies because of their production of high quantum yields for photoprocesses and the moderate intensity of their UV/vis absorptions.

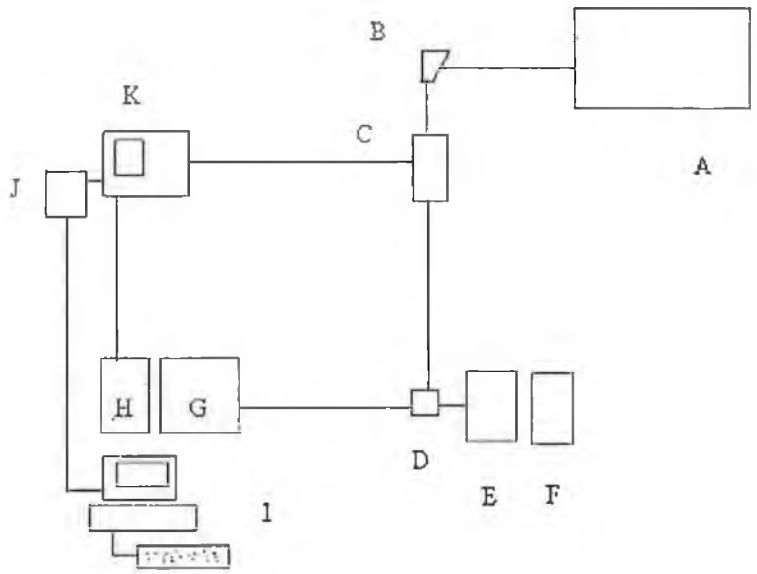

A = laser
B = prism
C = power meter
D = sample cell housing
E = xenon arc lamp
F = lamp power supply
G = monochromator
H = photomultiplier
I = computer
J = IEEE interface
K = oscilloscope

Figure 1.2.1 Block diagram of laser flash photolysis system.

1.3 Time Resolved InfraRed (TRIR) Spectroscopy

1.3.1 Step scan TRIR spectroscopy

The nanosecond point by point TRIR systems using single frequency detection are inconvenient for acquiring data over a broad IR range. Although frequencies of the commercially available diode lasers covers most of the range typically used for compound characterisation , the TRIR experiment is obtained by coupling together temporal absorbance data obtained one frequency per experiment. Thus it is a labour intensive process to produce a time-resolved IR spectrum with a resolution of 2 cm^{-1} even if the frequency range of interest to characterize a specific system is relatively narrow. In this context, it would be attractive to take advantage of the broad band of frequencies of available from a black body IR source in order to record a broader spectrum for short lived transient species. This can be achieved by using a step–scan interferometer electronically coupled to the repetitive pulse laser.

In Fourier transform infrared (FTIR), an interferogram is generated by recording the intensity of the signal from a black body source passed through the sample and the interferometer as a function of the displacement of the moving mirror of an interferometer. This information is converted to an intensity-v-frequency spectrum by taking its Fourier transform. Alternatively, the interferogram can be generated point by point if the mirror is precisely stepped from one fixed position to another and the intensity measured accurately as a function of that mirror position. If the sample is subjected to laser flash photolysis precisely coupled to the detection electronics, then one can record the time dependent intensity at each step of the mirror scan. A Fourier transform of the intensities recorded at a specific time delay over the entire range of the mirror step positions gives the IR spectrum of the sample at that time. A collection of these spectra as a function of time provides the three dimensional surface of frequency-v-time-v-absorbance. The spectral resolution is determined by the number of interferometer steps and the temporal resolution is determined by the rise time and sensitivity of the detector.[13]

The experimental setup used in step scan time resolved IR spectroscopy is shown in Figure 1.3.1.1. The advantages of this method over point by point TRIR spectroscopy are as follows : (1) Shorter experimental times compared with conventional methods of TRIR. (2) The entire mid IR region is available in one experiment. (3) High quality FTIR spectra are produced with a high spectral resolution. (4) The experiment is completely computer controlled and automated, with no need for tuning between laser shots.

The major disadvantages of using this method are the large number of laser shots required to obtain a spectrum. This can be overcome if the system is fully photoreversible or by continuously flowing fresh solution through the sample cell.

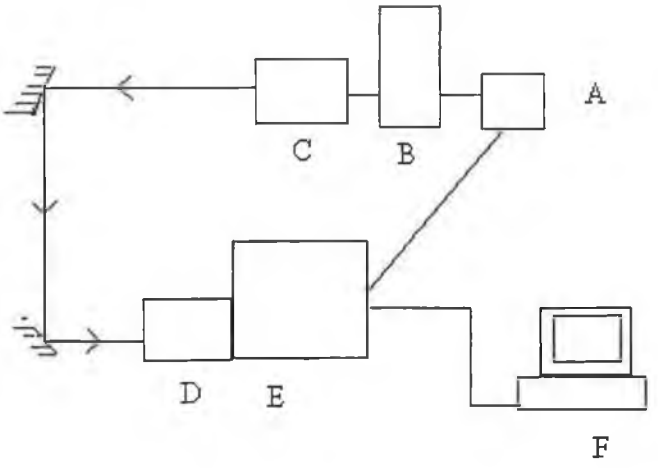

A = Pulse generator B = Laser power supply C = NdYAG laser
D = External bench E = Nicolet 860 step scan TRIR F = Computer

Figure 1.3.1.1 Block diagram for step scan TRIR spectroscopy.

1.3.2 Point by point TRIR

Point by point TRIR spectroscopy uses a continuous wave IR beam to probe the sample at a single frequency. The change in IR absorbance following the excitation pulse, is monitored with respect to time by a fast infra red detector coupled to a digital storage oscilloscope. The data is then transferred to a computer for analysis, in the same way a transient signal is recorded in UV/vis flash photolysis described earlier. This is repeated for a number of IR frequencies over a defined spectral range allowing a point by point difference spectrum to be constructed. The requirements for such a system are :

1. A monochromatic IR beam source.
2. A pulsed UV/vis light source.
3. A detector.

The intensity of the IR beam is always measured at each IR frequency of interest, thereby providing accurate values for the change in absorbance. The UV/vis source must also have good pulse to pulse stability to ensure the relative absorbance signals at various frequencies can be compared.

The IR beam is supplied in one of three ways; (1) a globar, (2) a CO laser or (3) a continuous wave semiconductor laser. The globar (black body source) is the most common way of generating the IR beam.[14] A monochromator is used to select a specific wavelength of light. The draw back with this method is that the photon flux at any frequency is low. This problem can be overcome by using a CO laser instead, which has a high photon flux.[15] This high photon flux provides a high signal to noise ratio, allowing traces to be obtained in a single shot. The disadvantage of using a CO laser is that it has a low resolution, it is only tuneable in 4 cm^{-1} steps and the laser is only tunable over the range 2010 – 1550 cm^{1}. For the study of metal carbonyl complexes this often proves inadequate as many complexes absorb above 2010 cm^{-1}. These problems maybe overcome by using IR diode lasers.[16] The IR diode lasers emit over the entire IR range, have high resolution and emit continuously over the entire range. These features make the semiconductor IR laser the most convenient probe for the nanosecond time resolved infra red studies of organometallic compound in the

condensed phase. These diodes are manufactured from single crystal lead salt semiconductor alloys. Varying the composition of the semiconductor can alter the band gap and such diode lasers are available over a broad infra red range (370-3050 cm^{-1}). An individual laser of this type usually has a scanning range of less then 200 cm^{-1} and is tuned over this region by changing the temperature and current through the diode. The diode IR laser operating temperature is less then 60 K and therefore requires a closed cycle helium refrigerator. However diodes that operate at liquid nitrogen temperatures are now available although they do have a lower output (a lower photon flux being emitted). The advantages of using a continuous wave IR semiconductor source over the continuous wave CO laser is that they allow the whole of the mid infra red region to be covered with high resolution (0.5 cm^{-1}). The output is two orders of magnitude lower then the CO laser and therefore precision optics are necessary to overcome the problem of lower power. Another disadvantage of using such a system over the CO laser is that a number of laser arrays must be used as each array emits over a narrow bandwidth of 200 cm^{-1}.

Signal detection in the nanosecond TRIR systems is typically achieved with liquid N_2 cooled HgCdTe or InSe diode IR detectors which have a rise time of about 10 ns and have a spectral range of 5000 – 400 cm^{-1}. A fast rise time pre amplifier is then use to boost the signal which is then recorded on an oscilloscope before being transferred to a computer.

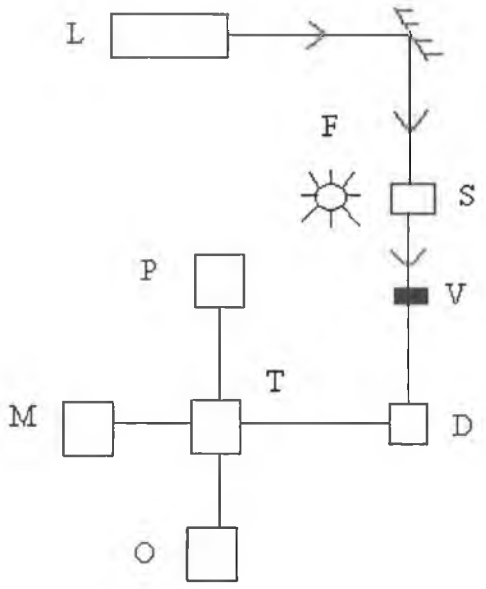

L = line tunable CO laser S = Sample Cell F = flash lamp
P = photodiode D = fast MCT IR detector
T = transient digitizer O = Oscilloscope M = Microcomputer

Figure 1.3.2 Block diagram of a point by point TRIR system.

1.4 Matrix isolation

Matrix isolation is the technique of trapping molecules or atoms in a solidified gas, at low temperatures and studying them with conventional spectrometers (IR and UV/vis). Matrix isolation is a powerful technique for the study of organometallic intermediates. The advantages of using this system is the complete transparency of the matrix from the far IR to the near vacuum UV, and of the rigidity of the matrix at a suitably low temperature (4-20 K). Therefore molecules which might have as low a lifetime a 10^{-8} seconds under fluid conditions are stable in matrices in their ground electronic and vibrational states.

George Pimentel was the first to carry out matrix isolation experiments in solidified noble gasses, CH_4 or CO.[17] However this was not the first example of the use of low

temperature solids as trapping media. Gilbert Lewis and his group in the 1930s had pioneered the use of low temperature organic glasses.[18] The technique has evolved into a far more prescient tool suited to a vast expanse of applications from environmental analysis to mimicking the conditions in interstellar dust clouds. Although IR and UV/vis are the most important spectroscopic techniques used in matrix isolation. A wide variety of spectroscopic techniques can be brought to bear in the study of a particular isolated metal fragment. Raman, fluorescence and even Mössbaeur spectroscopies have all been successfully used in the study of organometallic species.[19] Matrix isolation has a number of disadvantages and limitations when studying organometallic species. These include :

1. It cannot be used for the study of charged species.
2. Very little kinetic data may be attained.
3. It has also been found that the solid matrix cage can sometimes block some photochemical pathways.

In matrix isolation experiments the matrix is formed by deposition from the gas phase to a cold window. There are two ways of mixing the guest species with the host gas : (1) If the guest species has an easily measurable vapour pressure, it can be mixed with the host gas on a vacuum line by standard manometric techniques. This produces a gas mixture of known proportion. The ratio of host to guest is known as the matrix ratio. The gas mixture is then allowed into the vacuum chamber of the cold cell at a controlled rate and is deposited on the cold window. (2) If the guest has a low volatility (in the case of metal carbonyl complexes) it is usual to evaporate it from a side arm attached to the vacuum chamber of the cold cell while depositing the host gas.

For matrix isolation studies the equipment required includes :

1. A refrigeration system.
2. A sample holder.
3. A vacuum chamber.
4. A vacuum pumping system.
5. A gas handling system.
6. A method for generating the species of interest i.e a UV lamp.

1.4.1 The refrigeration system

These refrigerators consist of a compressor unit connected to a compact expander unit or head module by high pressure (feed) and low pressure (return) helium lines. The head module must be small and light enough to be incorporated into matrix cells for use with a wide variety of instrumentation. The helium gas is compressed and then allowed to expand within the head module. It is the expansion of the helium causes the cooling effect.

1.4.2 The sample holder

The sample holder is fixed to the lower heat station of the refrigerator, it is essential that it is made of a material that it is a good conductor at very low temperatures. Copper is the most cost effective material for the metal part of the sample holder. The windows are usually CsBr or CsI. They have the advantage over other materials like NaCl or KBr in that they are stronger and less brittle so do not deform as easily upon cooling.

1.4.3 The shroud

With the matrix sample held at 10K, it needs to be enclosed in a vacuum chamber. The shroud must therefore have the following features : (1) At least one inlet port for deposition of matrix must be provided. (2) There should be a pair of external windows suited for the spectroscopic technique to be used. (3) The shroud should fit comfortably into the sample compartment of the spectrometer to be used. (4) There should be convenient access to the interior of the shroud, when the head module is at room temperature for cleaning etc. (5) The head module of the refrigerator should be mated to the shroud by a rotatable seal, so that the cold window can be rotated within the shroud. (6) A means of connecting the vacuum system.

1.4.4. The vacuum system

The shroud enclosing the head module of the refrigerator must be evacuated to insulate the cold sample from warming by convection and conduction (Dewar vacuum). Pressures of 10^{-3} millibarr are sufficient to provide an efficient Dewar vacuum, however to minimise contamination the highest achievable vacuum is required. To attain a vacuum of the strength to achieve these two goals, a vacuum system of about 10^{-5} or 10^{-7} millibarr inside the sample chamber, is required when the cold window is at its experimental temperature (10-20 K). This vacuum can be achieved by using an oil diffusion pump backed by a two stage rotary pump.

In many ways both flash photolysis and matrix isolation are complementary techniques. Flash photolysis experiments have the advantage of giving the lifetimes of reactive intermediates. TRIR techniques become particularly powerful when combined with matrix isolation and studies in low temperature solvents. This provides a 'triad of techniques' with which to probe organometallic intermediates and excited states. A comparative summary of matrix isolation and flash photolysis techniques is given below :

1. In flash photolysis experiments reactive species are observed in the normal conditions of a reaction medium. A useful example of this is observed for the photochemistry of $Mn_2(CO)_{10}$. Photolysis of $Mn_2(CO)_{10}$ by matrix isolation provides

no evidence of the $\bullet Mn(CO)_5$ radical even though laser flash photolysis of $Mn_2(CO)_{10}$ produces the $\bullet Mn(CO)_5$ fragment. The explanation for this is that the two $\bullet Mn(CO)_5$ fragments combine in the matrix cage before one escapes. This cage effect can be overcome by generating the fragment via a different route.

2. The reactive species are transient and spectra are usually recorded at one wavelength per flash. This results in the need for multiple flashes which can be prohibitive in a number of ways. Firstly if the system is not photoreversible then numerous samples must be used to record a transient absorption spectrum. The amount of time needed to record an absorption spectrum of such a photo reversible system and the usually limited experimental time available on these costly apparatus, such studies can take an excessively long time. However the introduction of CCD (charge coupled device) detectors in UV/vis flash photolysis and step scan TRIR spectroscopy conjunction with a continuous flow system alleviate this problem. CCD cameras have a cut off of around 380nm making them unsuitable for the study of a large number of organometallic intermediates. While step scan TRIR is still a relatively new technology and is extremely costly.

1.5 Bonding in M-CO complexes

In metal carbonyl complexes the bonding between CO and a metal is a combination of σ and π bonding. The metal and the CO ligand yield a strong σ donor interaction from the CO molecule (Figure 1.5.1).[20] Delocalisation of π*d electrons from the central metal into the π* CO orbital gives rise to a π back bonding interaction.

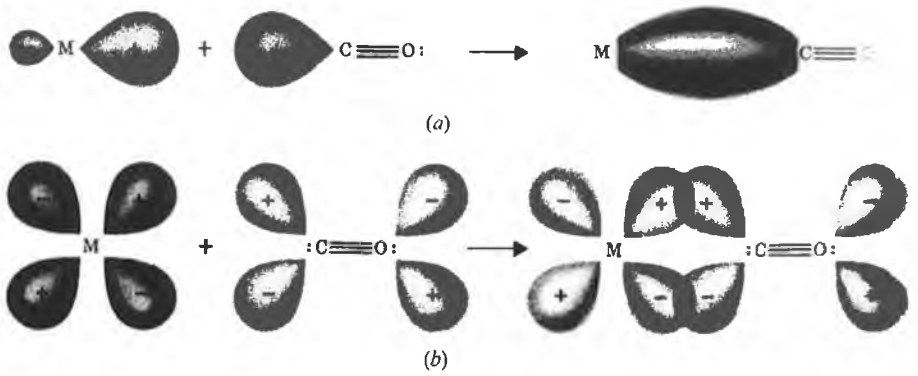

Figure 1.5.1 (a) The formation of the metal←CO σ bond using a lone electron pair. (b) The formation of the metal→CO π backbonding.

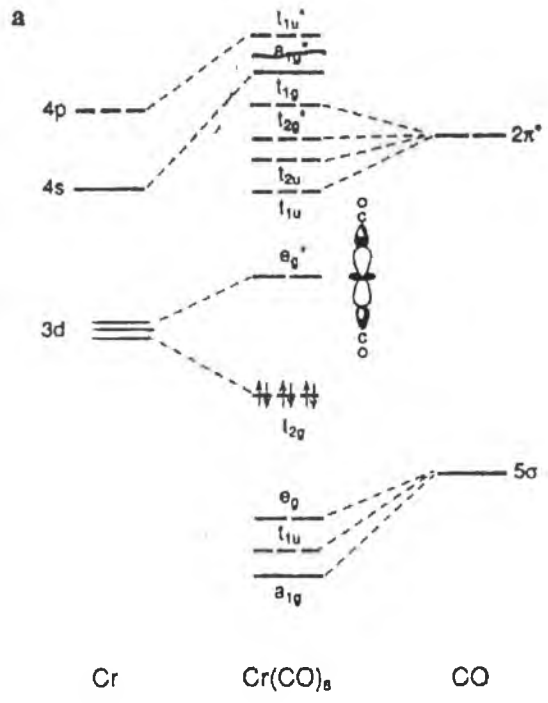

Figure 1.5.2 The molecular orbital diagram for a d^6 metal carbonyl complex.

In transition metal complexes it is the d orbitals that are involved in the π and σ bonding between the metal atoms and the ligands. When considering the effects of photochemical excitation of metal carbonyl complexes, the population of these metal d orbitals must be considered. For the d^6 $M(CO)_6$ (M=Cr, W or Mo) type metal carbonyl complexes the orbital and state diagrams are appropriate (Figures 1.5.2 and 1.5.3). The d_{z2} and d_{x2-y2} orbitals of e_g symmetry are antibonding (σ*), with respect to the metal ligand σ interactions. However the d_{xz}, d_{yz} and d_{xy} orbitals of t_{2g} symmetry are weakly π bonding between the metal and the CO ligands. The lowest lying excited state in these $M(CO)_6$ complexes have been traditionally assigned as ligand field states arising from the t_{2g} (π) → e_g (σ*) transitions, specifically the $^1A_g \rightarrow {}^{1,3}T_{1g}, {}^{1,3}T_{2g}$ transition. The $^3T_{1g}$ state lies lowest in energy and it is generally believed to be the photo excited state from which CO loss occurs.

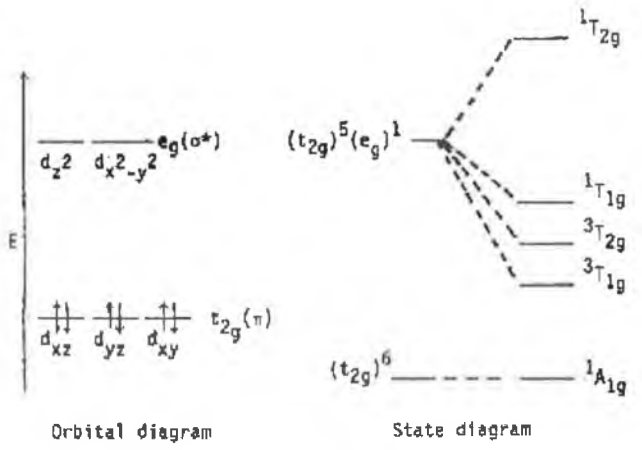

Figure 1.5.3 The orbital and state diagrams for octahedral $Cr(CO)_6$.

These transitions involve depopulation of a metal ligand bonding orbital and a population of an orbital that is strongly antibonding between the ligand and the metal. Thus the metal-ligand bonding is greatly weakened in the excited state. This assignment seemed to be confirmed by extended Huckel calculations.[21] This confirmed by semi empirical INDO/S CI and ab initio RHF calculations.[22] Pollak and co-workers carried out density functional calculation on the excited states of $Cr(CO)_6$. They found that symmetry forbidden transitions to low energy CT states and not ligand field excited states are responsible for the photolytic metal – CO bond cleavage.[23] Some of these CT states were calculated to be photodissociative. Upon Cr – CO bond lengthening there is a rapid lowering in energy of the LF states. This demonstrated that it was not necessary to excite to ligand field states in order to induce photo dissociation of ligands. However the accepted picture that metal ligand dissociation occurs from the LF excited state is based on the assumption that ligand field states are dissociative and this is true. The calculations also showed that these states are so strongly dissociative that even if they are too high in energy to be populated directly by irradiation into the lowest absorption band, they cross so soon with the lowest excited states that the lowest excited state potential energy curve along the metal – CO coordinate becomes dissociative.

Perutz and Turner showed using UV/vis monitoring, that photolysis of $Cr(CO)_6$ resulted in CO loss and generation of the unsaturated $Cr(CO)_5$ intermediate. There were two possible structures either (C_{4v})-$Cr(CO)_5$ or trigonal bypyramidal (D_{3h}). The $Cr(CO)_5$ fragment was assigned the C_{4v} symmetry by a combination of isotopic labelling and energy factored force field analysis.[24] Kelly *et al.* identified $Cr(CO)_5$(cyclohexane) by laser flash photolysis of $Cr(CO)_6$, as the primary photoproduct.[25] $Cr(CO)_6$ displayed a broad absorption band at 503nm, which was very similar to that observed in methane. This maximum was found at 489nm. Laser flash photolysis of $Cr(CO)_6$ in weakly coordinating perfluorocarbons a decrease in the order of magnitude of 103 for the lifetime of the solvated species $Cr(CO)_5$(s) over cyclohexane was noted.[26] This degree of stabilisation afforded to the metal alkane bond in cyclohexane compared to perfluorocyclohexane would suggest that for the complex $Cr(CO)_5(C_6H_{12})$, the metal-alkane bond energy is significant. Further information on the structure of $Cr(CO)_5$ in cyclohexane solution came in 1985 when isotopic data was obtained by TRIR following laser photolysis of $Cr(^{12}CO_5)(^{13}CO)$ in cyclohexane.[27, 28] The axial equatorial bond angle of C_{4v} $Cr(CO)_5(C_6H_{12})$ was estimated to be 93° identical to that calculated for $Cr(CO)_5(CH_4)$ in CH_4 matrix.[27, 28]

Reducing the symmetry of the system from O_h to C_{4v} symmetry upon substitution of CO substitution of $M(CO)_6$ to form $M(CO)_5L$ causes changes in the energy levels as illustrated by the Figure 1.5.4 which compares the d level splitting of the octahedral $M(CO)_6$ complex compared with the $M(CO)_5L$ complexes.

The low lying ligand field excitation will arise from the $d\pi \rightarrow d_{z2}$ excitation, and the principal antibonding M-L interaction will be localised along the z axis, a result that would predict photochemical loss of either ligand (L) or the CO ligand, which lie upon the z axis. The relative efficiency of this process has been found to be very dependent on the nature of the ligand (L). For certain ligands such as THF, complete conversion of $M(CO)_6$ to $M(CO)_5THF$ can occur without further reaction. However when the ligand resembles CO in its bonding properties, further CO loss and substitution by the ligand (L) can occur.

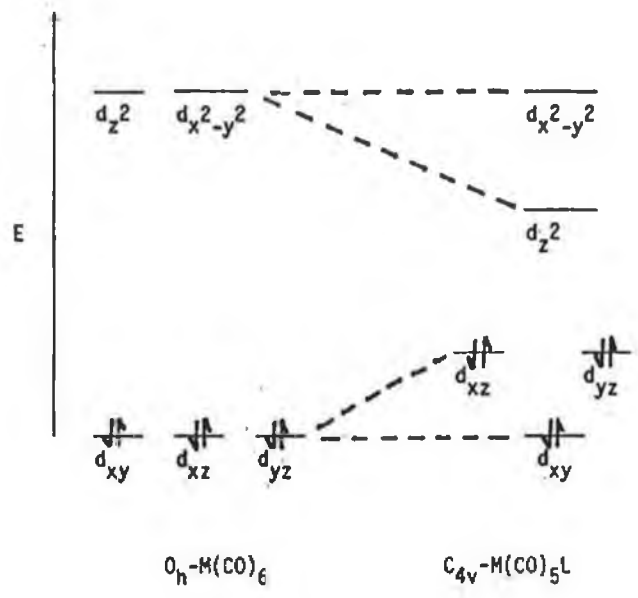

Figure 1.5.4 Orbital diagram comparing the d level splitting in an octahedral $M(CO)_6$ complex with a $M(CO)_5L$ complex.

1.6 Metal-Arene bonding

In the case of (η^6-arene)$M(CO)_3$ complexes, the planar ligand lies above the metal, forming a perpendicular bond between the arene ring and the metal.[29] The π orbitals of benzene are shown below in Figure 1.6.1.

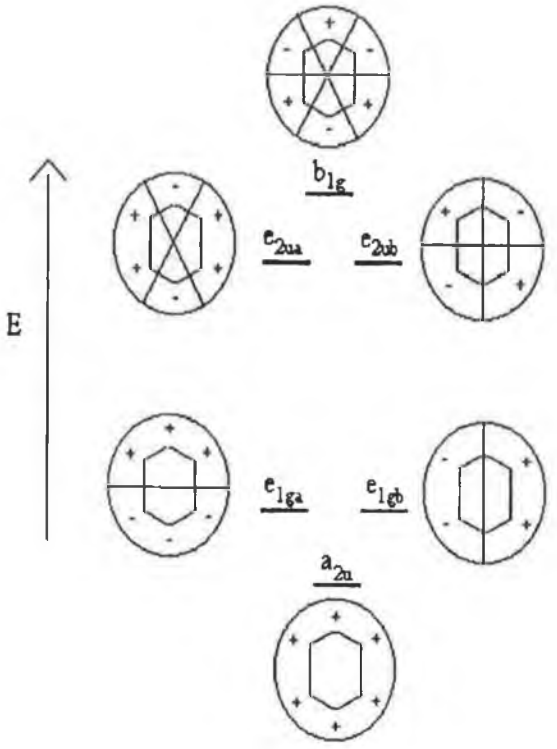

Figure 1.6.1 The molecular π orbitals of benzene.

If the z direction is assigned to the axis from the centre of the arene ligand, the d_{z2} orbital should have the correct symmetry to interact with the a_{2u} orbital (Figure 1.6.1). The interaction results in very little overlap as the d_{z2} points at the centre of the benzene ring. The two degenerate orbitals the e_{1gb} and e_{1ga} on the benzene ring donate electrons to the d_{xz} and d_{yz} orbitals and in this instance the overlap is large. The e_{2u} orbital set does not have the correct symmetry to interact with the metal orbitals except for a weak interaction with the d_{xy} and d_{x2-y2} orbital. Figure 1.6.2 depicts the orbital interaction diagram for formation of $M(CO)_3$ and M(η^6-benzene). Thus benzene is a good electron donor, but a poor electron acceptor. However its electronic properties can be altered by varying the substituents on the arene ring.

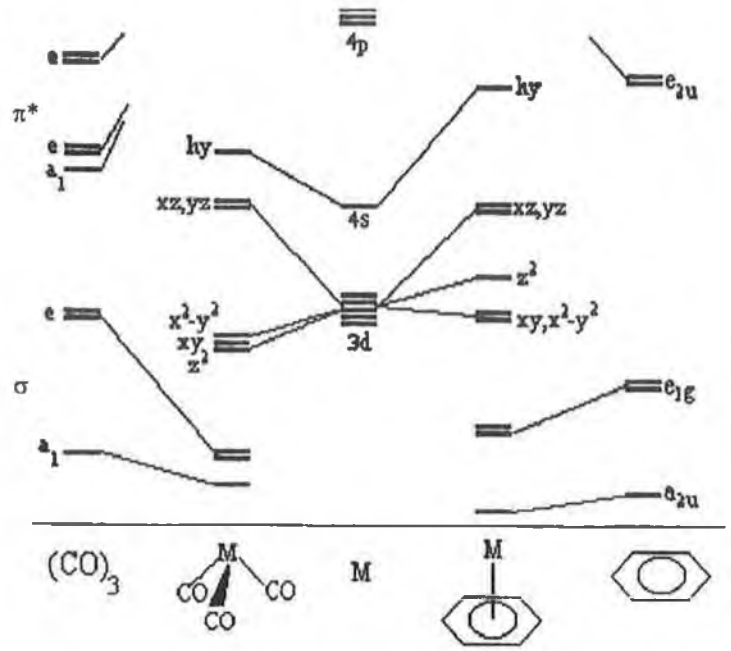

Figure 1.6.2 The molecular orbitals of $(CO)_3$,$M(CO)_3$, M, M(η^6-arene) and arene.

1.7 The electronic absorption spectra of (η^6-arene)Cr(CO)$_3$ complexes

The UV/vis absorption spectra of (η^6-arene)Cr(CO)$_3$ complexes are dominated by metal to ligand charge transfers (MLCT) absorptions. These complexes are characterised as having an absorption band in the vicinity of ~ 260 nm which is characteristic of the M-π^* CO CT absorption. The lower energy band at ~ 320 nm is assigned as a M $\rightarrow$ arene CT.[30] Some quantitative evidence for the assignment can gained by the examination of the colours of the (η^6-arene)Cr(CO)$_3$ complexes.[31] For example (η^6-benzene)Cr(CO)$_3$ is yellow, (η^6-trans stilbene)Cr(CO)$_3$ is red and (η^6anthracene)Cr(CO)$_3$ is dark violet. The energy of the onset of absorption of these compounds would seem to be related to the energy of the first $\pi \rightarrow \pi^*$ absorption of the arene ring.[32] Although the low energy region has not been studied in detail, these are probably low energy ligand field (LF) transitions.

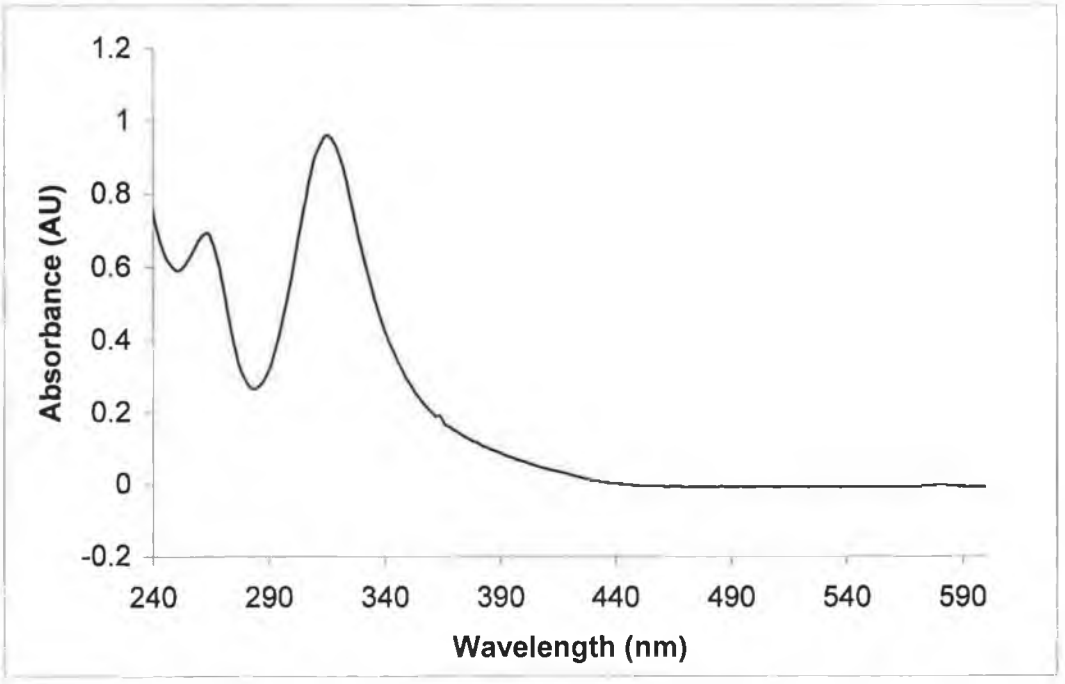

Figure 1.7.1 The UV/vis absorption spectrum of (η^6-benzene)Cr(CO)$_3$ recorded in cyclohexane.

1.8 Photochemistry of (η^6-arene)$M(CO)_3$ complexes

The earliest observation of the photo-reactions of (η^6-arene)$Cr(CO)_3$ were made by Strohmeier and von Hobe, who proposed the following, Scheme 1.8.1.[33]

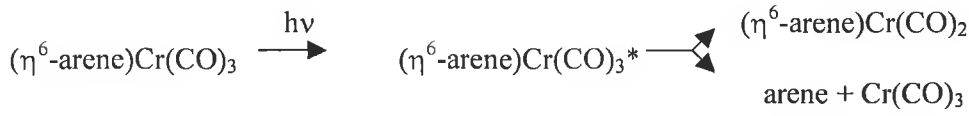

Scheme 1. 8. 1 The photochemical pathways of (η^6-arene)$Cr(CO)_3$.

Yavorskii *et al.* have also described spectral changes which occur during irradiation of (η^6-arene)$Cr(CO)_3$ in cyclohexane solution, which are compatible with the formation of the arene and chromium hexacarbonyl during reaction.[34] Wrighton and Haverty examined the photo-substitution of CO from (η^6-arene)$Cr(CO)_3$.[35]

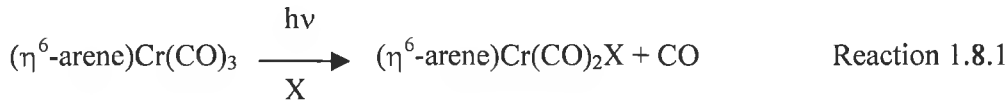

Reaction 1.8.1

The quantum yield for formation of (η^6-arene)$Cr(CO)_2$(pyridine) was found to be 0.72 +/- 0.07, independent of wavelength (313 nm, 366 nm, 436 nm), for solvent (isooctanol, benzene), arene (benzene or mesitylene) and light intensity.

Gilbert, Kelly, Budzwait and Koernor von Gustaff also studied the photo-induced CO exchange of (η^6-C_6H_6)$Cr(CO)_3$ in solution and obtained a quantum yield in accordance with that reported by Wrighton and Haverty (0.72).[36] The efficiency of arene exchange was found to be 0.12 (under an inert atmosphere). Under CO the yields, were considerably less. Flash photolysis in cyclohexane solution revealed the formation of a transient species which reacted to form a second species. Both species were found to be strongly quenched in the presence of CO. From these observations it was concluded that the species first formed is (η^6-C_6H_6)$Cr(CO)_2$ and that exchange with benzene involves this intermediate and does not occur through a one step dissociation of the excited molecule.

Bamford found that arene loss from (η^6-arene)$Cr(CO)_2$ was not a simple dissociation and offered a possible explanation involving the more complex route shown below involving formation of a multi centre complex.[38]

(η^6-arene)$Cr(CO)_2$ + 2(η^6-arene)$Cr(CO)_3$ ⟶ arene +

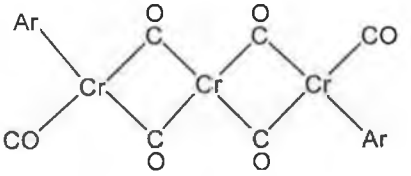

Reaction 1.8.2 Bamfords proposed reaction scheme of arene dissociation of the arene ring from (η^6-arene)$Cr(CO)_2$ to yield a multicentre complex.

The proposed route for arene dissociation agrees with Gilberts analysis.[36] A transient possibly (η^6-arene)$Cr(CO)_2$ which reacted further within the first few milliseconds to form a second transient species which absorbed throughout the visible spectrum. Rest and Sodeau provided IR evidence for the formation of coordinatively unsaturated species (η^6-arene)$Cr(CO)_2$ complexes in argon and methane and dinitrogen complexes in nitrogen matrices at 12 K.[37] Creaven *et al.* used both laser flash photolysis and TRIR to elucidate that (η^6-arene)$Cr(CO)_2$(alkane) was the primary photoproduct upon photolysis of (η^6-arene)$Cr(CO)_3$ in alkane solution.[39] UV/vis monitored flash photolysis was used to determine the kinetic behaviour of the (η^6-arene)$Cr(CO)_2$(alkane) fragment. For the $Cr(CO)_6$ system, the $Cr(CO)_5$ fragment which is generated upon photolysis coordinates to a solvent molecule in less then one picosecond. The enthalpy of activation for the recombination of CO with $Cr(CO)_5$(s) approximates the bond energy of the metal to solvent bond. Extending the example to (η^6-arene)$Cr(CO)_3$ complexes, enthalpy of activation for the recombination of CO with (η^6-arene)$Cr(CO)_2$(s) approximates the bond energy of the metal to solvent bond. For all the systems surveyed enthalpy of activation for the recombination of CO with (η^6-arene)$Cr(CO)_2$(s) was found to constant at 24 +/- 2 kJ mol^{-1}. The activation entropies for all the complexes surveyed were found to be negative for the CO recombination reaction. These changes are more consistent with an interchange mechanism for the CO reacting with the (η^6-arene)$Cr(CO)_2$(s) fragment than a

dissociative mechanism. For a dissociative mechanism the entropy of activation values should be closer to zero or positive.

The nature of the metal-alkane bond was investigated by Salliard and Hoffmann who measured the activation of the C- H bond upon coordination of a methane molecule and a hydrogen molecule to a sixteen electron intermediate.[40] There are two modes of bonding, (Figure 1.8.1) between the 16 electron metal fragment and methane or the hydrogen molecule. Firstly it could bind in a perpendicular fashion, where the C-H or H-H bond is colinear with the metal. The second mode they suggested is where the C-H or H-H bond approaches the metal in such a manner that the metal to carbon distance, and the metal to hydrogen distance are the same. This type of bond is known as an agostic bond.[41] The second mode was found to be the energetically more favourable for a H-H interaction with a metal centre, while for methane (the finding of their study could be applied to longer chain alkanes) it was found that the end on approach was more energetically favourable. This was because the second mode of interaction, resulted in overlap of the filled d_{xz} and the occupied C-H σ orbital. This repulsive effect dominated causing the d_{xz} orbital to be raised in energy, thus diminishing the stabilisation that was observed for H-H interaction.

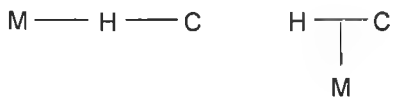

Figure 1.8.1 The two types of metal alkane interaction as proposed by Salliard and Hoffmann.[41]

Intramolecular examples of metal–alkane interaction, have showed details of the initial stages of the metal-CH interaction. Evidence for both linear and triangular interaction geometries was observed.[41]

(1) (2)

Figure 1.8.2 The (1) linear and (2) triangular interaction geometries of metal and alkane fragment.

The effect of electron donating and electron withdrawing groups have been investigated by Trembovler.[42] The systems investigated for the (η^6-arene)$Cr(CO)_2L$ (arene = C_6H_6, $C_6H_3(CH_3)_3$, $C_6H_5(OCH_3)$, $C_6H_5(COOCH_3)$ or $C_6H_5(COCH_3$ and L = CO or PPh_3). It was shown that for (η^6-arene)$Cr(CO)_3$ complexes containing electron donating substituents promote the decomposition of the complexes while electron accepting substituents slightly retard it. However only for benzene chromium tricarbonyl were the products shown to be free arene and $Cr(CO)_6$. It was also found that the introduction of a triphenyl phosphate ligand in place of a CO group leads to a four fold increase in the rate of decomposition. For arene metal tricarbonyl compounds carrying side chains with coordinating groups the photochemical loss of CO has led to produce of chelating species.[43] For complexes such as (η^6-3,5$Me_2C_6H_2(CH_2)_nOP(OPh)_2$)$Cr(CO)_3$, (where n = 1-3) upon irradiation a self chelating species is formed. Where n= 2 or 3 a dichelate species is formed or in the case of n =1, the monochelate complex is formed. Three bridged species have also been reported upon irradiation of the arene difluorophosphate complex, Scheme 1.8.2.

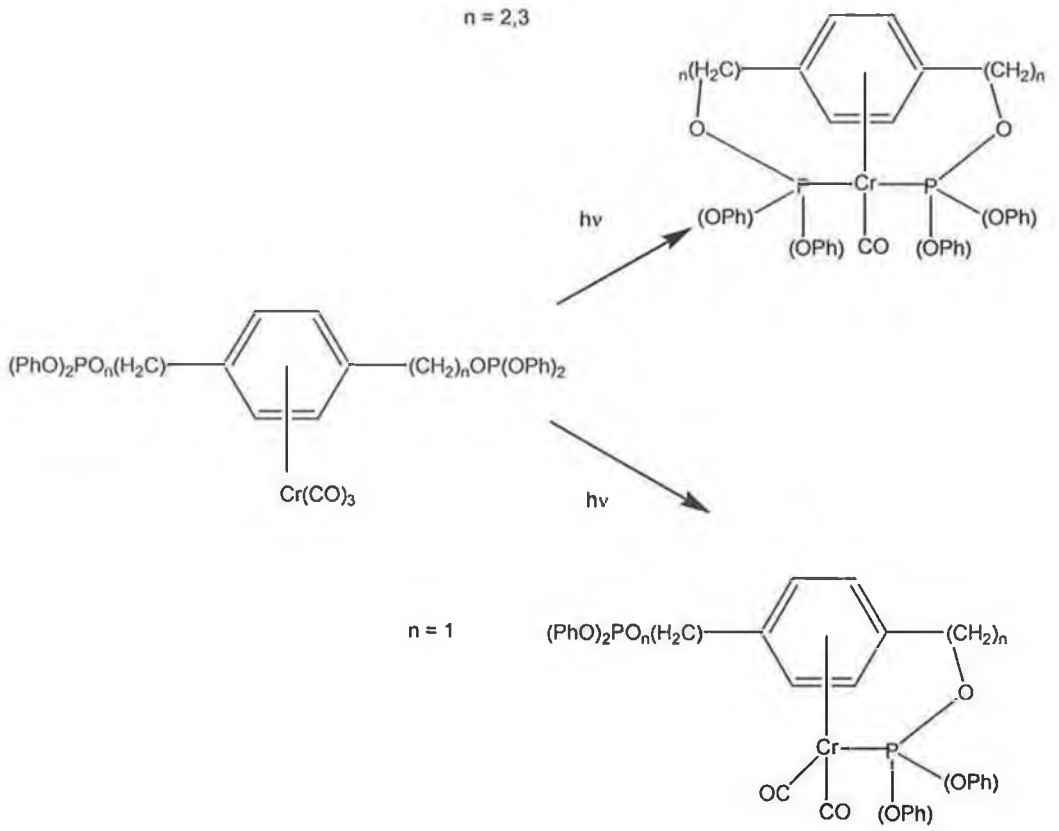

Scheme 1.8.2 Self chelating arene chromium tricarbonyl compounds upon photochemical loss of CO.

Arene chromium tricarbonyl complexes are also known to undergo photochemical redox reactions, Reaction 1.8.4 and Reaction 1.8.5. Two examples of photolysis of $(\eta^6\text{-arene})Cr(CO)_3$ to yield redox reactive intermediates are shown below.[44]

$$(\eta^6\text{-arene})Cr(CO)_3 \xrightarrow[MeOH]{h\nu} Cr(OMe)_3 \qquad \text{Reaction 1.8.4}$$

$$(\eta^6\text{-arene})Cr(CO)_3 \xrightarrow[S_2R_2]{h\nu} Cr(SR)_3 \qquad \text{Reaction 1.8.5}$$

The oxidative addition of Cl_3SiH to $(\eta^6\text{-benzene})Cr(CO)_2L$ intermediate by the photolysis of $(\eta^6\text{-benzene})Cr(CO)_3$ with Cl_3SiH has also been observed, reaction 1.8.6.[45]

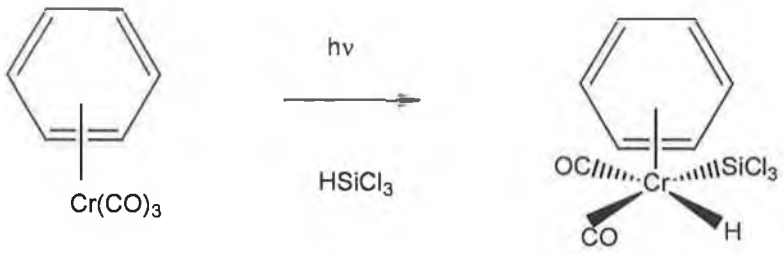

Reaction 1.8.6 The Photochemical addition of Cl_3SiH to (η^6-benzene)$Cr(CO)_3$.

1.9 Photochemistry of (η^5-C_5H_5)$Mn(CO)_3$ complexes

The absorption spectrum of (η^5-C_5H_5)$Mn(CO)_3$ is shown in Figure 1.9.1. The absorption band at ~ 330 nm is charge transfer in character with considerable M $\rightarrow$ η^5 C_5H_5 CT character, but ligand field transitions are likely to occur to be in the same region.[46,47,48] This absorption band also has some M $\rightarrow$ CO π*CT character. The absorption at ~ 260 nm is thought to be ligand field in character. These ligand field transitions being obscured by more intense charge transfer bands.

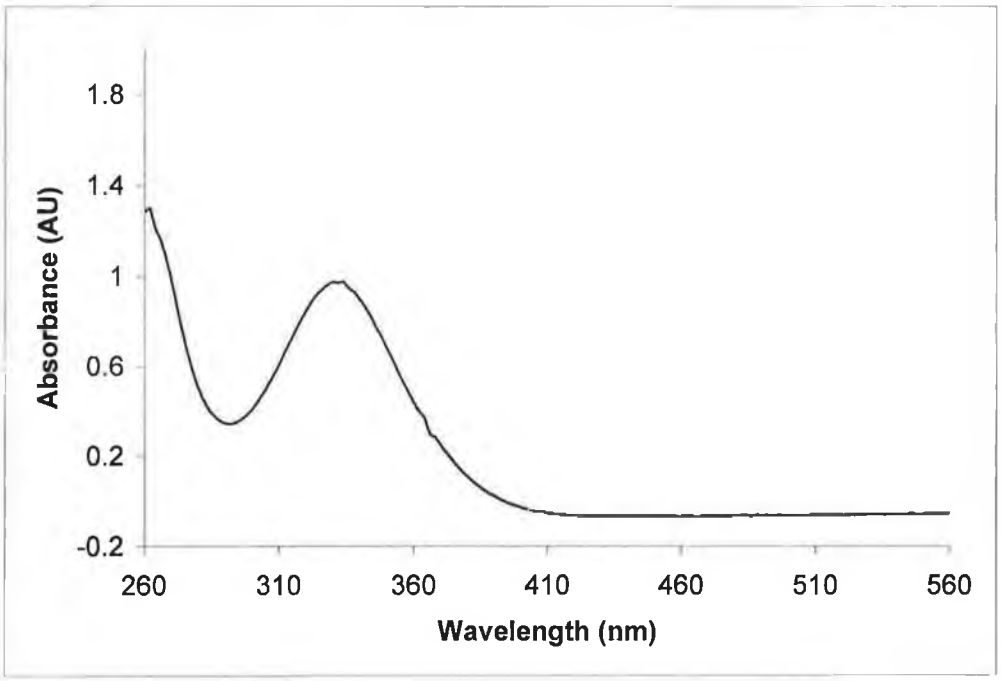

Figure 1.9.1 The UV/vis absorption spectrum of (η^5-C_5H_5)$Mn(CO)_3$.

Two transient species were observed for $(\eta^5\text{-}C_5H_5)Mn(CO)_3$ using both UV/vis flash photolysis and TRIR.[49] The first species was identified as $(\eta^5\text{-}C_5H_5)Mn(CO)_2$(solvent) which reacts with CO to reform the parent, Scheme 1.9.1.

$$(\eta^5\text{-}C_5H_5)Mn(CO)_3 \xrightarrow[\text{solvent}]{h\nu} (\eta^5\text{-}C_5H_5)Mn(CO)_2(\text{solvent}) + CO$$

$$(\eta^5\text{-}C_5H_5)Cr(CO)_2(\text{solvent}) + CO \rightarrow (\eta^5\text{-}C_5H_5)Mn(CO)_3$$

Scheme 1.9.1.

Rest and Sodeau have also shown the existence of the $(\eta^5\text{-}C_5H_5)Mn(CO)_2(CH_4)$ species by photolysis of $(\eta^5\text{-}C_5H_5)Mn(CO)_3$ in a CH_4 matrix at 20K.[50] Batterman and Black recorded a similar metal alkane interaction, by photolysis of $(\eta^5\text{-}C_5H_5)Mn(CO)_3$ in a methylcyclohexane/nujol mixture at 175K as the low temperature solid.[51] The second transient species was identified as $(\eta^5\text{-}C_5H_5)_2Mn(CO)_5$, which was formed by the reaction of $(\eta^5\text{-}C_5H_5)Mn(CO)_2$(solvent) with unphotolysed $(\eta^5\text{-}C_5H_5)Mn(CO)_3$, Scheme 1.9.2.

$$(\eta^5\text{-}C_5H_5)Mn(CO)_3 \xrightarrow[\text{solvent}]{h\nu} (\eta^5\text{-}C_5H_5)Mn(CO)_2(\text{solvent}) + CO$$

$$(\eta^5\text{-}C_5H_5)Mn(CO)_2(\text{solvent}) + (\eta^5\text{-}C_5H_5)Mn(CO)_3 \rightarrow (\eta^5\text{-}C_5H_5)_2Mn_2(CO)_5$$

Scheme 1.9.2.

Yang and Yang have also characterised the alkyl halide complex $(\eta^5\text{-}C_5H_4CH_2CH_2)Mn(CO)_2XR$ (X = Cl or Br, R = *n*-BU, *n*-C_5H_{11}) by low temperature spectroscopy.[52] Casey *et al.* showed that photolysis in a toluene glass matrix of $(\eta^5\eta^1\text{-}C_5H_4CH_2CH_2Br)Mn(CO)_2$ and $(\eta^5\eta^1\text{-}C_5H_4CH_2CH_2I)Mn(CO)_2$ and resulted in CO loss to yield intramolecular coordination of the alkyl halide to the manganese atom, Reaction 1.9.1, yielding both the $(\eta^5\eta^1\text{-}C_5H_4CH_2CH_2Br)Mn(CO)_2$ or $(\eta^5\eta^1\text{-}C_5H_4CH_2CH_2I)Mn(CO)_2$ species.[53] Both species were found to be stable up to -20°C.

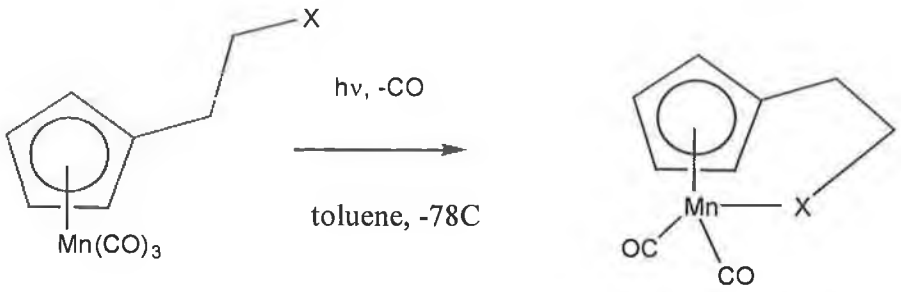

Reaction 1.9.1 Intramolecular alkyl halide coordination to manganese, by photolysis of $(\eta^5\text{-}C_5H_4CH_2CH_2X)Mn(CO)_2$ derivatives (X= I or Br).

As with $(\eta^6\text{-arene})Cr(CO)_3$ complexes the dominant process is again loss of CO and its replacement by a ligand (L) to yield the monosubstituted product $(\eta^5\text{-}C_5H_5)Mn(CO)_2(L)$ complex. Further loss of CO and replacement by a ligand (L) has been noted in several cases most notably when the ligand is a good π acceptor, for example all COs have been lost in the generation of $(\eta^5\text{-}C_5H_5)Mn(\eta^6\text{-}C_6H_6)$. The coordinatively unsaturated intermediate $(\eta^5\text{-}C_5H_5)Mn(CO)_2$ is susceptible to oxidative addition as in its $(\eta^6\text{-arene})Cr(CO)_2$ analogue, Reaction 1.9.2.[54]

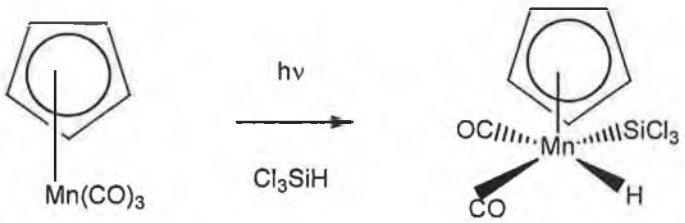

Reaction 1.9.2.

1.10 Arene exchange reactions

The exchange of arene ligands is a characteristic reaction of many transition metal π arene complexes and this is especially useful in the synthesis of complexes which by other methods it would be difficult or impossible.

$(\eta^6\text{-arene})ML + arene' \leftrightarrow (\eta^6\text{-arene}')ML + arene$. Reaction 1.10.1.

There are two types of exchange processes as in transition metal π complexes. These are thermal or photoinitiated and the rate of exchange and mechanism depends significantly on the solvent.

Strohmeier was the first to report kinetic studies for arene exchange reactions.[55] The rate law showed a first and second order dependence on the concentration of the starting arene complex as well as a first order dependence on the arene concentration. In accordance with these kinetic studies the following mechanism was proposed.

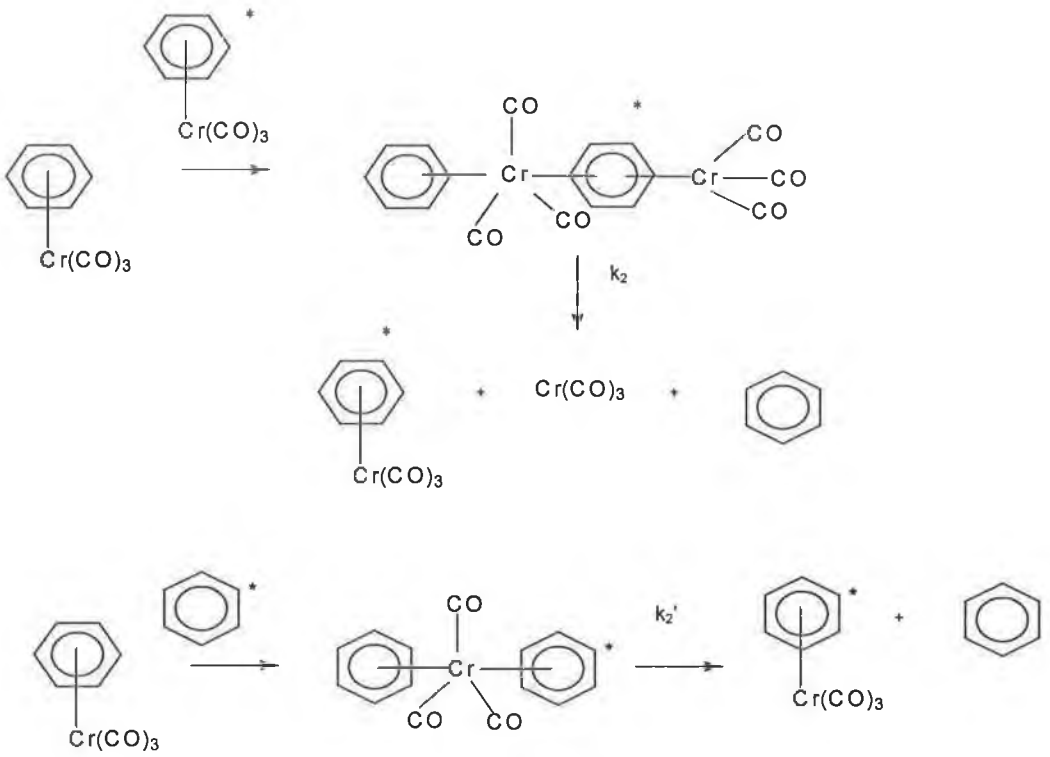

Scheme 1.10.1 A proposed mechanism for arene exchange.

The mechanism proposed by Strohmeier, in particular the dissociation of the (η^6-arene)$Cr(CO)_3$ to the arene and $Cr(CO)_3$ has received some criticism because it does not account for the acceleration by donor solvent, in addition the expected inversion observed when the two sides of the arene ring were distinguishable was not observed. A reinvestigation of the reaction by Traylor *et al.* (Scheme 1.10.2) gave a new insight into the rate laws and mechanisms involved in arene exchange.[56, 57] The nature of the second order dependence on the reactant arene complex on the rate of arene exchange was reexamined. When an inert Cr complex is added a first order dependence on the added Cr complex is observed for arene exchange. It was

concluded that in the absence of a co-ordinating solvent the reaction is likely to be catalysed by another molecule of the arene complex forming a dimeric intermediate.

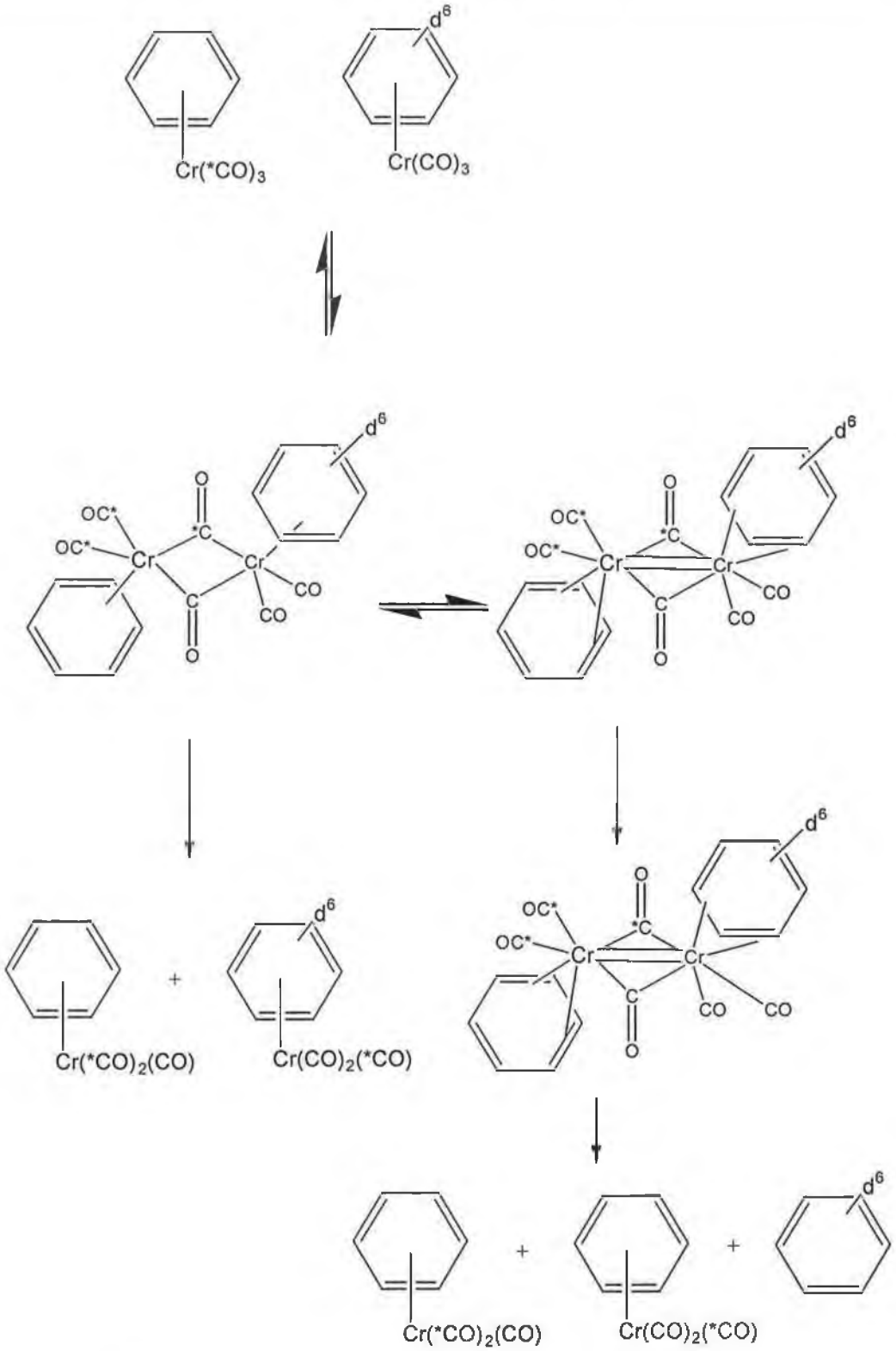

Scheme 1.10.2 The revised mechanism for arene exchange.

The occurrence of both ^{13}CO species and arene exchange can be satisfied by the CO bridging species shown. It should not be ruled out that the ^{13}CO scrambling between the two systems occurred by thermal CO loss.

Mahaffy and Pausson proposed that the arene exchange reaction is initiated by the presence of a donor solvent molecule (Scheme 1.10.6).[58]

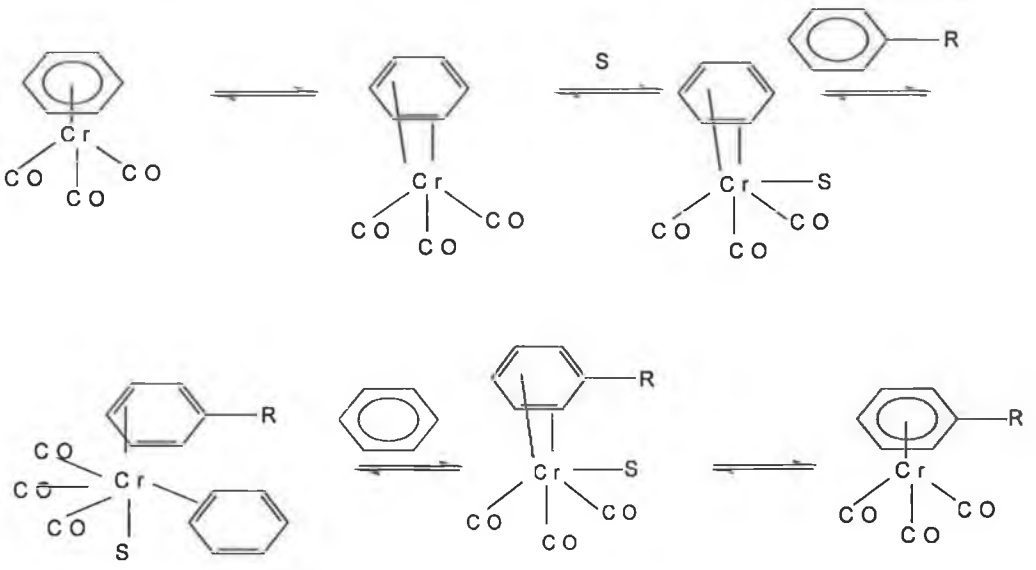

Scheme 1.10.6 Mahaffy and Pauson's mechanism for arene exchange in the presence of a donor solvent.

In the absence of a coordinating ligand, it was suggested that the reaction may proceed through the formation of a dimer formation via coordination of the oxygen of the carbonyl group of a (η^6-arene)$Cr(CO)_3$ complex. It is found that by extending the conjugation in the arene system from benzene to naphthalene to phenanthrene, the arene exchange reaction becomes more facile and the rate of arene exchange increases.

The arene displacement reaction was first investigated by the mechanism proposed by Zingales, Scheme 1.10.7.[59] (η^6-naphthalene)$Cr(CO)_3$ reacts 10 times faster then does (η^6-benzene)$Cr(CO)_3$. Zingales was the first to account for the second order rate law on the basis of ring slippage pathways for the reaction. Zhang *et al.* carried out a number of experiments concerning arene displacement.[61] The experiments involved a

number of (η^6-arene)$Cr(CO)_3$ complexes reacting with phosphines or phosphites to attempt to learn what factors influence the arene displacement reaction.

Considering what happens to the resonance energy alone of the ring ligand during the first slow rate determining step of the reaction, a rationalization of the increased reactivity of (η^6-naphthalene)$Cr(CO)_3$ over (η^6-benzene)$Cr(CO)_3$ may be offered. If the resonance energy of benzene is assumed to be unchanged in its (η^6-benzene)($Cr(CO)_3$ 20 kcal/ mole (84 kJ / mole) and zero energy in its (η^4-benzene)$Cr(CO)_3L$ configuration.[60] It seems safe to assume that it takes this amount of energy for the reaction to occur. Naphthalene has a resonance energy of 30 kcal/mole (136 kJ / mole), yet its (η^6-arene)$Cr(CO)_3$ compound reacts 10^6 times as fast as the (η^6-benzene)$Cr(CO)_3$ complex. Although the resonance energy of (η^6-naphthalene)$Cr(CO)_3$ is 30 kcal/mole (136 kJ / mole) the transition state (η^4-naphthalene)$Cr(CO)_3L$ can be given a resonance energy of 20 kcal / mole (84 KJ / mole) because of the fused benzene ring. This results in a net change of 10 kcal / mole (42 KJ / mole) going from the (η^6-naphthalene)$Cr(CO)_3$ to the (η^4-naphthalene)$Cr(CO)_3L$ complex. This difference may be responsible in part for the increased reactivity of the naphthalene complex. Zhang *et al.* found a good correlation between the rates of reaction and loss of resonance energy of the ring ligand as assumed by the $\eta^6 \rightarrow \eta^4$ step is the rate determining step.[61]

Howells used molecular orbital calculations at the extended Hückel level to construct full potential energy surface for ring slippage in (η^6-C_6H_6)Mn(η^5-C_5H_5), (η^6-$C_{10}H_8$)Mn(η^5-C_5H_5) and (η^6-pyrene)Mn(η^5-C_5H_5).[62] The overall form of the potential energy surface in a qualitative sense is insensitive to the substitution of MnCp by $Cr(CO)_3$, since both fragments are isoelectronic. The calculations correctly predicted arene lability in the order benzene << naphthalene < pyrene. However an $\eta^6 \rightarrow \eta^2$ path for naphthalene and a $\eta^6 \rightarrow \eta^1$ path for pyrene were found to be most favourable requiring the least energy. In benzene both paths were found to be comparable. No evidence was found for a discrete η^4 intermediate for (η^6-C_6H_6)Mn(η^5-C_5H_5).

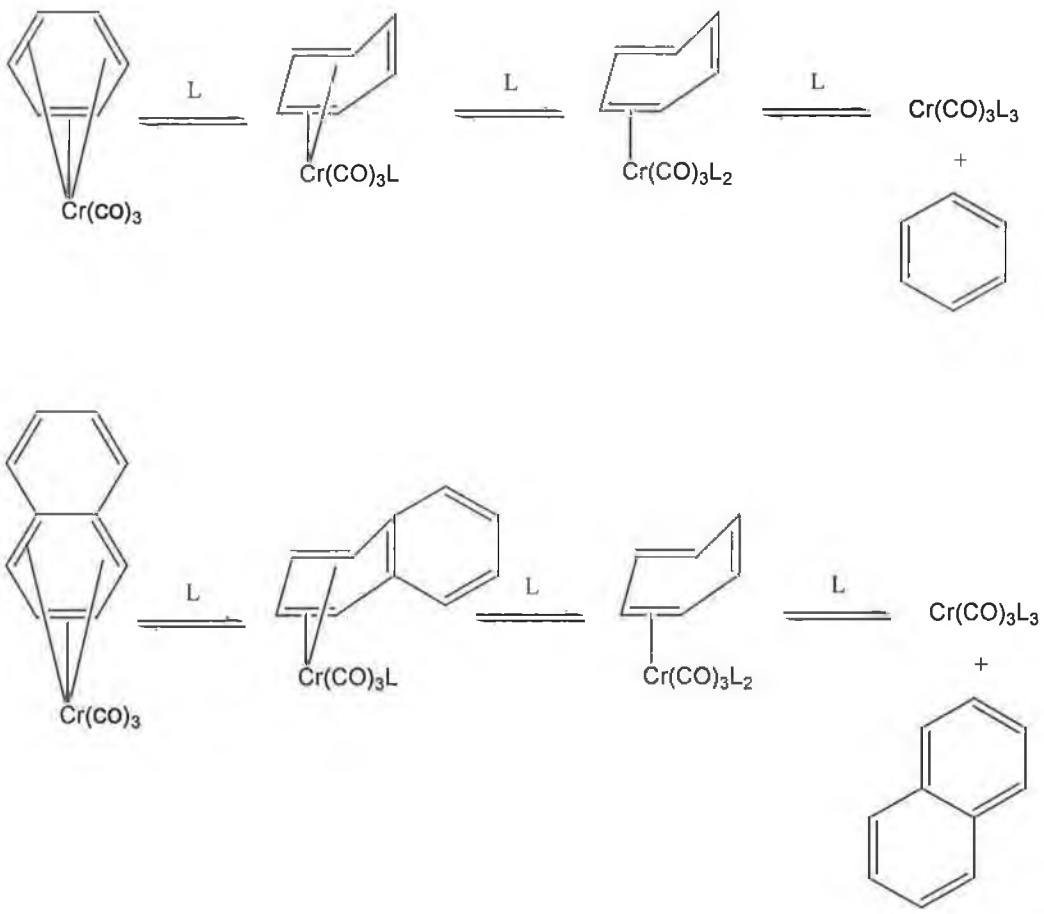

Scheme 1.10.7 The proposed mechanism for arene exchange, showing aromatisation of the second ring in the case of (η^6-naphthalene)$Cr(CO)_3$.

Likewise the rate of catalytic hydrogenation for (η^6-arene)$Cr(CO)_3$ complexes, increases in the order phenanthrene > naphthalene > anthracene.[63] In selectively deuterated naphthalene complexes, intramolecular ring exchange occurs at a much faster rate then intermolecular arene exchange with benzene. The haptotropic rearrangement clearly indicates the facility of ring slippage in naphthalene that provides a free coordination site for an incoming ligand.[64] This would indicate that the arene exchange reaction of (η^6-$C_{10}H_8$)$Cr(CO)_3$ with C_6H_6 could take place through an 16 electron η^3-allyl intermediate as shown in Figure 1.10.8.

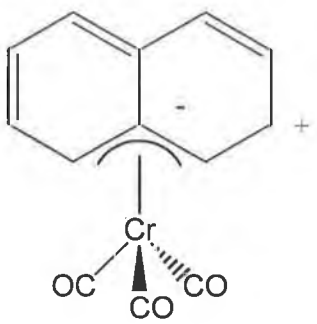

Figure 1.10.8 The η^3 allyl intermediate in migration of the $Cr(CO)_3$ fragment in (η^6-naphthalene)$Cr(CO)_3$.

1.11 Ring slippage reactions

Two types of haptotropic ring slip reaction are known. The first type of ring slip reaction is migration of the metal carbonyl fragment between different positions on the ligand. In rearrangements of the second type the metal shifts over the ligand, accompanied by reversible migrations of the hydrogen endo atoms between the metal and the ligand via agostic and hydride type intermediates.

An investigation into the reaction kinetics of $(\eta^5\text{-}C_5H_5)M(CO)_2L$ (where M = Co, Rh, Ir and L = PR_3) with a ligand L showed it to have first order dependence on both the concentration of the metal carbonyl fragment and the entering ligand, L.[65] To maintain the electron count in an associative process, an electron pair must be localised between two of the carbons of the C_5H_5 ring. This results in a ring slippage to a π allyl bonding interaction. An overall $\eta^5 \rightarrow \eta^3 \rightarrow \eta^5$ process was proposed for the process, Scheme 1.11.1.[66] Validation of this mechanism was the rationale that electron withdrawing substituents would increase the reaction rates while electron donating groups would reduce it if a pair of electrons were localised on the two carbons not forming the allyl bond is the rate determining step. This logic was tested and found to be correct. An electron withdrawing group (NO_2) was found to increase the rate and the electron donating group (CH_3) was found to decrease the rate.

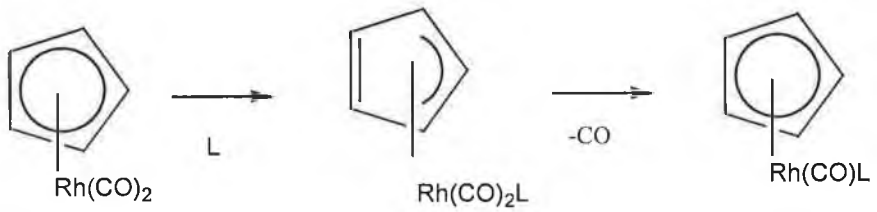

Scheme 1.11.1 $\eta^5 \rightarrow \eta^3 \rightarrow \eta^5$ process proposed by Cramer *et al.*, showing the associative addition of nucleophile, followed by CO loss.[66]

Casey and co workers have studied the reactions of $(\eta^5\text{-}C_5H_5)Re(CO)_3$ with $P(CH_3)_3$. Heating both reactants in hexane at 64 °C for 50 hours resulted in formation of the *fac*-$(\eta^1\text{-}C_5H_5)Re(CO)_3(P(CH_3)_3)_2$ adduct (Scheme 1.11.2).[67] Prolonged heating of the $(\eta^5\text{-}C_5H_5)Re(CO)_3$ complex with $P(CH_3)_3$, at 102°C in toluene, afforded the

substitution product, $(\eta^5\text{-}C_5H_5)Re(CO)_2P(CH_3)_3$. The only reasonable common intermediate is the $\eta^3\text{-}C_5H_5$ complex would seem to be a probable intermediate in the formation of both the hapticity change species $(\eta^1\text{-}C_5H_5)Re(CO)_3(P(CH_3)_3)_2$ and the substitution product $(\eta^5\text{-}C_5H_5)Re(CO)_2P(CH_3)_3$.

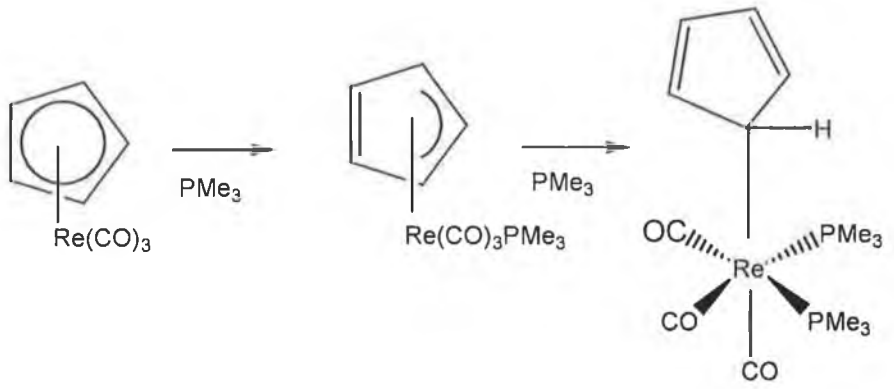

Scheme 1.11.2 Thermal substitution of CO by $P(CH_3)_3$ in $(\eta^5\text{-}C_5H_5)Re(CO)_3$ leading to formation of the diphosphine adduct fac $(\eta^1\text{-}C_5H_5)\ Re(CO)_3(PMe_3)_2$, through an $(\eta^5\text{-}C_5H_5)Re(CO)_3(PMe_3)$ monophosphine intermediate.

The thermal substitution reactions of $(\eta^5\text{-}C_4H_4N)Mn(CO)_3$ by $P(n\text{-}Bu_3)$ at 130°C, are 10^8 times faster than $(\eta^5\text{-}C_5H_5)Mn(CO)_3$.[68] This large rate enhancement was attributed to the more electronegative nitrogen, resulting in greater electron withdraw from the metal by the C_4H_4N compared to C_5H_5. Substitution reactions of cyclopentadienyl metal complexes are believed to involve a $\eta^5 \rightarrow \eta^3 \rightarrow \eta^5$ ring slippage. These processes enhance ligand substitution reactions, by localising a pair of electrons on the ring which permits a nucleophilic attack on the metal. This results in a low energy associative reaction pathway involving an 18 electron intermediate. It is possible that the $(\eta^3\text{-}C_4H_4N)Mn(CO)_2L$ intermediate may be more stable then the equivalent $(\eta^3\text{-}C_5H_5)Mn(CO)_2L$ complex. For the $(\eta^3\text{-}C_4H_4N)Mn(CO)_2L$ intermediate this would then result in a low energy associative reaction pathway involving an 18-electron intermediate, Scheme 1.11.3.

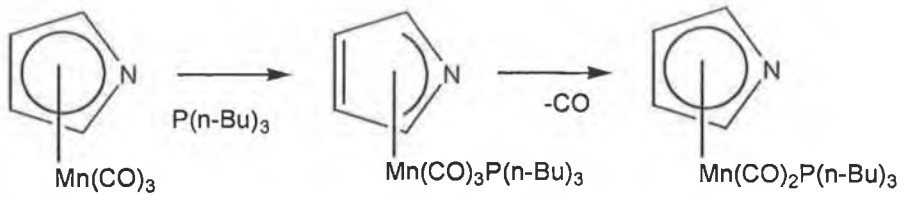

Scheme 1.11.3. Thermal substitution of CO by $P(n\text{-}Bu)_3$ in $(\eta^5\text{-}C_4H_4N)Mn(CO)_3$ involving an η^3-azaallyl type intermediate.

1.12 The Indenyl ligand effect

Mawby *et al.* were the first to report and study the kinetics and mechanisms of the $(\eta^5\text{-}C_9H_7)$ metal carbonyl compounds compared with their corresponding (η^5-cyclopentadienyl) analogues.[69] They found that the thermal CO substitution with $P(Ph)_3$ in $(\eta^5\text{-}C_9H_7)Mo(CO)_3CH_3$ gave the phosphine substituted acyl complex $(\eta^5\text{-}C_9H_7)Mo(CO)_3(P(Ph)_3)(C(O)CH_3)$. The substitution reaction of CO was found to be approximately 10 times faster for $(\eta^5\text{-}C_9H_7)Mo(CO)_3CH_3$ than for the analogous $(\eta^5\text{-}C_5H_5)Mo(CO)_3CH_3$, an η^3-indenyl intermediate was proposed to explain the rate acceleration and the observed second order kinetics for the reaction.

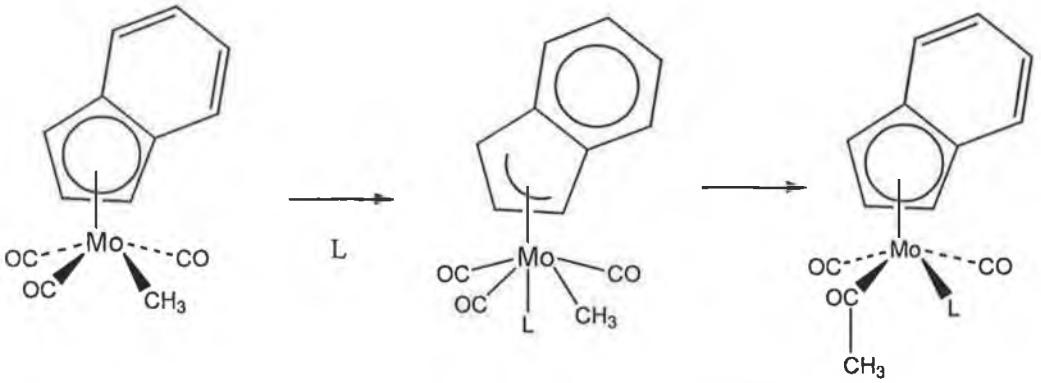

Scheme 1.12.1 Proposed mechanism for the associative substitution of CO in $(\eta^5\text{-}C_9H_7)Mo(CO)_3CH_3$ complex involving an η^3-indenyl intermediate.

Similar rapid substitution of η^5-indenyl complexes has been observed in a number of systems. No evidence for the η^3-intermediate could be obtained in the CO substitution

reaction of (η^5- C_9H_7)Re(CO)$_3$ with L (L = P(OC_2H_5)$_3$), Reaction 1.12.1. However η^1 formation was found to be much faster than for the (η^5-C_5H_5)Re(CO)$_3$ complex. Again the reaction is thought to proceed through an η^3-intermediate.[70]

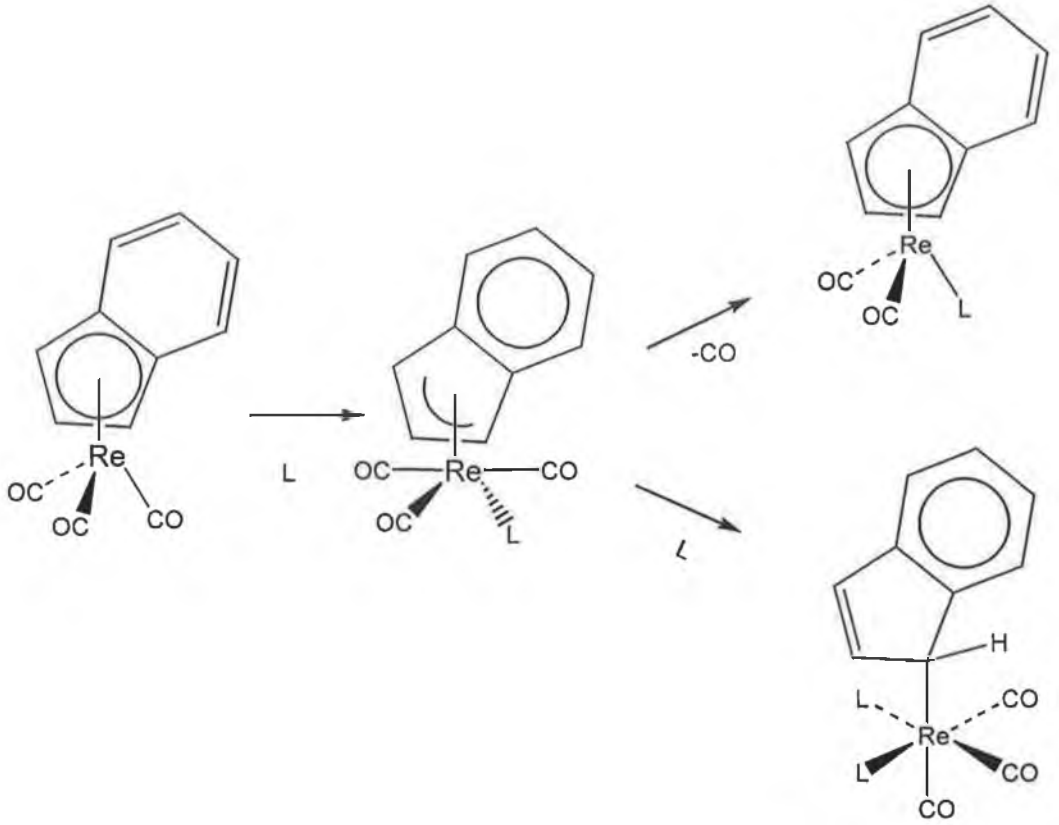

Scheme 1.12.2 Formation of either the η^1 or η^5 complexes indicates that both species originated from the same active intermediate the η^3 species.

By varying the conditions of this reaction, it was possible to form either the ring slip species (η^1-C_9H_7)Re(CO)$_3$L$_2$ or the CO substitution species (η^5- C_9H_7)Re(CO)$_2$L. [71] At low temperatures and high ligand concentration the (η^1-C_9H_7)Re(CO)$_3$L$_2$ was formed. At high temperatures and low concentrations of ligand the product was (η^5-Indene)Re(CO)$_2$L was formed. Treatment of the kinetic data for the formation of either the η^1 or η^5 complexes showed that both species originated from the same active intermediate, the (η^3-C_9H_7)Re(CO)$_3$L species. Ji, Rerek and Basolo have also reported the reaction of ($\eta^5C_{13}H_{19}$)Mn(CO)$_3$ (L = P(n-Bu)$_3$ where Bu = n butyl).[72] At low PBu_3 concentrations the reaction proceeded cleanly to the monosubstituted complex (η^5-$C_{13}H_9$)Mn(CO)$_2$L presumably through an unobserved η^3-fluorenyl

intermediate (η^3-$C_{13}H_9$)$Mn(CO)_3L$. Biagioni *et al.* reinvestigated the reaction of (η^5-$C_{13}H_{19}$)$Mn(CO)_3$ with alkyl phosphines at higher concentrations, producing the η^1 fluorenyl complex, (η^1-$C_{13}H_9$)$Mn(CO)_2L_2$.[73]

1.13 References

1. Ziegler, K.; Holtzkampf, E.; Breil, H.; Martin, M. *Angew. Chem.* 1955, **67**, 543.
2. Schiller, G. *German Patent.* 963, 605, *Chem abstract.* 11226, **53**, 1959.
3. Cotton, F.A and Wilkinson G, 'Advanced Inorganic Chemistry' 5th edition, Wiley New York 1988.
4. Holderich, W.; Hesse, M.; Naumann, F. *Angew. Chem. Int. Ed. Engl.* 1988, **27**, 246.
5. (a) Foster, D. *Adv. Organomet. Chem.* 1979, **17**, 255. (b) Drury, D.J. *Aspects of Homogonous Catalysis.* 1984, **5**, 197.
6. Orchin, M. *Acc. Chem. Res.* 1981, **14**, 259.
7. Heck, R.F.; Breslow, D.S. *J. Am. Chem. Soc.* 1961, **83**, 4025.
8. Magnus, P.; Principle, L.M. *Tetrahedron letters.* 1985, **26**, 4851.
9. Pagenkopf, B.L.; Livinghouse,. *J. Am. Chem. Soc.* 1996, **118**, 2285.
10. Gordon, CM., Kiscka, M., Jinka, I.R., Kerr, W.J., Scott, J.S., Gebicki, J. *J Organomet. Chem.* 1998, **556**, 147.
11. Draper, S.M.; Long, C.; Meyers, B.M. *J. Organomet. Chem.* 1999, **588**, 195.
12. R.G.W. Norrish; G. Porter, *Disc. Farad. Soc.* 1954, **17**, 40.
13. McFarlane, K.; Lee, B.;Ford, P.C.; Bridgewater J.S.; Lee, B. *J.Organomet. Chem.* 1998, **554**. 49.
14. Hermann, H.; Grevels, F.W.; Henne, H.; Schaffner, K. *J. Phys. Chem.* 1982. **86**. 5151.
15. Poliakoff, M and Weitz, E. *Adv. Organomet. Chem.* 1986. **26**. 277.
16. Laser Photonics. L5600 series tunable diode lasers.; *Laser photonics Inc. Analytical Division Brochure*. Laser Photonics, Andover, MA.
17. Whittle, E.; Dows, D.; Pimentall, G.C. *J. Phys. Chem.*, 1954, **22**, 1943.
18. Lewis, G.N.; Lipkin, D. *J. Am. Chem. Soc.* 1942, **64**, 2801.
19. Perutz, R.N. *Chem. Rev.* 1985, **85**, 278.
20. Abel E.W.; Stone F.G.A. *Quart. Rev. Chem. Soc.* 1969, **23**, 325.
21. Beach, N.A.; Gray, H.B. *J. Am.Chem. Soc*. 1968, **90** 5731.
22. (a) Kotzian, M.; Rösch, N.; Schroeder, H.; Zerner, M.C. *J. Am.Chem. Soc*. 1989, **11**, 7687. (b) Pierloot, k.; Verhulst, J.; Verbeke, P.; Vanquickenborne, L.G. *Inorg. Chem.* 1989, **28**, 3059.
23. Pollak, C.; Rose, A.; Baerando, E.J. *J. Am. Chem. Soc.* 1997, **119**, 7324.

24. Perutz ,R.N.; Turner, J. J. *Inorg. Chem.* 1975, **14**, 365.

25. Kelly, J.M.; Hermann, H.; Von Gustorf, E.K. *J. Chem. Soc., Chem. Commun.* 1973, 105.

26. Kelly, J.M; Bonneau, R. *J. Am. Chem. Soc.* 1980, **102**, 1220.

27. Hermann, H. Grevels, F.W.; Henne, A.; Schaffner K. *J. Phys. Chem.* 1982, **86**, 5151.

28. Church ,P. Grevels, F.W.; Hermann, H. Schaffner, K. *Inorg. Chem.* 1985, **24**, 418.

29. Ellian, M.; Chen, M.M.l.; Mingos D.M.P.; Hoffman R. *Inorg. Chem.* 1976, **15**, 149.

30. Carrol, D.G.; McGlynn, S.P. *Inorg . Chem.* 1968, **7**, 1285.

31. Wender, I .; Pino, P. *Organic synthesis via metal carbonyls. Vol 1. Ed Wiley. New York. N.Y.* 1968, p173.

32. Chalvert, J.G.; Pitts, J.N. *Photochemisty.* New York, NY, 1966.

33. Strohmeier, W.; Van Hobe, D. *Z . Naturforsch.* 1963, **109**, 981.

34. Yavorski, B.M, Barantskaya N.K, Trembovler V.M. *Akad Nauk, SSR.* 1972, **207**, 119.

35. Wrighton, M.S.; Haverty, J.L. *Z. Naturforsch.* 1975, **806**, 254.

36. Gilbert, A.; Kelly J.M.; Budzwait, M.; Koerner von Gustaff, E. *Z. Naturforsch.* 1976, **31b**, 1091.

37. Rest, A.J.; Sodeau, J.R. *J. Chem. Soc. Dalton Trans.* 1978, 651.

38. Bamford, C.H; Al-Lamee, K.G.; Konstantinov, C.J. *J . Chem. Soc.* 1977, 1406.

39. Creaven B.S.; George, M.W.; Ginsburg, A.G. Hughes, C.; Kelly, J.M.; Long, C.; McGrath, I.M.; Pryce, M.T. *Organometallics.* 1993, **12**, 3127.

40. Salliard, J.Y.; Hoffmann, R. *J. Am. Chem. Soc.* 1989, **106**, 2006.

41. Brookheart, M.; Grenn, M.L.H. *J. Organomet. Chem.* 1983, **250**, 395.

42. Trembovler, V.N.; Baranetskaya, N.K.; Fok, N.V.; Zaslauskaya, G.B.; Yavorskii, B.M.; Setkina, V.N. *J. Organomet. Chem.* 1976, **117**, 339.

43. Nesmeyanov, A.N., Struchkov, Yu.T., Andrianov, V.G.; Krivykh, V.V. and Rybinskaya, M.I. *J. Organomet. Chem.* 1979, **164**, 51.

44. (a) Brown D.A; Cunningham D; Glass W.K. *J. Chem. Soc. Chem. Commun.* 1966, 306.(b) Brown, D.A.; Glass, W.K.; Kumar; B. *J. Chem. Soc. Chem. Commun.* 1967, 736.

45. Jetz.W.; Graham, W.A.G. *Inorg. Chem.* 1841, **10**, 1971.

46. Giordiano, P.J.; Wrighton, M.S. *Inorg. Chem.* 16, **160**, 1977.

47. Lundquist, R.T.; Cais M. *J. Org. Chem.* 27, **1167**, 1967.

48. Gogan N.J.; Chu C.K. *J. Organomet. Chem.* 1975, **93**, 363.

49. Creaven, B.S; Dixon, A.J.; Kelly, J.M.; Long, C.; Poliakoff, M.; *Organometallics.* 1987, **6**, 2600.

50. Rest A.J; Sodeau J.R; Taylor D.J. *J. Chem. Soc., Dalton. Trans.* 1978, 681.

51. Batterman P.S.; Black, J.D. *J. Organomet. Chem.* 1977, C3, 39.

52. Yang, P.F; Yang, G.K. *J. Am. Chem. Soc.* 1992, **114**, 6937.

53. Casey, C.P.; Czerwinski, C.J.; Fraaley, M.E. *Inorg. Chim. Acta.* 1998, **280**, 316.

54. Jetz, W.; Graham, W.A.G. *Inorg. Chem.* 1971, **10**, 4.

55. Strohmeier, W.; Mittnacht, H. *Z. Phys. Chem (Munich).* 1959, **29**, 339.

56. Traylor, T.G.; Stewart, K.J. *J. Am. Chem. Soc.* 1984, **106**, 4445.

57. Traylor T.G.; Stewart, K.J. *J. Am. Chem. Soc.* 1986, **108**, 6977.

58. (a) Mahaffy, C.A.L.; Pauson, P.L. *J. Chem. Res .(S)* 1979, 126. (b) Mahaffy, C.A.L.; Pauson, P.L.; *J. Chem. Res. (M)*; 1979, 1752.

59. Zingales, F. Chiesa, A.; Basolo, F. *J. Am. Chem. Soc.* 1966, **88**, 2707.

60. Dewar, M.J.; Linn, C.D. *J. Am. Chem. Soc.* 1969, **91**, 789.

61. (a) Shen, J.K.: Zhang, S.S; Basolo, F.; Johnson, S.E.; Hawthorne, F.M. *Inorg. Chim. Acta.* 1995, **235**(1-2), 89. (b) Basolo, F. *New. J. Chem.* 1994, **18**, 19.

62. Howell J.A.S.; Ashford N.F.; Dixon D.T.; Kola J.C. *Organometallics* 1991, **10**, 1852-1869.

63. Yagupsky, M.G.; Cais, M. *Inorg. Chim. Acta.* 1975, **12**, 227.

64. Albright, T.A.; Hoffmannn, P.; Hoffmann, R.; Cillya, C.P.; Dobosh, P.A. *J. Am. Chem. Soc.* 1983, **105**, 3396.

65. Schuter – Wolden, H.G.; Basolo, F. *J. Am. Chem. Soc.* 1966, **88** 1657.

66. Cramer, R.; Selwell, L.D. *J. Organomet. Chem.* 1975, **92**, 245.

67. Casey, C.P.; O'Connor, J.M.; Jones W.D.; Haller K.J. *Organometallics* 1983, **2**, 535.

68. Kershner, D.; Rheingold, A.L.; Basolo, F. *Ogranometallics* 1987, **6**, 196-1.

69. (a) Hart-Davis, A.J.; Mawby, R. *J. Chem. Soc. A.* 1969, 2403. (b) Hart-Davis, A.J.; White, C.; Mawby, R. J. *Inorg. Chim. Acta.* 1970, **4**, 441. (c) White, C.; Mawby, R. *Inorg. Chim. Acta.* 1972, **6**, 157. (d) Jones, D.J.; Mawby, R.J. *Inorg .Chim. Acta.* 1972, **6**, 157.

70. Casey, C.P.; O'Connor, J.M. *Organometallics* 1985, **4**, 384.

71. Bang H.; Lynch T.J.; O'Connor; J.M. *Organometallics* 1992, **11**, 40.

72. Ji L.N.; Rerek M.E.; Basolo F. *Organometallics* 1984, **3**, 740.

73. Biagioni, R.N.; Lokovic, I.M.; Sketton, J.; Hartuny, J.B. *Organometallics* 1990, **9**, 547.

Chapter 2

The photochemistry of substituted (η^6-arene)$Cr(CO)_3$ compounds

2.1 Introduction to the photochemistry of (η^6-arene)$Cr(CO)_3$ complexes

Previous photochemical studies on the (η^6-arene)$Cr(CO)_3$ system, have found that the primary reaction is CO loss, proceeding with a high quantum yield (Φ) 0.72 (Reaction 2.1.2).[2] However under an inert atmosphere, the arene exchange reaction takes place, but with a much lower quantum yield (0.12) (Reaction 2.1.1).[1] This second process thought to proceed through a ring slip process, was less extensively studied while the first reaction was studied in some detail.

$$(\eta^6\text{-arene})Cr(CO)_3 \xrightarrow[\text{arene*}]{h\nu} (\eta^6\text{-arene*})Cr(CO)_3 + \text{arene} \qquad \text{Reaction 2.1.1}$$

$$(\eta^6\text{-arene})Cr(CO)_3 \xrightarrow[L]{h\nu} (\eta^6\text{-arene})Cr(CO)_2(L) + CO \qquad \text{Reaction 2.1.2}$$

Attempts to observe this ring slip reaction were made by Creaven *et al* who obtained some evidence for a ring slip process, by UV/vis monitored flash photolysis.[3] Upon laser flash photolysis of (η^6-C_6H_6)$Cr(CO)_3$, additional transient signals were observed besides those relating to the known photoproduct (η^6-C_6H_6)$Cr(CO)_2$(alkane), or any species formed by a subsequent reaction of this intermediate. Pryce *et al.* carried out a photochemical study of various arene substituted (η^6-arene)$Cr(CO)_3$ complexes.[6] The rate constant for the reaction of the photogenerated (η^6-arene)$Cr(CO)_2$(alkane) fragment with CO was found to be dependent on the nature and degree of the substitution of the arene ligand and upon the alkane solvent. Activation parameters for recombination of the (η^6-arene)$Cr(CO)_2$(alkane) fragment with CO were consistent with an interchange mechanism. Neither a ring slip adduct or ultimately $Cr(CO)_6$ were seen upon photolysis of (η^6-arene)$Cr(CO)_3$ complexes in carbon monoxide saturated alkane solutions.

Breheny, subsequently carried out a study of the photochemistry of (η^6-C_5H_5N)$Cr(CO)_3$ and its 2,6 methyl and silyl disubstituted derivatives by matrix isolation, TRIR and UV/vis flash photolysis in the hope of detecting haptotropic changes at the heteoarene.[4] Solution photochemistry provided evidence for the formation of (η^1-C_5H_5N)$Cr(CO)_5$. Ultimately $Cr(CO)_6$ was observed along with

formation of the solvated dicarbonyl. Matrix isolation studies showed that long wavelength irradiation results in a haptotropic change of the pyridine ring coordination from η^6- η^1. At shorter wavelength irradiation the ring slip product was observed in addition to the CO loss species. In this study it was thought that by placing a functional group on the arene ring to induce an alternative photochemical pathway to CO loss.

2.2 Spectroscopic properties of $(\eta^6\text{-}C_6H_6)Cr(CO)_3$, $(\eta^6\text{-}C_6H_5NH_2)Cr(CO)_3$, $(\eta^6\text{-}C_6H_5OCH_3)Cr(CO)_3$, $(\eta^6\text{-}C_6H_5CO_2CH_3)Cr(CO)_3$ and $(\eta^6\text{-}C_6H_5COH)Cr(CO)_3$

All of the tricarbonyl systems studied have two IR bands in the carbonyl region except for $(\eta^6\text{-}C_6H_5NH_2)Cr(CO)_3$, in which the lower energy band is resolved into two distinct bands. These complexes all have C_s symmetry (except $(\eta^6\text{-}C_6H_6)Cr(CO)_3$ which has C_{3v} symmetry. A decrease in the frequency of the CO bands is observed as the substituent on the ring is varied from H to an electron donating group, for the series $(\eta^6\text{-}C_6H_5NH_2)Cr(CO)_3$, $(\eta^6\text{-}C_6H_5OCH_3)Cr(CO)_3$, $(\eta^6\text{-}C_6H_5CO_2CH_3)Cr(CO)_3$ or $(\eta^6\text{-}C_6H_5COH)Cr(CO)_3$, a decrease in the ν_{co}. This is a result of the increased electron density at the metal atom, resulting in donation to the antibonding orbitals of the CO ligand, thus decreasing the CO bond order and the ν_{co}.

$(\eta^6$-arene$)Cr(CO)_3$ complex	UV/vis bands Cyclohexane (nm)	IR bands Cyclohexane (cm^{-1})
$(\eta^6\text{-}C_6H_5NH_2)Cr(CO)_3$	270, 332.	1967, 1893, 1888.
$(\eta^6\text{-}C_6H_5OCH_3)Cr(CO)_3$	262, 324.	1978, 1907.
$(\eta^6\text{-}C_6H_6)Cr(CO)_3$	263, 315.	1983, 1913.
$(\eta^6\text{-}C_6H_5CO_2CH_3)Cr(CO)_3$	260, 325,395.	1991, 1926.
$(\eta^6\text{-}C_6H_5COH)Cr(CO)_3$	320, 420.	1998, 1938.

Table 2.2.1 Spectroscopic parameters of all $(\eta^6$-arene$)Cr(CO)_3$ complexes. All spectra were recorded in cyclohexane.

The UV/vis spectrum for all four complexes are broadly similar and are given in Figure 2.2.1-2.2.5. The UV/vis spectrum contains a valley at 280 nm through which it is possible to observe transient species in the UV/vis flash photolysis experiments. The band with the λ_{max} at approximately 320 nm is assigned as a M→ arene CT band with some M → π*CO CT character.[5] There is also an absorption centred around 265 nm which is assigned to a M → π* CO CT transition.

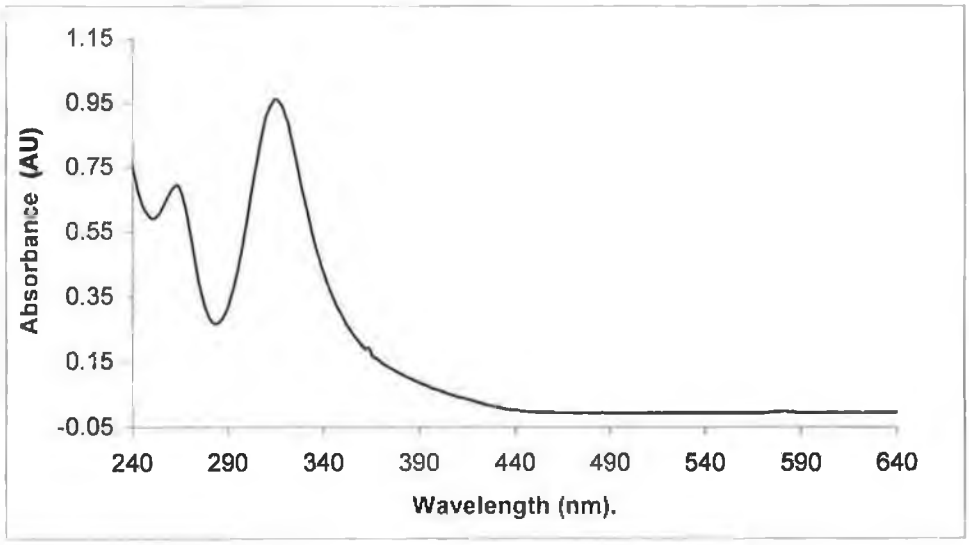

Figure 2.2.1 The UV/vis spectrum of $(\eta^6\text{-}C_6H_6)Cr(CO)_3$ recorded in cyclohexane.

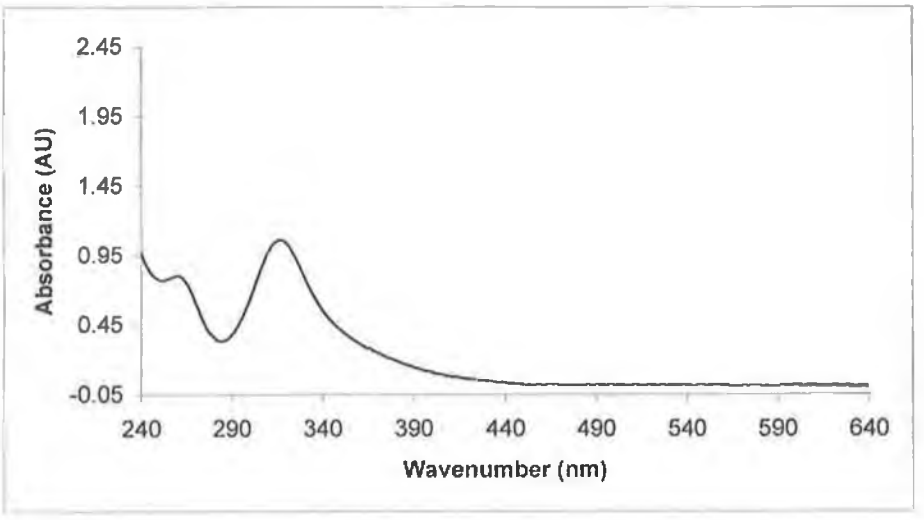

Figure 2.2.2 The UV/vis spectrum of $(\eta^6\text{-}C_6H_5NH_2)Cr(CO)_3$ recorded in cyclohexane.

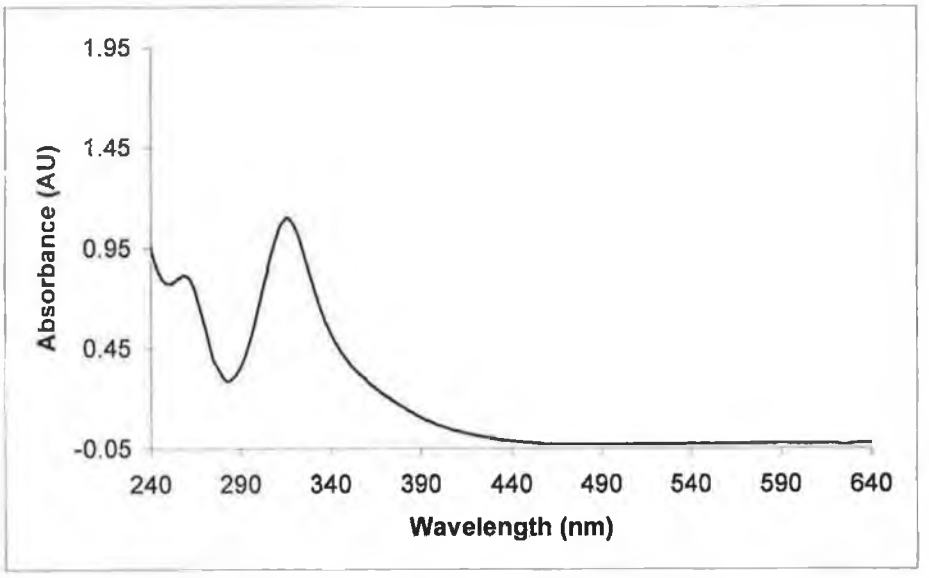

Figure 2.2.3 The UV/ vis spectrum of $(\eta^6\text{-}C_6H_5OCH_3)Cr(CO)_3$ recorded in cylohexane.

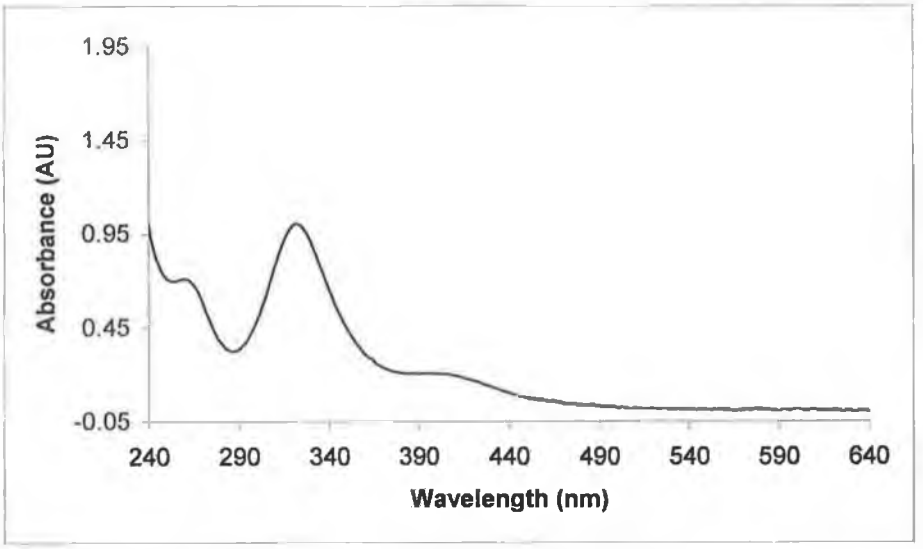

Figure 2.2.4 The UV/vis spectrum of $(\eta^6\text{-}C_6H_5CO_2CH_3)Cr(CO)_3$ recorded in cyclohexane.

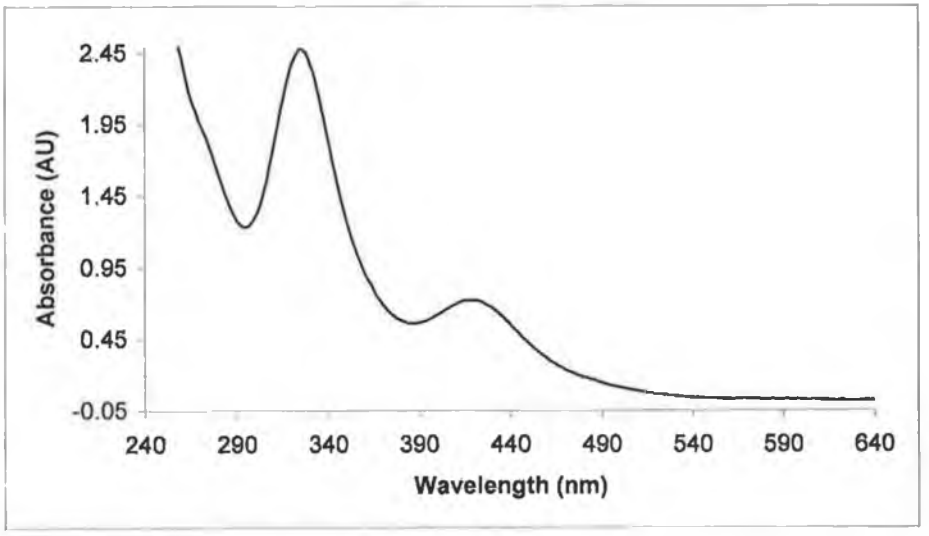

Figure 2.2.5 The UV/vis spectrum of $(\eta^6\text{-}C_6H_5COH)Cr(CO)_3$ recorded in cyclohexane.

2.3 X-ray crystallography of substituted (η^6-arene)$Cr(CO)_3$ complexes

Hunter and Shillday undertook a systematic investigation using X- ray crystallography to quantify the effect of main group π donor and π acceptor substituents on the planarity of the arene ring in (η^6-arene)$Cr(CO)_3$ complexes.[7] They found that π donor substituents and their ipso carbon (the carbon atom in the ring attached to the functional group) are bent away from the $Cr(CO)_3$ moiety, while π acceptor substituents and their ipso carbon atoms are in the plane of the arene ring and are bent slightly towards the $Cr(CO)_3$ unit. The effect of a substituent on the planarity of the arene ring is best measured by the angle θ_i. The parameter θ_i is defined as the angle between the least squares planes defined by the ipso and ortho carbon atoms of the arene and the least squares plane defined by the ortho- and meta- carbon atoms of the arene. These values along with the distance of the Cr atom to the centroid of the substituted arene ring (D_{cent}) are shown below in Table 2.3.1. It was also found that the magnitudes of these structural distortions are dependent on the π donor or π acceptor abilities of the substituent. The amino ($-NH_2$) substituent displayed very large distortions from planarity of the ring, while the more weakly donating group (the methoxy substituent), shows less distortion of ring planarity. Those substituents having moderate π acceptor characteristics remain approximately in the plane of the ring, while those bearing strong π acceptor substituents are bent out of the plane towards the $Cr(CO)_3$ unit.

(η^6-arene)$Cr(CO)_3$ complex	D_{cent}	θ_i
(η^6-$C_6H_5NH_2$)$Cr(CO)_3$	1.724	5.78
(η^6-$C_6H_5OCH_3$)$Cr(CO)_3$	1.740	1.90
(η^6-$C_6H_5CO_2CH_3$)$Cr(CO)_3$	1.719	0.40
(η^6-C_6H_5COH)$Cr(CO)_3$	1.717	-1.04

Table 2.3.1 Structural parameters for (η^6-arene)$Cr(CO)_3$ complexes as measured by Hunter and Shillday.[7]

Hunter and Shillday explained this behaviour using simple valence bond theory to predict the qualitative behaviour of any of π donation and π acceptor interactions. Therefore π donation from a substituent, D, would be expected to result in the contribution of a second resonance form of these complexes. This second resonance form has a positive charge localised on D and a negative charge on the $Cr(CO)_3$ fragment. The anionic $Cr(CO)_3$ centre in the charge-seperated zwitterionic (η^5-cyclohexadienyl)$Cr(CO)_3$ resonance form has an 18 electron configuration and would be expected to repel the electron density of the exocyclic bond.

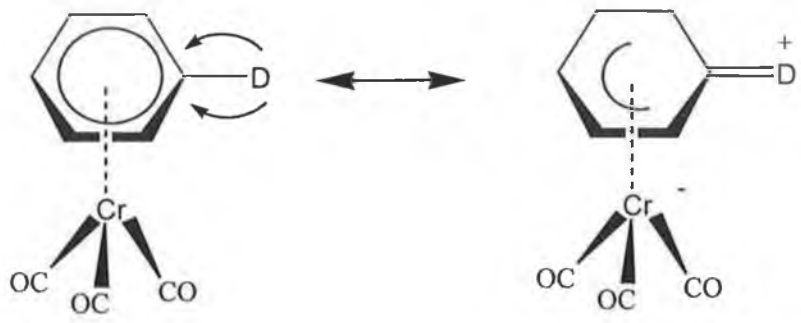

Figure 2.3.1 The two different resonance forms of (η^6-C_6H_5D)$Cr(CO)_3$ (D = electron donating group).

Hence the π donor substituent and its ipso carbon atom would be expected to bend away from the $Cr(CO)_3$ centre. In extreme cases, such a π-donor interaction would produce a cyclohexadienyl complex in which the exocyclic double bond was completely nonbonding with respect to the $Cr(CO)_3$ unit.

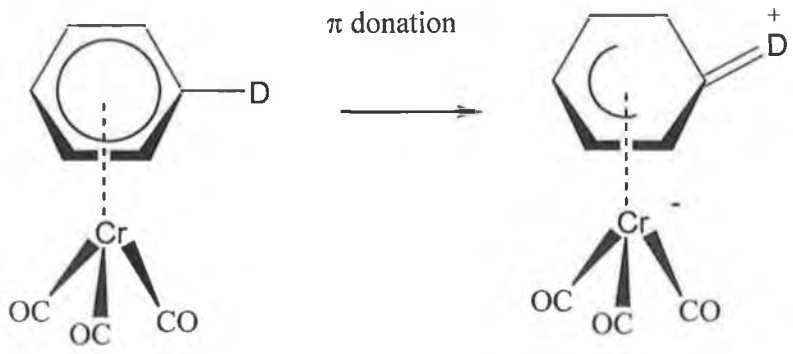

Figure 2.3.2 The two different resonance forms of $(\eta^6\text{-}C_6H_5D)Cr(CO)_3$, (D = electron donating group) showing the structural distortions to the arene ring.

This is in accordance with the calculated structure of the hypothetical species $[(\eta^5\text{-}C_6H_5{=}CR_2)Cr(CO)_3]^-$. In calculations by Albright, Hoffmann and Hofmann for these species, the exocyclic bond was found to bend away from the $Cr(CO)_3$ unit in the $[(\eta^5\text{-}C_6H_5{=}CR_2)Cr(CO)_3]^-$ complex.[8]

For π acceptor substituents the opposite situation to that of the π donor substituent is expected. Here the exocyclic bond would be expected to bend towards instead of away from the $Cr(CO)_3$ centre, and bond to the 16 electron cationic $Cr(CO)_3$ centre.

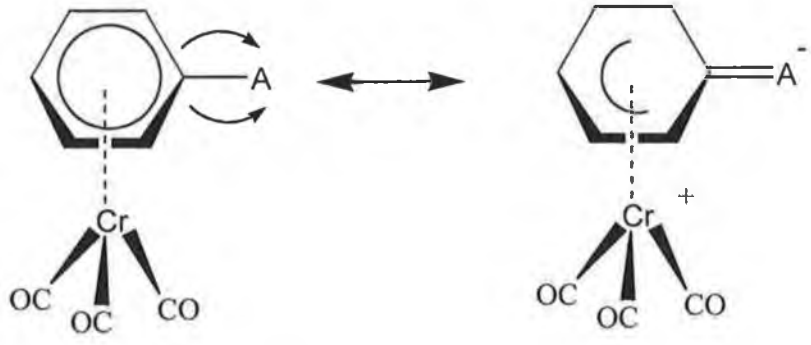

Figure 2.3.3 The two different resonance forms of $(\eta^6\text{-}C_6H_5A)Cr(CO)_3$ (A = electron withdrawing group).

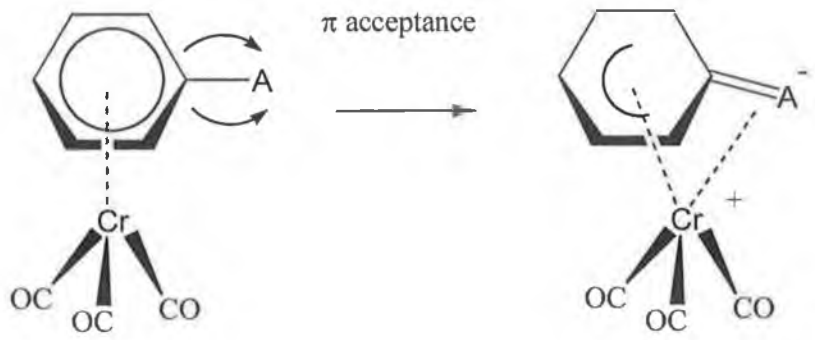

Figure 2.3.4 The two different resonance forms of $(\eta^6\text{-}C_6H_5A)Cr(CO)_3$ (A = electron withdrawing group) showing the structural distortions to the arene ring.

Again this is in accordance with what was predicted by the calculated structure of the hypothetical species $[(\eta^5\text{-}C_6H_5{=}CR_2)Cr(CO)_3]^+$. In calculations by Albright, Hoffmann and Hofmann for these species, the exocyclic bond was found to bend towards the $Cr(CO)_3$ unit.[8]

2.4 Steady state photolysis of $(\eta^6$-arene$)Cr(CO)_3$ complexes in CO saturated cyclohexane and 1,1,2 trifluorotrichloroethane

The photochemistry of the substituted $(\eta^6$-arene$)Cr(CO)_3$ complexes were investigated in either CO or argon saturated cyclohexane or 1,1,2 trifluorotrichloroethane solution. All samples were degassed by three "freeze pump thaw" cycles (see experimental section) before addition of CO or argon, at a pressure of one atmosphere. The solutions were protected from light during this period.

The $(\eta^6$-arene$)Cr(CO)_3$ complexes were photolysed in cyclohexane solution saturated with CO at various wavelengths beginning with long wavelength irradiation using a xenon arc lamp with a succession of cut off filters. Upon photolysis at λ_{exc} >400 nm, no changes in the UV/vis spectrum of the solutions were observed. Upon switching the filter to λ_{exc} >340nm, spectral changes consistent with a reduction in intensity of the parent bands with formation of 'uncoordinated arene' and $Cr(CO)_6$ were observed. These assignments were confirmed by comparison of the spectral changes observed by

Trembovler *et al.*, Yavorskii *et al.* and by comparison with authentic samples of the relevant compounds.[9, 10, 11, 12]

An IR spectrum obtained following the photolysis experiment confirmed the formation of $Cr(CO)_6$ (band at 1985 cm^{-1}). Similar experiments were carried out using $(\eta^6\text{-}C_6H_5OCH_3)Cr(CO)_3$ and $(\eta^6\text{-}C_6H_5CO_2CH_3)Cr(CO)_3$ and it was found that all complexes showed similar spectral changes upon photolysis at $\lambda_{exc} > 340nm$. However formation of free arene and $Cr(CO)_6$ appeared to be faster for $(\eta^6\text{-}C_6H_5NH_2)Cr(CO)_3$ than for $(\eta^6\text{-}C_6H_5COH)Cr(CO)_3$, $(\eta^6\text{-}C_6H_5OCH_3)Cr(CO)_3$ or $(\eta^6\text{-}C_6H_5CO_2CH_3)Cr(CO)_3$. $(\eta^6\text{-}C_6H_6)Cr(CO)_3$ was also photolysed under the same conditions and even after prolonged periods, no significant spectral changes were observed. The spectral changes are summarized in Table 2.4.1.

	UV/vis.		IR.
$(\eta^6$-arene$)Cr(CO)_3$ complex	Depletion nm	Grow in nm	Grow in cm^{-1}
$(\eta^6\text{-}C_6H_5NH_2)Cr(CO)_3$	332	250, 280	1985
$(\eta^6\text{-}C_6H_5OCH_3)Cr(CO)_3$	324	260, 280	1985
$(\eta^6\text{-}C_6H_5CO_2CH_3)Cr(CO)_3$	325, 395	260, 280	1985
$(\eta^6\text{-}C_6H_6)Cr(CO)_3$	-	-	-
$(\eta^6\text{-}C_6H_5COH)Cr(CO)_3$	320, 420	260, 280	1985

Table 2.4.1 The spectral changes observed in the UV/vis and the IR spectra of the $(\eta^6$-arene$)Cr(CO)_3$ complexes upon photolysis at λ_{exc} >340nm in CO - saturated cyclohexane.

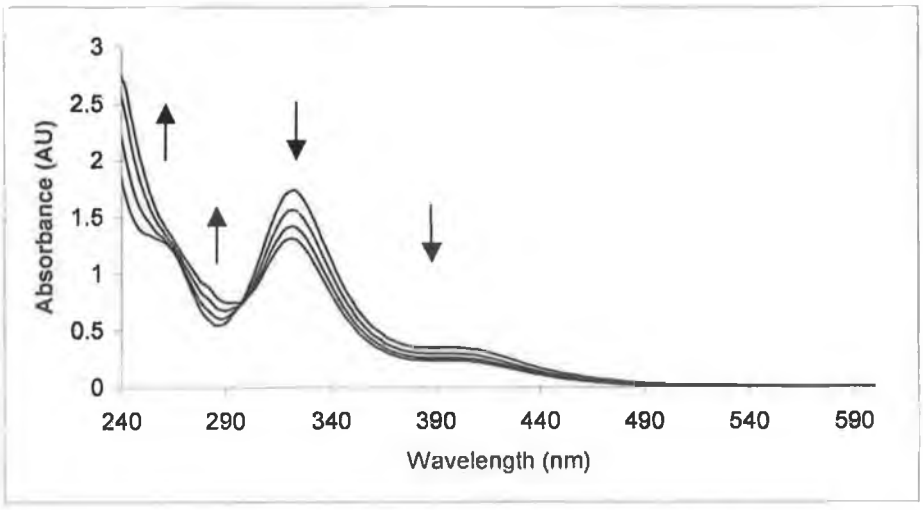

Figure 2.4.1 UV/ vis spectra recorded following photolysis of $(\eta^6\text{-}C_6H_5CO_2CH_3)Cr(CO)_3$ in CO saturated cyclohexane over a period 36 minutes at λ_{exc} >340nm filter with a Xe arc lamp.

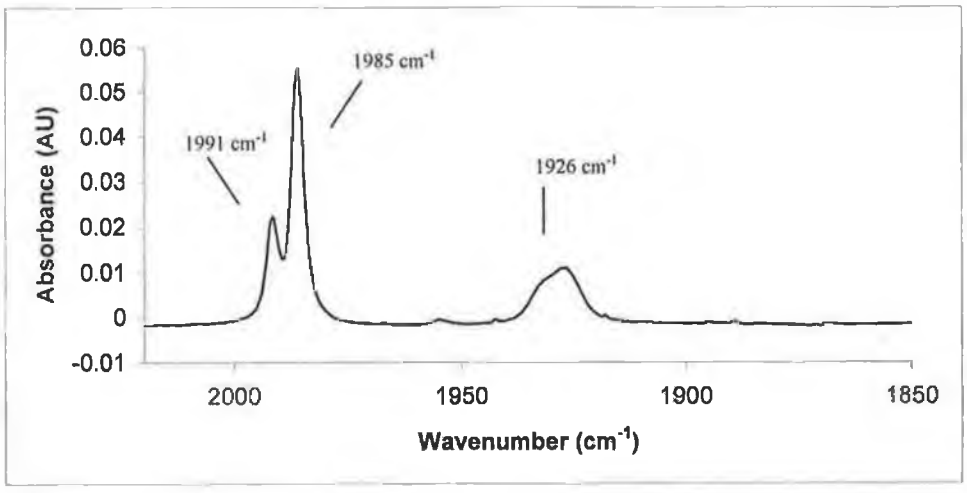

Figure 2.4.2 IR spectrum recorded following photolysis of $(\eta^6\text{-}C_6H_5CO_2CH_3)Cr(CO)_3$ in CO saturated cyclohexane over a period 36 minutes at λ_{exc} > 340 nm filter with a Xe arc lamp. $(\eta^6\text{-}C_6H_5CO_2CH_3)Cr(CO)_3$ ν_{co} : 1991 and 1926 cm^{-1}. $Cr(CO)_6$ ν_{co} : 1985 cm^{-1}.

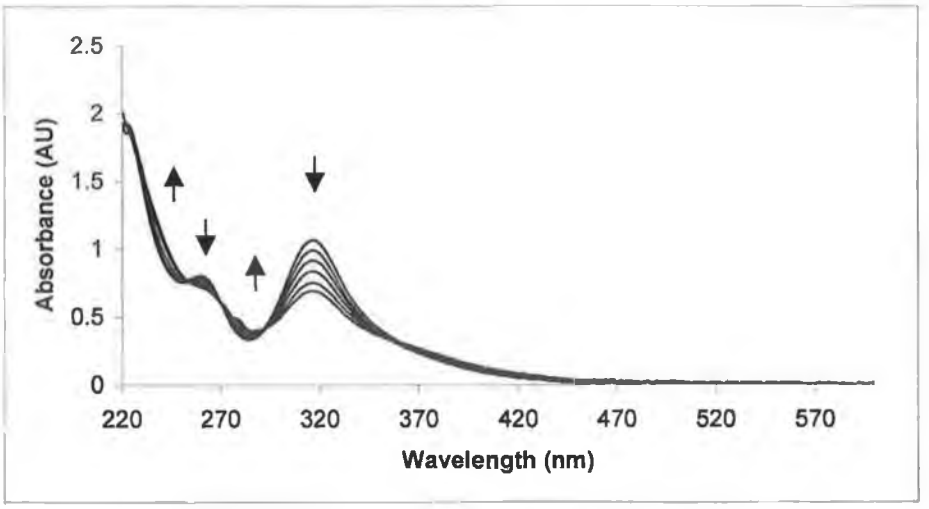

Figure 2.4.3 UV/ vis spectra recorded following photolysis of $(\eta^6\text{-}C_6H_5NH_2)Cr(CO)_3$ in CO saturated cyclohexane over a period 6 minutes at λ_{exc} >340nm filter with a Xe arc lamp.

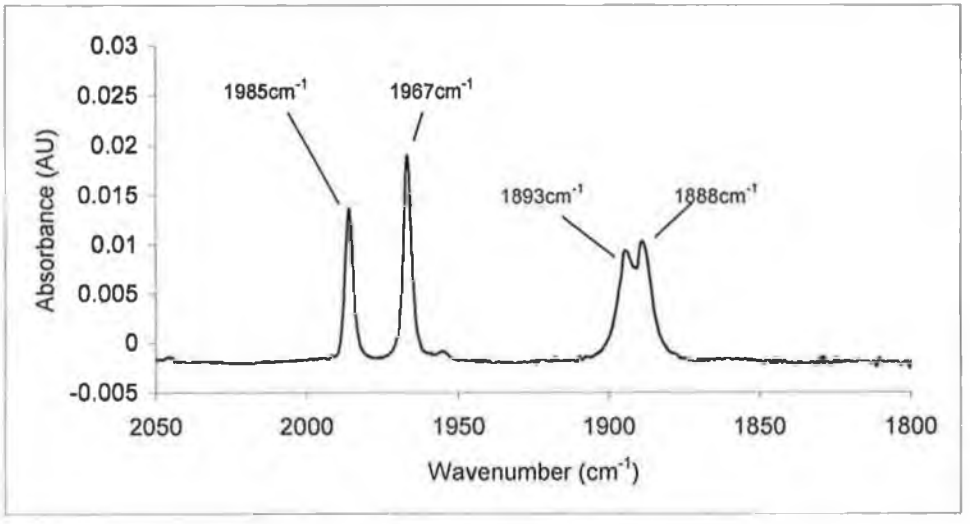

Figure 2.4.4 IR spectrum recorded following photolysis of $(\eta^6\text{-}C_6H_5NH_2)Cr(CO)_3$ in CO saturated cyclohexane over a period 6 minutes at λ_{exc} >340nm filter with a Xe arc lamp. $(\eta^6\text{-}C_6H_5NH_2)Cr(CO)_3$ ν_{co} : 1967, 1893 and 1888 cm^{-1}. $Cr(CO)_6$ ν_{co} : 1985 cm^{-1}.

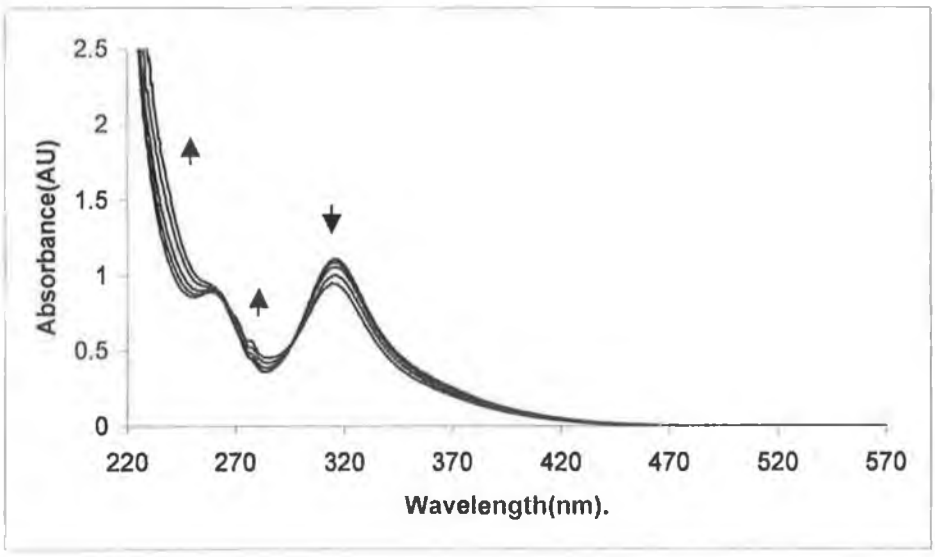

Figure 2.4.5 UV/ vis spectra recorded following photolysis of $(\eta^6\text{-}C_6H_5OCH_3)Cr(CO)_3$ filter in CO saturated cyclohexane over a period 22 minutes at λ_{exc} >340nm filter with a Xe arc lamp.

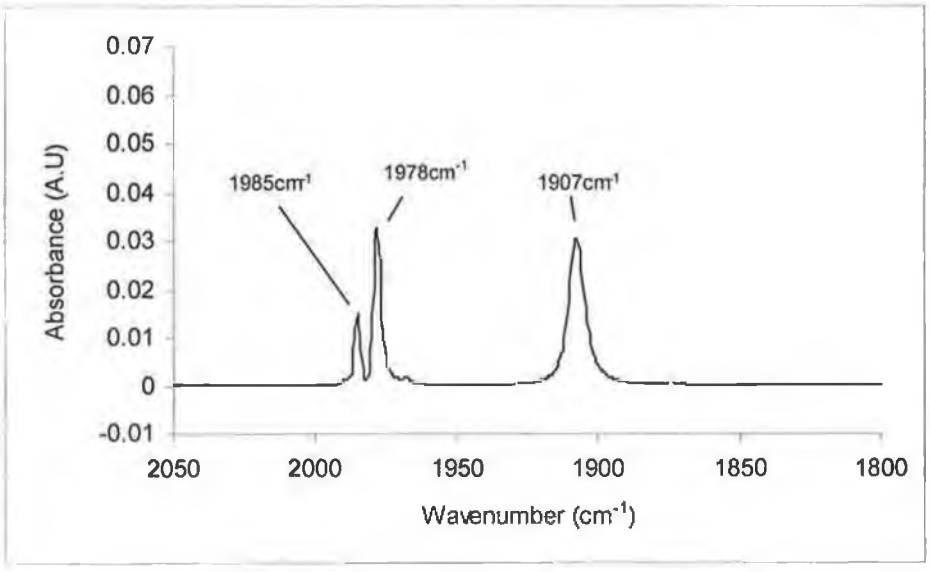

Figure 2.4.6 IR spectrum recorded following photolysis of $(\eta^6\text{-}C_6H_5OCH_3)Cr(CO)_3$ in CO saturated cyclohexane over a period 22 minutes at λ_{exc} >340nm filter with a Xe arc lamp. $(\eta^6\text{-}C_6H_5COCH_3)Cr(CO)_3$ ν_{co} : 1980 and 1907 cm^{-1}. $Cr(CO)_6$ ν_{co} : 1985 cm^{-1}.

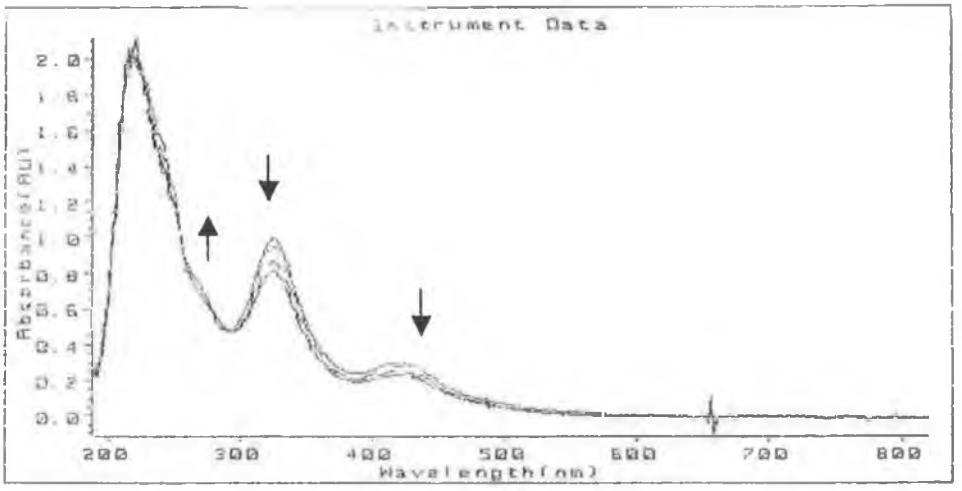

Figure 2.4.7 UV/vis spectra recorded following photolysis of $(\eta^6\text{-}C_6H_5COH)Cr(CO)_3$ in CO saturated cyclohexane over a period 7 minutes at λ_{exc} >340nm filter using a Xe arc lamp.

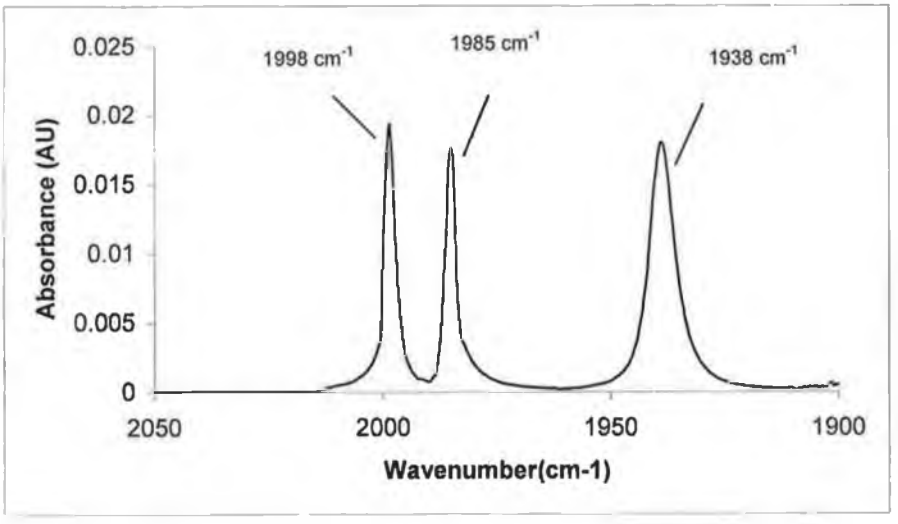

Figure 2.4.8 IR spectrum recorded following photolysis of $(\eta^6\text{-}C_6H_5COH)Cr(CO)_3$ in CO saturated cyclohexane over a period 7 minutes at λ_{exc} >340nm filter using a Xe arc lamp. $(\eta^6\text{-}C_6H_5COH)Cr(CO)_3$ ν_{co} : 1998, 1938 cm^{-1}. $Cr(CO)_6$ ν_{co} : 1985 cm^{-1}.

Pryce had previously observed that photolysis of $(\eta^6\text{-}C_6H_6)Cr(CO)_3$ at λ_{exc} = 355 nm produced free benzene and $Cr(CO)_6$ in 1,1,2 trifluorotrichloroethane [23] Photolysis at λ_{exc} = 355 nm of $(\eta^6\text{-}C_6H_5NH_2)Cr(CO)_3$, $(\eta^6\text{-}C_6H_5OCH_3)Cr(CO)_3$, $(\eta^6\text{-}C_6H_5CO_2CH_3)Cr(CO)_3$ and $(\eta^6\text{-}C_6H_5COH)Cr(CO)_3$ in CO saturated 1,1,2 trifluorotrichloroethane again produced $Cr(CO)_6$ and free arene. An IR spectrum recorded on completion of photolysis at λ_{exc} = 355 nm, showed formation of $Cr(CO)_6$. Quantum efficiency of the arene loss reaction of $(\eta^6\text{-}C_6H_6)Cr(CO)_3$, $(\eta^6\text{-}C_6H_5NH_2)Cr(CO)_3$, $(\eta^6\text{-}C_6H_5OCH_3)Cr(CO)_3$, $(\eta^6\text{-}C_6H_5CO_2CH_3)Cr(CO)_3$ and $(\eta^6\text{-}C_6H_5COH)Cr(CO)_3$ were measured in both CO saturated cyclohexane and 1,1,2 trifluorotrichloroethane at λ_{exc} = 355 nm. The results are shown in the Table 2.4.2.

$(\eta^6$-arene$)Cr(CO)_3$	Φ in Cyclohexane	Φ in 1,1,2 Triflouro trichloroethane.
$(\eta^6\text{-}C_6H_5NH_2)Cr(CO)_3$	0.08	0.24
$(\eta^6\text{-}C_6H_5OCH_3)Cr(CO)_3$	0.0001575	0.27
$(\eta^6\text{-}C_6H_6)Cr(CO)_3$	0	0.15
$(\eta^6\text{-}C_6H_5COH)Cr(CO)_3$	0.04883	0.17
$(\eta^6\text{-}C_6H_5CO_2CH_3)Cr(CO)_3$	0.0004479	0.32

Table 2.4.2 Quantum yields recorded at λ_{exc} = 355 nm in CO saturated cyclohexane and 1,1,2 trifluorotrichloroethane for the $(\eta^6$-arene$)Cr(CO)_3$ complexes. The data used to calculate the quantum yields in this table is given in Appendix A.

The data in Table 2.4.2 indicates that only photolysis of $(\eta^6$-arene$)Cr(CO)_3$ complexes bearing either strong electron withdrawing or electron donating groups results in arene displacement in CO saturated cyclohexane. Unlike cyclohexane, the quantum yields for arene loss measured in 1,1,2 trifluorotrichloroethane, indicates that arene displacement is efficient for all systems investigated. Bamford found that $(\eta^6$-benzene$)Cr(CO)_3$ had a quantum yield for arene displacement of 0.41 in CCl_4 when photolysed at 365 nm which is higher then that recorded for arene displacement in 1,1,2 trifluortrichlororethane.[17] UV/vis and IR spectroscopy indicated the formation

of $Cr(CO)_6$ and free arene (contained in appendix A). The spectral changes observed were similar to those observed by Yavorskii for the displacement of the arene ring from (η^6-arene)$Cr(CO)_3$ to give free arene and $Cr(CO)_6$.[11,12,13]

2.5 UV/vis flash photolysis of the substituted (η^6-C_6H_5X)$Cr(CO)_3$ systems (X = NH_2, OCH_3, $C(CO)OCH_3$, C(O)H) at λ_{exc} = 355 nm in CO / argon saturated cyclohexane

A series of UV/vis flash photolysis experiments were undertaken in a variety of solvents and in the presence of CO and Ar. The effect of changing the solvent media was examined for the four complexes under investigation.

2.5.1 UV/vis flash photolysis of the substituted (η^6-C_6H_5X)$Cr(CO)_3$ systems (X = NH_2, OCH_3, $C(CO)OCH_3$, C(O)H) at λ_{exc} = 355 nm in CO saturated cyclohexane, the primary photoproduct.

The photochemistry of (η^6-$C_6H_5NH_2$)$Cr(CO)_3$, (η^6-$C_6H_5OCH_3$)$Cr(CO)_3$, (η^6-$C_6H_5CO_2CH_3$)$Cr(CO)_3$ and (η^6-C_6H_5COH)$Cr(CO)_3$ was investigated by UV/vis flash photolysis with λ_{exc} = 355nm in CO - saturated cyclohexane. Figure 2.5.1.1 contains a difference absorption spectrum for the (η^6-$C_6H_5NH_2$)$Cr(CO)_3$ obtained 5 μs and 70 μs after the laser pulse. The negative absorbance at 340 nm represents the depletion of the parent compound. A photoproduct band was observed with a λ_{max} at 280 nm. Both the (η^6-$C_6H_5OCH_3$)$Cr(CO)_3$ and (η^6-$C_6H_5CO_2CH_3$)$Cr(CO)_3$ appear to be fully reversible when their photochemistry is investigated in CO saturated cyclohexane. However in the case of (η^6-$C_6H_5NH_2$)$Cr(CO)_3$ there was a residual absorption at 280 nm, furthermore the parent absorption at 340 nm did not completely recover to pre-irradiation value. The difference transient absorption spectrum of (η^6-C_6H_5COH)$Cr(CO)_3$ could not be obtained because the sample was extremely photosensitive and rapidly decomposed during the experiment.

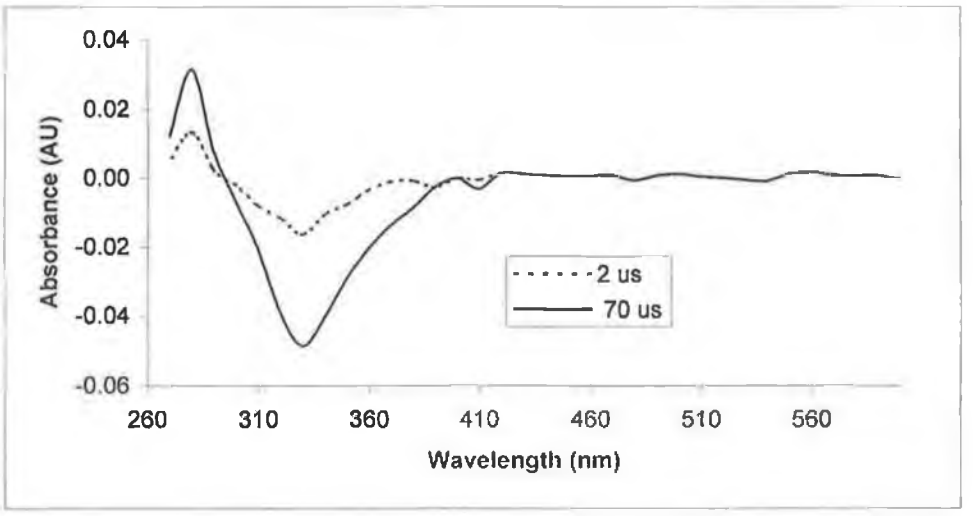

Figure 2.5.1.1 UV/vis difference spectrum of $(\eta^6\text{-}C_6H_5NH_2)Cr(CO)_3$, obtained at room temperature in CO - saturated cyclohexane, 5 μs and 70 μs after excitation (λ_{exc} = 355 nm).

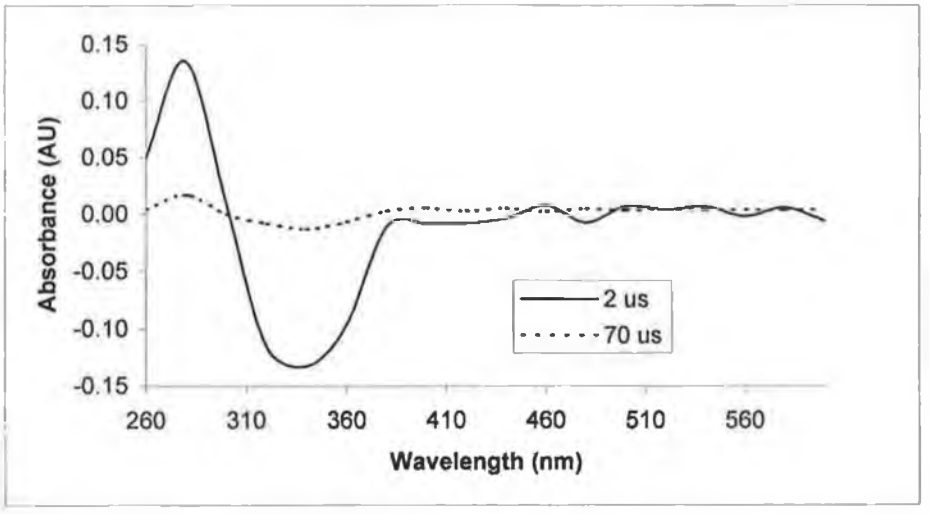

Figure 2.5.1.2 UV/vis difference spectrum of $(\eta^6\text{-}C_6H_5COCH_3)Cr(CO)_3$, obtained at room temperature in CO - saturated cyclohexane, 5 μs and 70 μs after excitation (λ_{exc} = 355 nm).

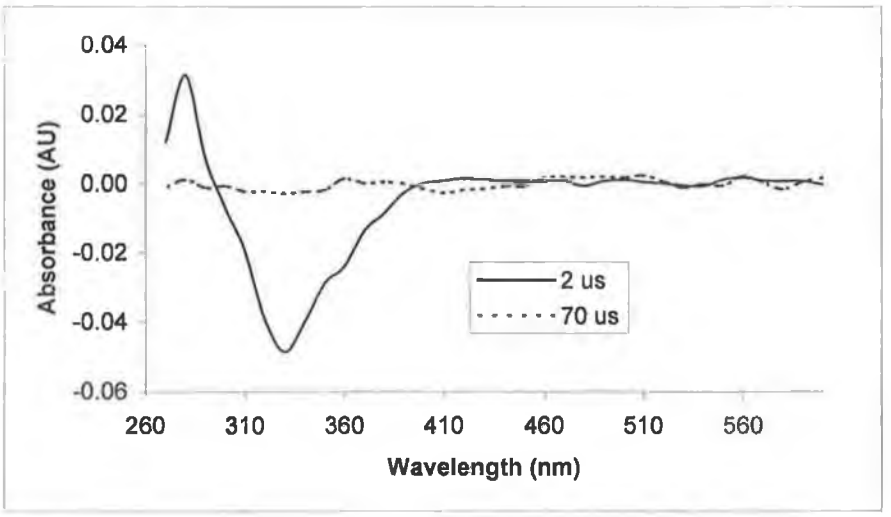

Figure 2.5.1.3 UV/vis difference spectrum of $(\eta^6\text{-}C_6H_5CO_2CH_3)Cr(CO)_3$, obtained at room temperature in CO - saturated cyclohexane, 5 μs and 70 μs after excitation (λ_{exc} = 355 nm).

The transient absorption spectra indicated the signals recorded at 280nm and 340nm are not fully reversible for the $(\eta^6$-arene$)Cr(CO)_3$ complexes with strong electron donating/electron withdrawing ($-NH_2$/-CHO) substituents on the arene. For $(\eta^6$-arene$)Cr(CO)_3$ complexes with a weakly electron donating/electron withdrawing ($-OCH_3$/$-CO_2CH_3$) substituents, the system appears to be fully reversible.

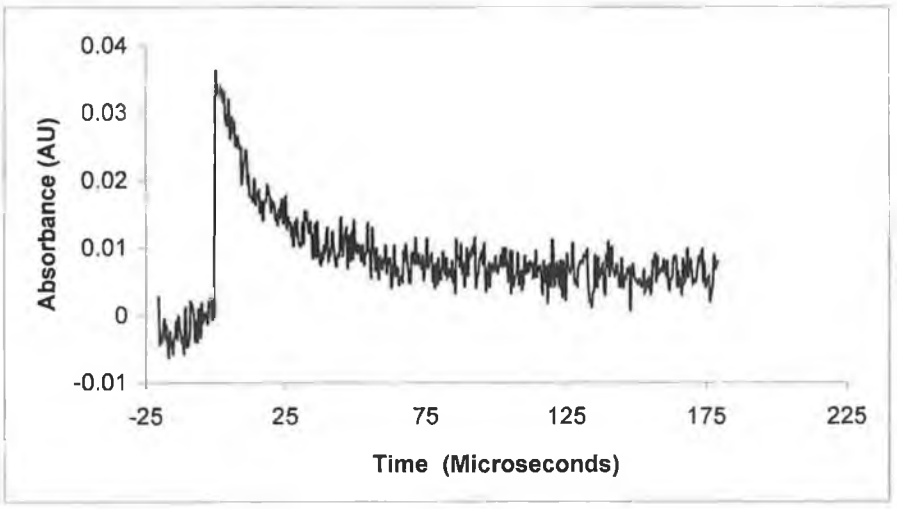

Figure 2.5.1.5 Typical transient signal observed following laser excitation at λ_{exc} = 355 nm of $(\eta^6\text{-}C_6H_5NH_2)Cr(CO)_3$ monitored at 280nm in CO saturated cyclohexane.

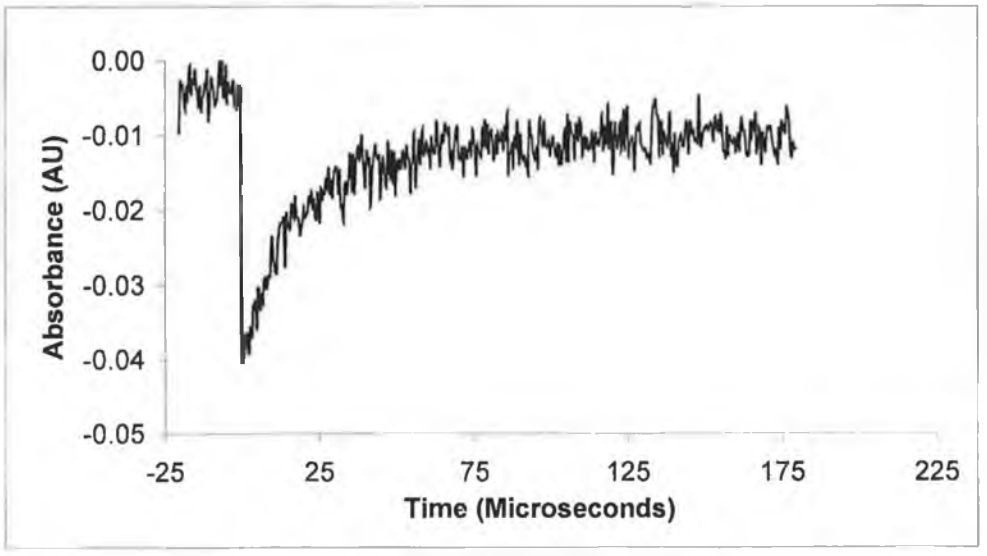

Figure 2.5.1.6 Typical transient signal observed following laser excitation at λ_{exc} = 355 nm of $(\eta^6\text{-}C_6H_5NH_2)Cr(CO)_3$ monitored at 340 nm in CO saturated cyclohexane.

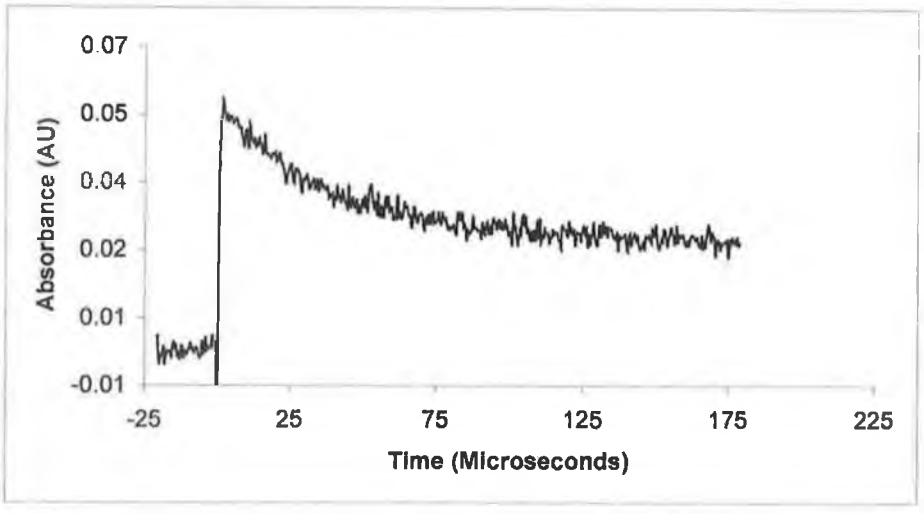

Figure 2.5.1.7 Typical transient signal observed following laser excitation at λ_{exc} = 355 nm of $(\eta^6\text{-}C_6H_5COH)Cr(CO)_3$ monitored at 280 nm in CO saturated cyclohexane.

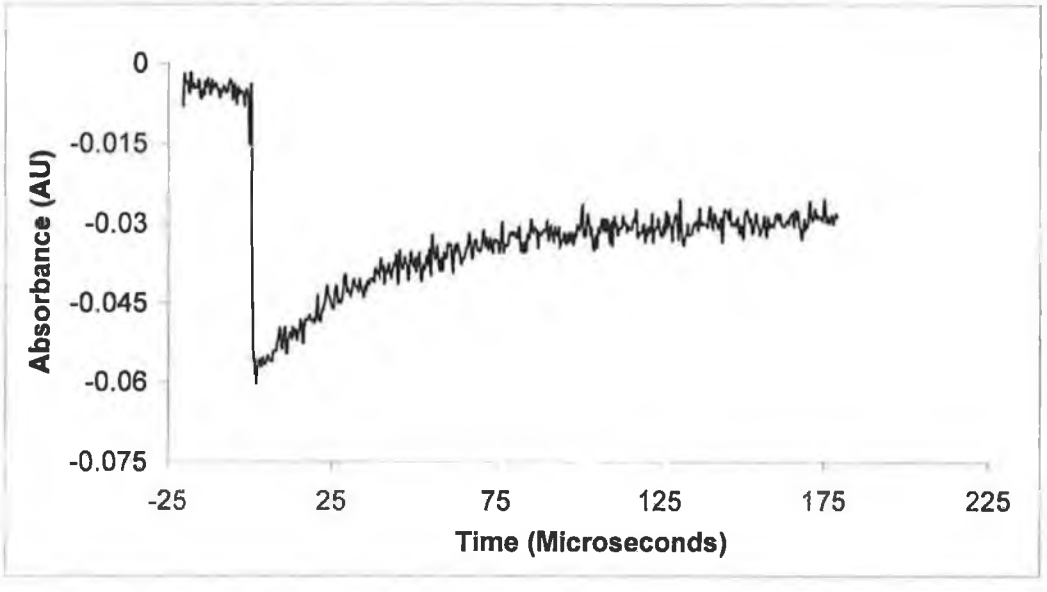

Figure 2.5.1.8 Typical transient signal observed following laser excitation at λ_{exc} = 355 nm of $(\eta^6\text{-}C_6H_5COH)Cr(CO)_3$ monitored at 340 nm in CO saturated cyclohexane.

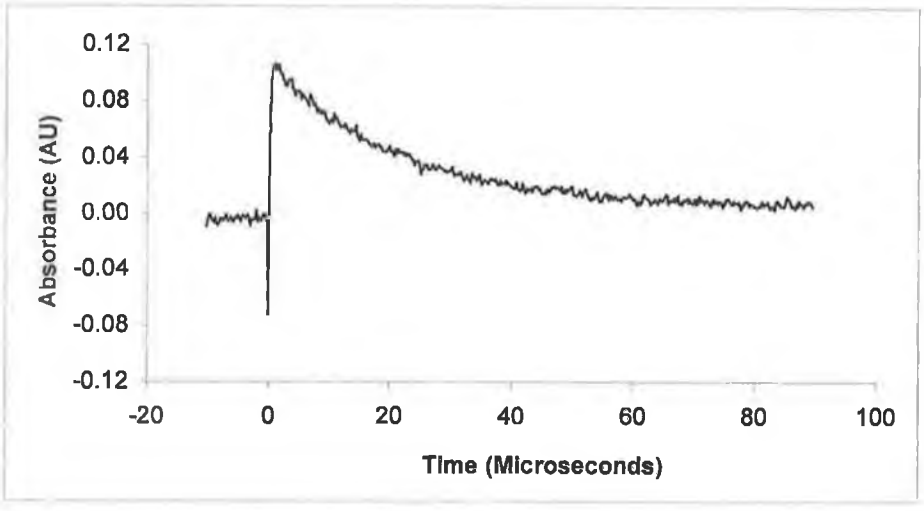

Figure 2.5.1.9 Typical transient signal observed following laser excitation at λ_{exc} = 355 nm of $(\eta^6\text{-}C_6H_5CO_2CH_3)Cr(CO)_3$ monitored at 280nm in CO saturated cyclohexane.

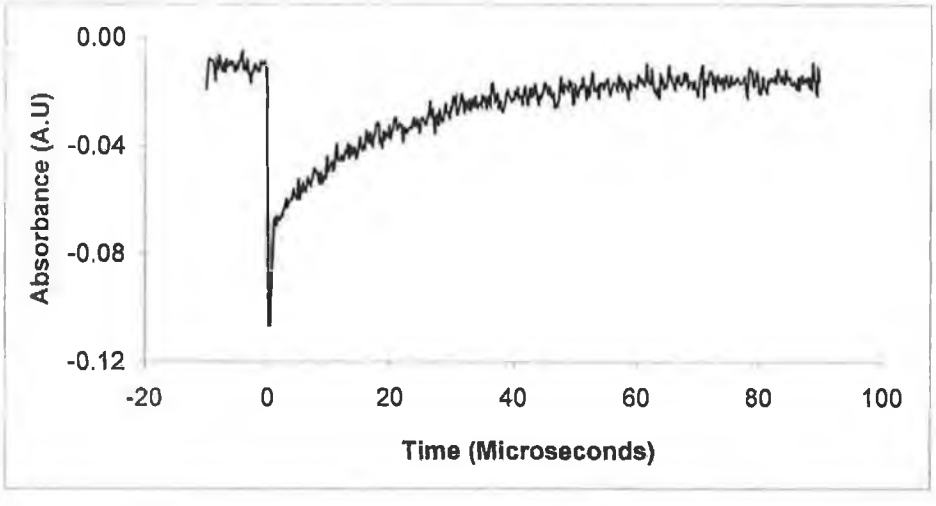

Figure 2.5.1.10. Typical transient signal observed following laser excitation at λ_{exc} = 355 nm of $(\eta^6\text{-}C_6H_5CO_2CH_3)Cr(CO)_3$ monitored at 340 nm in CO saturated cyclohexane.

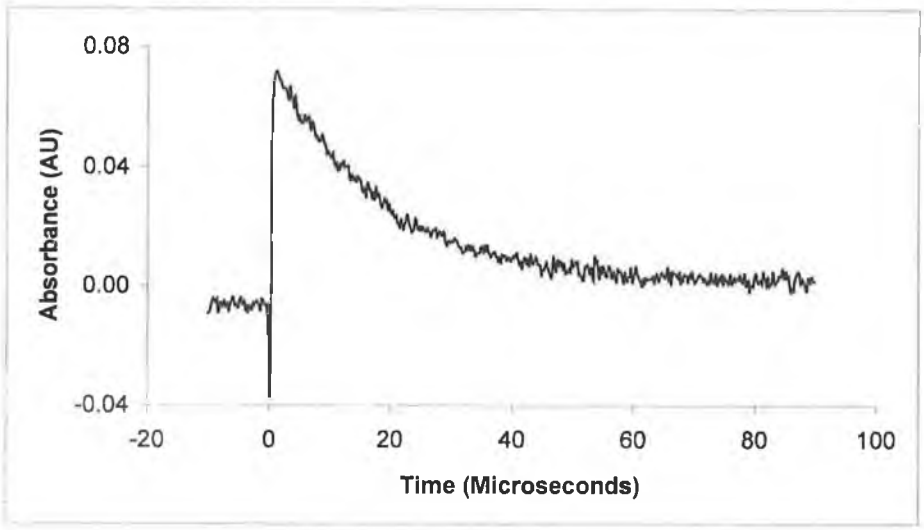

Figure 2.5.1.11 Typical transient signal observed following laser excitation at λ_{exc} = 355 nm of $(\eta^6\text{-}C_6H_5OCH_3)Cr(CO)_3$ monitored at 280 nm in CO saturated cyclohexane.

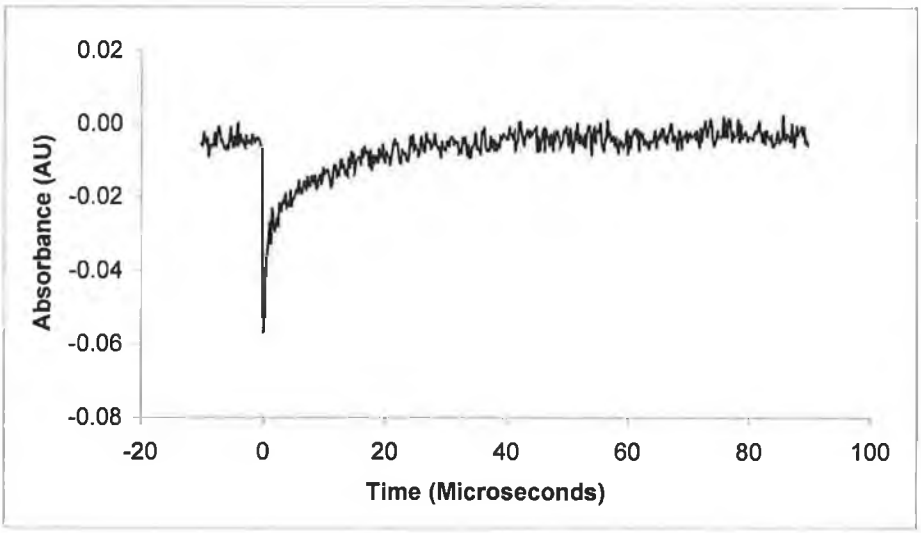

Figure 2.5.1.12 Typical transient signal observed following laser excitation at λ_{exc} = 355 nm of $(\eta^6\text{-}C_6H_5OCH_3)Cr(CO)_3$ monitored at 320 nm in CO saturated cyclohexane.

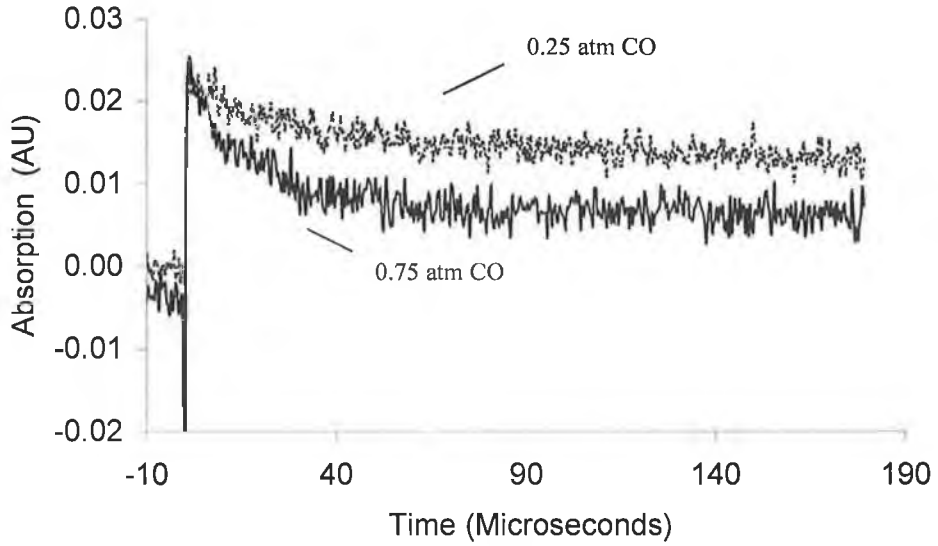

Figure 2.5.1.13 Transients signals observed following photolysis at λ_{exc} = 355 nm for (η^6-$C_6H_5NH_2$)$Cr(CO)_3$ in CO saturated (0.75 and 0.25 atm CO) cyclohexane, monitored at 280 nm.

For the (η^6-arene)$Cr(CO)_3$ complexes bearing strongly electron donating/electron withdrawing (-NH_2/-CHO)substituents there is a large increase in the residual baseline of the transient signal of the decay of the solvated dicarbonyl to the parent compound. The plot above represents the decay of the solvated dicarbonyl to the parent compound for the (η^6-$C_6H_5NH_2$)$Cr(CO)_3$ complex. It should also be noted that the residual baseline increases under lower concentrations of CO. This indicates that another species may absorb in the same area and this second decay path exists for the dicarbonyl species. Under a CO atmosphere the signal observed which relates to recovery of the parent monitored between 320 nm and 340 nm was found to recover, however as can be seen from Figures 2.5.1.5 – 2.5.1.12 for (η^6-arene)$Cr(CO)_3$ complexes with strong electron donating / withdrawing (-NH2/-CHO) substituents, the signals do not return to pre irradiation baselines. The k_2 value for the recovery was found to be identical to that obtained of the decay signal monitored at 280 nm. This confirms the assignment of this process to the recombination of the dicarbonyl species

with CO, reforming the parent, Reaction 2.5.1.3. The observed 1st order rate constants for the disappearance of the 280 nm feature was dependent on the concentration of CO. This signal was assigned to the CO loss product (η^6-arene)$Cr(CO)_2$(solvent) reacting with CO to regenerate the parent (η^6-arene)$Cr(CO)_3$ species.

$$(\eta^6\text{-arene})Cr(CO)_3 \xrightarrow[-CO]{\lambda_{exc}\ 355nm} (\eta^6\text{-arene})Cr(CO)_2. \quad \text{Reaction 2.5.1.1}$$

$$(\eta^6\text{-arene})Cr(CO)_2 + \text{cyclohexane} \longrightarrow (\eta^6\text{-arene})Cr(CO)_2(\text{cyclohexane}) \quad \text{Reaction 2.5.1.2}$$

In CO saturated solution the solvated dicarbonyl reacts with CO to reform the parent.

$$(\eta^6\text{-arene})Cr(CO)_2(\text{cyclohexane}) \xrightarrow[\text{cyclohexane}]{CO} (\eta^6\text{-arene})Cr(CO)_3. \quad \text{Reaction 2.5.1.3}$$

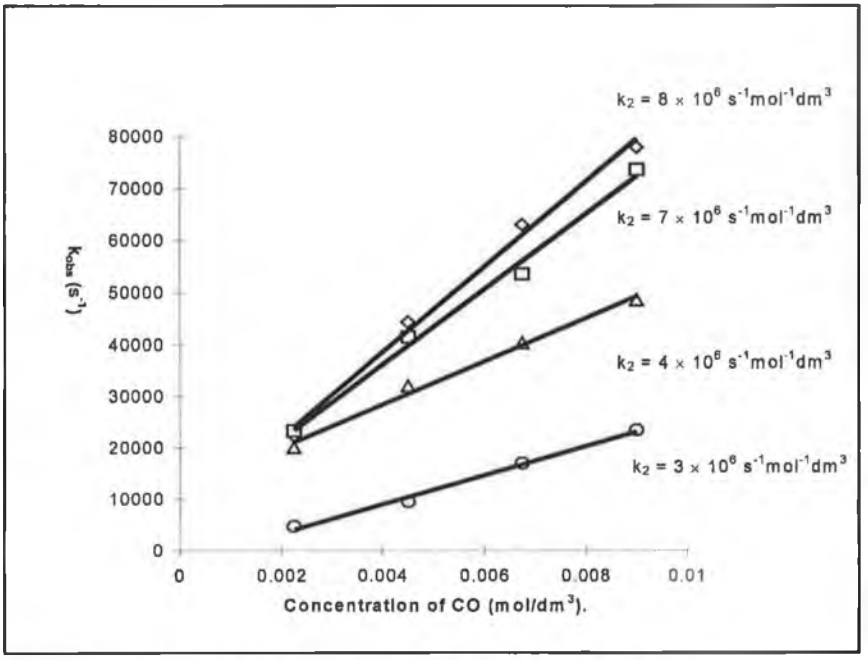

◇- (η^6-$C_6H_5NH_2$)$Cr(CO)_3$, □ - (η^6-$C_6H_5OCH_3$)$Cr(CO)_3$,

△ - (η^6-$C_6H_5CO_2CH_3$)$Cr(CO)_3$, ○ - (η^6-C_6H_5COH)$Cr(CO)_3$.

Figure 2.5.1.4 Plot of k_{obs} (s^{-1}) versus CO concentration for the reaction of (η^6-arene)$Cr(CO)_2$(solvent) with CO.

The k_2 values are shown in the Table 2.5.1.1.

Compound	k_2 $s^{-1}mol^{-1}dm^3$ 298 K.
$(\eta^6-C_6H_5NH_2)Cr(CO)_3$	8×10^{-6}
$(\eta^6-C_6H_5OCH_3)Cr(CO)_3$	7×10^{-6}
$(\eta^6-C_6H_5CO_2CH_3)Cr(CO)_3$	4×10^{-6}
$(\eta^6-C_6H_5COH)Cr(CO)_3$	3×10^{-6}

Table 2.5.1.1 The second order rate constant values recorded for the reaction of the solvated dicarbonyl species with CO to yield the parent tricarbonyl complex.

2.5.2 UV/vis flash photolysis of the substituted $(\eta^6-C_6H_5X)Cr(CO)_3$ systems (X = NH_2, OCH_3, $C(CO)OCH_3$, C(O)H) at λ_{exc} = 355 nm in argon saturated cyclohexane, the secondary photoproduct

The photochemistry of $(\eta^6-C_6H_5NH_2)Cr(CO)_3$, $(\eta^6-C_6H_5OCH_3)Cr(CO)_3$, $(\eta^6-C_6H_5CO_2CH_3)Cr(CO)_3$ and $(\eta^6-C_6H_5COH)Cr(CO)_3$ was also investigated by UV/vis flash photolysis with λ_{exc} = 355 nm in argon flushed cyclohexane. The transient absorption difference spectrum of $(\eta^6-C_6H_5COH)Cr(CO)_3$ could not be obtained as the sample decomposed too quickly upon excitation at λ_{exc} = 355 nm. Figures 2.5.2.1 – 2.5.2.3 show the difference spectra obtained 70 μs after the laser pulse.

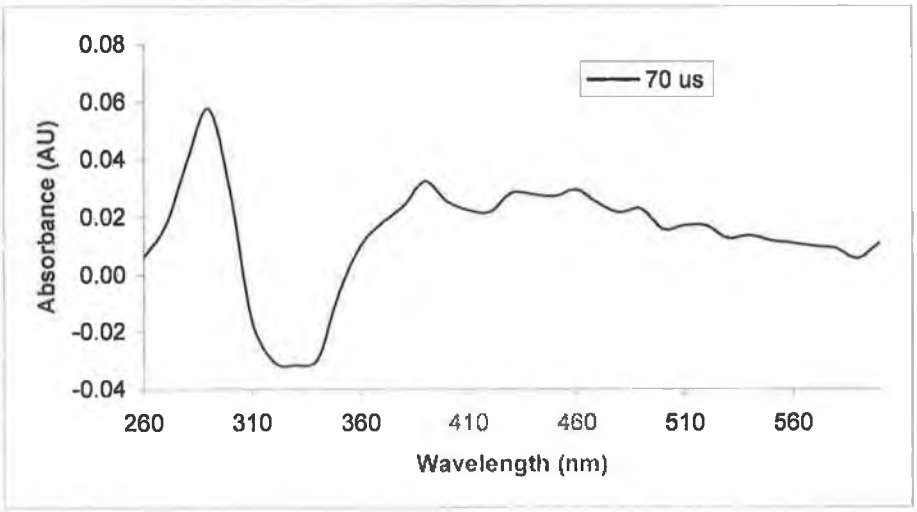

Figure 2.5.2.1 The UV/vis difference spectrum recorded 70 μs after excitation at λ_{exc} = 355 obtained for $(\eta^6\text{-}C_6H_5CO_2CH_3)Cr(CO)_3$ in argon saturated cyclohexane.

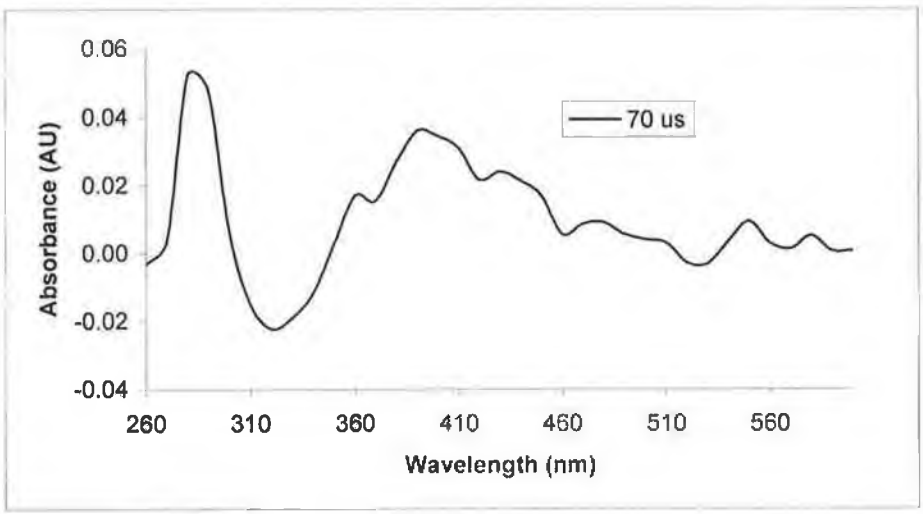

Figure 2.5.2.2 The UV/vis difference spectrum recorded 70 μs after excitation at λ_{exc} = 355 obtained for $(\eta^6\text{-}C_6H_5OCH_3)Cr(CO)_3$ in argon saturated cyclohexane.

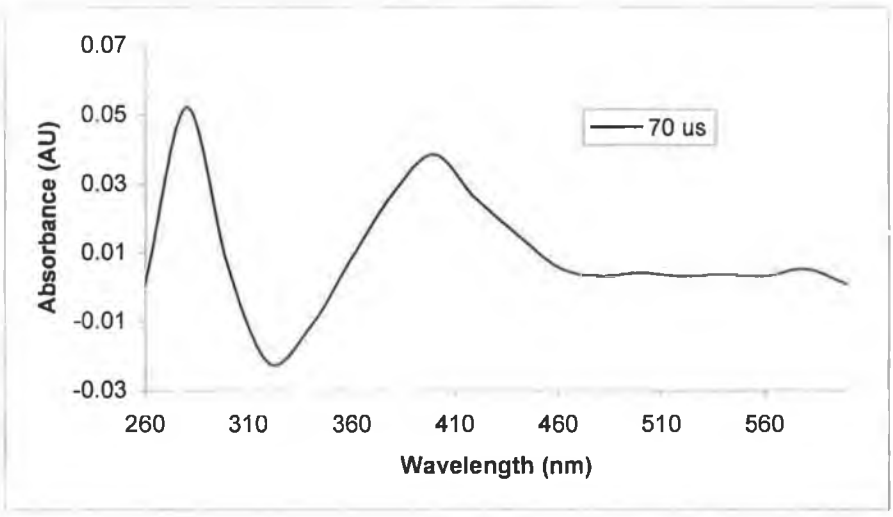

Figure 2.5.2.3 The UV/vis difference spectrum recorded 70 μs after excitation at λ_{exc} = 355 obtained for $(\eta^6\text{-}C_6H_5NH_2)Cr(CO)_3$ in argon saturated cyclohexane.

For $(\eta^6\text{-}C_6H_5NH_2)Cr(CO)_3$ a grow in with a λ_{max} at 400nm was observed upon excitation at 355nm in argon saturated cyclohexane. The observed rate of this grow in was found to be dependent on the concentration of starting material (Figure 2.6.2.4). By plotting the k_{obs} of this signal against the concentration of the parent complex, the second order rate constant was determined to be for this species was found to be 8×10^8 $s^{-1}moles^{-1}$ dm^3. This behaviour would be consistent with formation of a dinuclear species.

Comparison of the UV/vis spectra recorded throughout the laser experiment at λ_{exc} = 355 nm, with the transient absorption spectrum shows some similarities. Examination of the UV/vis spectra reveals that the band is produced at ~ 400 nm is consistent with the grow in recorded at 400 nm using laser flash photolysis. The depletion of the parent band at 340 nm can also be observed in the UV/vis spectra and is consistent with the negative absorption at 340 nm observed in the transient absorption spectra. Formation of a band with a λ_{max} at 280 nm in the ground state spectrum is consistent with a band with a λ_{max} at 280 nm in the transient absorption spectra. The band at 280 nm in the transient absorption spectra would be consistent with reaction of the solvated dicarbonyl species with parent to form a dimeric species.

$$(\eta^6\text{-}C_6H_5NH_2)Cr(CO)_3 \xrightarrow[-CO]{\lambda_{exc} = 355nm} (\eta^6\text{-}C_6H_5NH_2)Cr(CO)_2 \qquad \text{Reaction 2.5.2.1}$$

$$(\eta^6\text{-}C_6H_5NH_2)Cr(CO)_2 + \text{cyclohexane} \longrightarrow (\eta^6\text{-}C_6H_5)Cr(CO)_2(\text{cyclohexane})$$

Reaction 2.5.2.2

In argon saturated solution the solvated dicarbonyl reacts with parent to form the dinuclear species.

$$(\eta^6\text{-}C_6H_5NH_2)Cr(CO)_2(\text{cyclohexane}) \xrightarrow{(\eta^6\text{-}C_6H_5NH_2)Cr(CO)_3} (\eta^6\text{-}C_6H_5NH_2)_2Cr_2(CO)_5$$

Reaction 2.5.2.3

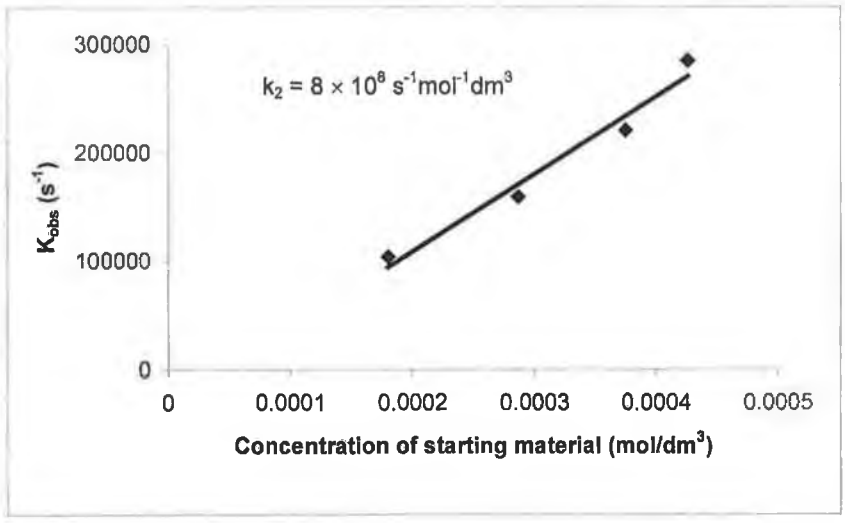

Figure 2.5.2.4 The plot of observed rate constant at 400nm with respect to the concentration of $(\eta^6\text{-}C_6H_5NH_2)Cr(CO)_3$.

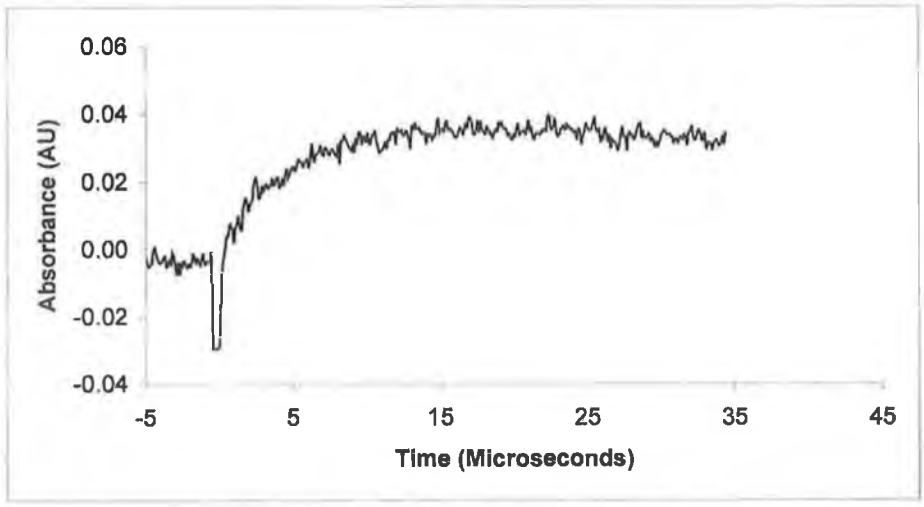

Figure 2.5.2.4 Transient signal observed following laser flash photolysis at λ_{exc} = 355 nm of $(\eta^6\text{-}C_6H_5NH_2)Cr(CO)_3$ in cyclohexane under 1 atmosphere of argon at 400nm.

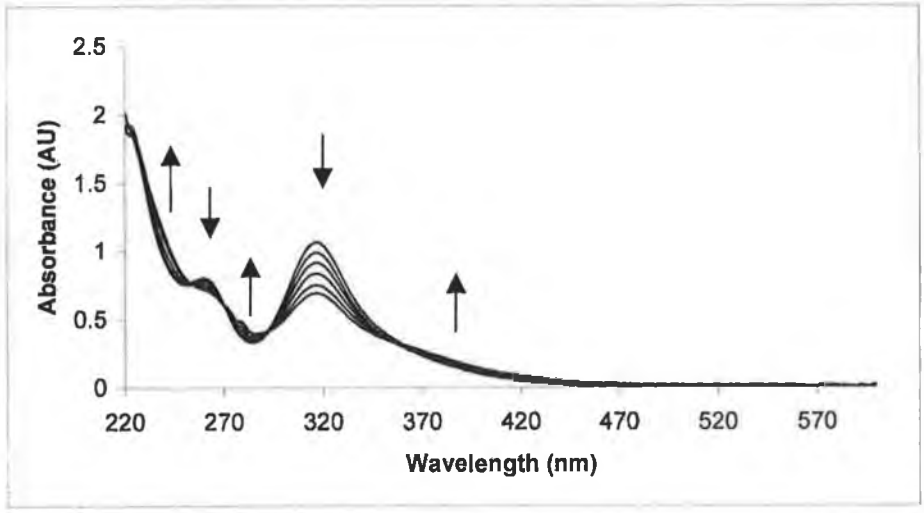

Figure 2.5.2.5 UV/vis changes upon photolysis at λ_{exc} =355 nm of $(\eta^6\text{-}C_6H_5NH_2)Cr(CO)_3$ in argon saturated cyclohexane.

For the other systems $(\eta^6\text{-}C_6H_5CO_2CH_3)Cr(CO)_3$ and $(\eta^6\text{-}C_6H_5OCH_3)Cr(CO)_3$, the difference absorption spectra obtained following flash photolysis at $\lambda_{exc} = 355$ nm were quite similar to those observed for $(\eta^6\text{-}C_6H_5NH_2)Cr(CO)_3$. Additionally the changes in the UV/vis spectrum obtained following photolysis at $\lambda_{exc} = 355$ nm were also quite similar to those observed for the $(\eta^6\text{-}C_6H_5NH_2)Cr(CO)_3$. The observed rate of the grow in measured at 400 nm was not found to be dependent on the concentration of starting material indicating a more complex reaction than formation of a dimeric species. The changes in the UV/vis spectrum of $(\eta^6\text{-}C_6H_5CO_2CH_3)Cr(CO)_3$ and the grow in recorded at 400 nm are displayed below which is similar to the signal recorded for the $(\eta^6\text{-}C_6H_5OCH_3)Cr(CO)_3$ and $(\eta^6\text{-}C_6H_5COH)Cr(CO)_3$ complex, while the UV/vis state spectrum recorded under argon is similar to that of $(\eta^6\text{-}C_6H_5NH_2)Cr(CO)_3$.

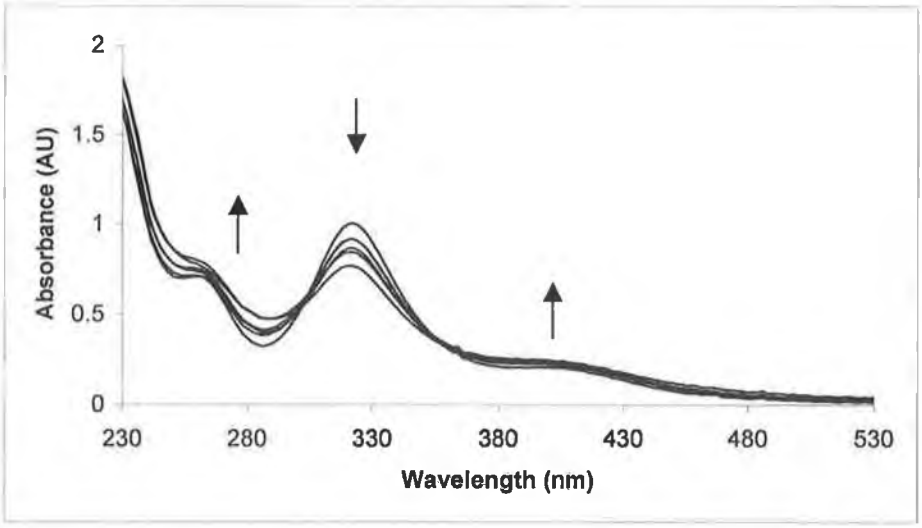

Figure 2.5.2.6 UV/vis changes upon photolysis at λ_{exc} = 355 nm of $(\eta^6\text{-}C_6H_5CO_2CH_3)Cr(CO)_3$ in argon saturated cyclohexane over a period 4 minutes.

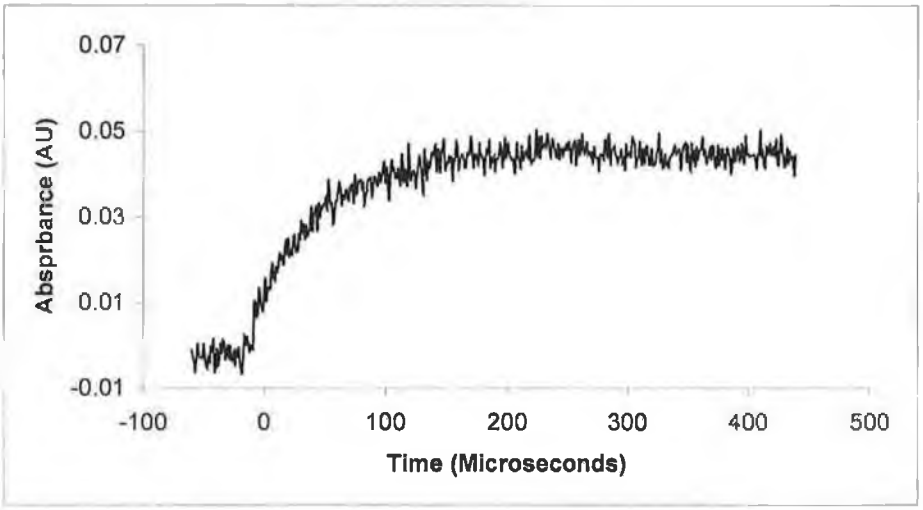

Figure 2.5.2.7 Transient signal observed following laser flash photolysis of $(\eta^6\text{-}C_6H_5CO_2CH_3)Cr(CO)_3$ in cyclohexane under 1 atmosphere of argon at 400 nm following excitation at λ_{exc} = 355 nm.

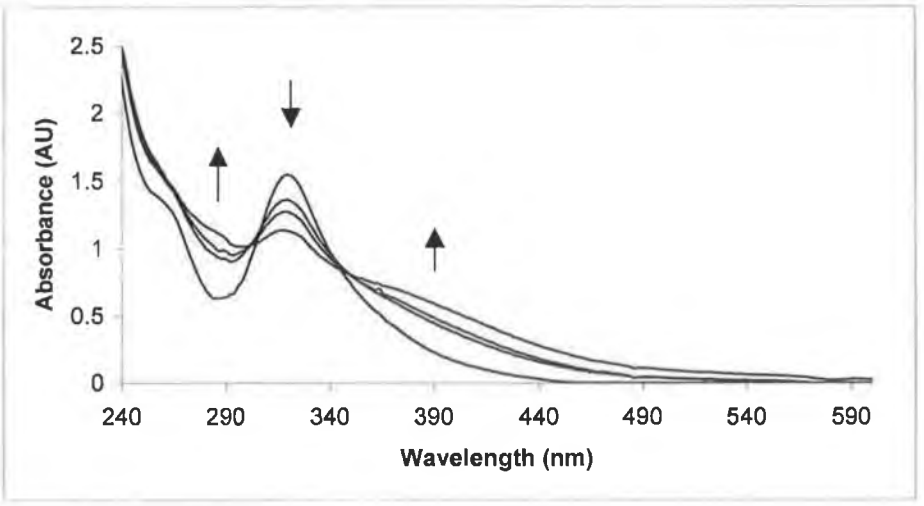

Figure 2.5.2.8 UV/vis changes upon photolysis at λ_{exc} = 355nm of $(\eta^6\text{-}C_6H_5OCH_3)Cr(CO)_3$ in argon saturated cyclohexane.

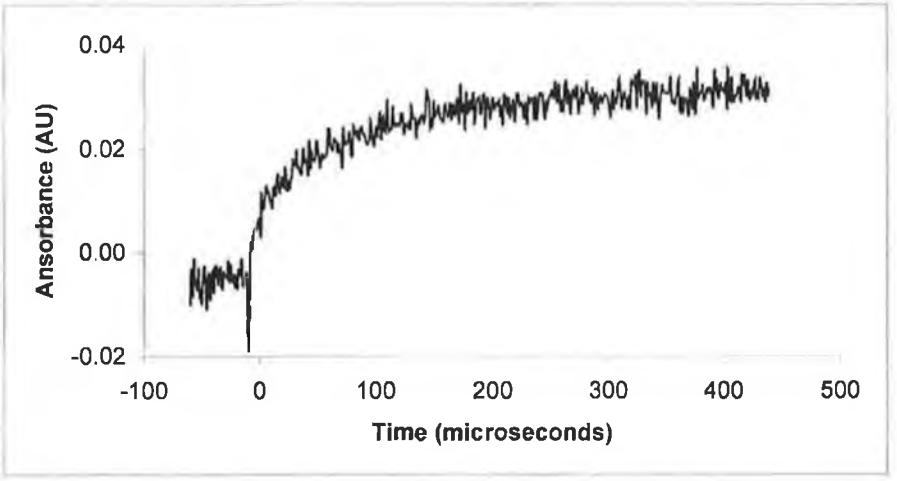

Figure 2.5.2.9 Transient signal observed following laser flash photolysis of $(\eta^6\text{-}C_6H_5OCH_3)Cr(CO)_3$ in cyclohexane under 1 atmosphere of argon at 400 nm following excitation at λ_{exc} = 355 nm.

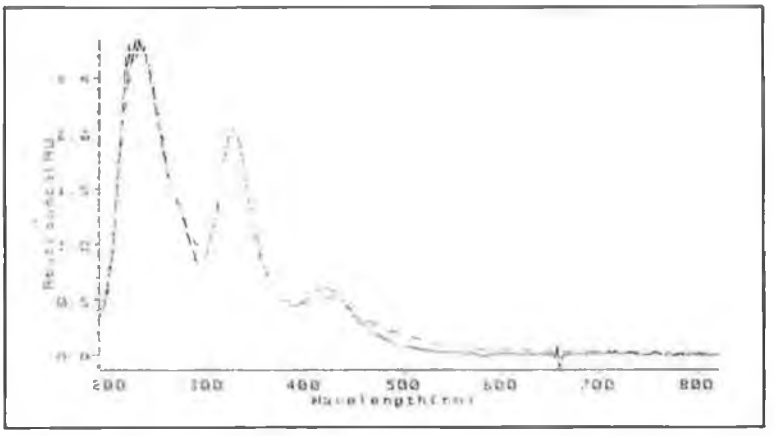

Figure 2.5.2.10 UV/vis changes upon photolysis at λ_{exc} = 355 nm of $(\eta^6\text{-}C_6H_5COH)Cr(CO)_3$ in argon saturated cyclohexane.

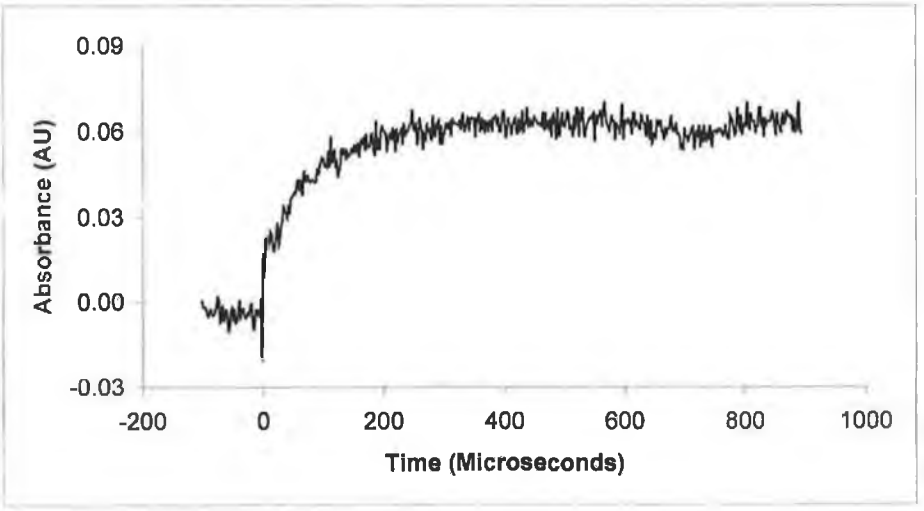

Figure 2.5.2.11 Transient signal observed following laser flash photolysis of $(\eta^6\text{-}C_6H_5COH)Cr(CO)_3$ in cyclohexane under 1 atmosphere of argon at 400 nm following excitation at λ_{exc} = 355 nm.

2.6 UV /vis flash photolysis of the substituted (η^6-C_6H_5X)$Cr(CO)_3$ systems (X = NH_2, OCH_3, $C(CO)OCH_3$, C(O)CH) at λ_{exc} = 355 nm in 1,1,2 trichlorotrifluoroethane

The photochemistry of (η^6-$C_6H_5NH_2$)$Cr(CO)_3$, (η^6-$C_6H_5OCH_3$)$Cr(CO)_3$, (η^6-$C_6H_5CO_2CH_3$)$Cr(CO)_3$ and (η^6-C_6H_5COH)$Cr(CO)_3$ was also investigated in a CO saturated 1,1,2 trichlorotrifluoro ethane solution. For all complexes, similar signals were observed. Two signals were observed following laser flash photolysis at 355 nm for all complexes. A grow in at 280 nm with no decay and at 330 nm a depletion followed by non recovery, signals typical of all signals are shown in Figure 2.6.1 and 2.6.2.

For all complexes, photolysis at λ_{exc} = 355 nm led to spectral changes in the UV/vis and IR which were consistent with depletion of the parent and formation of $Cr(CO)_6$. These changes had been previously observed for (η^6-C_6H_6)$Cr(CO)_3$ by Pryce.[23] Flash photolysis studies carried out on (η^6-C_6H_6)$Cr(CO)_3$ in 1,1,2 trifluorotrichloro ethane, revealed that the only signals observed upon excitation at λ_{exc} = 355 nm, was that of a step form which occurred at 280 nm and a corresponding depletion at 330 nm. In that study two photolysis pathways were thought to exist. The first being the cleavage of the metal – arene bond, resulting in the formation of a $Cr(CO)_3$ fragment which rapidly combines with CO to form $Cr(CO)_6$. The second being CO loss to yield the dicarbonyl intermediate. As $Cr(CO)_6$ absorbs at 280 nm, the dicarbonyl intermediate is masked by the formation of $Cr(CO)_6$. At 330 nm where the depletion of the parent is observable, no recovery of the parent is evident. The quantum yield for the photochemical substitution of CO with piperdine in $Cr(CO)_6$ was determined by Wieland and van Eldik in a number of solvents ranging from *n*-pentane (0.72), *n*-dodecane (0.58) to perfluorocyclohexane (0.47).[14] By increasing the hydrocarbon chain length of the solvent, the quantum yield for CO substitution was found to decrease. In halogenated solvents such as perfluorohexane, a more pronounced decrease in quantum yield was noted. This again illustrates how the photochemistry of metal carbonyl complexes can be altered by varying the solvent medium (alkane to halogenated solvent).

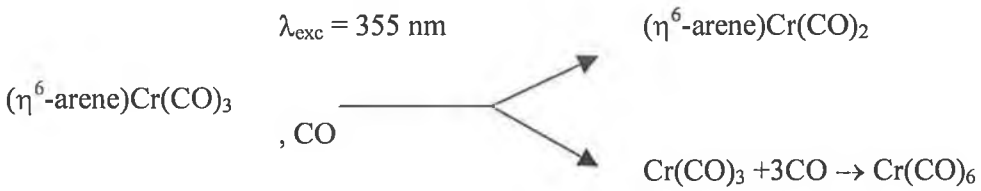

Scheme 2.6.1 The proposed photochemical pathways observed for $(\eta^6\text{-arene})Cr(CO)_3$ (arene = $C_6H_5NH_2$, $C_6H_5OCH_3$, $C_6H_5CO_2CH_3$ and C_6H_5COH) in CO saturated 1,1,2 trifluorotrichloroethane upon photolysis at λ_{exc} = 355 nm.

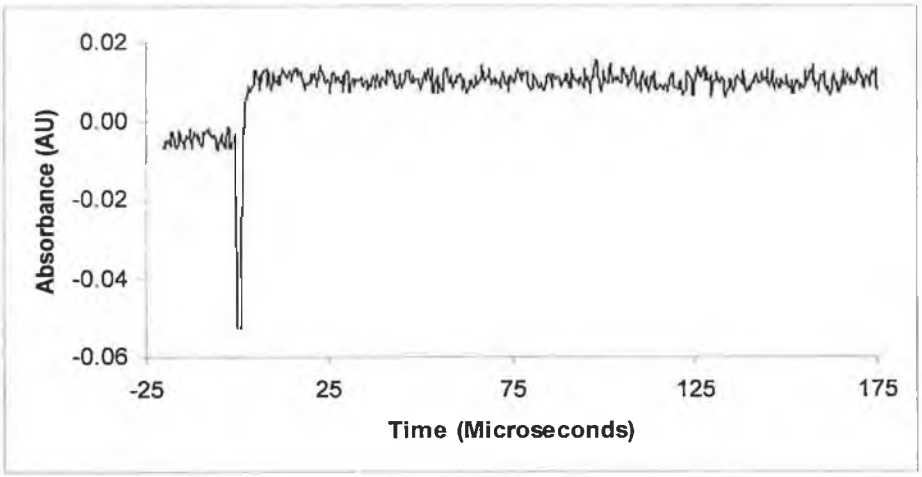

Figure 2.6.1 Transient signal observed in CO saturated 1,1,2 trichlorotrifluoro ethane at 280 nm for $(\eta^6\text{-}C_6H_5NH_2)Cr(CO)_3$ after after photolysis at λ_{exc} = 355nm.

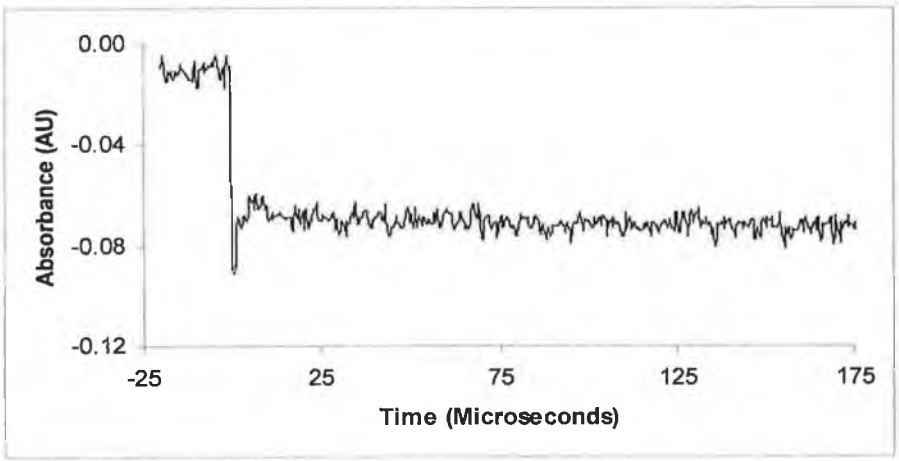

Figure 2.6.2 Transient signal observed in CO saturated 1,1,2 trichlorotrifluoro ethane at 330 nm for $(\eta^6\text{-}C_6H_5NH_2)Cr(CO)_3$ after photolysis at λ_{exc} = 355nm.

2.7 Discussion

The formation of $Cr(CO)_6$, as a result of the photolysis of the functionalised $(\eta^6$-arene$)Cr(CO)_3$ in the presence of CO, demonstrates that CO loss is not the only photochemical route accessible to these complexes. The efficiency of arene displacement is dependent on the nature of the solvent and also the substituent on the arene ring. From the actinometry experiments, photolysis at λ_{exc} = 355 nm of the $(\eta^6$-arene$)Cr(CO)_3$ complexes in CO saturated cyclohexane led to a significant quantum yield value (Φ) for displacement of the arene for those complexes carrying a strongly electron withdrawing/electron donating ($-NH_2$/-COH) substituent on the arene ring. For all the $(\eta^6$-arene$)Cr(CO)_3$ complexes studied (both bearing electron withdrawing and donating groups), the quantum yield (Φ) for arene displacement in 1,1,2 trifluorotrichloroethane was higher than that measured in alkanes. On photolysis in fluorinated solvents there is a dramatic increase in the quantum yield (Φ) for arene displacement mainly for the weakly electron donating / electron withdrawing groups as opposed to a modest increase for quantum yield Φ for strongly electron donating / withdrawing groups. This increase in quantum yield Φ in flourinated solvents is attributed to the increased relaxation times for the metal arene tricarbonyls in flourinated solvents as compared to in alkane solution.[14]

There is a difference in the photochemistry between the hydrocarbon and fluorinated solvents, and a difference in reactivity of the intermediates produced in hydrocarbon and fluorinated solvents. However, this cannot explain a difference in photochemistry i.e. why $(\eta^6$-$C_6H_6)Cr(CO)_3$ efficiently loses CO in hydrocarbon solvents and efficiently loses arene in perfluoro solvents. For an explanation of this, the vibrational relaxation of excited states must be considered which is clear from Heilwell *et al.* that vibrational relaxation is more efficient in hydrocarbon solvents than in chlorinated solvents.[13] One possible explanation for the difference in the observed photochemistry in this study is that in perfluorosolvents, different photochemistry pathways are available to vibrationally excited species which are not accessible in hydrocrbon solvents.

Kinkaid carried out a series of ground state calculations on a series of functionalised (η^6-arene)$Cr(CO)_3$ complexes in order to explain these photochemical observations.[15] Results indicated that the energy difference between the HOMO-2 and HOMO-3 orbitals are smaller in the complexes which undergo arene loss, i.e those complexes where the arene carries a strongly electron donating or withdrawing substituent. As a result these calculations suggest that there are two excited states which are accessible to these compounds, one leading to arene loss, the other leading to CO loss.

Two possible routes exist for arene displacement. The photochemical arene displacement reaction of (η^6-arene)$Cr(CO)_3$ may proceed through either cleavage of the arene–metal bond. This would result in a 12 electron $Cr(CO)_3$ fragment, which would react with CO to yield $Cr(CO)_6$. The other proposed route for the arene displacement of (η^6-arene)$Cr(CO)_3$ may take place through a ring slip intermediate.

The earliest observation of the photo-reactions of (η^6-arene)$Cr(CO)_3$ complex were made by Strohmeier and von Hobe, who proposed the Scheme 2.7.1.

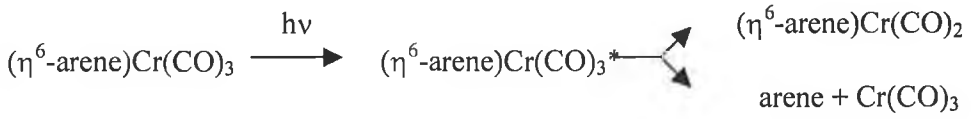

Scheme 2.7.1 The photochemical pathways of (η^6-arene)$Cr(CO)_3$.

The 12 electron $Cr(CO)_3$ fragment would then presumably further react with CO to give $Cr(CO)_6$, Reaction 2.7.1.

$$Cr(CO)_3 + 3CO \longrightarrow Cr(CO)_6 \qquad \text{Reaction 2.7.1}$$

Mahaffy and Pausson have proposed a ring slip intermediate in the thermal arene exchange reactions of (η^6-arene)$Cr(CO)_3$ complexes. A photochemical arene exchange was observed, hinting at a possible decrease of hapticity of the benzene ligand on irradiation. For the photochemical displacement of the arene ring for

$(\eta^6\text{-arene})Cr(CO)_3$ complexes in CO saturated cyclohexane leading to $Cr(CO)_6$, a ring slip intermediate could be proposed.

$$(\eta^6\text{-arene})Cr(CO)_3 \xrightarrow[CO]{h\nu} (\eta^4\text{-arene})Cr(CO)_4 \xrightarrow[CO]{} (\eta^2\text{-arene})Cr(CO)_5$$

$$\xrightarrow[CO]{} Cr(CO)_6 + \text{arene.} \qquad \text{Scheme 2.7.2.}$$

However neither steady state or time resolved methods obtained evidence for intermediates for either route leading to arene displacement.

Besides undergoing arene loss, the $(\eta^6\text{-arene})Cr(CO)_3$ complexes all underwent photodissociation of a CO ligand. For all compounds in this investigation, the difference spectra obtained by UV/vis flash photolysis at $\lambda_{exc} = 355$ nm in CO saturated cyclohexane exhibits a maximum at approximately 280 nm. A depletion of the parent between 320 to 340 nm was also observed. By analogy with the difference spectra obtained by UV/vis flash photolysis of $(\eta^6\text{-}C_6H_6)Cr(CO)_3$, the feature at 280 nm was assigned as the primary photoproduct, to the appropriate $(\eta^6\text{-arene})Cr(CO)_2(\text{cyclohexane})$ species. The rate of decay of the signal recorded in CO saturated cyclohexane at 280 nm was found to be dependent on the concentration of CO. This transient signal represents the reaction of the solvated dicarbonyl to regenerate the parent according to the reaction shown below, Reaction 2.7.5. The free metal carbonyl fragment lifetime is short, since it coordinates the solvent molecules into a vacant site within 1 ps of formation, Reaction 2.7.3 and 2.7.4.[24]

$$(\eta^6\text{-arene})Cr(CO)_3 \xrightarrow[S]{\lambda_{exc} = 355nm} (\eta^6\text{-arene})Cr(CO)_2 + CO \qquad \text{Reaction 2.7.3}$$

$$(\eta^6\text{-arene})Cr(CO)_2 + CO \longrightarrow (\eta^6\text{-arene})Cr(CO)_2S \qquad \text{Reaction 2.7.4}$$

$$(\eta^6\text{-arene})Cr(CO)_2Solv \xrightarrow{CO} (\eta^6\text{-arene})Cr(CO)_3 \qquad \text{Reaction 2.7.5}$$

The second order rate constants for the reaction of the solvated dicarbonyl with CO for all systems studied are quite similar. The second order rate constants for the reaction of the solvated dicarbonyl with CO are marginally higher for the two arene complexes containing an electron donating substituent on the ring compared to the two with electron withdrawing substituents.

For (η^6-arene)$Cr(CO)_2$(solvent) where the arene contains an electron donating complex, electron density is donated to the metal centre which causes a weakening of the interaction between the metal and the solvent. The solvent molecule is thus easier to displace leading to a higher rate of reaction of CO with the solvated dicarbonyl. While for (η^6-arene)$Cr(CO)_2$(solvent) complexes where the arene contains an electron withdawing group, electron density is withdrawn from the electron deficient metal centre which causes formation of a stronger interaction between the metal and the solvent . Thereby the solvent molecule is harder to displace leading to a lower rate of reaction of CO with the solvated dicarbonyl.

Following photolysis of λ_{exc} = 355 nm (η^6-$C_6H_5NH_2$)$Cr(CO)_3$ a secondary species was found to form in argon saturated cyclohexane. The transient signal recorded at 280 nm did not decay, indicating that the photo generated (η^6-$C_6H_5NH_2$)$Cr(CO)_2$(solvent) species did not reform the parent, nor was there any evidence for recovery of the parent at 340 nm. This would imply that the solvated dicarbonyl is reacting further to form a secondary species. A grow in was observed with a λ_{max} at 400 nm. The k_{obs} for this signal showed a linear dependence on the concentration of starting material, (η^6-$C_6H_5NH_2$)$Cr(CO)_3$. This would suggest that the photo generated (η^6-$C_6H_5NH_2$)$Cr(CO)_2$(s) fragment was reacting with starting material to form a secondary dinuclear species as shown in Scheme 2.7.3.

$(\eta^6\text{-}C_6H_5NH_2)Cr(CO)_3 \longrightarrow (\eta^6\text{-}C_6H_5NH_2)Cr(CO)_2 + CO \xrightarrow[S]{}$

$(\eta^6\text{-}C_6H_5NH_2)Cr(CO)_2S.$

$(\eta^6\text{-}C_6H_5NH_2)Cr(CO)_2(s) \longrightarrow (\eta^6\text{-}C_6H_5NH_2)_2Cr(CO)_5$ Scheme 2.7.3.
$(\eta^6\text{-}C_6H_5NH_2)Cr(CO)_3$

The formation of dinuclear species was also observed following laser flash photolysis of $(\eta^6\text{-}C_6H_6)Cr(CO)_3$, $(\eta^5\text{-}C_5H_5)Mn(CO)_3$ and $(\eta^5\text{-}C_5H_5)Co(CO)_2$.[6,21,22] Two plausible structures exist for this species a bridging species **(1)** or the amino coordinated species **(2)**.

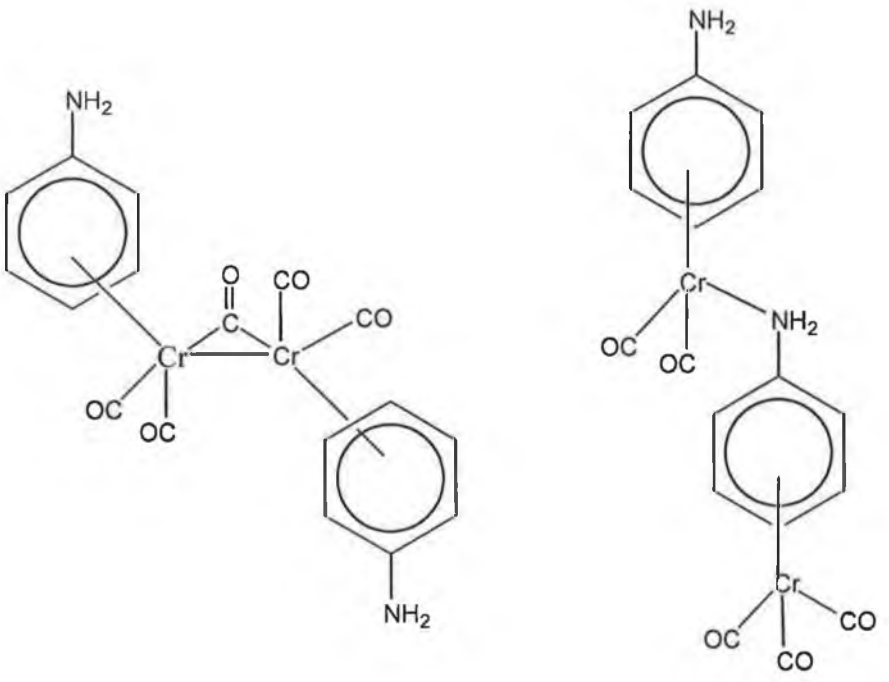

Figure 2.7.3 Possible structures of secondary species observed in argon saturated cyclohexane after excitation at λ_{exc} = 355 nm for $(\eta^6\text{-}C_6H_5NH_2)Cr(CO)_3$.

For (η^6-$C_6H_5CO_2CH_3$)$Cr(CO)_3$, (η^6-$C_6H_5CO_2CH_3$)$Cr(CO)_3$ and (η^6-$C_6H_5OCH_3$)$Cr(CO)_3$ complexes, similar spectral changes were observed for the UV/vis spectra and the UV/vis transient absorption spectra upon excitation at

λ_{exc} = 355 nm in argon saturated cyclohexane to those observed for the (η^6-$C_6H_5NH_2$)$Cr(CO)_3$ complex. However, the grow in observed at λ_{max} at 400 nm following excitation at 355 nm does not show a linear dependence of the observed rate constant and the concentration of starting material. This would suggest that the (η^6-arene)$Cr(CO)_2$(s) is not reacting with starting material to give a dinuclear species, but a more complex reaction must be considered. For the (η^6-$C_6H_5CO_2CH_3$)$Cr(CO)_3$, (η^6-C_6H_5COH)$Cr(CO)_3$ and (η^6-$C_6H_5OCH_3$)$Cr(CO)_3$ complexes, formation of chelate species involving a hapticity change of the arene ring or CO loss is possible

For arene metal tricarbonyls complexes carrying side chains with coordinating groups the photochemical loss of CO has led to the production of chelating species. For example irradiation of (η^6-3,5 $(CH_3)_2C_6H_2(CH_2)_nOP(OPh)_2$)$Cr(CO)_3$, (where n = 1-3) produced a chelating species. Low temperature photolysis of (η^6-allylbenzene)$Cr(CO)_3$ at -20°C in pentane by Pryce resulted in formation of an orange solid.[23] A mass spectrum of this orange product was recorded and the results were consistent with the formation of an ion of a three carbonyl complex. These results indicate that the product formed on photolysis does not result in CO loss. These results were consistent with a ring coordination change from η^6-arene to η^4-arene with a subsequent formation of η^2-coordination of the double bond.

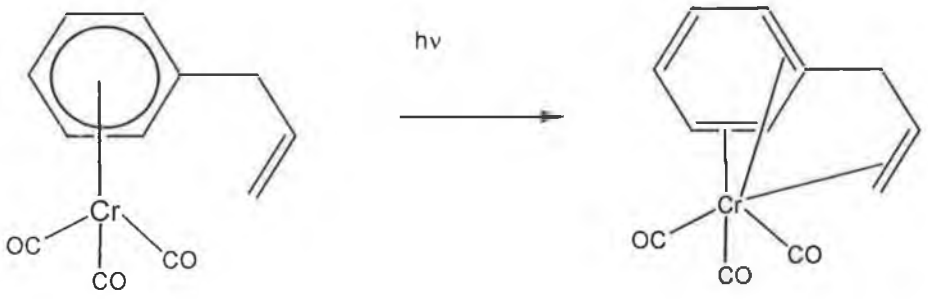

Reaction 2.7.7. Possible formation of chelate species upon low temperature at -20°C photolysis of (η^6-allylbenzene)$Cr(CO)_3$.

2.8 Conclusions

The effect of the addition of a functional group to (η^6-arene)$Cr(CO)_3$ was found to affect its photochemistry. (η^6-C_6H_6)$Cr(CO)_3$ was found to undergo only CO loss as a primary photo-process. This is not the case for the (η^6-arene)$Cr(CO)_3$ complexes studied here, where a functional group was attached to the ring. Besides undergoing CO loss as a primary photoprocess, functionalised η^6-arene ligands containing strongly electron withdrawing/donating (-NH_2/-CHO) groups also undergo photochemical displacement of the arene ring in a CO atmosphere. These results have been explained in terms of density functional theory calculations on (η^6-arene)$Cr(CO)_3$ complexes, where it was found that the energy difference between the HOMO-2 and the HOMO-3 orbitals are smaller in the complexes which undergo arene loss as opposed to those which only undergo CO loss. This suggests that the two excited states, i.e the one leading to arene loss and the one leading to CO loss are both accessible.

All functionalised (η^6-arene)$Cr(CO)_3$ complexes investigated were found to lead to formation of a secondary photoproduct under argon. Although classification of structure can not be made on just laser flash photolysis studies alone, from the results obtained it is thought that (η^6-$C_6H_5NH_2$)$Cr(CO)_3$ forms a dinuclear species. The identity of the species formed following flash photolysis in the presence of argon of (η^6-$C_6H_5CO_2CH_3$)$Cr(CO)_3$, (η^6-$C_6H_5OCH_3$)$Cr(CO)_3$ and (η^6-C_6H_5COH)$Cr(CO)_3$, remains unknown, a chelate species is possible through the carbonyl oxygen of the functional group binding to the metal centre.

2.9 References

1. Strohmeier, W.; von Hobe, D. *Z. Naturforsch,Teil B.* 1963, **18**, 981.
2. Wrighton, M.S.; Haverty, J. *Z. Naturforsch, Teil B.* 1975, **30**, 254.
3. Creaven, B.S. *Ph.D Thesis,* Dublin City University, 1987.
4. Breheny, C. *Ph.D Thesis*, Dublin City University, 1996.
5. Carrol, D.G.; McGlynn, S.P. *Inorg . Chem.* 1968, **7**, 1285.
6. Creaven, B.S.; George, M.W.; Ginzburg, A.G.; Hughes, C.; Kelly, J.M.; Long, C.; McGrath, I.M.; Pryce, M.T. *Organometallics* 1993, **12**, 3127.
7. Hunter, A.D.; Shillday, L. *Organometallics* 1992, **11**, 1550.
8. (a) Albright, T.A.; Hoffmann, R.; Hofmann, P. *Chem. Ber.* 1978, **111**, 1591. (b) Hoffmann, R.; Hofmann, P. *J. Am. Chem. Soc.* 1976, **98**, 598. (c) Top, S. Jaouen, G.; Sayer, B.G.; McGlinchey, M. J. *J. Am. Chem. Soc.* 1983, **105**, 6426.
9. Trembovler, V.N; Baranentskaya, N.K.; Fok, N.V; Zaslavskaya, G.B.; Yavorskii B.M; Setkina V.N. *J.Organomet.Chem.* 1976, **117**, 339.
10. Yavorskii, B.M.; Barentskaya, N.K.; Trembovler, V.N.; Setkina, V.N. *Doklady Akad. Nauk.* S.S.R. 1972, **207**, 1147.
11. Yavorskii, B.M.; Trembovler, V.N.; Setkina, V.N.; Barentskaya, N.K.; Zaslavskaya, G.B.; Evdokimora, M.G. *Russ. J. Phys. Chem.* 1974, **3**, 1231.
12. Yavorskii, B.M.; Trembovler, V.N.; Setkina, V.N.; Barentskaya, N.K.; Zaslavskaya, G.B.; Doklady. Akad. Nauk. S.S.R. 1974, **218**, 1153.
13. Heilwell, E.J.; Cavanagh, R.R.; Stephenson J.C. *Chem. Phys. Lett* 1987, **134**, 181.
14. Wieland, S.; van Eldik, R.; *Coord. Chem. Rev.* 1990, **97**, 155.
15. Kincaid, K. *DFT calculations on (η^6-arene)Cr(CO)$_3$ complexes* Dublin City University, 2000.
16. Hill, R.S.; Wrighton, M.S. *Organometallics* 1987, **6**, 632.
17. Bamford, C.H; Al-Lamee, K.G. Konstantinov, C.J. *J . Chem. Soc.* 1977, 1406.
18. Graham, M.A.; Poliakoff, M.; Turner, J.J. *J. Chem. Soc. A.*; 2939 , 1971.
19. Zingales, F. Chiesa, A.; Basolo, F. *J. Am. Chem. Soc.* 1966, **88**, 2707.
20. Shen, J.K.; Zhang, S.S; Basolo, F.; Johnson, S.E.; Hawthorne, F.M. *Inorg. Chim. Acta.* 1995, **235**, (1-2), 89.
21. Creaven, B.S.; Dixon, A.J.; Kelly, J.M.; Long, C.; Poliakoff, M. *Organometallics*

1987, **6**, 2600.

22. Vollhardt, K.P.C.; Bercaw, J.E.; Bergman, R.G. *J. Organomet. Chem.* **1975**, **97**, 283.
23. Pryce M.T. *Ph.D Thesis*, Dublin City University, 1993.
24. Simon, J.D.; Xie, X. *J. Phys. Chem.* 1986, **90**, 6751.

Chapter 3

The photochemistry of $(\eta^5\text{-}C_4H_4S)Cr(CO)_3$ and $(\eta^5\text{-}C_4H_4Se)Cr(CO)_3$

3.1 Introduction to the use of transition metal complexes as models for hydrodesulphurisation

Hydrodesulphurisation catalytic reactions, have become of immense industrial significance, due to its application to remove sulphur from petroleum compounds. Hydrodesulphurisation is the reaction of sulphur containing organic molecules with hydrogen in the presence of a transition metal sulphide (T.M.S) catalyst leading to formation of a mixture of hydrocarbons and hydrogen sulphide (Reaction 3.1.1).

$$R\text{-}SH + H_2 \rightarrow RH + H_2S \qquad \text{Reaction 3.1.1}$$

The study of this reaction has become essential, due to the dwindling amount of pure "petroleum feedstocks" and the more stringent environmental demands enforced by governments. This has led to the development of more active catalysts to convert low quality hydrocarbon reserves into clean burning fuels. Transition metal sulphides are the most active and least expensive catalysts used in the hydrodesulphurisation reaction. The most common catalysts in commercial use are Co or Ni promoted MoS_2 / WS_2 catalysts supported on alumina oxide. Hydrodesulphurisation is carried out under high temperature conditions of about 200°C - 400°C under a hydrogen flow.[1] The sulphide catalysts are formed by treating the metal oxide catalyst with either hydrogen and hydrogen sulphide or with hydrogen and thiophene during the initial stages of the catalytic process to create the active metal sulphide catalyst.[2]

3.1.1 Thiophene complexes as model compounds for the hydrodesulphurisation process

Thiophene is thought to bond to the metal sulphide catalyst surface through both a η^1 coordination and a η^5 coordination mode adsorption. The horizontal η^5 coordination adsorption mode is reported to be the most favourable adsorption mode to weaken the C-S bond.[3] Therefore regarding the different modes of adsorption the η^1 coordination is favoured for adsorption, while reaction takes place in the more effective horizontal η^5

coordination. Because of the interest in the mechanism of the hydrodesulphurisation reaction, numerous organometallic thiophene complexes have been synthesised as models for possible intermediates in the hydrodesulphurisation reaction. Thiophene was found to have five possible modes of coordination η^1,η^2,η^4, η^5 and the ring insertion coordination mode, which are shown in Figure 3.1.1.1.[4,5,6,7] In the η^1 and η^2 mode of coordination, thiophene is regarded as a two electron donor. In these two latter modes, thiophene is coordinated very weakly and is thus easily replaced from the metal surface by reactants. The η^5 coordination (a six electron donor) mode is the most common for the thiophene ring. In this mode the metal withdraws electron density from the π electron system and makes the thiophene susceptible to be attacked by nucleophiles. This effect decreases with the addition of an alkyl-substituent to the two or five positions on the thiophene ring.

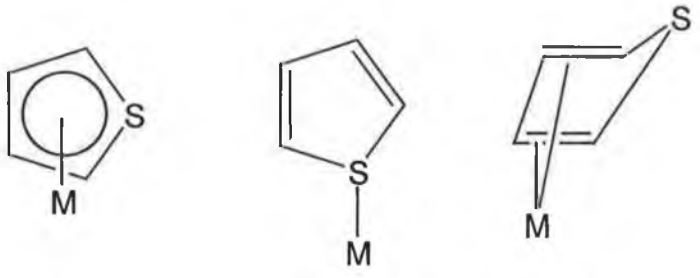

η^5–coordination η^1–s-coordination η^4–coordination

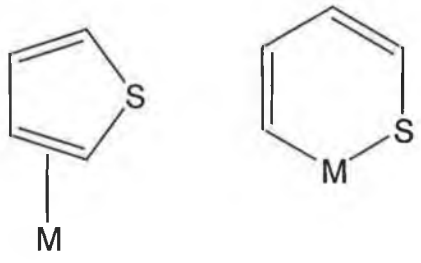

η^2–coordination ring insertion coordination

Figure 3.1.1.1 The coordination modes of thiophene

In the η^4 coordination (four electron donor to the metal) mode of thiophene, the complexes were also found to be reactive. For example (η^5-C_5H_5)Ir(η^5-2,5-$C_4H_2S(CH_3)_2$)

can be reduced to $(\eta^5\text{-}C_5H_5)Ir(\eta^4\text{-}2,5\text{-}C_4H_2S(CH_3)_2)$.[6,7] The η^4 isomer quickly isomerises to the more stable ring insertion C-S isomer in the presence of a base catalyst or ultraviolet light (Reaction 3.1.1.2).

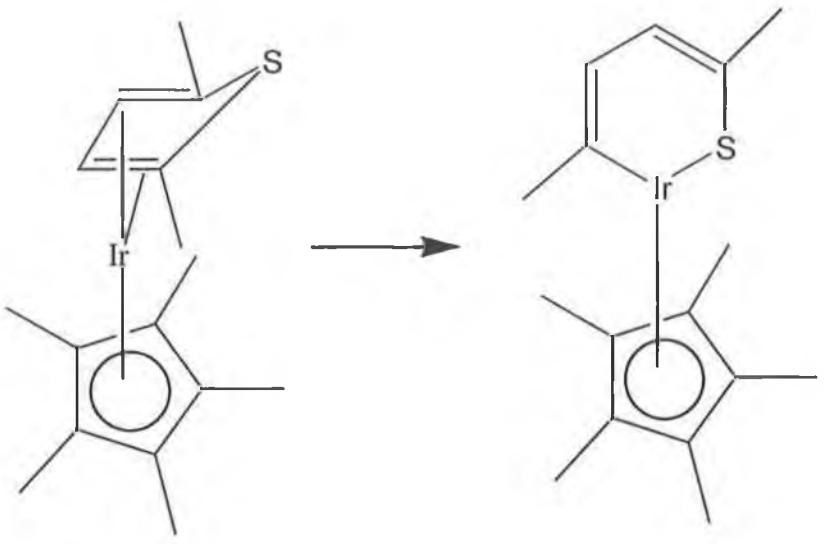

Reaction 3.1.1.2

Similarly it has been shown that it is possible to electrochemically derive the $(\eta^4\text{-}C_4H_4S)$ mode by two electron reduction from the $(\eta^5\text{-}C_5(CH_3)_5)Rh(\eta^4\text{-}C_4H_4S)$ at –78 °C, while further reaction with CO yields $(\eta^5\text{-}C_5(CH_3)_5)Rh(CO)_2$ with displacement of the thiophene ring.[8]

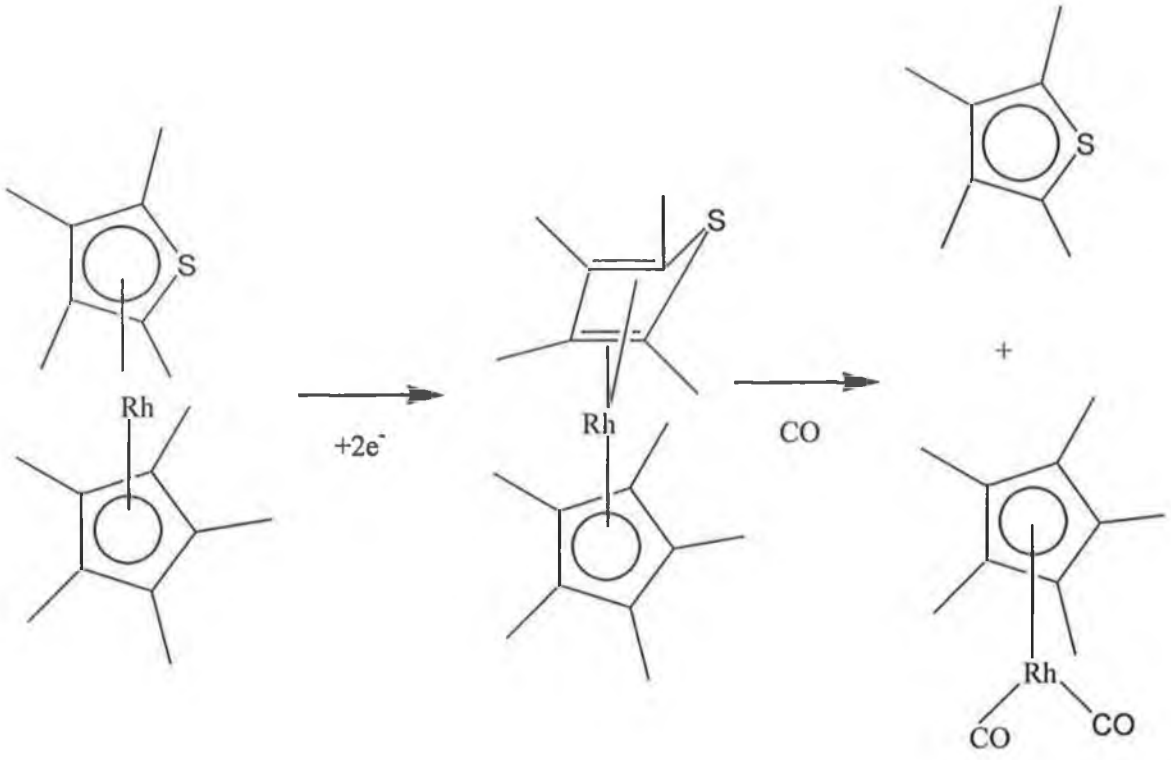

Reaction 3.1.1.3

Angelici has also synthesised the stable η^4 thiophene complex by reacting $(\eta^5\text{-}C_5(CH_3)_5)Re(CO)_2(\eta^1\text{-}C_4H_4S)$ with $Fe_2(CO)_9$ in THF to yield $(\eta^5\text{-}C_5(CH_3)_5)Re(CO)_2(\eta^1\text{-}C_4H_4S)(\eta^4\text{-}C_4H_4S)Fe(CO)_3$ as shown in Reaction 3.1.14.[9]

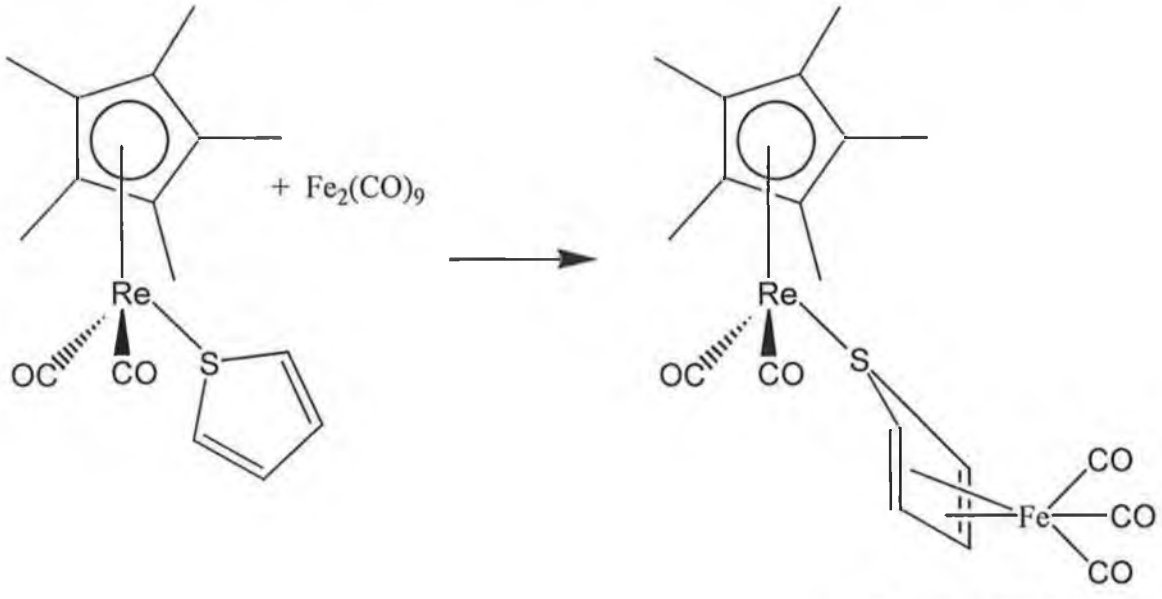

Reaction 3.1.1.4

Zhang *et al.* have shown that benzothiophene can undergo hydrodesulphurisation upon coordination to manganese.[12] The coordination of $Mn(CO)_3^+$ to the benzothiophene ligand activates the benzothiophene to reductive insertion and subsequent desulphurisation upon hydrogenation, Scheme 3.1.1.1.

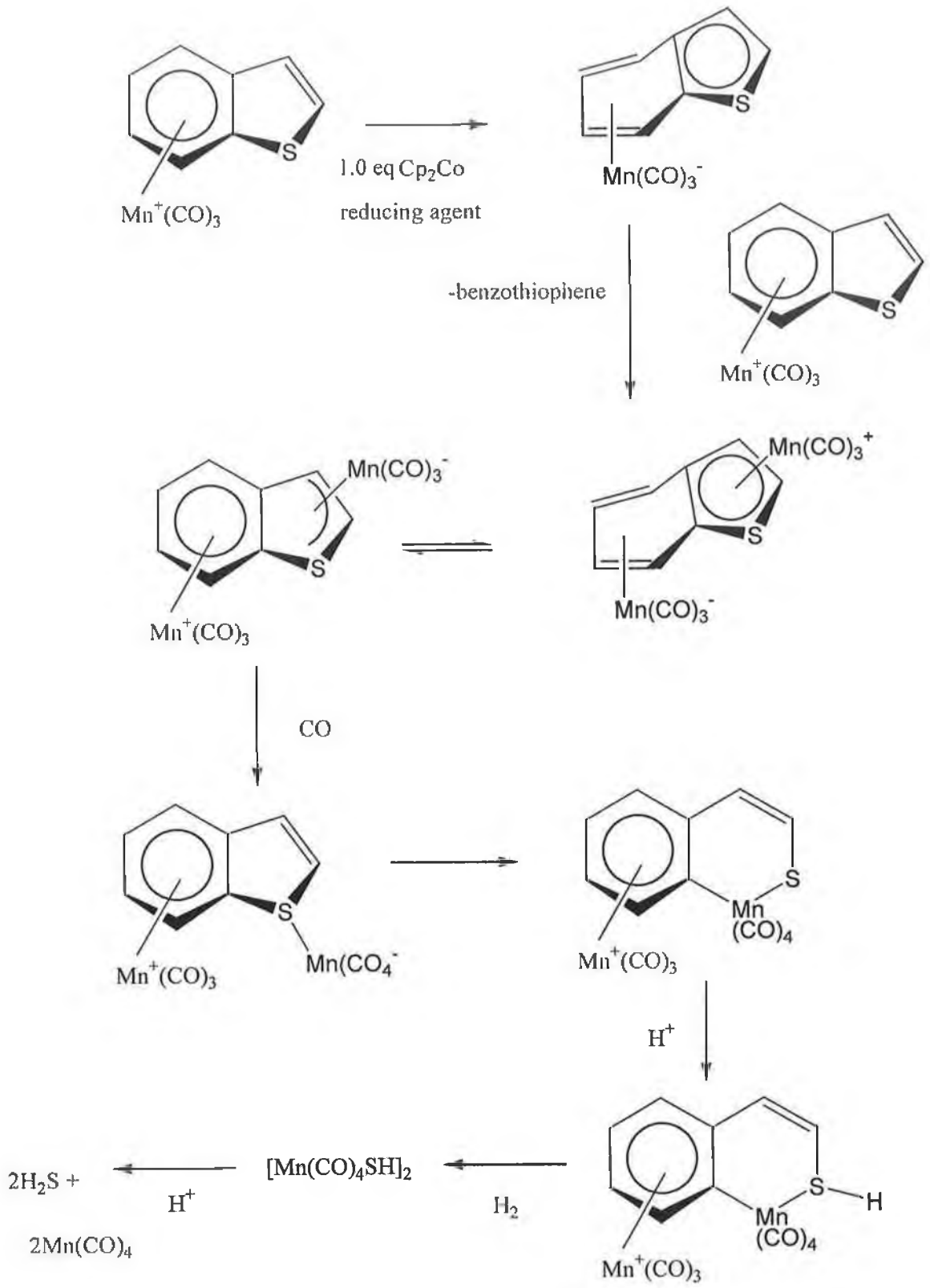
Mn+(CO)3
1.0 eq Cp2Co
reducing agent
Mn(CO)3-
-benzothiophene
Mn(CO)3+
CO
Mn(CO4-
H+
[Mn(CO)4SH]2
H2
2H2S +
H+
2Mn(CO)4

Scheme 3.1.1.1

Dullaghan *et al.* have also shown that $Mn(CO)_3^+$ coordination activates the thiophene to reductive insertion and subsequent desulphurisation upon hydrogenation.[13] Cobaltocene reduction of $(\eta^5\text{-}C_4H_4S)Mn(CO)_3^+$ at room temperature under an atmosphere of CO yielded the bimetallic species with a $Mn(CO)_4$ moiety inserted into a C-S bond. Hydrogenation of the bimetallic C-S insertion product yielded a bridging hydride complex. This species was found to react with CO giving a proposed bridging diene thiolate ligand bonded to each manganese through the sulphur and a carbon – carbon bond (as shown below).

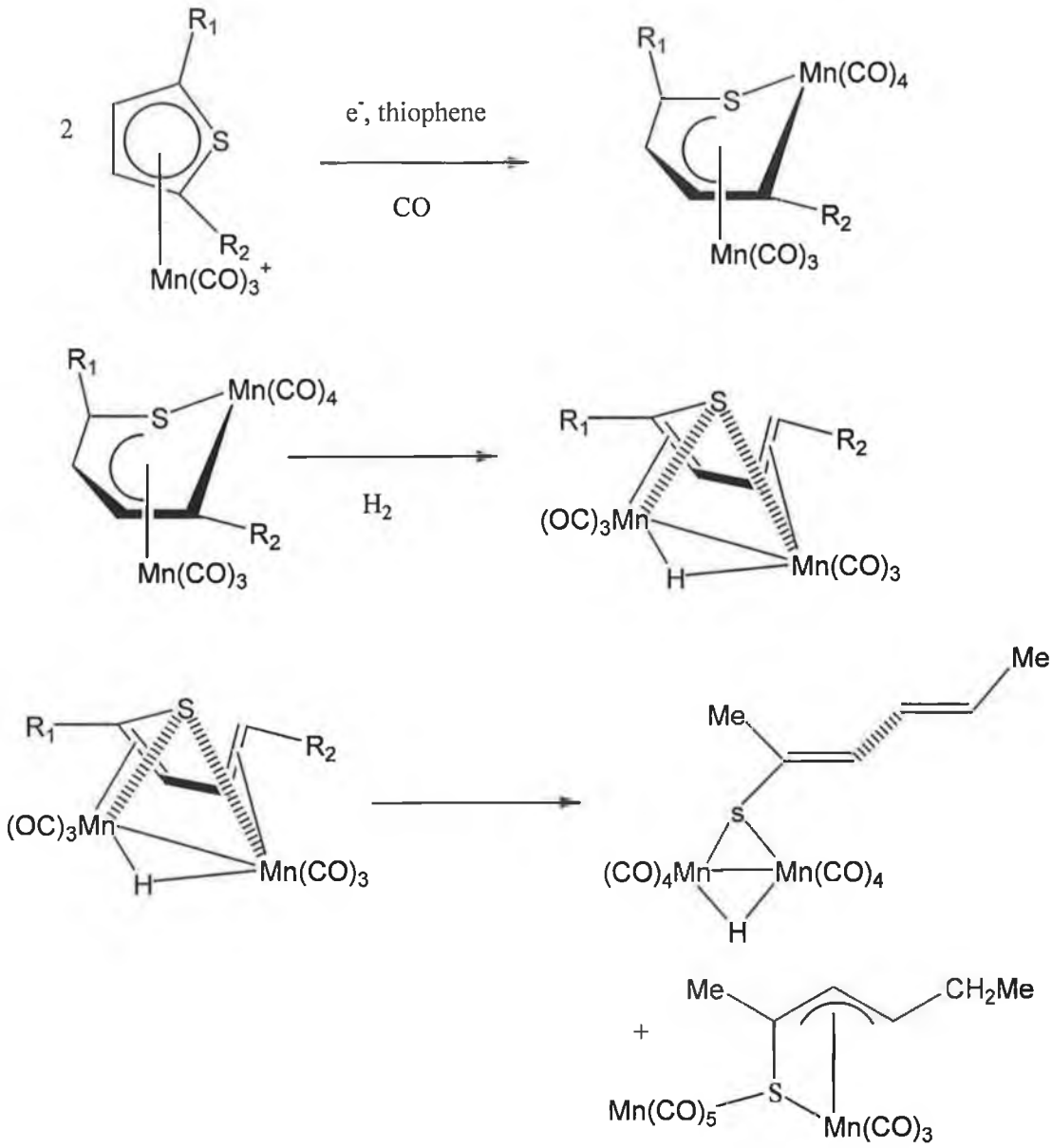

Scheme 3.1.1.2

3.1.2 Selenophene complexes as model compounds for the hydrodesulphurisation process

Like thiophene, selenophene has a number of coordination modes, which include, η^1 ,η^2 , η^4, η^5, η^5 ring opened, and the C-Se metal ring insertion mode.[14,15,16]

In the electron rich complex $(\eta^5\text{-}C_5(CH_3)_5)Re(CO)_2(\eta^y\text{-}C_4X_nH_{4-n}Se)$ (y = 1 or 2, X = CH_3 ; n=0, 1, or 2), the selenophene ligand is found to bind in either the η^1 or η^2 binding mode depending on the substituent at the two and five position on the ring. [14,15] In the η^2 mode the selenophene coordinates through the two carbons in the ring, while for the 2,5 dimethyl derivative coordination occurs in a η^1 fashion, through the Se atom. For the related monomethyl substituted derivative both the η^1 and η^2 isomers exist, Figure 3.1.2.1. It was also found that the binding mode of the selenophene depended on the nature of the C_5R_5 ring. For the less electron donating C_5R_5 ring (C_5H_5) compared to $C_5(CH_3)_5$ it was found that η^1 coordination of the selenophene ring is favoured. By lowering the electron density on the Re atom the η^1 Se binding mode is favoured.

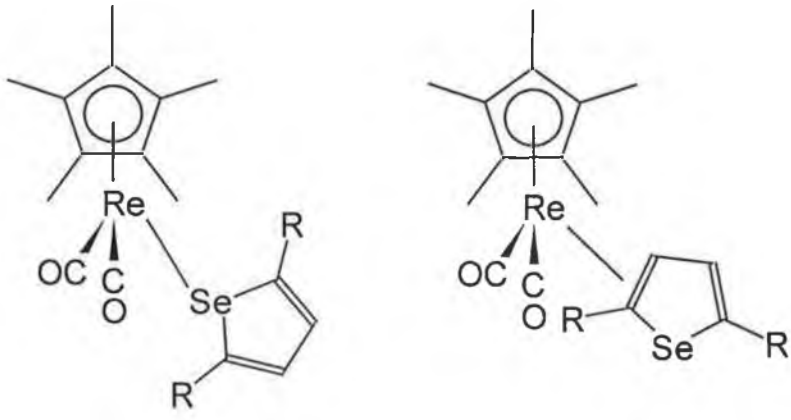

Figure 3.1.2.1 η^1 or η^2 binding modes for $(\eta^5\text{-}C_5(CH_3)_5)Re(CO)_2(\eta^y\text{-}C_4X_nH_{4-n}Se)$ (y = 1 or 2, R = CH_3 ; n=0, 1, or 2).

The reaction of $(\eta^5\text{-}C_4H_4Se)Mn(CO)_3^+$ with $NaBH_4$ as the hydride source gives $(\eta^4\text{-}C_4H_5Se)Mn(CO)_3$, Reaction 3.1.2.1.[16]

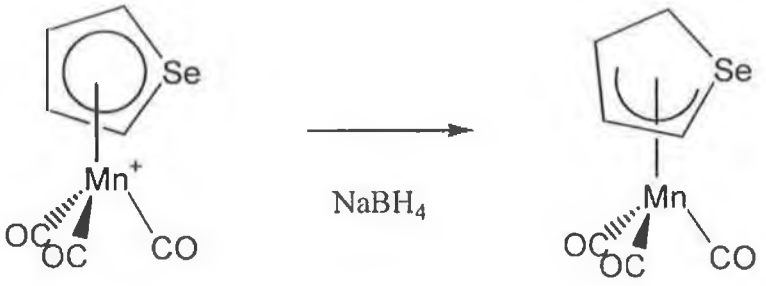

Reaction 3.1.2.1

In contrast to the addition of hydride to the selenophene ring in $(\eta^5\text{-}C_4H_4Se)Mn(CO)_3^+$, hydride addition to $(\eta^5\text{-}C_4H_4Se)Ru(\eta^5\text{-}C_5H_5)^+$ results in cleavage of the C-Se bond, Reaction 3.1.2.2.[16]

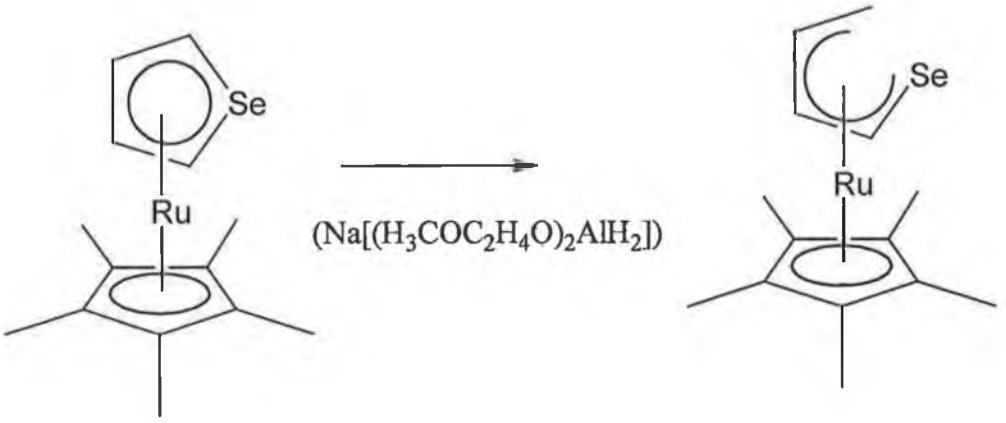

Reaction 3.1.2.2

The reaction of $(\eta^5\text{-}2,5\ (CH_3)_2C_4H_2Se)Ir(C_5(CH_3)_5)^{2+}$ with $Na[(CH_3\text{-}OC_2H_4O)_2AlH_2]$ gives the ring opened product, in which iridium is inserted into a C-Se bond to give a planar six membered ring, Reaction 3.1.2.3.[16]

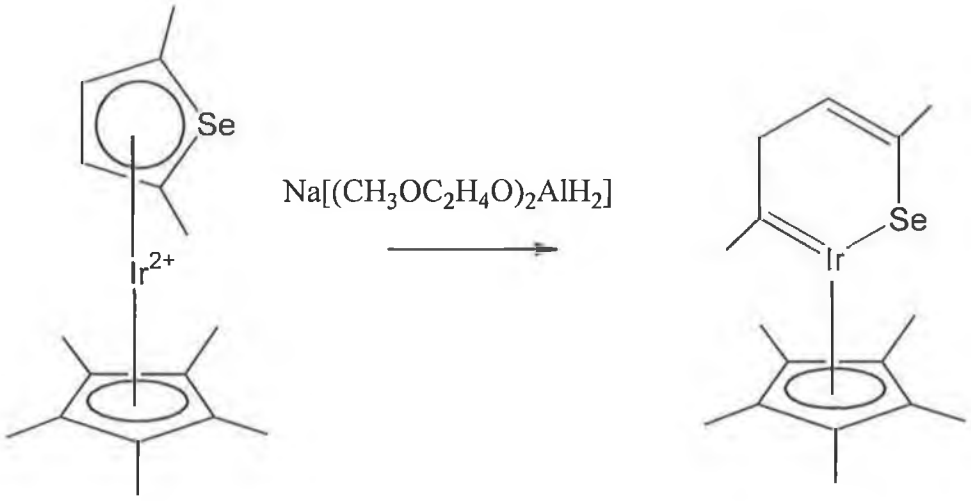

Reaction 3.1.2.3

Unlike the analogous thiophene complex $(\eta^5\text{-}2,5\ (CH_3)_2C_4H_2S)Ir(C_5(CH_3)_5)^{2+}$, where reaction with $Na[(CH_3\text{-}OC_2H_4O)_2AlH_2]$ results first in the formation of $(\eta^4\text{-}2,5\ (CH_3)_2C_4H_2S)Ir(C_5(CH_3)_5)$ and subsequent rearrangement to give the ring opened product. No such intermediate is observed prior to insertion in the case of the selenophene system, $(\eta^5\text{-}2,5\ (CH_3)_2C_4H_2Se)Ir(C_5(CH_3)_5)^{2+}$ where only the ring opened species is observed.

3.2 Bonding and reactivity in $(\eta^5\text{-}C_4H_4S)Cr(CO)_3$ complexes

In the η^5-binding mode, thiophene can be viewed as a formal six electron donor. The metal-ligand binding in η^5-thiophene complexes can be compared to metal ligand binding in their η^5-cyclopenadienyl analogues. Introduction of the sulphur atom into the five membered ring lowers the symmetry of the ring from D_{5h} in the $C_5H_5^-$ anion , to C_2v in thiophene, C_4H_4S. The molecular orbitals of both $C_5H_5^-$ anion and C_4H_4S are shown in Figure 3.2.1. In the $C_5H_5^-$ anion the degenerate e_1" pair of orbitals is the HOMO and these two orbitals serve as the principal donor orbitals in metal ligand bonding. Although the lower energy a_2" orbital has the ability to serve as a donor orbital most of the electron donation involves the e_1" HOMO. The LUMO is a pair of degenerate e_2" π orbitals.

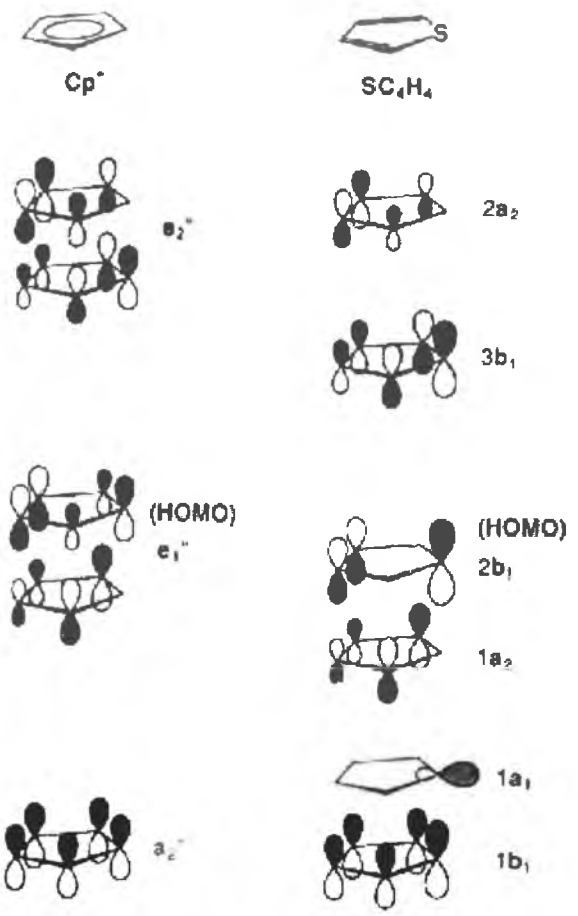

Figure 3.2.1 The molecular orbitals of both $C_5H_5^-$ and C_4H_4S.

In thiophene the two highest energy occupied orbitals are the $1a_2$ and $2b_1$ orbitals. These are similar in character to the degenerate e_2" HOMO in $C_5H_5^-$ ring. The presence of the S atom in C_4H_4S results in a high energy $1a_1$ occupied orbital which has no counterpart in the $C_5H_5^-$ ring. Although this orbital is of minor importance when thiophene binds through the η^5 mode it becomes an important donor orbital when thiophene binds to a metal in a η^1-S fashion. The two LUMO orbitals are the $3b_1$ and $2a_2$ orbitals which resemble the e_2" set of orbitals of $C_5H_5^-$.

Bonding in both types of complexes can be considered in terms of interactions between the $Cr(CO)_3$ fragment and the $C_5H_5^-$ or C_4H_4S ligand. The important levels of $Cr(CO)_3$ and of $C_5H_5^-$ and C_4H_4S are shown in Figure 3.2.2.[17]

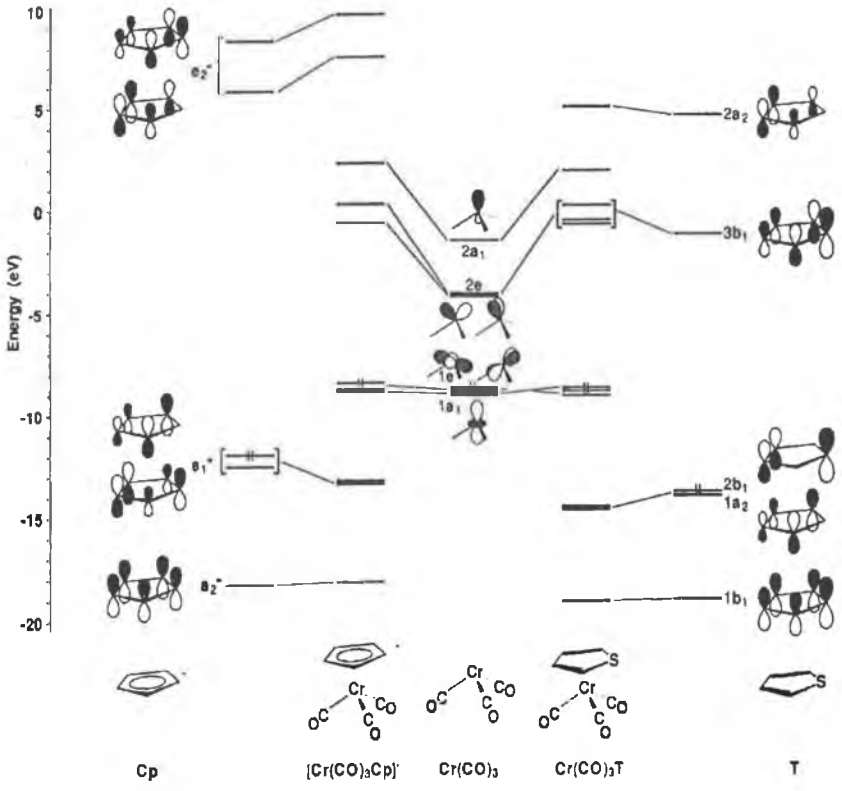

Figure 3.2.2 The calculated energy levels for $(\eta^5\text{-}C_4H_4S)Cr(CO)_3$ and $(\eta^5\text{-}C_5H_5)Cr(CO)_3^-$.

For $(\eta^5\text{-}C_5H_5)Cr(CO)_3^-$, the three $C_5H_5^-$ orbitals e_1" and a_2" interact with the vacant 2e and $2a_1$ orbitals on the $Cr(CO)_3$ unit. The $C_5H_5^-$ a_2" orbital also interacts weakly, in an antibonding manner, with the filled $1a_1$ orbital on the $Cr(CO)_3$ unit, but this weak interaction is counter balanced by the bonding interaction between a_2" and $2a_1$ with the $Cr(CO)_3$ unit $1a_1$ orbital. The unoccupied $C_5H_5^-$ e_2" orbital interacts with the filled $Cr(CO)_3$ 1e orbitals, but this interaction is weak. In $(\eta^5\text{-}C_4H_4S)Cr(CO)_3$ the occupied $2b_1$,$1a_2$ and $1b_1$ thiophene orbitals act as donors and the empty $3b_1$ and $2a_2$ orbitals act as acceptors. The $C_5H_5^-$ donor orbitals e_1", lie about 1.5 eV closer in energy to the metal based orbitals than the corresponding thiophene donor orbitals, $1a_2$ and $2b_1$. The C_4H_4S acceptor orbitals $3b_1$ and $2a_2$, lie much lower in energy and therefore closer in energy to

the occupied metal-based orbitals than the corresponding $C_5H_5^-$ acceptor orbitals. These differences would suggest that C_4H_4S is a better acceptor but poorer donor than $C_5H_5^-$. The relative donor and acceptor strengths are also reflected in the Mulliken populations of the ligand donor and acceptor orbitals in the complexes.

Orbital	$(\eta^5\text{-}C_5H_5)Cr(CO)_3^-$	$(\eta^5\text{-}C_4H_4S)Cr(CO)_3$
e_2"	0.04 0.05	
e_1"	1.69 1.77	
$2a_2$		0.06
$3b_1$		0.20
$2b_1$		1.75
$1a_2$		1.80

Table 3.2.1 The orbital occupations of $(\eta^5\text{-}C_5H_5)Cr(CO)_3^-$ and $(\eta^5\text{-}C_5H_4S)Cr(CO)_3$.

The magnitude of the donor and acceptor orbital occupations in both $(\eta^5\text{-}C_5H_5)Cr(CO)_3^-$ and $(\eta^5\text{-}C_4H_4S)Cr(CO)_3$ is a measure of the relative donor and acceptor properties of $C_5H_5^-$ and C_4H_4S. The population of these orbitals are shown in Table 3.2.1. In the $C_5H_5^-$ and C_4H_4S ligands each of the donor orbitals, e_1" in $C_5H_5^-$ and $1a_2$ and $2b_1$ in C_4H_4S are occupied by two electrons. While each of the acceptor orbitals, e_2" in $C_5H_5^-$ and $3b_1$ and $2a_2$ in C_4H_4S are empty. The increased acceptor ability of the C_4H_4S ligand over the $C_5H_5^-$ ligand results almost entirely from the much lower energy C_4H_4S $3b_1$ and $2a_2$ orbitals compared to the corresponding $C_5H_5^-$ acceptor orbitals, e_2". This increase however is not large and even though thiophene is a better π-acceptor than $C_5H_5^-$, it still cannot be described as a good π-acceptor. Although there are many similarities in the binding between $C_5H_5^-$ and C_4H_4S, the inclusion of a larger S atom in C_4H_4S instead of a carbon atom in $C_5H_5^-$ (or in the case of C_4H_4Se the inclusion of a much larger selenium atom) changes both the character of the ring molecular orbitals and

the nature of the metal ring interaction in these complexes. The large size of the sulphur atom in the C_4H_4S ring and its effect on the η^5 binding geometry of the C_4H_4S ring can be seen clearly from Figure 3.2.3, depicting the binding geometry of the $C_5H_5^-$ ring in $(\eta^5\text{-}C_5H_5)Cr(CO)_3^-$ **1** and $(\eta^5\text{-}C_4H_4S)Cr(CO)_3$ **2**. In **1,** the $C_5H_5^-$ ring lies approximately in the plane orthogonal to the plane formed by the C atoms of the three CO ligands indicated by the two parallel broken lines. In **2** however, the large size of the S atom results in the tilting of the entire ring relative to the plane orthogonal to the plane of the three CO ligands. Tilting of the ring is also accompanied by a slight slip of the ring. This combined tilt and slip accommodates the larger S atom and serves to optimise rather then weaken the bonding between the metal and both the large S atom and the C atoms.

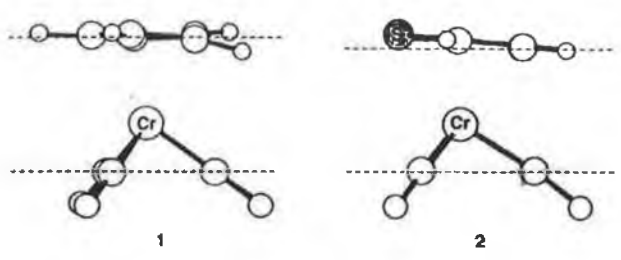

Figure 3.2.3 The molecular geometry of $(\eta^5\text{-}C_4H_4S)Cr(CO)_3$ complex and $(\eta^5\text{-}C_4H_5)Cr(CO)_3^-$.

The molecular geometry of the $(\eta^5\text{-}C_4H_4Se)Cr(CO)_3$ complex is similar to that of the $(\eta^5\text{-}C_4H_4S)Cr(CO)_3$ complex. The selenophene ring binds to the chromium tricarbonyl fragment through the selenium and the two C=C bonds each *trans* to a carbonyl ligand, thereby giving a pseudo octahedral coordination around the Cr atom with the selenium atom bent out of the plane of the ring. This is the same geometry as found in the $(\eta^5\text{-}C_4H_4S)Cr(CO)_3$ complex. However for $(\eta^5\text{-}C_4H_4Se)Cr(CO)_3$, the selenium atom is further from the plane of the other ring atoms than sulphur in comparison to sulphur in $(\eta^5\text{-}C_4H_4S)Cr(CO)_3$. For the $(\eta^5\text{-}2,5\ (CH_3)_2C_4H_2Se)Cr(CO)_3$ complex the selenium atom

is found to be bent out of the ring by 6.7° (the dihedral angle between the plane of the ring carbons).[16] This angle is 2.2° greater then the thiophene analogue and is expected considering the larger size of the selenium atom.

3.3 Photoinduced ring slippage in cyclopentadienyl metal carbonyl systems

Although quite rare, there have been some reports of photo-induced ring slip in cyclopentadienyl metal carbonyl systems. Crichton, Rest and Taylor have reported that photolysis of $(\eta^5\text{-}C_5H_5)Co(CO)_2$ in a pure CO matrix monitored by IR spectroscopy yielded depletion of the parent bands at 2032 and 1972 cm^{-1} and the appearance of bands at 2075 cm^{-1} and 2018 cm^{-1} which were assigned to $(\eta^3\text{-}C_5H_5)Co(CO)_3$, Reaction 3.3.1.[18]

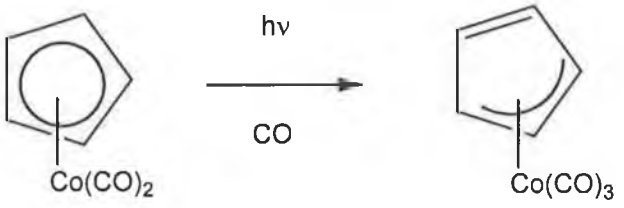

Reaction 3.3.1.

Rest *et al.* carried out a related study on $(\eta^5\text{-}C_5H_5)Fe(CO)_2CH_3$ and again observed a shift of the ν_{co} bands to a higher wavenumber (2050, 1982 and 1975 cm^{-1}), as is expected for a increase in the number of CO bands to yield $(\eta^3\text{-}C_5H_5)Fe(CO)_3CH_3$, Reaction 3.3.2.[19]

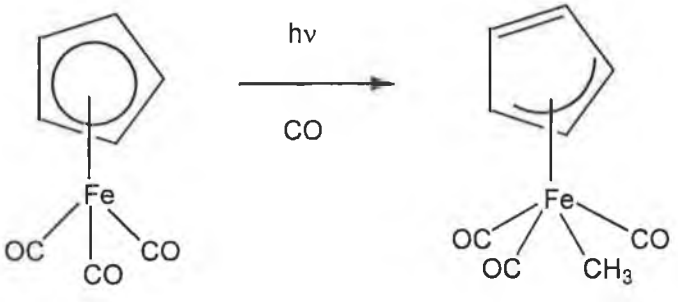

Reaction 3.3.2.

Blaha and Wrighton also observed a ring slip product, when $(\eta^5\text{-}C_5H_5)Fe(CO)_2CH_2Ph$ was irradiated in the presence of added ligand (L = CO or PPh_3), with the formation of

$(\eta^4\text{-}C_5H_4CH_2Ph)Fe(CO)_2L$.[20] Perutz and co-workers have also found evidence for the formation of $(\eta^3\text{-}C_5H_5)(\eta^5\text{-}C_5H_5)Re(CO)H$ (1918 cm^{-1}), upon photolysis of $(\eta^5\text{-}C_5H_5)_2ReH$ in the presence of CO.[21] Prolonged irradiation leads to formation of the $\eta^1\text{-}C_5H_5$ dicarbonyl species, $(\eta^1\text{-}C_5H_5)(\eta^5\text{-}C_5H_5)Re(CO)_2H$ (1918 and 1872 cm^{-1}).

3.4 Organometallic complexes in modelling the hydrodesulphurisation process

The homogeneous solution chemistry of discrete metal complexes has provided an interesting molecular model for the heterogeneous catalysed process.[10] A coordinatively unsaturated transition metal fragment ML_n simulates a surface absorption site where a reactive molecule is chemisorbed. A prototype of such a fragment has been proposed by removing some of the CO ligands from a metal carbonyl complex $M(CO)_n$. These fragments have been proposed as intermediates in the reactions of metal carbonyl complexes and have been detected by matrix isolation techniques. Such fragments can be seen as molecular analogues of adsorption sites on the solid catalyst (known as vacancies), where surface coordination bonds are incomplete. Because chemisorption can be considered a local phenomena only a few atoms are necessary to simulate an adsorption site, thus the concept of using organometallic complexes and intermediates generated there from is justified. However there are some limitations in this model, where mononuclear complexes are involved. Chemisorption can occur in multicentre adsorption sites, and the neighbouring metallic atom participation could be of great importance in subsequent steps of the catalytic process. On the other hand, fragments and complexes offer the advantages of varying the number of and the nature of the ligands, thereby allowing the study of the influence of oxidation states, coordinative unsaturation and the electronic role of promoters in the first step of the catalytic process.

In contrast to heterogeneous catalysis, homogeneous catalysis using organometallic transition metal complexes offers a catalytic reaction in solution. The main difficulty arising with homogeneous catalysis is to cleave both carbon sulphur bonds of the thiophenes, since most studies only describe insertion of the thiophene and breaking of one bond.

It was therefore decided to investigate the photochemistry of the thiophene hydrodesulphurisation model compounds $(\eta^5\text{-}C_4H_4S)Cr(CO)_3$ and $(\eta^5\text{-}C_4H_4Se)Cr(CO)_3$ to determine if it is possible to photochemically induce a hapticity change in these complexes.

3.5 Spectroscopic parameters of $(\eta^5\text{-}C_4H_4S)Cr(CO)_3$

The spectroscopic parameters for $(\eta^5\text{-}C_4H_4S)Cr(CO)_3$ are given in Table 3.5.1. The UV/vis spectrum of $(\eta^5\text{-}C_4H_4S)Cr(CO)_3$ is shown in Figures 3.5.1, two bands are observed at λ_{max} 417 nm and 325 nm.

$(\eta^5\text{-}C_4H_4S)Cr(CO)_3$ has C_s symmetry and three absorption bands are observed in the carboyl region of the IR at 1981,1911 and 1897 cm^{-1}. The ^1H NMR data for $(\eta^5\text{-}C_4H_4S)Cr(CO)_3$ are shown in Table 3.5.1.[22]

Complex	UV/vis bands λ_{max} nm	IR bands cm^{-1}	^1H NMR ppm
$(\eta^5\text{-}C_4H_4S)Cr(CO)_3$	417 315	1981 1911 1897	H2 5.37 H3 5.59 H4 5.59 H5 5.37

Table 3.5.1 Spectroscopic parameters for $(\eta^5\text{-}C_4H_4S)Cr(CO)_3$. UV/vis and IR spectra were recorded in cyclohexane, with the NMR spectrum obtained in $CDCl_3$.

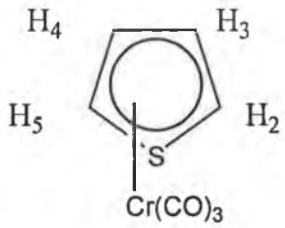

Figure 3.5.1 NMR numbering pattern for $(\eta^5\text{-}C_4H_4S)Cr(CO)_3$.

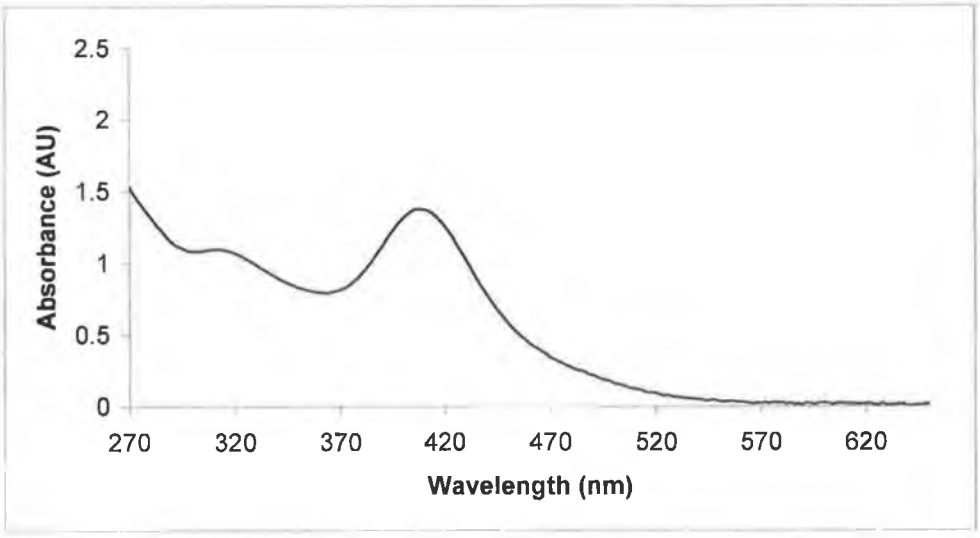

Figure 3.5.2. The UV/vis spectrum of $(\eta^5\text{-}C_4H_4S)Cr(CO)_3$ recorded in cyclohexane.

3.6 UV/vis, IR and NMR monitored steady state photolysis of $(\eta^5\text{-}C_4H_4S)Cr(CO)_3$

The photochemistry of $(\eta^5\text{-}C_4H_4S)Cr(CO)_3$ was investigated in CO and argon saturated cyclohexane, and in the presence of trapping ligands such as triphenylphosphine. Prior to photolysis, all samples were degassed by three "freeze pump thaw" cycles. The solutions were protected from light during preparation. UV/vis monitored photolysis of $(\eta^5\text{-}C_4H_4S)Cr(CO)_3$ in CO saturated cyclohexane was carried out with irradiation wavelengths of : $\lambda_{exc} > 500$ nm, > 400 nm and > 340 nm. Following photolysis at $\lambda_{exc} > 500$ nm, > 400 nm and > 340 nm, no changes were observed in the UV/vis spectrum. However when the sample was irradiated with the xenon arc lamp, changes were observed in the UV/vis spectrum that were consistent with the formation of $Cr(CO)_6$ and displacement of thiophene. An increase in absorption in the region 260–280 nm which is indicative of formation of $Cr(CO)_6$ together with depletion of the band at 420 nm which indicates displacement of thiophene from the $(\eta^5\text{-}C_4H_4S)Cr(CO)_3$ complex, Figure 3.6.1. An IR spectrum of the solution recorded after photolysis indicated the presence of $Cr(CO)_6$ with a band at 1985 cm^{-1}, in addition to starting material, Figure 3.6.2.

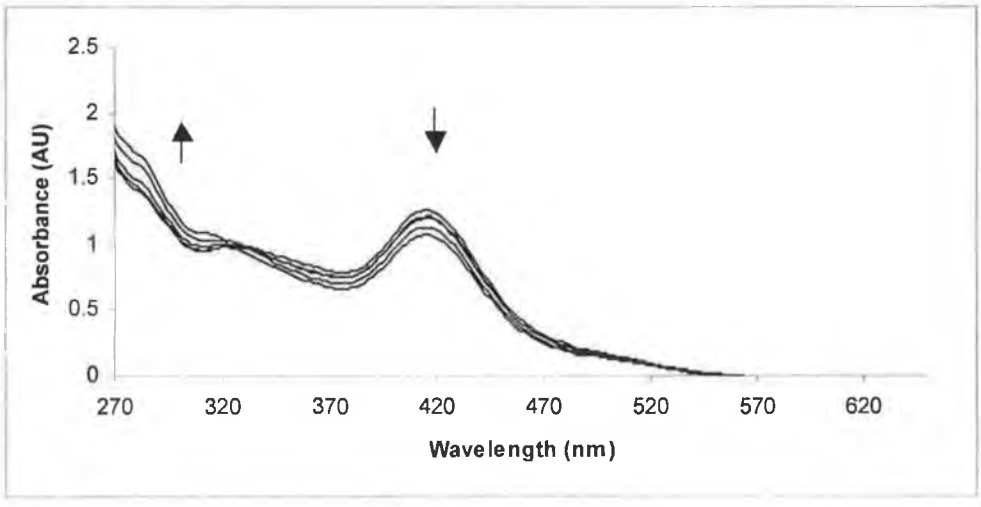

Figure 3.6.1 UV/vis changes following photolysis of $(\eta^5\text{-}C_4H_4S)Cr(CO)_3$ in CO saturated cyclohexane, at high energy (no filter) using a xenon arc lamp over a period of 22 minutes.

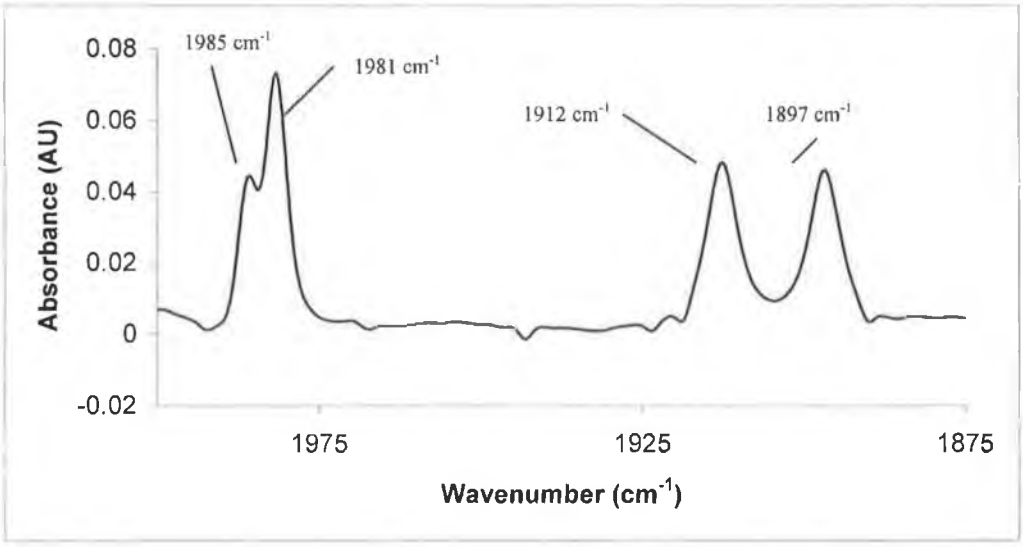

Figure 3.6.2 An IR spectrum obtained following photolysis of $(\eta^5\text{-}C_4H_4S)Cr(CO)_3$ after 22 minutes in CO saturated cyclohexane using a xenon arc lamp. $(\eta^5\text{-}C_4H_4S)Cr(CO)_3$ ν_{co} : 1981,1912 and 1897 cm^{-1}, $Cr(CO_6$ ν_{co} : 1985cm^{-1}.

To obtain further information on the arene displacement reaction of the $(\eta^5\text{-}C_4H_4S)Cr(CO)_3$ complex, it was decided to investigate the photochemical arene exchange reaction of $(\eta^5\text{-}C_4H_4S)Cr(CO)_3$ in argon saturated C_6D_6 by NMR spectroscopy. The samples were prepared in degassable NMR tubes. All samples were degassed by three "freeze pump thaw" cycles before addition of argon at 1 atmosphere. The sample was initially irradiated at $\lambda_{exc} > 500nm$, > 400nm and subsequently with $\lambda_{exc} > 340nm$, with no changes observed in the NMR spectrum, for $(\eta^5\text{-}C_4H_4S)Cr(CO)_3$.

However, photolysis at high energy using a xenon arc lamp only, led to rapid displacement of the thiophene ring by the benzene ring which was confirmed by disappearance of the complexed thiophene bands (4.18 and 3.7 ppm) and appearance of new "free" thiophene bands (6.82 and 6.78 ppm), Figure 3.6.3. A change in colour from dark red to pale yellow was also noted. On completion of photolysis, removal of excess solvent under vacuum left a yellow residue. This residue was dissolved in acetone and its IR spectrum was recorded, showing bands at 1967 and 1887 cm^{-1}, which are consistent

with formation of $(\eta^6\text{-}C_6D_6)Cr(CO)_3$, Reaction 3.6.1. Further studies on the arene exchange reaction of $(\eta^5\text{-}C_4H_4S)Cr(CO)_3$ showed that the reaction is suppressed by the presence of CO as only $Cr(CO)_6$ was observed with no evidence for $(\eta^6\text{-}C_6D_6)Cr(CO)_3$, Reaction 3.6.2.

$$(\eta^5\text{-}C_4H_4S)Cr(CO)_3 \xrightarrow[C_6D_6,\ \text{argon}]{h\nu} (\eta^6\text{-}C_6D_6)Cr(CO)_3 + C_4H_4S \qquad \text{Reaction 3.5.1}$$

$$(\eta^5\text{-}C_4H_4S)Cr(CO)_3 \xrightarrow[C_6D_6,\ CO]{h\nu} Cr(CO)_6 + C_4H_4S \qquad \text{Reaction 3.5.2}$$

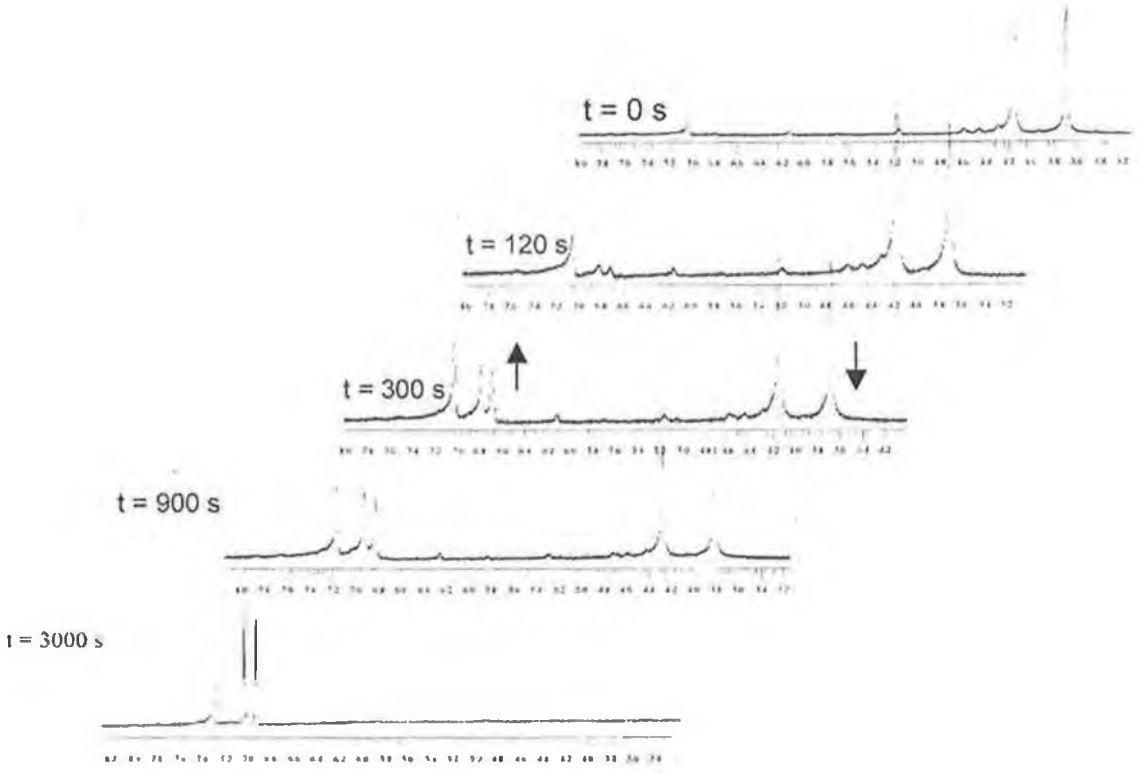

Figure 3.6.3 NMR spectrum of $(\eta^5\text{-}C_4H_4S)Cr(CO)_3$ in C_6D_6 recorded various time intervals over 50 minutes following photolysis using a xenon arc lamp. $(\eta^5\text{-}C_4H_4S)Cr(CO)_3$: 4.18 and 3.78 ppm. C_4H_4S : 6.82 and 6.77 ppm. The bands at 4.18 and 3.78 ppm disappear as the bands at 6.82 and 6.82 ppm form.

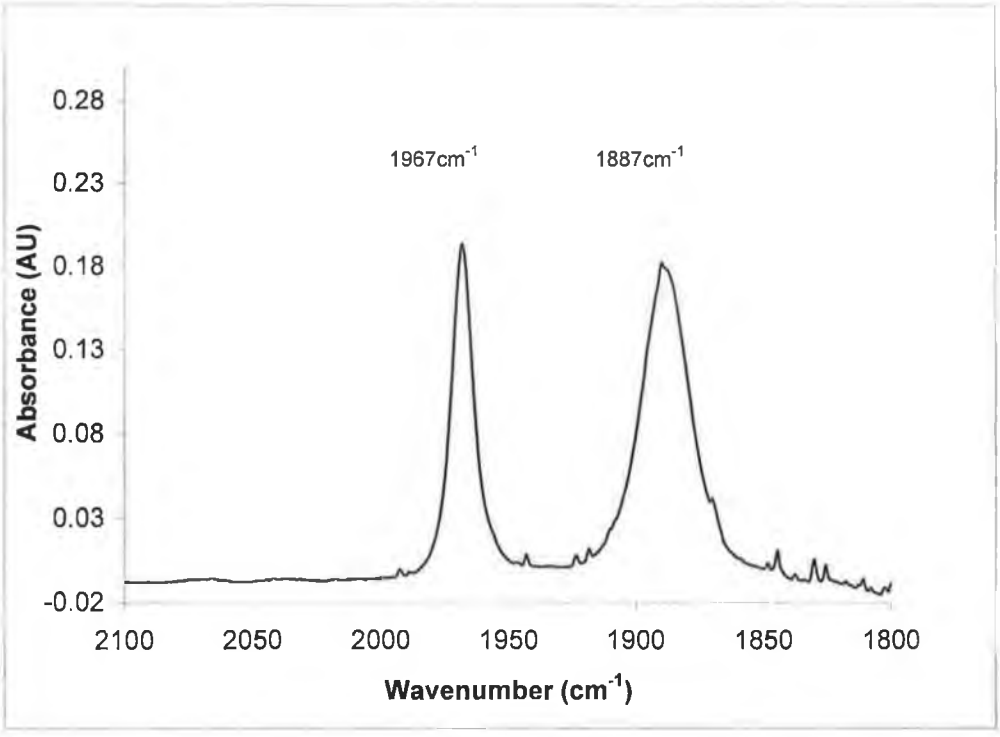

Figure 3.6.4 The IR spectrum (solvent acetone) obtained following photolysis of $(\eta^5\text{-}C_4H_4S)Cr(CO)_3$ in argon saturated C_6D_6 using a xenon arc lamp. $(\eta^5\text{-}C_6D_6S)Cr(CO)_3$ ν_{co} : 1967 and 1887 cm^{-1}.

Irradiation of $(\eta^5\text{-}C_4H_4S)Cr(CO)_3$ in the presence of a trapping ligand (PPh_3, 5 times molar excess) with both a xenon arc lamp (no filter) and a band pass filter λ_{exc} 320 - 390 nm (xenon arc lamp) led to the formation of the dicarbonyl species. The changes observed in UV/vis spectrum were, an increase in absorption from 330 – 390 nm, and from 430 – 480 nm approximately. An IR spectrum obtained on completion of the photolysis showed formation of two new bands at 1906 and 1850 cm^{-1} which were assigned to the dicarbonyl species, $(\eta^5\text{-}C_4H_4S)Cr(CO)_2PPh_3$.

$$(\eta^5\text{-}C_4H_4S)Cr(CO)_3 \xrightarrow[PPh_3]{h\nu} (\eta^5\text{-}C_4H_4S)Cr(CO)_2PPh_3 + CO \qquad \text{Reaction 3.5.3}$$

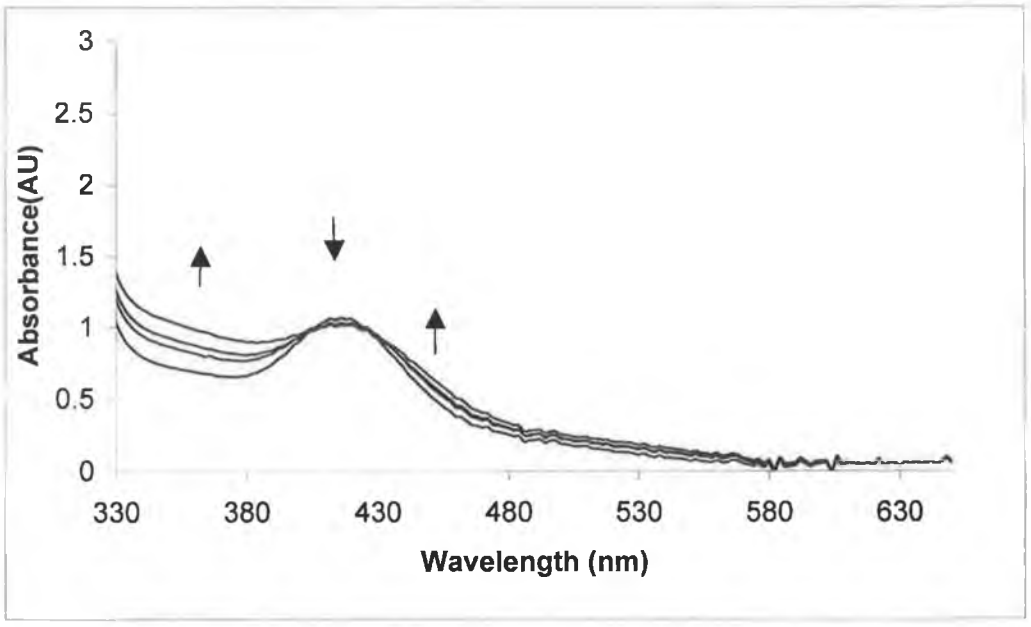

Figure 3.6.5 UV/vis changes observed following photolysis a xenon arc lamp of $(\eta^5\text{-}C_4H_4S)Cr(CO)_3$ 1.9×10^{-4} M in cyclohexane containing PPh_3 1×10^{-3} M.

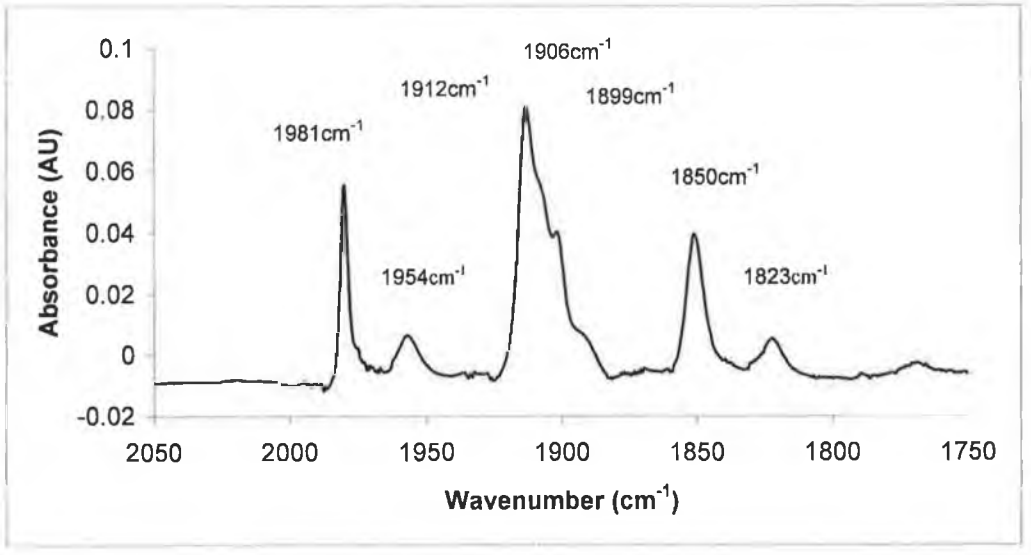

Figure 3.6.6 IR spectrum recorded following photolysis a xenon arc lamp of $(\eta^5\text{-}C_4H_4S)Cr(CO)_3$ 1.9×10^{-4} M in cyclohexane containing PPh_3 1.2×10^{-3} M . $(\eta^5\text{-}C_4H_4S)Cr(CO)_3$ ν_{co} : 1981, 1912 and 1899 cm^{-1}, $(\eta^5\text{-}C_4H_4S)Cr(CO)_3$ ν_{co} : 1906 and 1850 cm^{-1}. Note that the bands at 1954 and 1823 cm^{-1} are due to PPh_3.

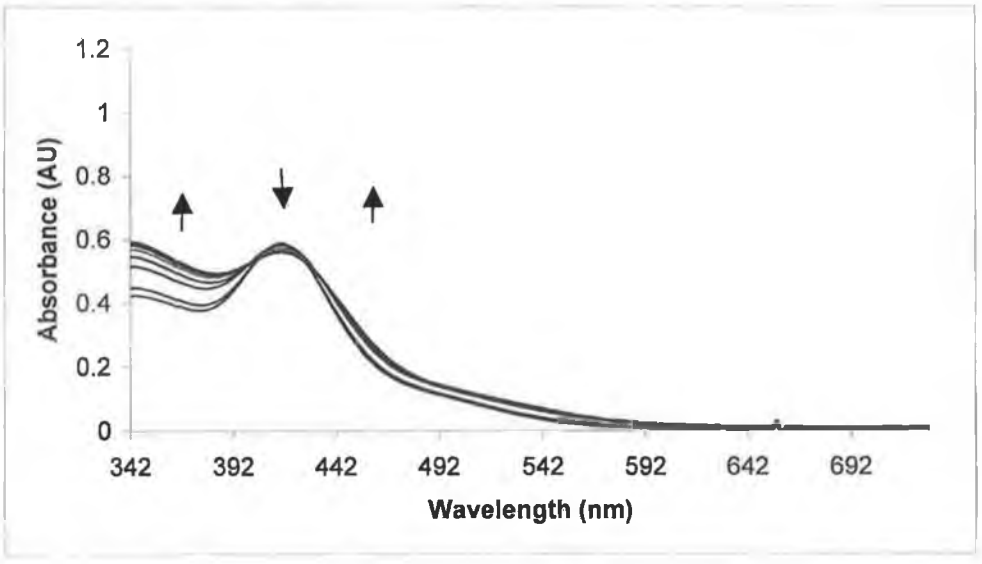

Figure 3.6.7 UV/vis changes following photolysis at λ_{exc} 320 – 390 nm of $(\eta^5\text{-}C_4H_4S)Cr(CO)_3$ 1.2×10^{-4} M at in cyclohexane containing an excess of PPh_3 7×10^{-4} M.

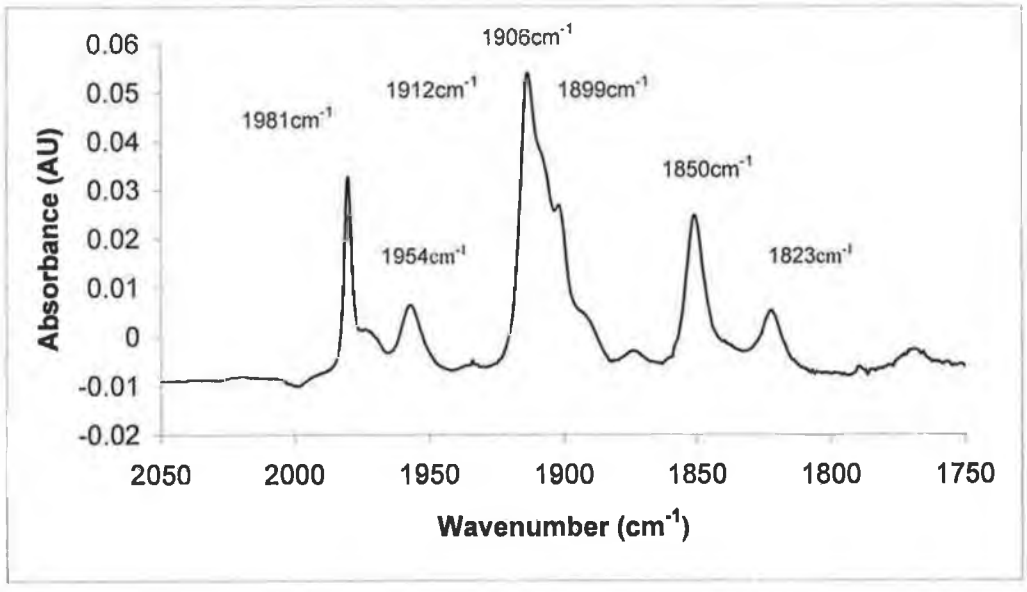

Figure 3.6.8 An IR spectrum recorded following photolysis of $(\eta^5\text{-}C_4H_4S)Cr(CO)_3$ 1.2×10^{-4} M in cyclohexane containing PPh_3 7×10^{-4} M at 355 nm. $(\eta^5\text{-}C_4H_4S)Cr(CO)_3$ ν_{co} : 1981, 1912 and 1899 cm^{-1}, $(\eta^5\text{-}C_4H_4S)Cr(CO)_2PPh_3$ ν_{co} : 1906 and 1850 cm^{-1}. Note that the bands at 1954 and 1823 cm^{-1} are due to PPh_3.

3.7 Photochemical investigations of $(\eta^5\text{-}C_4H_4S)Cr(CO)_3$ using both step scan and point by point TRIR techniques

The photochemistry of $(\eta^5\text{-}C_4H_4S)Cr(CO)_3$ was investigated in CO saturated heptane solution and monitored by step scan TRIR spectroscopy and point by point TRIR spectroscopy at both 266 nm and 355 nm excitation. Figure 3.7.1 represents the step scan difference spectrum obtained after 0.65 μs following excitation at 355 nm. The negative peaks at 1984, 1914 and 1898 cm^{-1}, indicate depletion of the parent compound with two positive peaks at 1924 and 1860 cm^{-1}. These latter bands were assigned to the solvated dicarbonyl species, $(\eta^5\text{-}C_4H_4S)Cr(CO)_2$(heptane). No other bands were observed under these conditions at a longer time base.

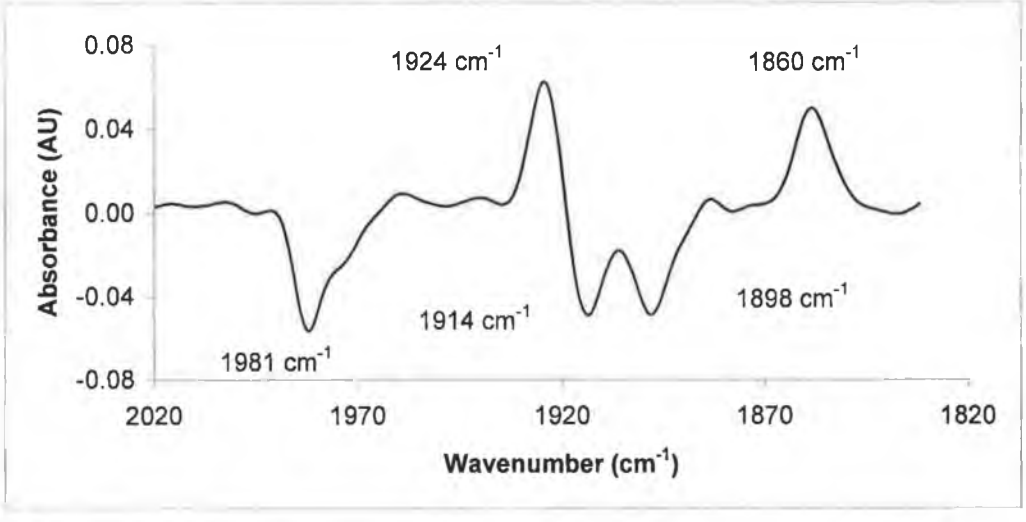

Figure 3.7.1 The stepscan TRIR spectrum recorded 0.65 μs after λ_{exc} = 355 nm of $(\eta^5\text{-}C_4H_4S)Cr(CO)_3$ in CO saturated heptane.

The TRIR difference spectrum obtained after 50 μs following 266 nm excitation is given in Figure 3.7.2. At least four new bands were observed at 2002, 1971, 1936 and 1886 cm^{-1} in addition to depletion of the parent bands at 1984, 1914 and 1898 cm^{-1}. The bands at 2002, 1971, 1936 and 1886 cm^{-1} are tentatively assigned to a tetra carbonyl species, $(\eta^4\text{-}C_4H_4S)Cr(CO)_4$. No other bands were observed at a shorter timebase.

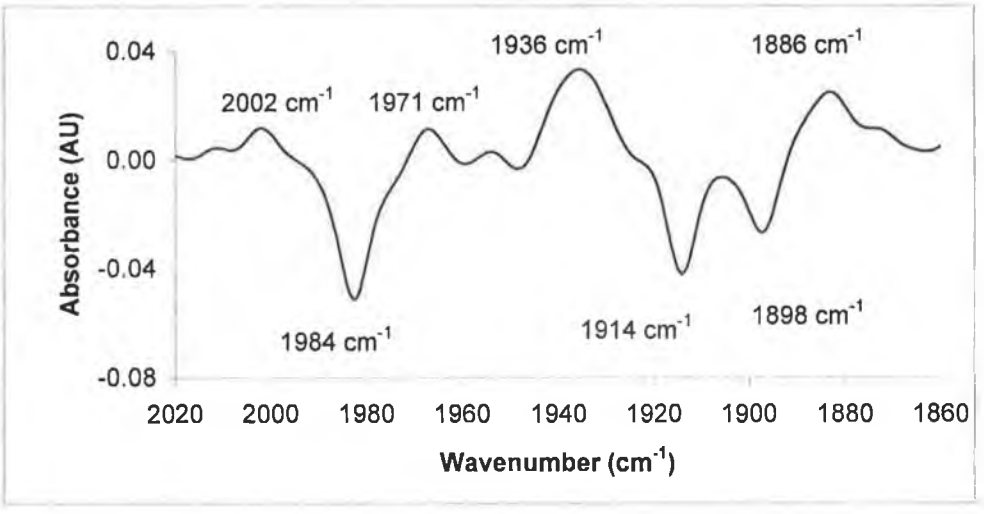

Figure 3.7.2 The stepscan TRIR spectrum recorded 50 μs after excitation of $(\eta^5\text{-}C_4H_4S)Cr(CO)_3$ at λ_{exc} 266 nm in CO saturated heptane.

In addition to the stepscan experiments, point by point TRIR measurements were also carried out. Given in Figure 3.7.3 is the difference spectrum obtained using point by point TRIR spectroscopy at both 800 ns and 30 us after excitation at 266 nm. After 800 ns four bands are observed at 1960, 1924, 1886 and 1860 cm^{-1}. There also appears to be a band absorbing under the parent band at 1895 cm^{-1}, as the band at 1895 cm^{-1} is not depleted to the same extent as the band at 1912 cm^{-1} indicating the presence of a band growing underneath the 1895 cm^{-1} band. The two bands at 1924 and 1860 cm^{-1} had been previously observed using stepscan TRIR at λ_{exc} = 355 nm and assigned to the formation of $(\eta^5\text{-}C_4H_4S)Cr(CO)_2$(heptane).

Given in Figures 3.7.4 and 3.7.6 are the kinetic traces of the transient species observed at 1924 and 1860 cm^{-1}, following λ_{exc} = 266 nm, under zero to two atmospheres of CO. On increasing the concentration of CO, the lifetime of the transient signals observed at 1924 and 1860 cm^{-1} decreases. The second order rate constant was obtained from the slope of this plot. For the signal at 1924 cm^{-1}, the second order rate constant was determined to be 1.88×10^6 $s^{-1}moles^{-1}dm^3$ and that at 1859 cm^{-1}, 2.55×10^6 $s^{-1}mol^{-1}dm^3$. The difference

between the two values of the second order rate constants, is due to the relative weakness of the signal observed at 1924 cm^{-1} compared to the signal at 1860 cm^{-1}. Following excitation of $(\eta^5\text{-}C_4H_4S)Cr(CO)_3$ at λ_{exc} = 355 nm using step scan TRIR in CO saturated heptane, two bands were again observed at 1924 and 1859 cm^{-1} 650 ns after excitation, thus indicating formation of $(\eta^5\text{-}C_4H_4S)Cr(CO)_2$(heptane). The bands at 1960, 1895 (absorbs under the parent band) and 1886 cm^{-1} are assigned to the formation of $(\eta^4\text{-}C_4H_4S)Cr(CO)_3$(heptane). These bands were not observed at 30 μs using point by point TRIR or at 50 μs using step scan TRIR.

The spectrum recorded 30 μs after excitation at λ_{exc} 266nm in CO saturated heptane displays depletion of the parent bands at 1981, 1912 and 1895 cm^{-1} and a grow in of four bands at 2002, 1971, 1936 and 1886 cm^{-1}. As before these four bands are assigned to the formation of a tetracarbonyl species, $(\eta^4\text{-}C_4H_4S)Cr(CO)_4$. The rate of formation of the photoproduct at 1936 cm^{-1} was determined from the kinetic traces, and was found to increase upon increasing the concentration of CO from zero to two atmospheres. From the plot of k_{obs} of the grow in of the signal at 1936 cm^{-1} versus concentration of CO in heptane the second order rate constant was determined to be 1.79×10^6 $s^{-1}mol^{-1}dm^3$ for the reaction of $(\eta^4\text{-}C_4H_4S)Cr(CO)_3$(heptane) with CO to form $(\eta^4\text{-}C_4H_4S)Cr(CO)_4$.

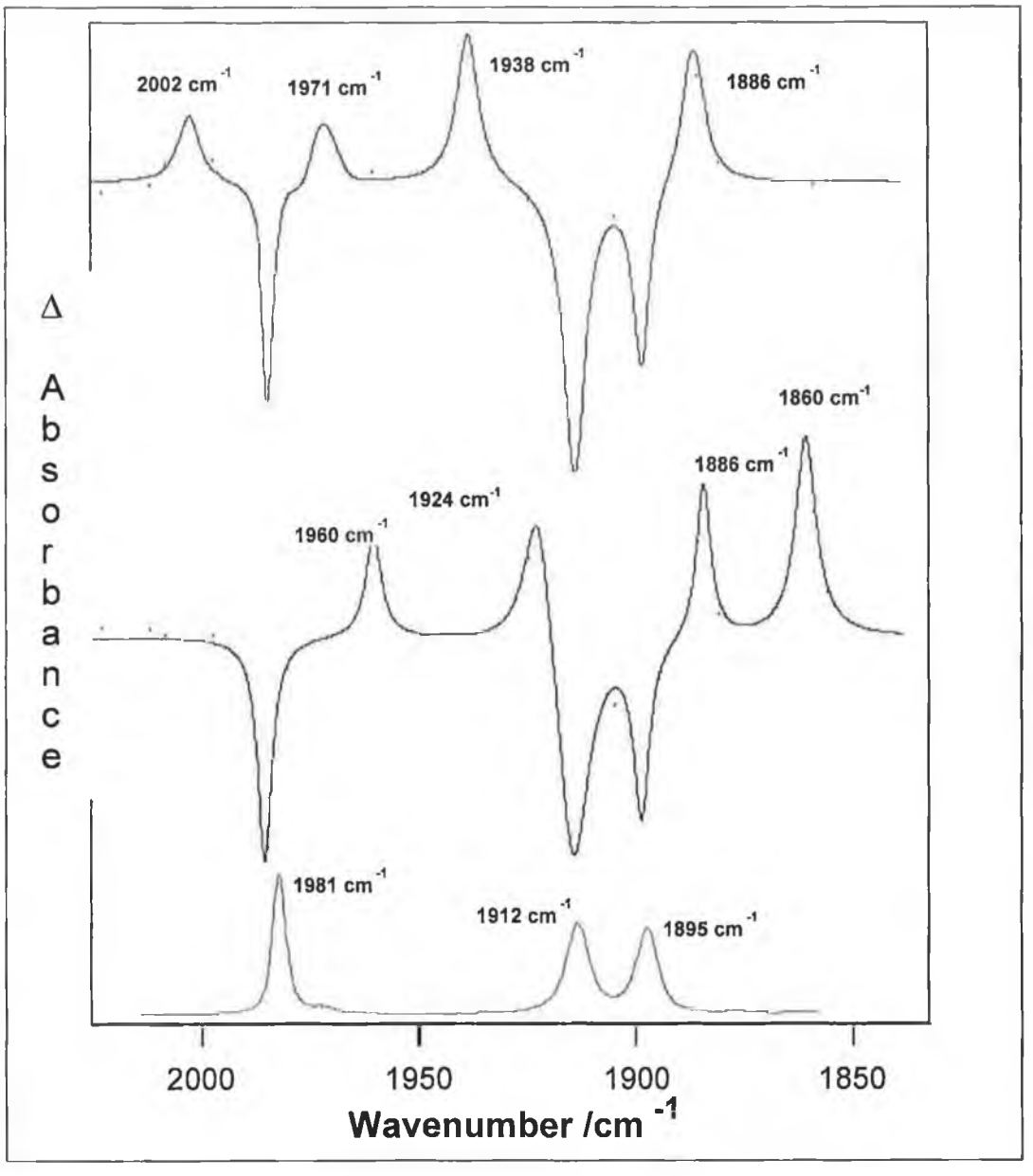

Figure 3.7.3 The point by point TRIR spectrum observed following excitation of $(\eta^5\text{-}C_4H_4S)Cr(CO)_3$ at 266 nm in CO saturated heptane spectra were recorded at 800ns and 30 μs after the laser pulse.

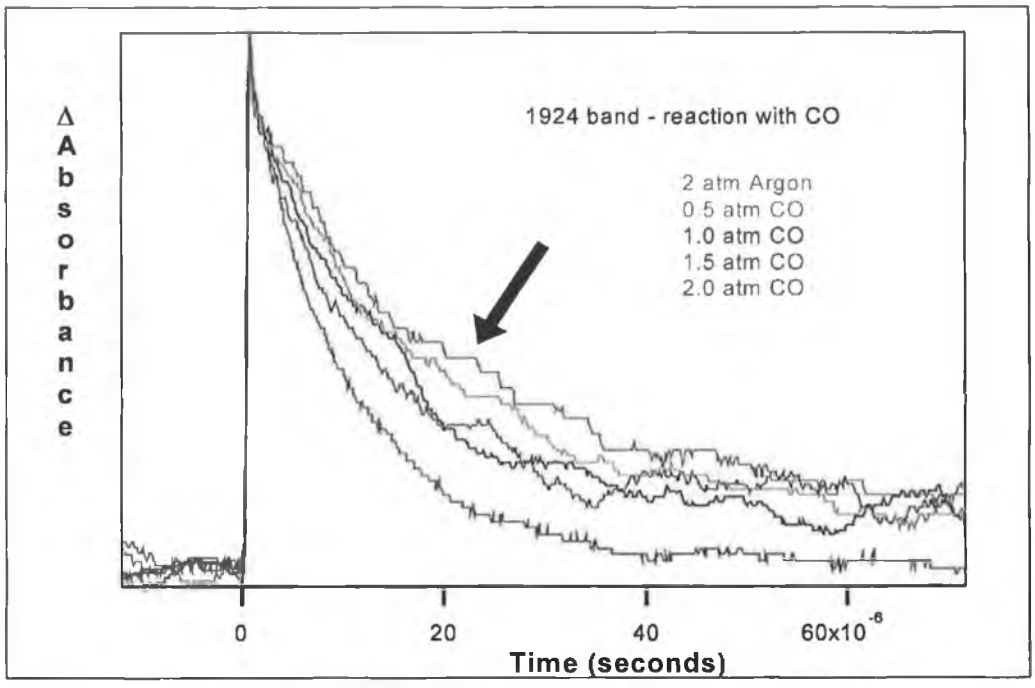

Figure 3.7.4 The kinetic traces observed at 1924 cm^{-1} following excitation of $(\eta^5\text{-}C_4H_4S)Cr(CO)_3$ at 266nm under various concentrations of CO in heptane.

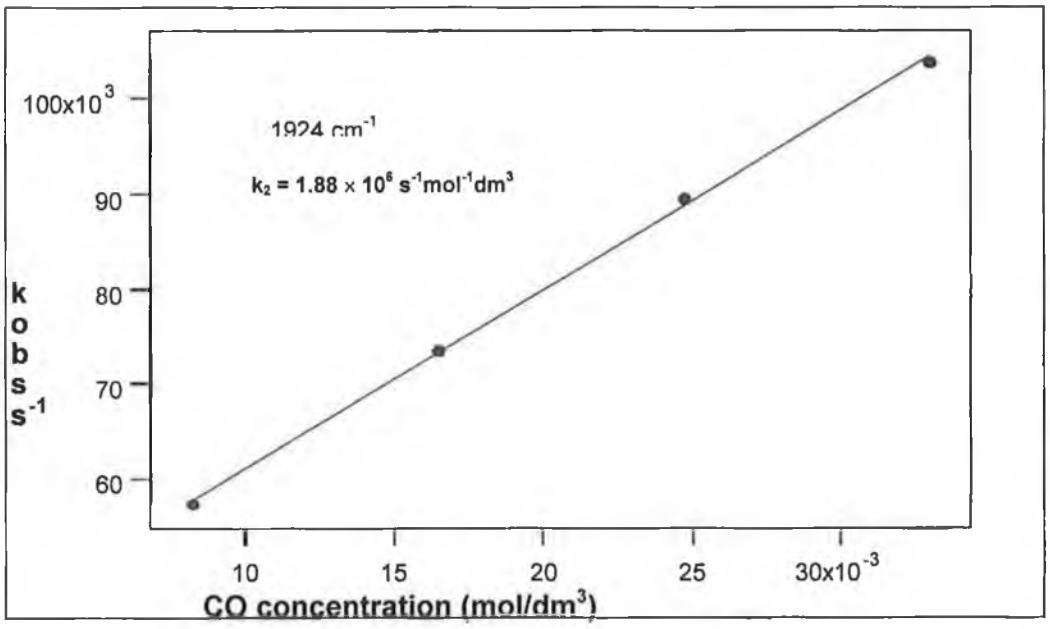

Figure 3.7.5 Plot of k_{obs} versus CO concentration at 1924cm^{-1} following 266nm excitation, for the reaction of $(\eta^5\text{-}C_4H_4s)Cr(CO)_2$(heptane) with CO.

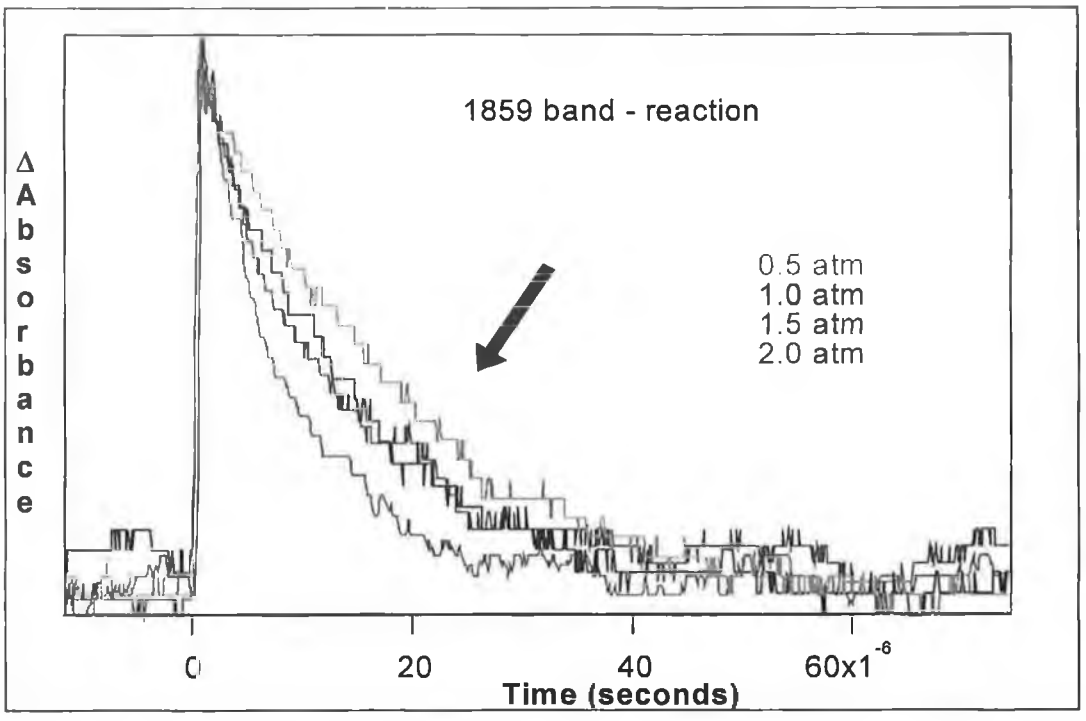

Figure 3.7.6 The kinetic trace observed at 1859 cm^{-1} following excitation of $(\eta^5\text{-}C_4H_4S)Cr(CO)_3$ at 266nm under various concentrations of CO in heptane.

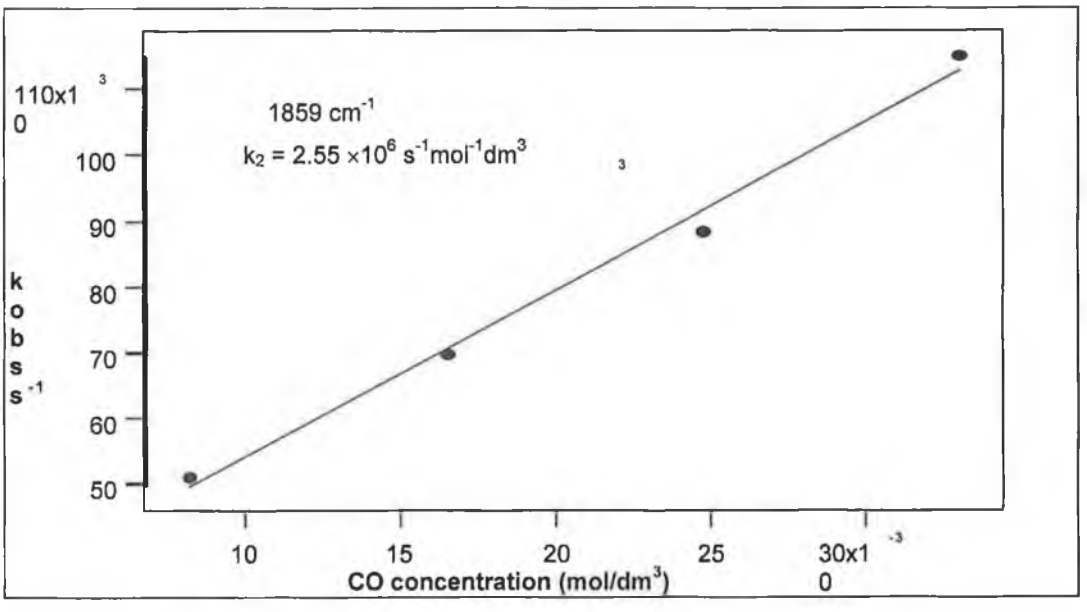

Figure 3.7.7 Plot of k_{obs} versus CO concentration at 1859 cm^{-1} following 266nm excitation, for the reaction of $(\eta^5\text{-}C_4H_4S)Cr(CO)_2$(heptane) with CO.

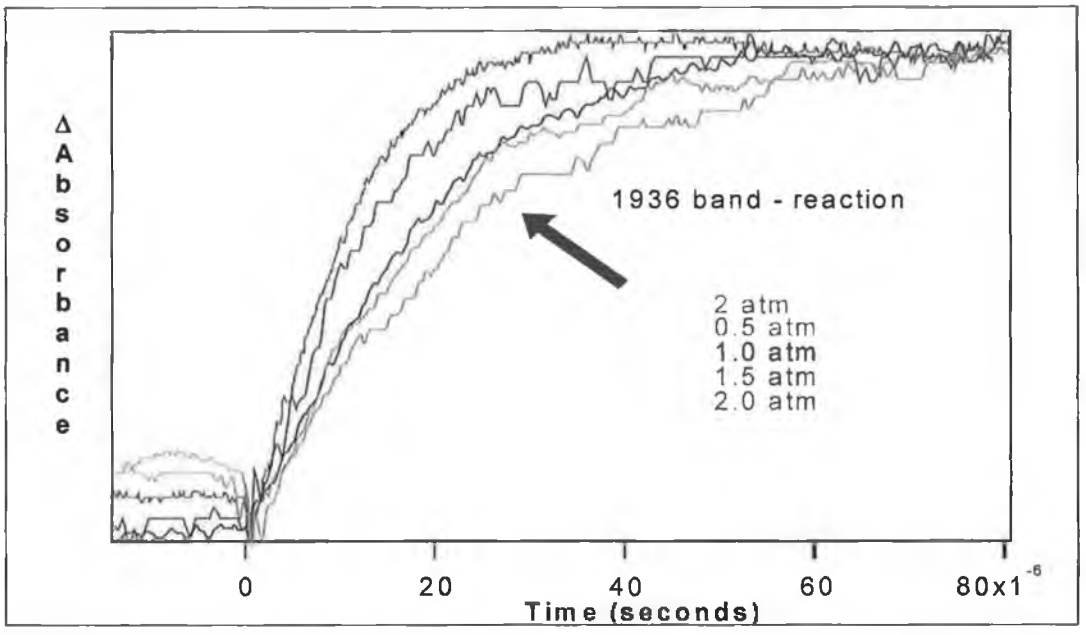

Figure 3.7.8 The kinetic traces observed at 1936cm^{-1} following excitation at 266nm under various concentrations of CO in heptane for (η^5-C_4H_4S)Cr(CO)$_3$.

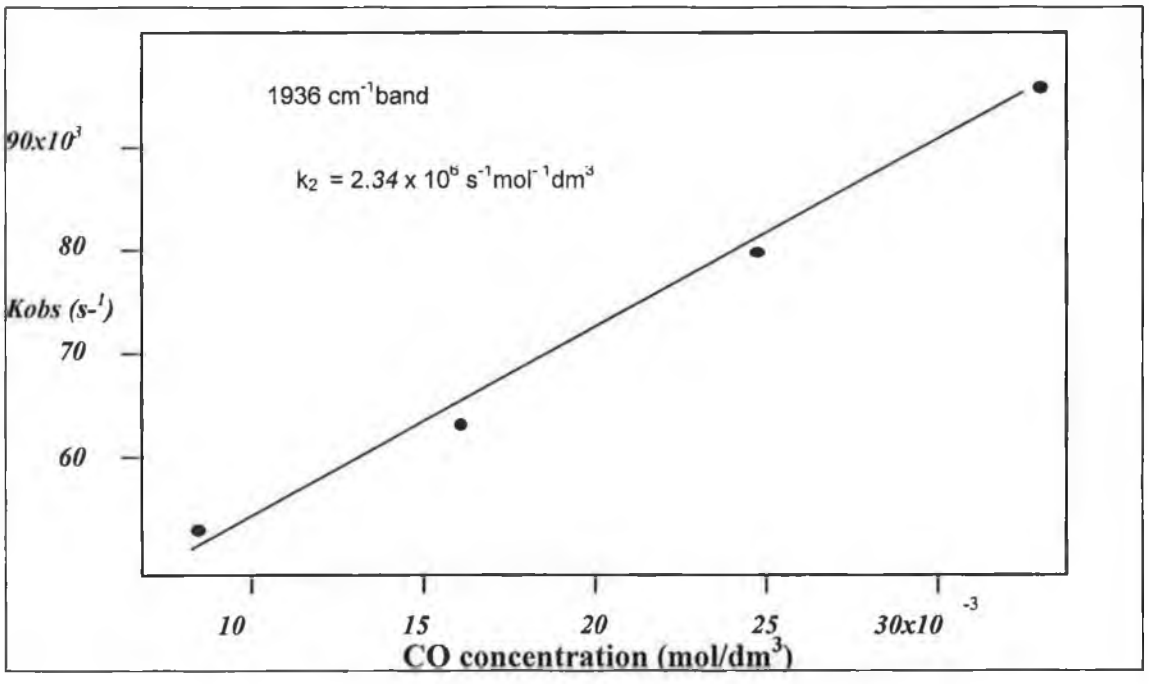

Figure 3.7.9 Plot of k_{obs} versus CO concentration at 1936 cm^{-1} following excitation at 266nm, for the reaction of (η^5-C_4H_4S)Cr(CO)$_2$(heptane) with CO.

3.8 Matrix isolation experiments on $(\eta^5\text{-}C_4H_4S)Cr(CO)_3$ with IR detection

Nitrogen matrix

The photochemistry of $(\eta^5\text{-}C_4H_4S)Cr(CO)_3$ was investigated in nitrogen and carbon monoxide doped argon matrices. The photochemistry was initially investigated in a nitrogen matrix at 12 K with various excitation wavelengths. Upon photolysis at $\lambda >$ 500nm, > 400nm, > 340nm or > 300nm, no changes were observed in the IR spectrum. However, upon high energy photolysis using the xenon arc lamp (no filters), the parent bands at 1979, 1912 and 1888 cm^{-1} decreased in intensity with formation of five new carbonyl bands at 1972, 1932, 1895, 1881 and 1863 cm^{-1}. In addition new bands were also observed at 2185, 2154 and 2139 cm^{-1}. The IR difference spectra are shown in Figure 3.8.1, where the depletion of the parent bands occur as negative peaks and product bands as positive peaks.

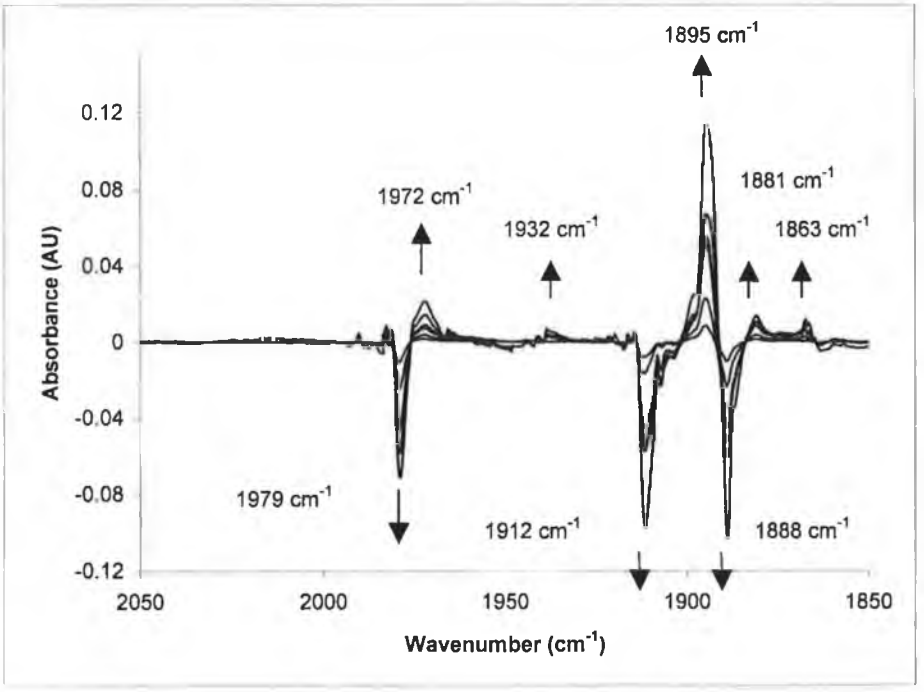

Figure 3.8.1 Spectral changes in the carbonyl region for $(\eta^5\text{-}C_4H_4S)Cr(CO)_3$ following irradiation for 7 hours with a xenon arc lamp in a nitrogen matrix at 12K.

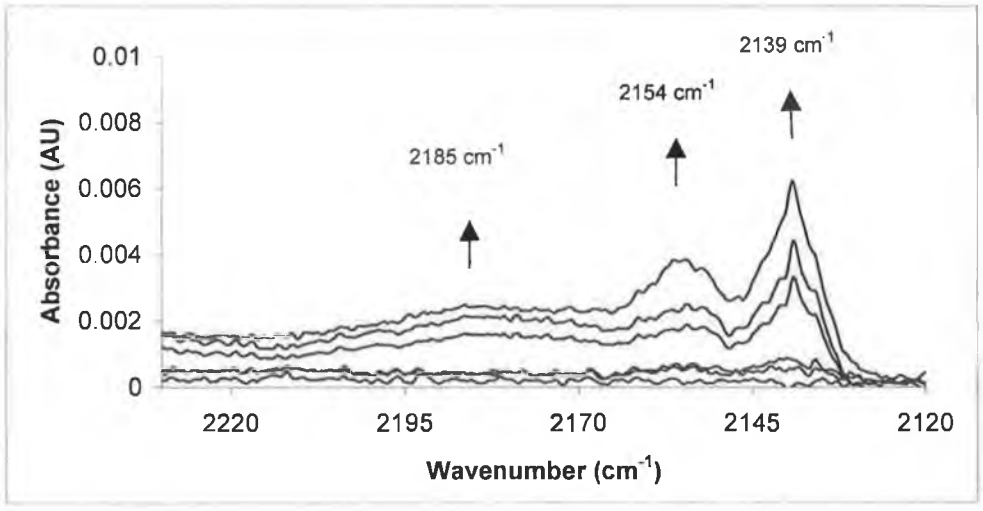

Figure 3.8.2 Spectral changes observed following photolysis of $(\eta^5\text{-}C_4H_4S)Cr(CO)_3$ in a nitrogen matrix at 12K after 7 hours with a xenon arc lamp. Free CO is evident at 2139 cm^{-1} and two $\nu(N{\equiv}N)$ stretches at 2185 and 2154 cm^{-1}.

The number of CO bands for this system is related to the number of carbonyl groups present in the photofragment. The two bands at 1972 and 1881 cm^{-1} in a N_2 matrix are similar in wavenumber (1960, 1886 cm^{-1}) to the bands observed after 800 ns using point by point TRIR following excitation at λ_{exc} = 266 nm of $(\eta^5\text{-}C_4H_4S)Cr(CO)_3$ in CO saturated heptane. These bands have previously been assigned to $(\eta^4\text{-}C_4H_4S)Cr(CO)_3$(heptane). Presumably, the third band is possibly obscured by the parent band at 1888 cm^{-1} in the matrix experiment, as was also suggested in the TRIR experiments. Therefore the bands in the matrix at 1972 and 1881 cm^{-1} are assigned to the $(\eta^4\text{-}C_4H_4S)Cr(CO)_3(N_2)$ species, with the $\nu(N{\equiv}N)$ stretch at 2185 cm^{-1}. These bands are assigned to the $(\eta^4\text{-}C_4H_4S)Cr(CO)_3(N_2)$ on the basis that they occur at a similar frequency to the bands observed for *fac* – $(\eta^4$-norboradiene$)Cr(CO)_3(N_2)$ (2207 $\nu(N{\equiv}N)$ and ν_{co} at 1988 and 1902 cm^{-1}).[27]

In addition there are further carbonyl bands at 1932 and 1867 cm^{-1}, evidence for free CO at 2139 cm^{-1} and a $\nu(N{\equiv}N)$ stretch at 2154 cm^{-1}. These ν_{co} at 1932 and 1867 cm^{-1} have been assigned to the dicarbonyl species, $(\eta^5\text{-}C_4H_4S)Cr(CO)_2(N_2)$.

2 % CO matrix

The photochemistry of $(\eta^5\text{-}C_4H_4S)Cr(CO)_3$ was also investigated in an 2% CO/ 98% argon matrix. Again, no changes were observed upon photolysis at $\lambda_{exc} > 500nm$, > 400nm, > 340nm or > 300nm. Upon photolysis with a xenon arc lamp, depletion of the parent bands (represented by the negative peaks) at 1978, 1907 and 1886 cm^{-1} and formation of bands (represented by the positive peaks) at 1986, 1979, 1911 and 1895 cm^{-1} were observed. It is possible that upon photolysis the $Cr(CO)_3$ unit rotates from a staggered formation with respect to the thiophene ring, to a eclipsed form. Therefore the bands at 1979, 1911 and 1895 cm^{-1} are assigned to the formation of a rotomer. Again no assignment can be made to the band at 1895 cm^{-1}. Prolonged photolysis, produced a band at 1986 cm^{-1} which corresponds to the formation of $Cr(CO)_6$. This photoreaction corresponds with what was observed upon photolysis of $(\eta^5\text{-}C_4H_4S)Cr(CO)_3$ using a xenon arc lamp in CO saturated cyclohexane.

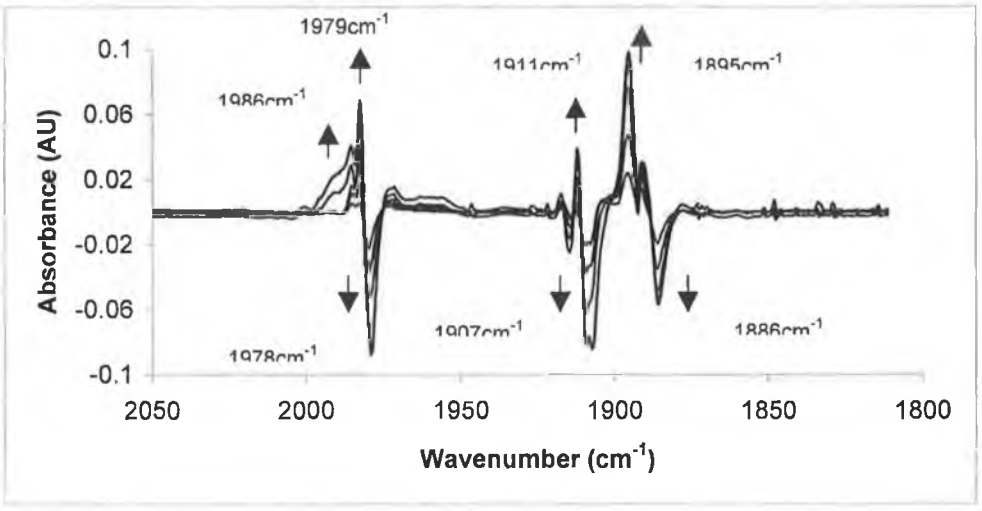

Figure 3.8.5 Spectral changes observed in the carbonyl region following photolysis of $(\eta^5\text{-}C_4H_4S)Cr(CO)_3$ in a 2% / 98% carbon monoxide / argon matrix, at 12K after 3 hours, with the xenon arc lamp.

3.9 UV/vis flash photolysis of $(\eta^5\text{-}C_4H_4S)Cr(CO)_3$ at λ_{exc} = 266 nm and 355 nm

The photochemistry of $(\eta^5\text{-}C_4H_4S)Cr(CO)_3$ was investigated by UV/vis flash photolysis at both 266 nm and 355 nm in cyclohexane and in the presence of either CO or argon. Following flash photolysis at both λ_{exc} = 266 or 355 nm in CO saturated cyclohexane only one signal was observed at 420 nm. Figures 3.9.1 and 3.9.2 depict the recovery observed under different concentrations of CO.

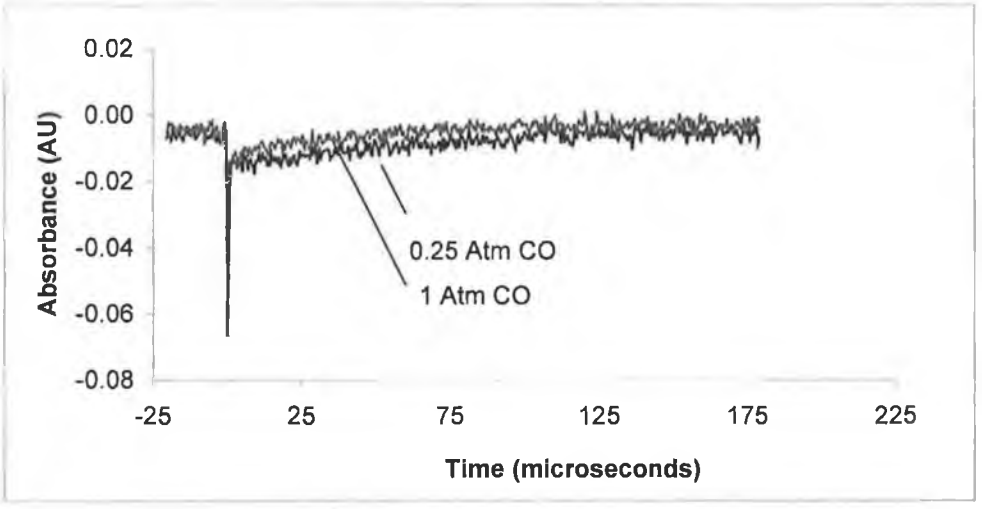

Figures 3.9.1 Transient signals at 420 nm observed following laser flash photolysis of $(\eta^5\text{- } C_4H_4S)Cr(CO)_3$ at 266 nm in cyclohexane in the presence of 0.25 and 1 atmospheres of CO.

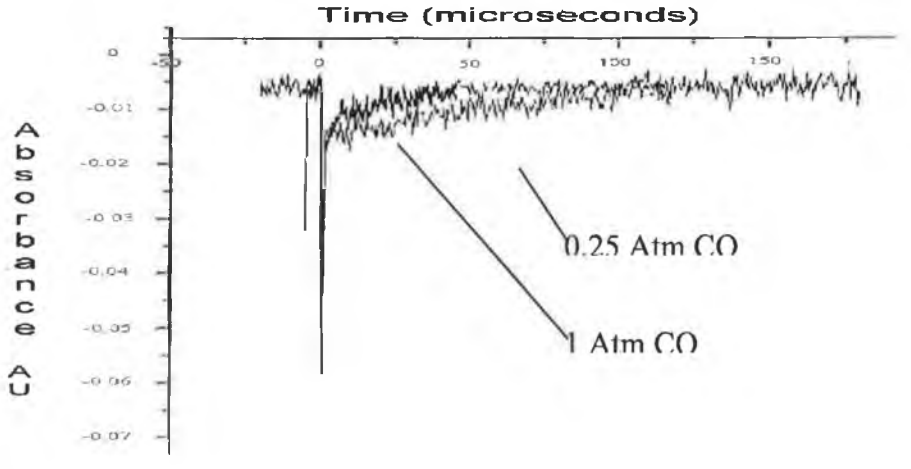

Figures 3.9.2 Transient signals observed at 420 nm following laser flash photolysis of $(\eta^5\text{-}C_4H_4S)Cr(CO)_3$ at 355 nm in the presence of 0.25 and 1 atmosphere of CO in cyclohexane.

The signal at 420 nm is thought to represent the depletion of the parent compound. Analysis of the kinetic parameters associated with the recovery at 420 nm proved difficult, as the signal was too weak to accurately measure the rate of recovery. Upon

increasing the concentration of CO however the lifetime of the signal decreases. Comparison of the kinetic traces of the bands assigned to the solvated dicarbonyl using point by point TRIR at both 266 nm with the signal observed using laser flash photolysis at 266 nm at a specific CO concentration, showed the signals to have a similar lifetime. Therefore this signal has been assigned to the recovery of the parent complex $(\eta^5\text{-}C_4H_4S)Cr(CO)_3$, from the reaction of the solvated dicarbonyl $(\eta^5\text{-}C_4H_4S)Cr(CO)_2$(cyclohexane) with CO. No signals were detected at either λ_{exc} = 266 nm or 355 nm that could be assigned to the $(\eta^4\text{-}C_4H_4S)Cr(CO)_4$ species. The UV/vis spectrum was monitored continuously throughout the flash photolysis experiments at λ_{exc} 355nm in CO saturated cyclohexane with no changes detected. The UV/vis spectrum was also monitored upon laser flash photolysis at λ_{exc} = 266 nm in CO saturated cyclohexane, but this time a 'new' absorption was observed to form in the region 260-300 nm. An IR spectrum recorded on completion of the experiment revealed formation of $Cr(CO)_6$. The changes in the UV/vis spectrum were the same as those recorded upon photolysis of $(\eta^5\text{-thiophene})Cr(CO)_3$ using a xenon arc lamp, Figure 3.9.3.

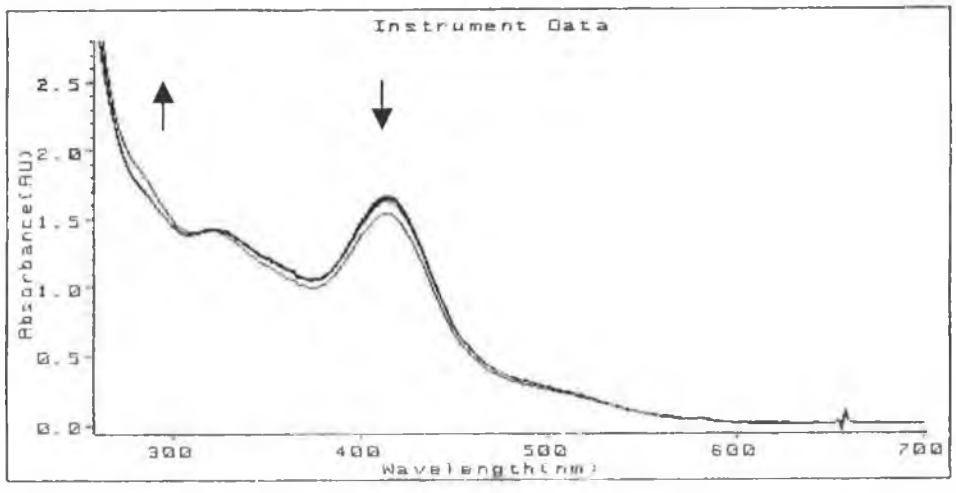

Figure 3.9.3 UV/vis changes recorded following laser flash photolysis of $(\eta^5\text{-}C_4H_4S)Cr(CO)_3$ at λ_{exc} =266 nm in CO saturated cyclohexane.

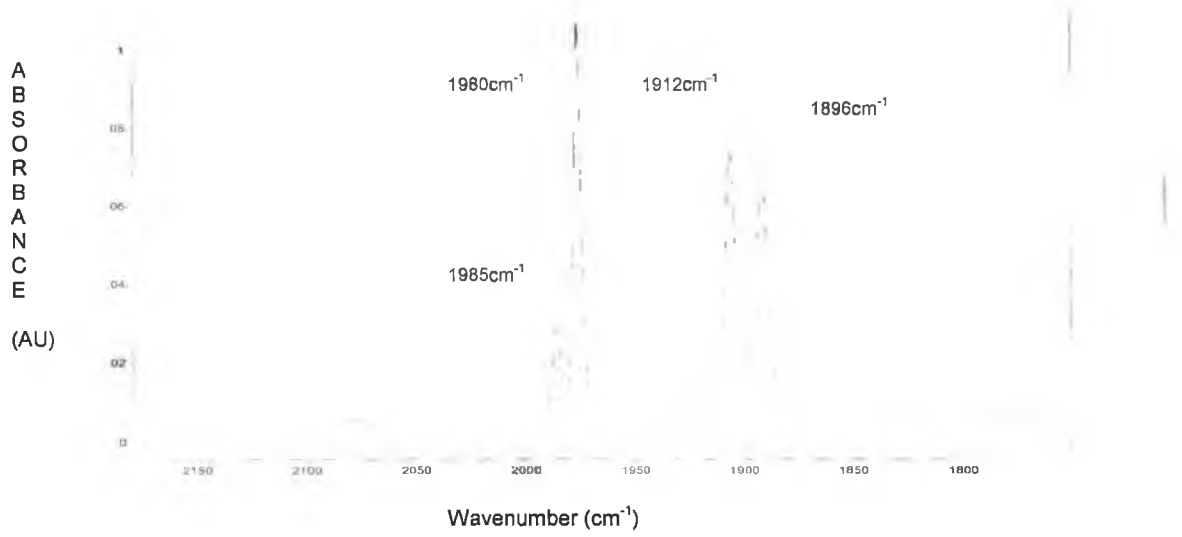

Figure 3.9.4 IR spectrum recorded following laser flash photolysis of $(\eta^5\text{-}C_4H_4S)Cr(CO)_3$ at $\lambda_{exc} = 266$ nm in CO saturated cyclohexane. $(\eta^5\text{-}C_4H_4S)Cr(CO)_3$ ν_{co} : 1981,1912 and 1896 cm^{-1}, $Cr(CO)_6$ ν_{co} : 1985 cm^{-1}.

3.10 Spectroscopic parameters for $(\eta^5\text{-}C_4H_4Se)Cr(CO)_3$

The spectroscopic parameters for $(\eta^5\text{-}C_4H_4Se)Cr(CO)_3$ are given in Table 3.9.1. The UV/vis spectrum of $(\eta^5\text{-}C_4H_4Se)Cr(CO)_3$ is shown in Figures 3.9.1. For the $(\eta^5\text{-}C_4H_4Se)Cr(CO)_3$ complex, three bands are observed at 515, 425, and 373 nm. One of the most stark differences between $(\eta^5\text{-}C_4H_4S)Cr(CO)_3$ and the $(\eta^5\text{-}C_4H_4Se)Cr(CO)_3$, is that the $(\eta^5\text{-}C_4H_4Se)Cr(CO)_3$ complex absorbs much further into the visible region.

Three absorption bands are observed in the IR region, as the $(\eta^5\text{-}C_4H_4Se)Cr(CO)_3$ complex has C_s symmetry. For $(\eta^5\text{-}C_4H_4Se)Cr(CO)_3$ compared to $(\eta^5\text{-}C_4H_4S)Cr(CO)_3$ the shift of the ν_{co} bands to a higher frequency is indicative of decreased electron density on the metal centre which leads to a decreased population of CO antibonding orbitals thus increasing the CO bond order and the ν_{co}. This would indicate that C_4H_4S is a better donor ligand than C_4H_4Se in the η^5-binding mode. The ^1H

nuclear NMR data for $(\eta^5\text{-}C_4H_4S)Cr(CO)_3$ and $(\eta^5\text{-}C_4H_4Se)Cr(CO)_3$ are shown in Table 3.10.1.[22]

Complex	UV/vis λ_{max} nm	IR bands cm^{-1}	^1H NMR ppm
$(\eta^5\text{-}C_4H_4Se)Cr(CO)_3$	515	1983	H_2 5.95
	425	1916	H_3 5.79
	373	1894	H_4 5.79
			H_5 5.95

Table 3.10.1 Spectroscopic parameters of $(\eta^5\text{-}C_4H_4Se)Cr(CO)_3$ 3. UV/vis and IR spectra were recorded in cyclohexane, with the NMR spectra obtained in $CDCl_3$.

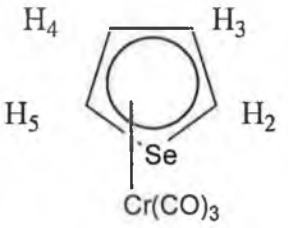

Figure 3.10.1 NMR numbering pattern for $(\eta^5\text{-}C_4H_4Se)Cr(CO)_3$.

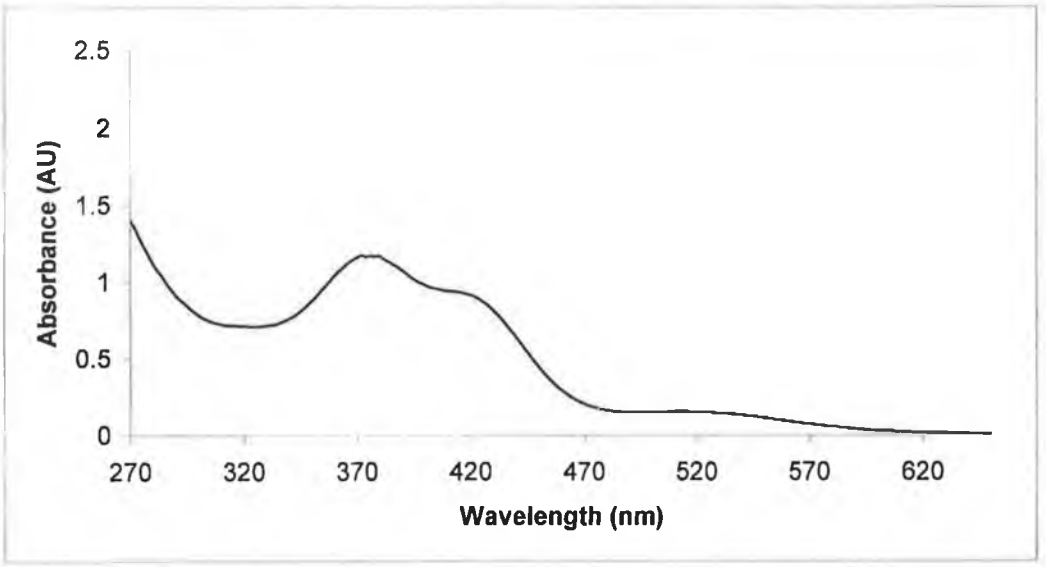

Figure 3.10.1 The UV/vis spectrum of $(\eta^5\text{-}C_4H_4Se)Cr(CO)_3$ recorded in cyclohexane.

3.11 UV/vis, IR and NMR monitored steady state photolysis of $(\eta^5\text{-}C_4H_4Se)Cr(CO)_3$

UV/vis monitored photolysis of $(\eta^5\text{-}C_4H_4Se)Cr(CO)_3$ in CO saturated cyclohexane at λ_{exc} = 355nm resulted in a grow in of a band from 270 – 330 nm and depletion of the parent bands in the region 330 – 570 nm. No spectral changes were recorded upon lower energy photolysis (i.e at λ_{exc} > 500nm or > 400nm). An IR spectrum recorded after photolysis revealed new bands a number of new bands at 2014, 1985, 1956 and 1914 cm^{-1}, in addition to the parent bands at 1983, 1916 and 1894 cm^{-1}. The assignment of a band formed at 1914 $cm^{-1}$is based on the fact that the parent band at 1914 cm^{-1} is not of the same intensity as the band at 1894 cm^{-1}. The band at 1985 cm^{-1} is assigned to $Cr(CO)_6$. The three new IR bands in the carbonyl region at 2014, 1956 and 1914 cm^{-1} are shifted to a higher frequency than the IR bands in the parent compound, $(\eta^5\text{-}C_4H_4Se)Cr(CO)_3$. These bands are assigned to the $(\eta^4\text{-}C_4H_4Se)Cr(CO)_4$ species. This assignment is based on comparison of the IR bands at 2014, 1956 and 1916 cm^{-1} in the carbonyl region, to the IR bands in the carbonyl region of other chromium tetracarbonyl species. For other chromium tetracarbonyl species such as $(\eta^4$-hexamethylbicyclo [2.2.0] hexadiene$)Cr(CO)_4$ and $(\eta^4$-noraboradiene$)Cr(CO)_4$ the IR bands in the carbonyl region occur at 2025, 1940, 1900 cm^{-1} and 2032, 1960, 1946 and 1915 cm^{-1} respectively.[23,24]

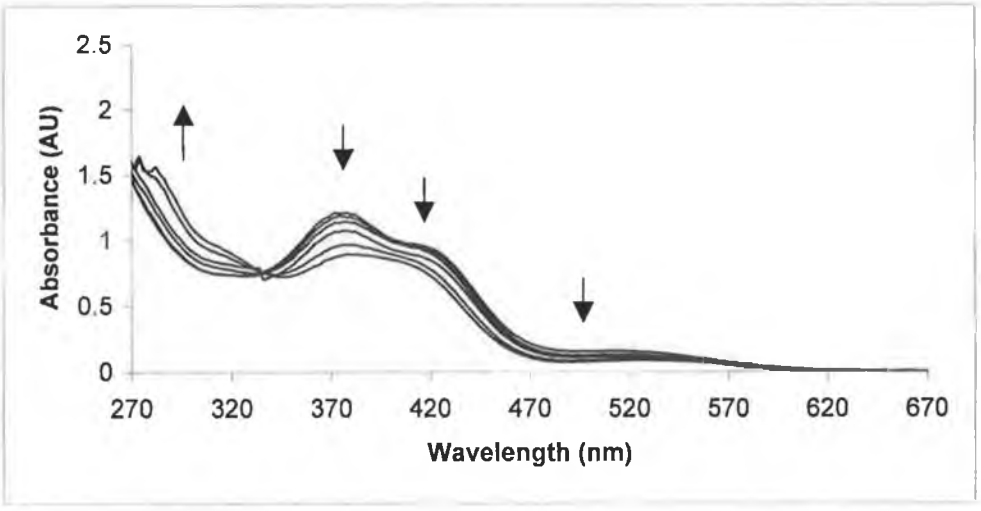

Figure 3.11.1 The UV/vis spectra recorded following photolysis of $(\eta^5\text{-}C_4H_4Se)Cr(CO)_3$ at λ_{exc} = 355 nm in CO saturated cyclohexane over a period of 4.5 minutes.

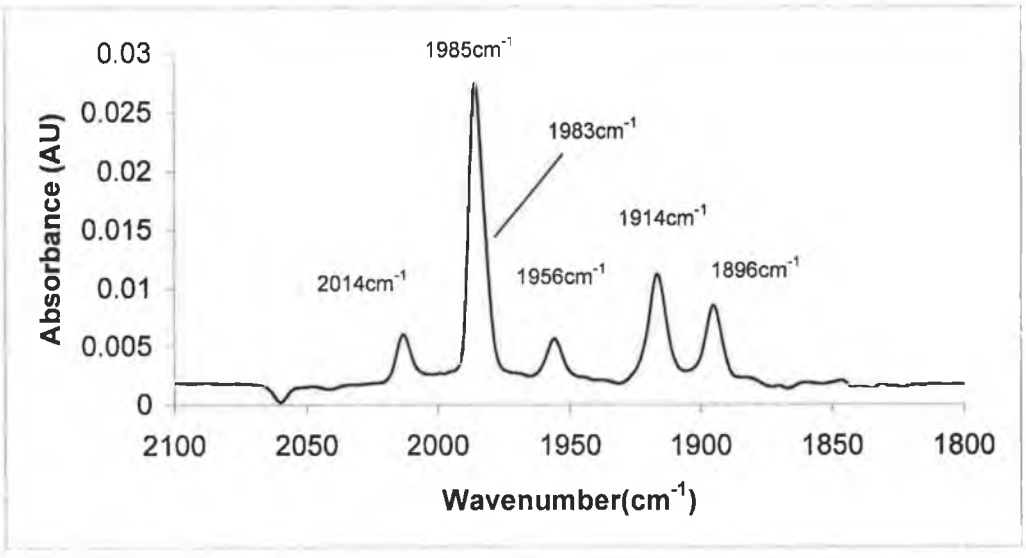

Figure 3.11.2 An IR spectrum recorded after photolysis of $(\eta^5\text{-}C_4H_4Se)Cr(CO)_3$ at λ_{exc} = 355nm in CO saturated cyclohexane over a period of 4.5 minutes.
$(\eta^5\text{-}C_4H_4Se)Cr(CO)_3$ ν_{co} : 1983, 1916 and 1894 cm^{-1}. $Cr(CO)_6$ ν_{co}: 1985 cm^{-1}.
$(\eta^4\text{-}C_4H_4Se)Cr(CO)_4$ ν_{co} : 2014, 1956 and 1916 cm^{-1}.

IR monitored photolysis of $(\eta^5\text{-}C_4H_4Se)Cr(CO)_3$ at λ_{exc} = 355 nm in CO purged cyclohexane solution, resulted in depletion of the parent bands at 1983, 1916 and 1894 cm^{-1}, and the grow in of bands at 1985 cm^{-1} ($Cr(CO)_6$) and formation of three bands at 2014, 1956 and 1916 cm^{-1} which were assigned to $(\eta^4\text{-}C_4H_4Se)Cr(CO)_4$.

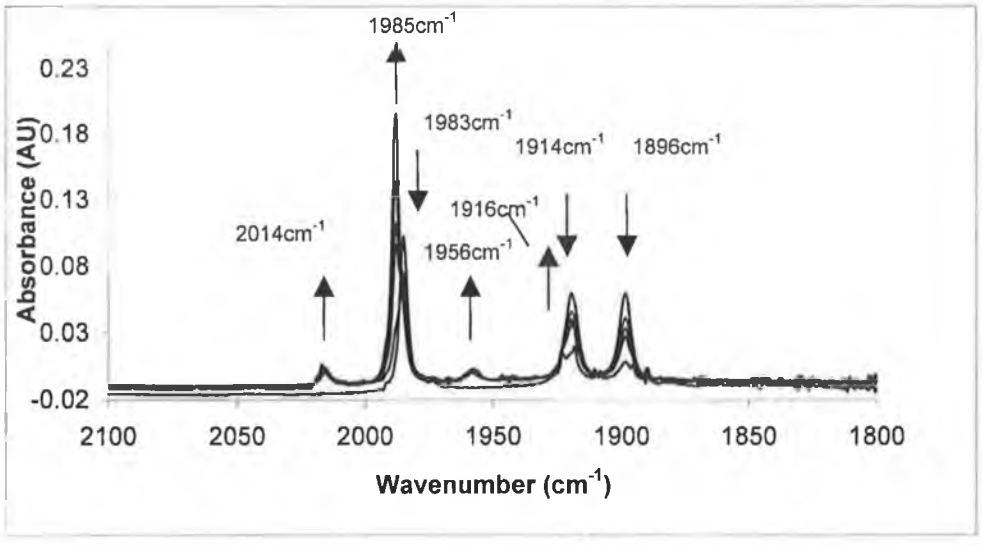

Figure 3.11.3 IR monitored photolysis of $(\eta^5\text{-}C_4H_4Se)Cr(CO)_3$ in CO saturated cyclohexane at λ_{exc} = 355nm for 10 minutes. $(\eta^5\text{-}C_4H_4Se)Cr(CO)_3$ ν_{co} : 1983, 1916 and 1894 cm^{-1}. $Cr(CO)_6$ ν_{co} : 1985 cm^{-1}, $(\eta^4\text{-}C_4H_4Se)Cr(CO)_4$ ν_{co} : 2014, 1956 and 1916 cm^{-1}.

NMR monitored photolysis of the $(\eta^5\text{-}C_4H_4Se)Cr(CO)_3$ complex was carried out at λ_{exc} > 340 nm in CO saturated C_6D_{12}. The bands at 5.5 and 5.4 ppm are due to $(\eta^5\text{-}C_4H_4Se)Cr(CO)_3$. The bands at 7.54 and 7.36 ppm are due to free C_4H_4Se which was initially produced by stray light photolysis. Upon photolysis at λ_{exc} > 340nm the parent bands at 5.5 and 5.4 ppm decrease in intensity while the bands at 7.54 and 7.36 ppm (free C_4H_4Se) increase in intensity with two other new bands at 7.9 and 7.1 ppm. On completion of the experiment, the solvent was removed, leaving an orange residue. The orange residue was dissolved in pentane and an IR spectrum was recorded. Bands were observed in the carbonyl region of the IR spectrum at 1983, 1916 and 1899 cm^{-1} $(\eta^5\text{-}C_4H_4Se)Cr(CO)_3$, 1985$cm^{-1}$ $Cr(CO)_6$ and 2014, 1956 and 1914 cm^{-1}

(η^4-C_4H_4Se)$Cr(CO)_4$. The NMR bands at 7.9 and 7.1 ppm are thought to possibly relate to the latter species, (η^4-C_4H_4Se)$Cr(CO)_4$, which has IR bands in the carbonyl region at 2014, 1955 and 1914 cm^{-1}.

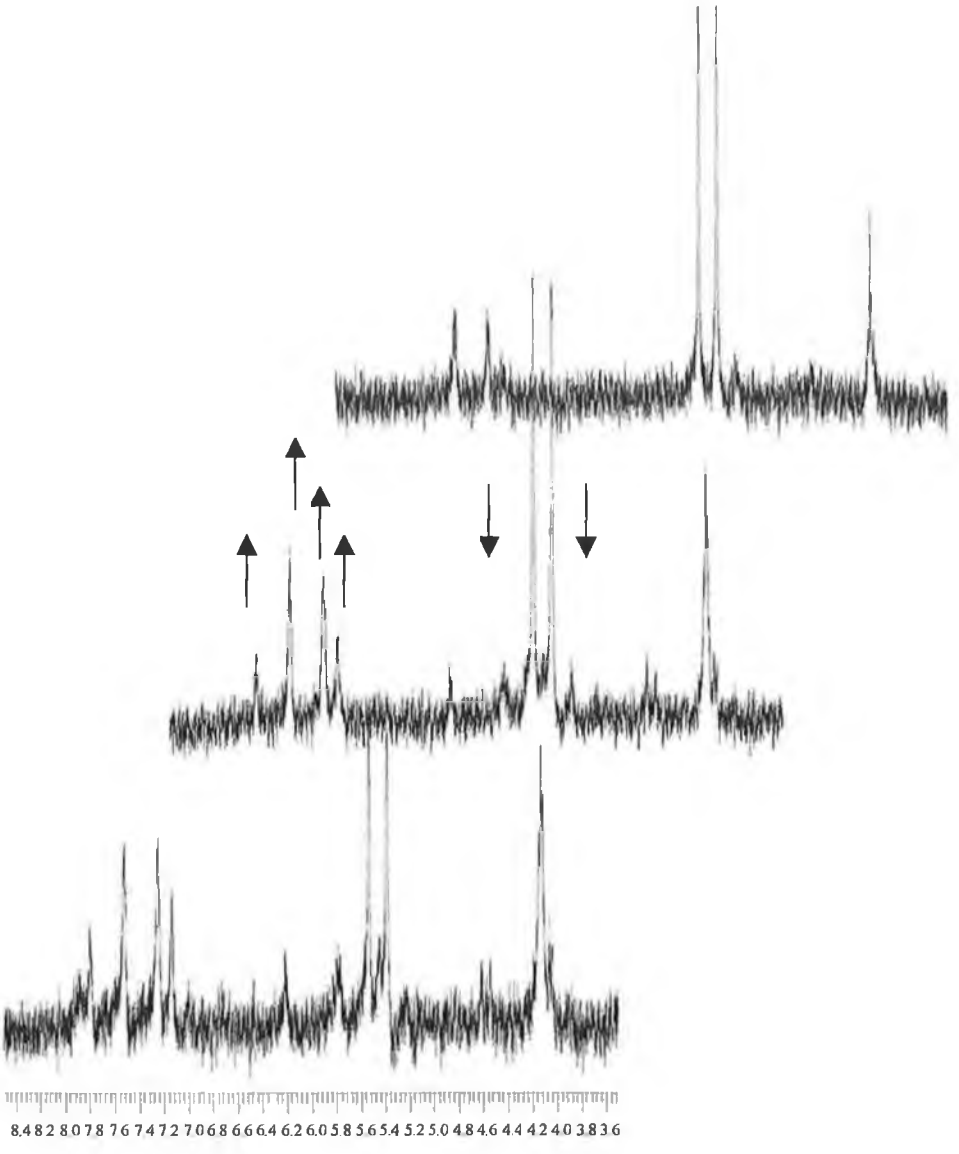

Figure 3.11.4 Photolysis of (η^5-C_4H_4Se)$Cr(CO)_3$ in CO saturated deuterared cyclohexane at $\lambda_{exc} > 340nm$ over 50 minutes. (η^4-C_4H_4Se)$Cr(CO)_4$. : 7.9 and 7.1 ppm (η^5-C_4H_4Se)$Cr(CO)_3$: 5.5 and 5.4 ppm, (η^4-C_4H_4Se)$Cr(CO)_4$. : 7.9 and 7.1 ppm, C_4H_4Se : 7.54 and 7.36 ppm.

Photolysis of $(\eta^5\text{-}C_4H_4Se)Cr(CO)_3$ was also carried out at λ_{exc} = 355 nm in the presence of a trapping ligand (5 times molar excess of pyridine). Figure 3.11.5, shows the spectral changes observed upon photolysis the UV/vis at λ_{exc} = 355 nm. An increase in absorption was observed between 323 – 363 nm and in the region 400 – 447 nm, with a depletion of the parent absorption at 373 nm. An IR spectrum of the solution recorded at the end of the experiment revealed new bands at 1974, 1920, 1859 and 1854 cm^{-1}. The bands at 1920 and 1859cm^{-1} are assigned to the formation of the dicarbonyl species, $(\eta^5\text{-}C_4H_4Se)Cr(CO)_2(\eta^1\text{-}C_5H_5N)$, Reaction 3.11.1.

$$(\eta^5\text{-}C_4H_4Se)Cr(CO)_3 \xrightarrow[C_5H_5N]{h\nu} (\eta^5\text{-}C_4H_4Se)Cr(CO)_2(\eta^1\text{-}C_5H_5N) \qquad \text{Reaction 3.11.1.}$$

While the bands at 1974 and 1854 cm^{-1} are tentatively assigned to the $(\eta^4\text{-}C_4H_4Se)Cr(CO)_3(\eta^1\text{-}C_5H_5N)$ species, Reaction 3.11.2.

$$(\eta^5\text{-}C_4H_4Se)Cr(CO)_3 \xrightarrow[C_5H_5N]{h\nu} (\eta^4\text{-}C_4H_4Se)Cr(CO)_3(\eta^1\text{-}C_5H_5N) \qquad \text{Reaction 3.11.2.}$$

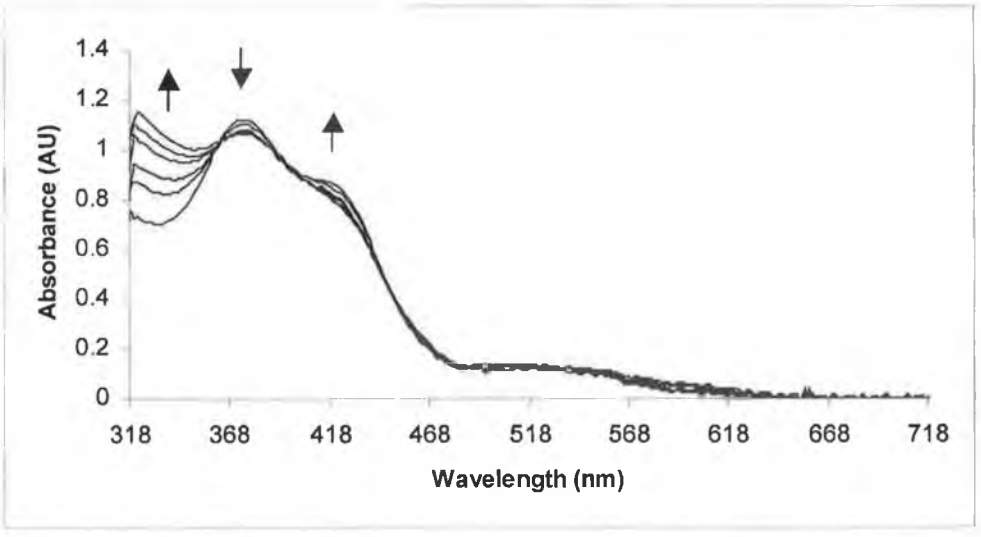

Figure 3.11.5 UV/vis changes observed upon photolysis of $(\eta^5\text{-}C_4H_4Se)Cr(CO)_3$ 2.2×10^{-4} M in cyclohexane at $\lambda_{exc} = 355$ nm for 2.5 minutes containing a 5 times molar excess of pyridine 1.1×10^{-3} M .

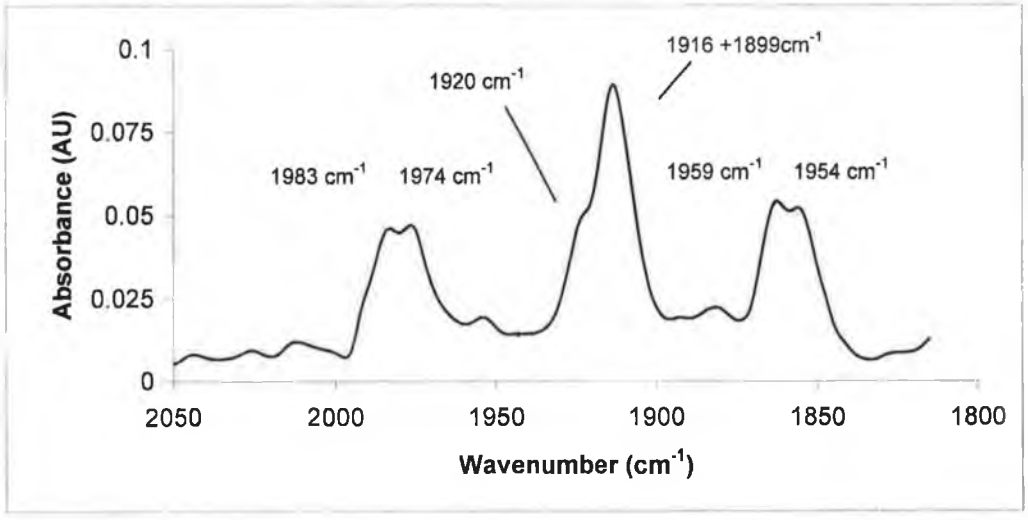

Figure 3.11.6 An IR spectrum recorded upon photolysis of $(\eta^5\text{-}C_4H_4Se)Cr(CO)_3$ 2.2×10^{-4} M in cyclohexane at $\lambda_{exc} = 355$ nm for 2.5 minutes containing a 5 times molar excess of pyridine 1.1×10^{-3} M . $(\eta^5\text{-}C_4H_4Se)Cr(CO)_3$ ν_{co} : 1983 cm^{-1}, 1912 and 1896, $(\eta^5\text{-}C_4H_4Se)Cr(CO)_2(\eta^1\text{-}C_5H_5N)$ ν_{co} : 1920 and 1859 cm^{-1} and $(\eta^4\text{-}C_4H_4Se)Cr(CO)_3(\eta^1\text{-}C_5H_5N)$ ν_{co} : 1974 and 1854 cm^{-1}.

3.12 TRIR spectroscopy experiments on $(\eta^5\text{-}C_4H_4Se)Cr(CO)_3$

The photochemistry of $(\eta^5\text{-}C_4H_4Se)Cr(CO)_3$ was investigated in a CO saturated heptane solution and monitored by step scan TRIR spectroscopy at λ_{exc} = 355 nm excitation (Figure 3.12.1).

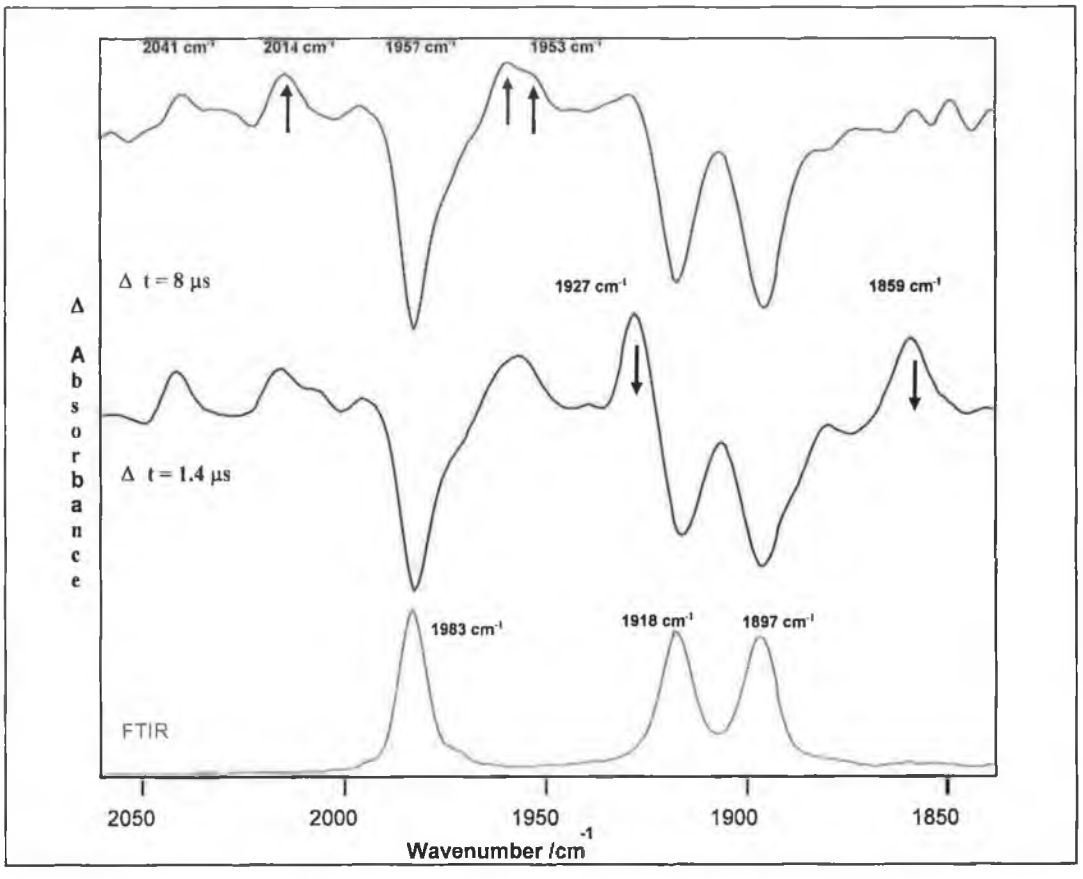

Figure 3.12.1 The step can TRIR spectrum collected at 1.4 and 8 μs following λ_{exc} = 355 nm in CO saturated heptane of $(\eta^5\text{-}C_4H_4Se)Cr(CO)_3$.

The negative peaks at 1983, 1918 and 1897 cm^{-1} are assigned to the depletion of the parent complex. Approximately 1.4 μs after excitation, eight bands are observed at 2041, 2015, 2003, 1957, 1953,1927 and 1859 cm^{-1} and a band at 1918 cm^{-1} obscured by the parent band in addition to the depletion of the parent bands at 1983,1918 and 1897 cm^{-1}. The two bands at 1927 and 1859 cm^{-1} bands are thought to belong to the $(\eta^5\text{-}C_4H_4Se)Cr(CO)_2$(heptane) species. The kinetic traces of the bands at 1927 and 1859

cm^{-1} are shown in Figures 3.12.3 and 3.12.4. From the plot of k_{obs} (s^{-1}) for the signal at 1927 and 1859 cm^{-1} against concentration of CO (moles/dm^3) the second order rate constant for the reaction of the solvated dicarbonyl with CO was determined to be 5.8 × 10^6 $s^{-1}mol^{-1}dm^3$, Figure 3.11.4.

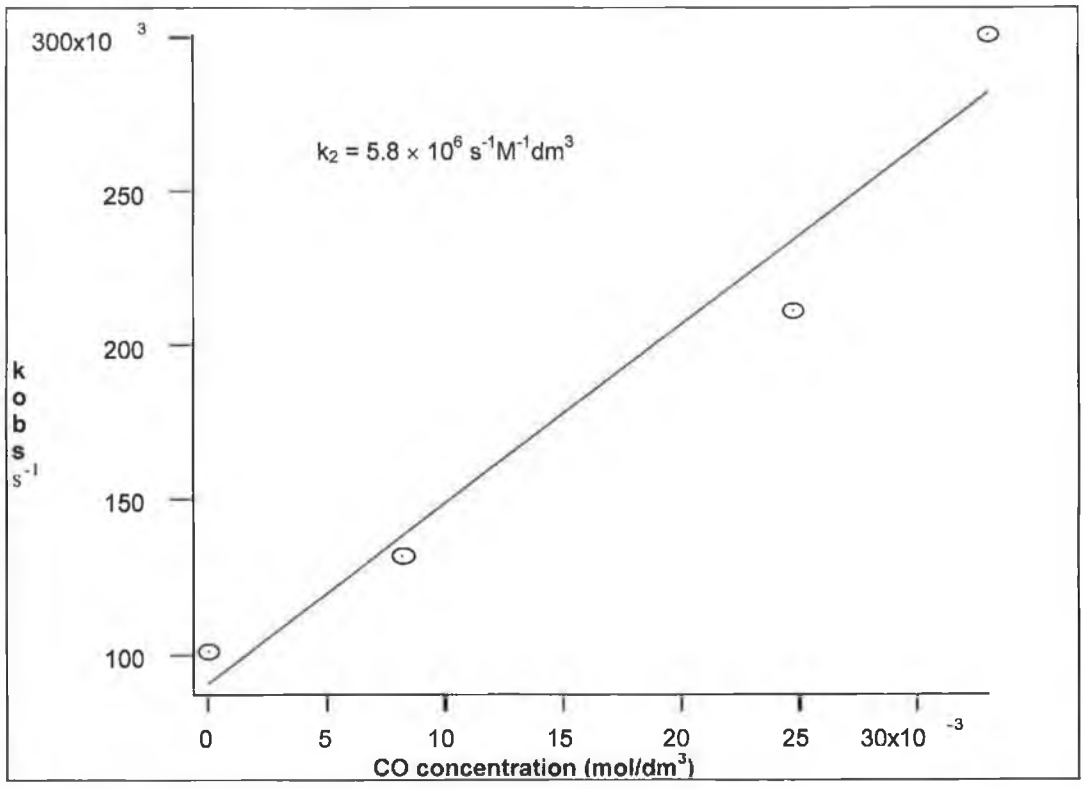

Figure 3.12.2 The kinetic traces observed at 1859 cm^{-1} following excitation at λ_{exc} = 355nm in CO saturated heptane (2 atmospheres) for $(\eta^5\text{-}C_4H_4Se)Cr(CO)_3$.

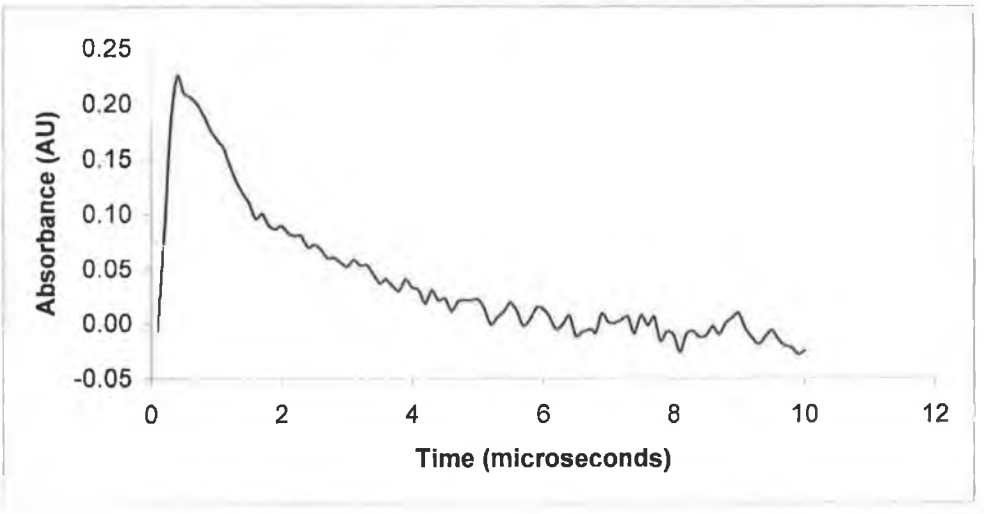

Figure 3.12.3 The kinetic trace observed at 1927 cm^{-1} following excitation at λ_{exc} = 355nm in CO saturated heptane (2 atmospheres) for $(\eta^5\text{-}C_4H_4Se)Cr(CO)_3$.

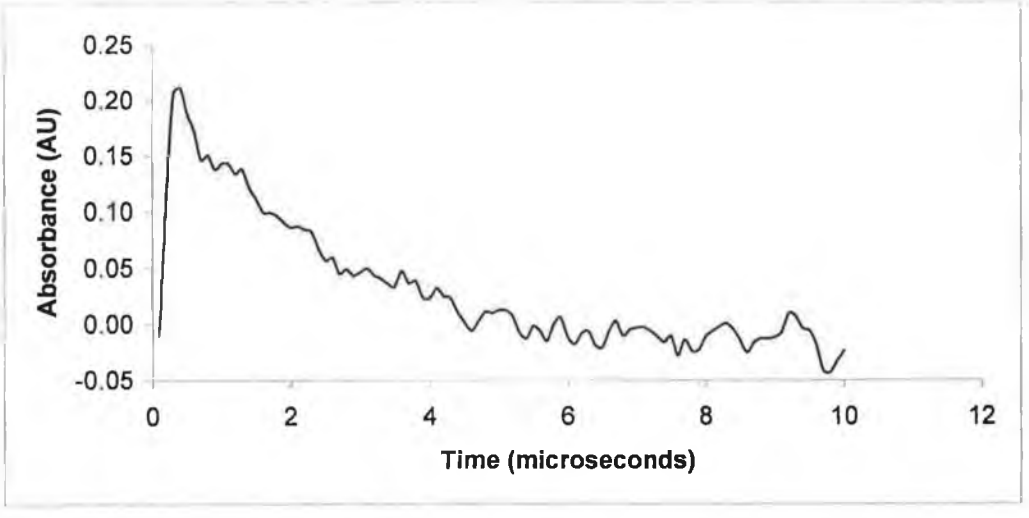

Figure 3.12.4 The kinetic trace observed at 1859 cm^{-1} following excitation at λ_{exc} = 355nm in CO saturated heptane (2 atmospheres) for $(\eta^5\text{-}C_4H_4Se)Cr(CO)_3$.

In addition to the bands observed at 1927 and 1859 cm^{-1}, five further bands were observed at 2041, 2015, 2003 1956, 1953 cm^{-1}. The three bands at 2015, 1956 and a third band at 1918 cm^{-1} is obscured by the parent absorption, are at similar wavenumber to the

bands observed using IR monitored steady state photolysis at $\lambda_{exc} = 355$ nm in CO saturated cyclohexane (2014, 1956 and 1914 cm^{-1}). The three bands at 2014, 1956 and 1914 cm^{-1}, therefore have been assigned to the $(\eta^4\text{-}C_4H_4Se)Cr(CO)_4$ species. In addition to these bands three further bands were observed at 2041, 2003 and 1953 cm^{-1} which were not observed in the steady state experiments. These bands were assigned to either the $(C,Se\text{-}C_4H_4Se)Cr(CO)_3$ or the *endo* – Se $(\eta^4\text{-}C_4H_4Se)Cr(CO)_3$ species.

3.13 Matrix isolation experiments on $(\eta^5\text{-}C_4H_4Se)Cr(CO)_3$ with IR detection

The photochemistry of $(\eta^5\text{-}C_4H_4Se)Cr(CO)_3$ was examined in an argon, a 2% CO doped argon matrix and a nitrogen matrix.

Argon matrix

Photolysis of $(\eta^5\text{-}C_4H_4Se)Cr(CO)_3$ in an argon matrix at $\lambda_{exc} > 500$ nm or 436nm resulted in no changes in the IR spectrum. Photolysis of $(\eta^5\text{-}C_4H_4Se)Cr(CO)_3$ at $\lambda_{exc} = 406$ nm saw depletion of the parent bands at 1987, 1921 and 1898 cm^{-1}, and a grow in of three bands at 2046, 2001 and 1957 cm^{-1}. These changes are shown below in Figure 3.13.1.

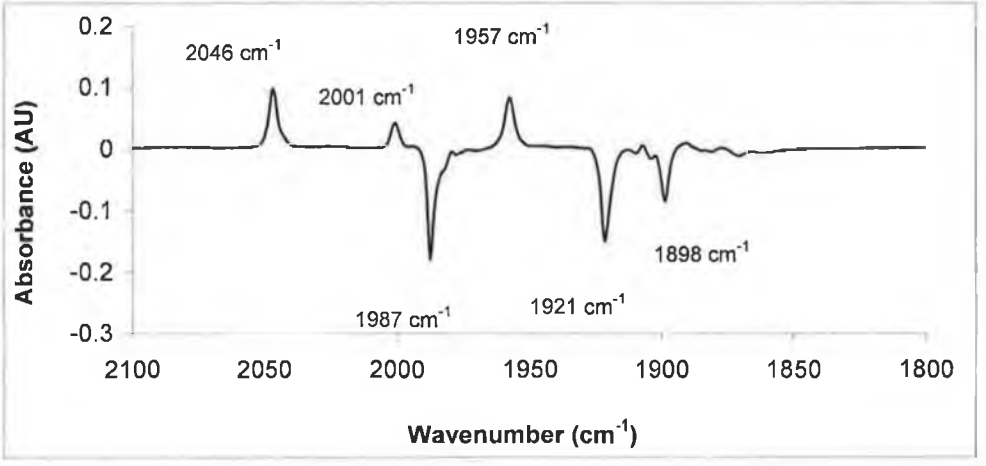

Figure 3.13.1 The difference spectrum in the carbonyl region following photolysis at λ_{exc} = 406 nm (mercury xenon lamp) of $(\eta^5\text{-}C_4H_4Se)Cr(CO)_3$ in an argon matrix at 12K for 150 minutes.

Photolysis at $320 < \lambda_{exc} < 390$ nm resulted in depletion of the bands at 2046, 2001 and 1957 cm^{-1} and the grow in of bands at 2034 and 1932 cm^{-1} along with a band at 2137 cm^{-1}.

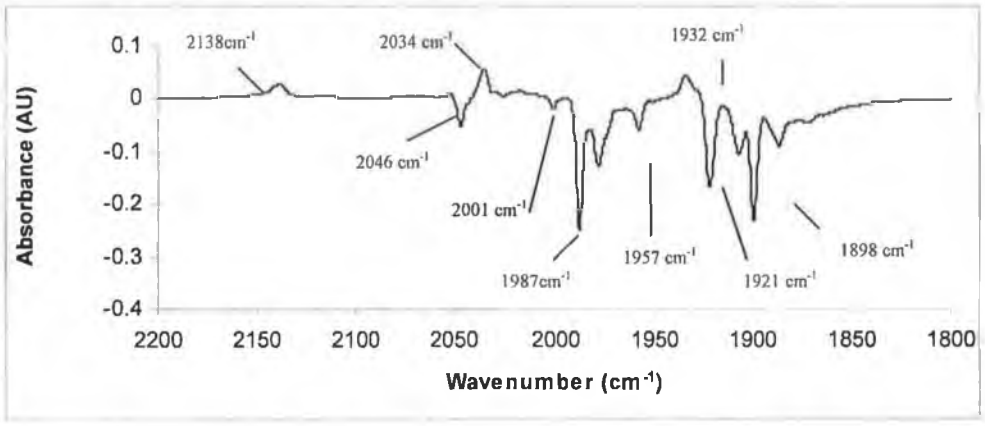

Figure 3.13.2 The difference spectrum in the carbonyl region following photolysis at $320 < \lambda_{exc} < 390$ nm (mercury xenon lamp) for $(\eta^5\text{-}C_4H_4Se)Cr(CO)_3$ in an argon matrix at 12K after 60 minutes.

Nitrogen matrix

The photochemistry of $(\eta^5\text{-}C_4H_4Se)Cr(CO)_3$ was also examined in a nitrogen matrix at 12 K. Again photolysis at $\lambda_{exc} > 500$ nm or 436 nm resulted in no changes. Photolysis of $(\eta^5\text{-}C_4H_4Se)Cr(CO)_3$ at 406 nm saw depletion of the parent bands at 1981, 1914 and 1890 cm^{-1} with formation of new bands at 2001 and 1957 cm^{-1}. An impurity in the nitrogen which absorbed strongly in the region 2035 – 2065 cm^{-1} obscured any band that absorbed in this region. These changes are shown below in Figure 3.13.3.

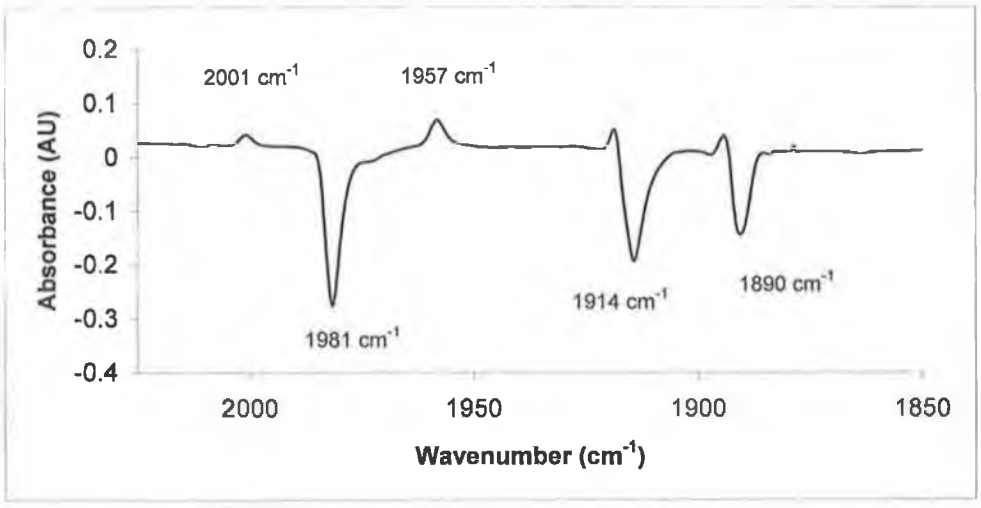

Figure 3.12.3 The difference spectrum of the carbonyl region following photolysis at λ_{exc} 406 nm (mercury xenon lamp) for $(\eta^5\text{-}C_4H_4Se)Cr(CO)_3$ in an nitrogen matrix at 12K after 60 minutes.

2 % CO matrix

The photochemistry of $(\eta^5\text{-}C_4H_4Se)Cr(CO)_3$ was also examined, in a 2%CO / 98% argon matrix at 12 K. Photolysis of $(\eta^5\text{-}C_4H_4Se)Cr(CO)_3$ at λ_{exc} >500nm and 436nm resulted in no changes in the IR spectrum. Upon photolysis at λ_{exc} = 406 nm depletion of the parent bands at 1979, 1910 and 1888 cm^{-1} with simultaneous formation of three bands at 2044, 1997 and 1954 cm^{-1} occurs. These spectral changes are shown in Figure 3.13.4.

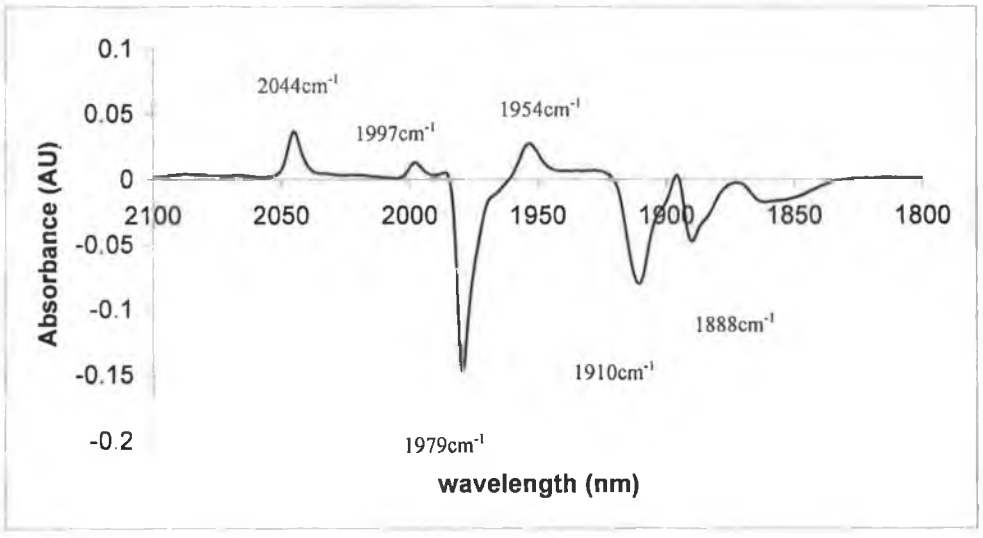

Figure 3.13.4 Spectral changes in the carbonyl region for $(\eta^5\text{-}C_4H_4Se)Cr(CO)_3$ following photolysis (mercury lamp) at λ_{exc} = 406 nm in a 2% / 98% carbon monoxide / argon matrix at 12K after 55 minutes.

Upon broad band photolysis at λ_{exc} >320 nm the bands formed upon photolysis decayed with formation of a new band at 1985 cm^{-1}. These changes are shown in Figure 3.13.5.

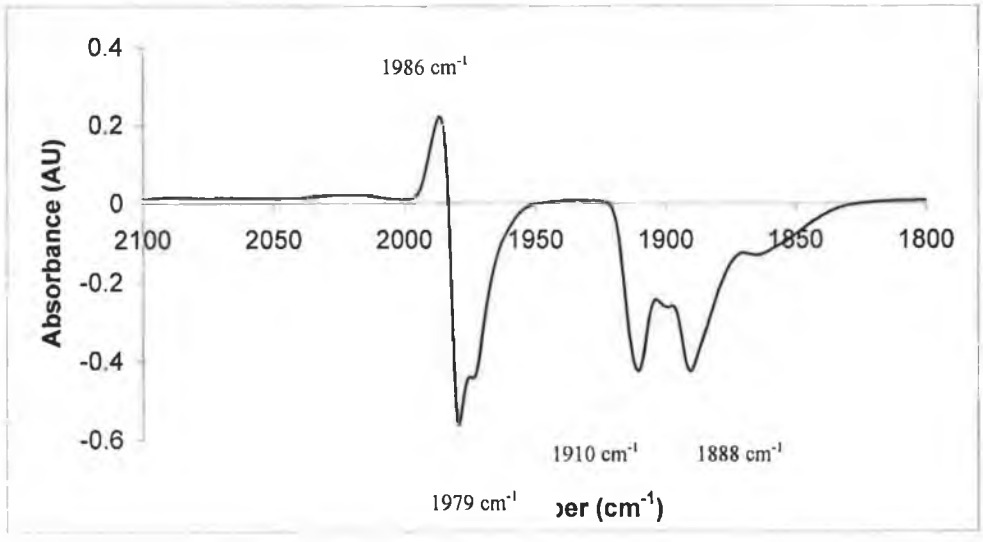

Figure 3.13.5 Spectral changes in the carbonyl region for $(\eta^5\text{-}C_4H_4Se)Cr(CO)_3$ following photolysis at λ_{exc} >320nm in a 2% CO matrix at 12K after 180 minutes.

Photolysis at 406nm, in all three matrix media (argon, nitrogen, 2% CO / 98% Ar) showed formation of a three band pattern at approximately the same wavenumbers 2046, 2001 and 1957 cm^{-1}, (in the nitrogen matrix the band at 2046 cm^{-1} is obscured by an impurity). These bands are also observed following excitation at λ_{exc} = 355 nm using step scan TRIR spectroscopy in CO saturated heptane.

Upon shorter wavelength irradiation (band pass filter 320 < λ_{exc} < 390 nm) depletion of the bands at 2046, 2001 and 1957 cm^{-1} was observed with formation of two bands at 2032 and 1935 cm^{-1} in a argon matrix.

3.14 UV/vis flash photolysis of (η^5-C_4H_4Se)$Cr(CO)_3$ at 266nm and 355nm

The photochemistry of (η^5-C_4H_4Se)$Cr(CO)_3$ was also investigated by UV/vis flash photolysis at λ_{exc} = 355nm in CO saturated cyclohexane. Depletion of the parent was followed by formation of a band in the region 460-520 nm with a λ_{max} at 490 nm, which did not decay within the timescale of the experiment. This grow in is seen to form on the same timescale as the bands assigned to the (η^4-C_4H_4Se)$Cr(CO)_4$ species (observed using stepscan TRIR at λ_{exc} = 355 nm) and the other species, which was tentatively assigned as either the (C,Se-C_4H_4Se)$Cr(CO)_3$ and *endo* – Se (η^4-C_4H_4Se)$Cr(CO)_3$ species.

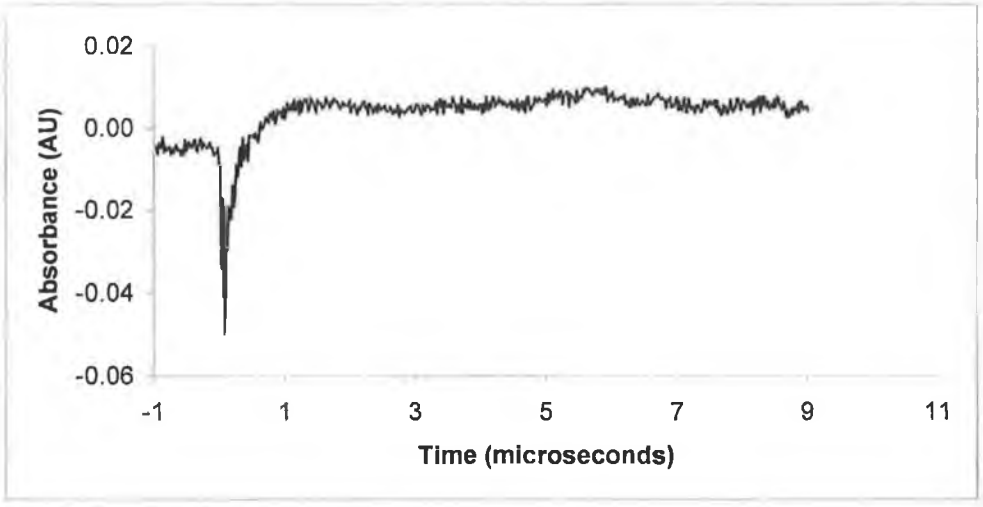

Figure 3.14.1 Transient signal observed at 480 nm following laser flash photolysis at λ_{exc} = 355 nm of (η^5-C_4H_4Se)$Cr(CO)_3$ in CO saturated cyclohexane (1 atmosphere).

In addition to the transient signals in the region 460 – 520 nm, upon flash photolysis at λ_{exc} = 355 nm in CO saturated cyclohexane, a recovery was observed at 420 nm. However the transient signal observed was too weak to accurately measure the rate of recovery.

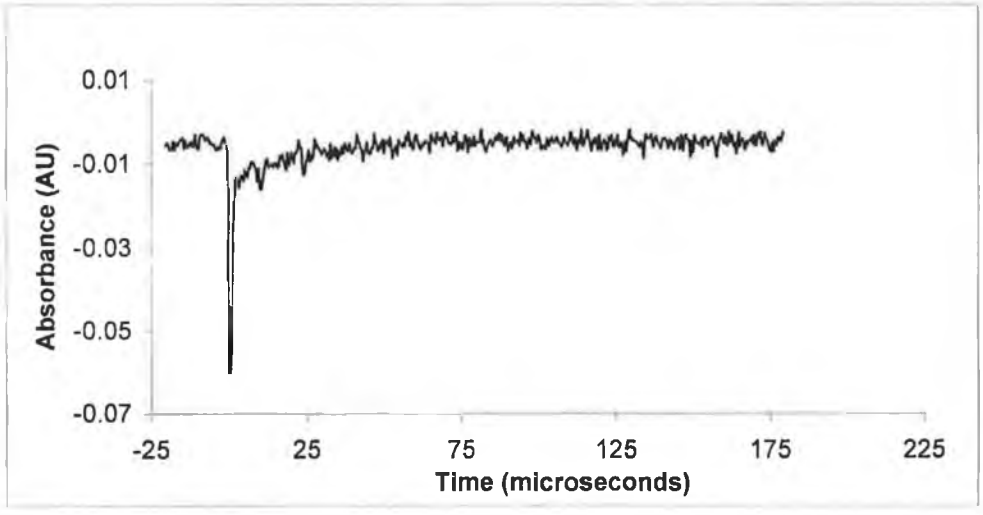

Figure 3.14.2 Recovery observed at 420nm following laser flash photolysis at λ_{exc} = 355 nm in CO saturated cyclohexane.

The photochemistry of $(\eta^5\text{-}C_4H_4Se)Cr(CO)_3$ was also investigated by UV/vis flash photolysis at λ_{exc} = 355 nm in cyclohexane containing a molar excess of a trapping ligand (pyridine). Transient signals were observed in the region 460 nm - 520 nm was observed with a λ_{max} at 480 nm. Figure 3.14.3 represents the signal observed, a depletion of the parent followed by a grow in which did not decay. The grow in forms in less then 2 μs of the flash. The rate of the grow in of the signal observed at 480 nm did not depend on the concentration of pyridine. The signal observed at 480 nm is assigned to the formation of the ring insertion species or the ring slip species $(C,Se\text{-}C_4H_4Se)Cr(CO)_3$, *endo*-$(\eta^5\text{-}C_4H_4Se)Cr(CO)_3$. No signals however were observed which could account for the formation of the $(\eta^5\text{-}C_4H_4Se)Cr(CO)_2(\eta^1\text{-}C_5H_5N)$ dicarbonyl species, section 3.11.

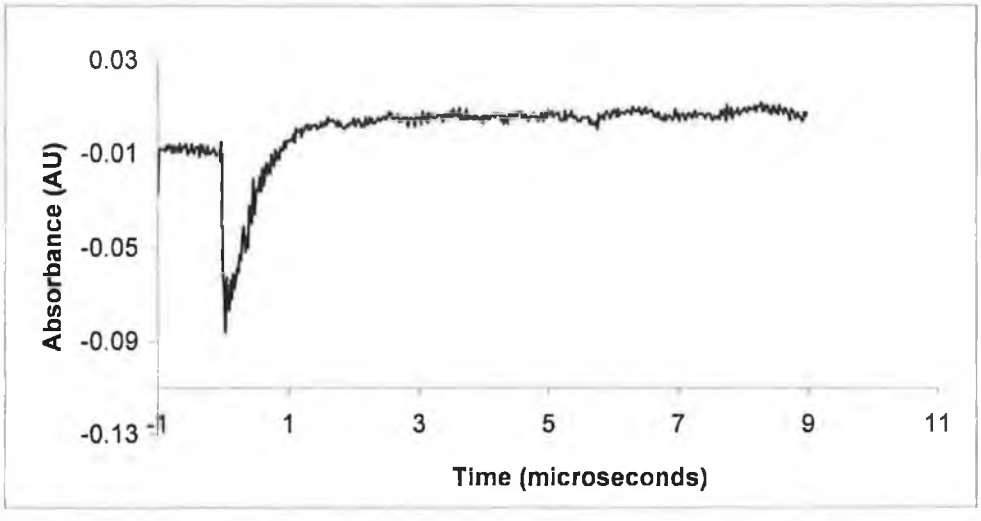

Figure 3.14.3 Transient signal observed at 480 nm following laser flash photolysis at λ_{exc} = 355nm of $(\eta^5\text{-}C_4H_4Se)Cr(CO)_3$ (2.2×10^{-4} M) concentration in cyclohexane containing a molar excess of pyridine 1.1×10^{-3} M.

3.15 Discussion

Photolysis of both $(\eta^5\text{-}C_4H_4S)Cr(CO)_3$ at λ_{exc} = 266 nm and with a xenon arc lamp and $(\eta^5\text{-}C_4H_4Se)Cr(CO)_3$ at λ_{exc} = 355 nm, resulted in displacement of the arene ring and formation of $Cr(CO)_6$. Using a mixture of time resolved techniques and low temperature matrix isolation experiments ring slip intermediate species for both $(\eta^5\text{-}C_4H_4S)Cr(CO)_3$ and $(\eta^5\text{-}C_4H_4Se)Cr(CO)_3$ were observed.

From the steady state experiments it can be seen that photolysis of $(\eta^5\text{-}C_4H_4S)Cr(CO)_3$ in the presence of an arene resulted in arene exchange following photolysis using a xenon arc lamp. This process was suppressed in the presence of CO. This would seem to imply that the arene exchange process occurs via the dicarbonyl solvated species as proposed by Gilbert *et al.*[26] This mechanism proposes that the dicarbonyl solvated species undergoes a ring slippage, to form two η^4 interactions with the metal centre. The benzene ring is then displaced. A CO molecule is captured from the solution and the benzene forms an η^6 interaction to give $(\eta^6\text{-}C_6H_6)Cr(CO)_3$, as shown in Scheme 3.15.1.

This mechanism however does not take into account that the concentration of CO would be so low (i.e the only CO in solution would be the CO displaced on photolysis of the parent complex) that the final stage of the reaction would be very inefficient. Therefore it would indicate that instead of the reaction taking place through the dicarbonyl solvent complex it takes place through an $(\eta^4\text{-}C_4H_4S)Cr(CO)_3$(solvent) species, the arene exchange product is then formed from this species. This would then account for the reduction in the arene exchange process in the presence of CO, Scheme 3.15.1.

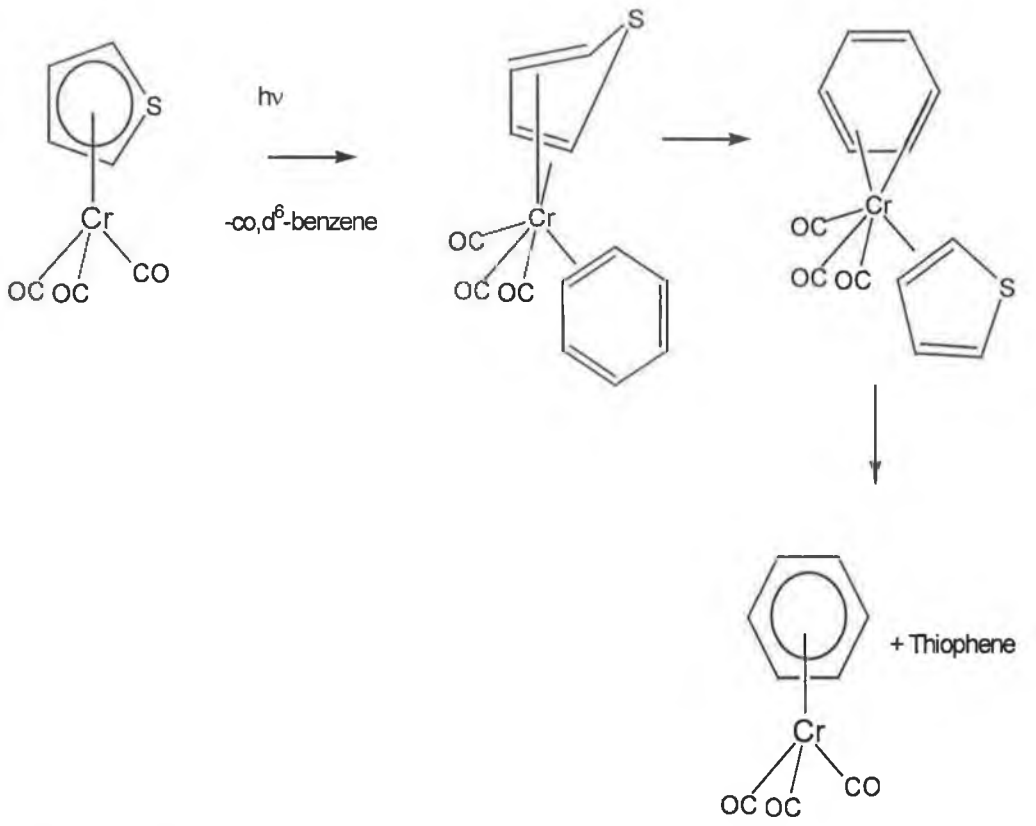

Scheme 3.15.1

Further evidence for arene loss in $(\eta^5\text{-}C_4H_4S)Cr(CO)_3$ was that high energy photolysis in CO saturated cyclohexane, resulted in formation of $Cr(CO)_6$. Presumably formation of the hexacarbonyl is the result of further reaction of the ring slip thiophene species, $(\eta^4\text{-}C_4H_4S)Cr(CO)_4$ with CO. Photolysis of $(\eta^5\text{-}C_4H_4S)Cr(CO)_3$ in the presence of a trapping ligand PPh_3 using a xenon arc lamp at and a $320 < \lambda_{exc} < 390$ nm filter or, no filter resulted in the formation of the dicarbonyl species $(\eta^5\text{-}C_4H_4S)Cr(CO)_2PPh_3$.

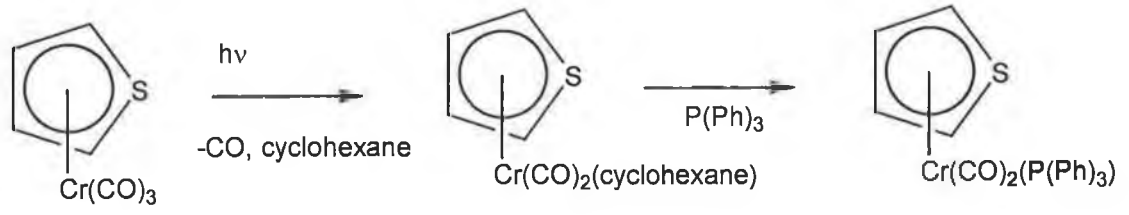

Scheme 3.15.2

The dicarbonyl species could however be formed through a ring slip intermediate. Formation of a $(\eta^4\text{-}C_4H_4S)Cr(CO)_3PPh_3$ species which then loses CO with accompanying η^4 to η^5 change in the co-ordination of the thiophene ring would occur in the formation of the dicarbonyl species $(\eta^5\text{-}C_4H_4S)Cr(CO)_2PPh_3$. This associative CO loss process is shown in scheme 3.15.3.

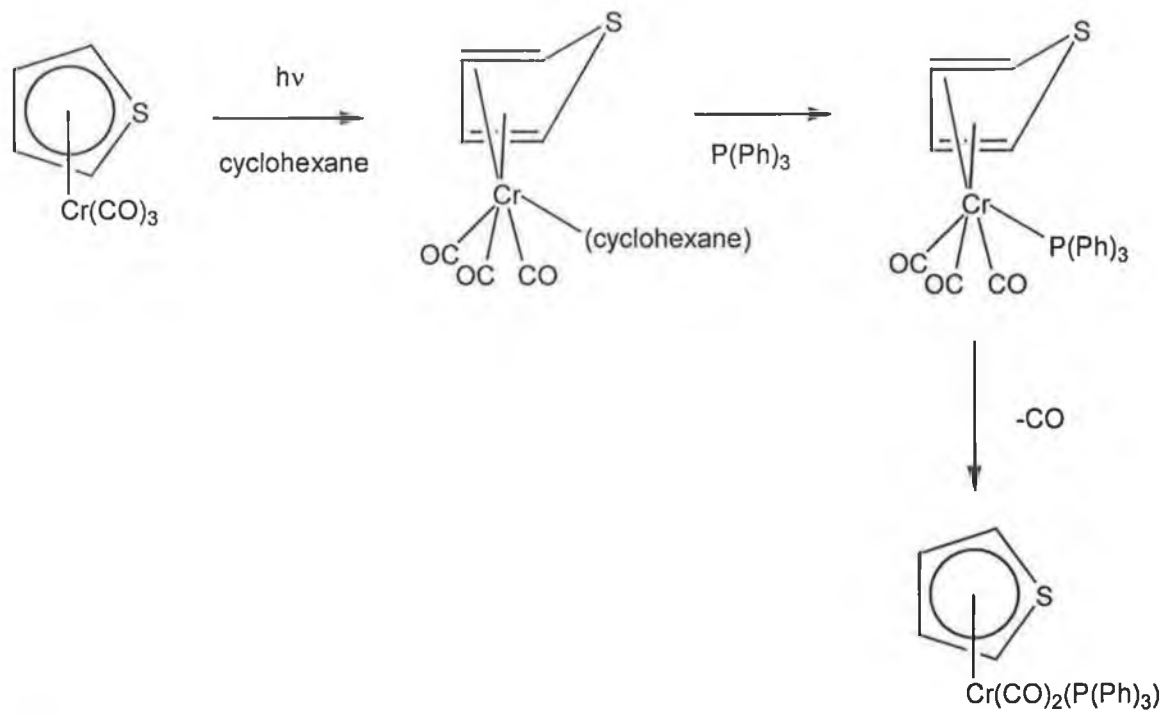

Scheme 3.15.3

The photochemistry of $(\eta^5\text{-}C_4H_4S)Cr(CO)_3$ was also investigated when isolated in 2% CO and nitrogen matrices. High energy irradiation of $(\eta^5\text{-}C_4H_4S)Cr(CO)_3$ in the nitrogen matrix resulted in formation of bands at 1972, 1932, 1895, 1881 and 1867cm^{-1} in the carbonyl region and formation of free CO at 2139 cm^{-1} and two $\nu(N\equiv N)$ at 2154 and 2185cm^{-1}. By comparison of the results obtained by TRIR studies of $(\eta^5\text{-}C_4H_4S)Cr(CO)_3$, the bands at 1972 and 1881 cm^{-1} are assigned to $(\eta^4\text{-}C_4H_4S)Cr(CO)_3(N_2)$, the $\nu(N\equiv N)$ stretch at 2185 cm^{-1}. Similarly the bands at 1932 and 1967 cm^{-1} are assigned to formation of the dicarbonyl species $(\eta^5\text{-}C_4H_4S)Cr(CO)_2(N_2)$, evidence for free CO at 2139 cm^{-1} and a $\nu(N\equiv N)$ stretch at 2154 cm^{-1}.

High energy photolysis of $(\eta^5\text{-}C_4H_4S)Cr(CO)_3$ in a 2%CO / 98% Ar matrix did not result in formation of $(\eta^4\text{-}C_4H_4S)Cr(CO)_4$. Instead the grow in of a band at 1986 cm^{-1} was observed relating to formation of $Cr(CO)_6$. The reason for the observation of the total displacement of the thiophene ring from η^5 to η^4 slip may have been due to the use of broad band filters when carrying out the reaction. Therefore upon photolysis of the starting material to give $(\eta^4\text{-}C_4H_4S)Cr(CO)_4$, this complex is itself quickly photolysed to form $Cr(CO)_6$. Three bands at 1979, 1911 and 1895 cm^{-1} were also seen to form upon high energy photolysis. Sanger and Angelici using variable temperature ^{13}C NMR, have shown that there is restricted rotation of the thiophene ring around the Cr-thiophene bond in both $(\eta^5\text{-}2\ (CH_3)C_4H_3S)Cr(CO)_3$ and $(\eta^5\text{-}2,5\ (CH_3)_2C_4H_2S)Cr(CO)_3$.[22] The $(\eta^5\text{-}C_4H_4S)Cr(CO)_3$ has a pseudo octahedral structure in which the CO ligands are approximately trans to a sulphur or a double bond of the thiophene ligand. Upon photolysis the $Cr(CO)_3$ unit rotates from a staggered formation with respect to the thiophene ring, to an eclipsed form, Reaction 3.15.1. The bands at 1979, 1911 and 1895 cm^{-1} are therefore assigned to the formation of this species.

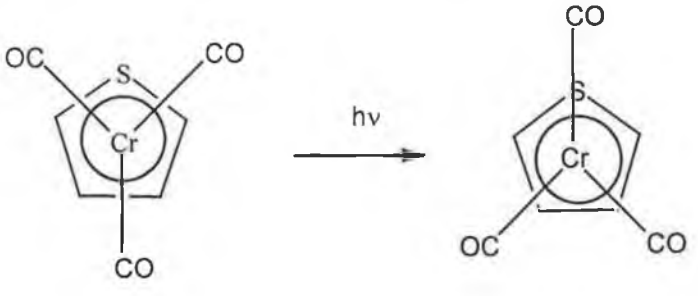

Staggered $(\eta^5$-thiophene)$Cr(CO)_3$ Eclipsed $(\eta^5$-thiophene)$Cr(CO)_3$

Reaction 3.15.1. Staggered and eclipsed forms of $(\eta^5\text{-}C_4H_4S)Cr(CO)_3$.

The photochemistry of $(\eta^5\text{-}C_4H_4S)Cr(CO)_3$ was also investigated in CO saturated heptane by TRIR at both λ_{exc} = 355 nm and 266 nm. The photochemistry of this system was investigated using a mixture of step scan and point by point techniques. Step scan TRIR

revealed that upon photolysis at λ_{exc} = 355 nm, two bands at 1923 and 1860 cm^{-1} were observed at 650 ns after excitation. These bands were assigned to formation of the $(\eta^5\text{-}C_4H_4S)Cr(CO)_2$(heptane) species.

Upon photolysis at λ_{exc} = 266 nm using step scan TRIR detection, four bands at 2002, 1971, 1938 and 1886 cm^{-1} associated with the formation of $(\eta^4\text{-}C_4H_4S)Cr(CO)_4$ were observed to form within 50 μs after excitation. Upon photolysis at λ_{exc} = 266 nm using point by point detection, at a short timebase (800 ns after excitation), carbonyl stretches were observed to form associated to the $(\eta^4\text{-}C_4H_4S)Cr(CO)_3$(solvent) species, (1960 and 1886 cm^{-1}) and the $(\eta^5\text{-}C_4H_4S)Cr(CO)_2$(heptane) species, (1923 and 1860 cm^{-1}). At a longer timebase (30 μs after excitation), bands associated with the formation of $(\eta^4\text{-}C_4H_4S)Cr(CO)_4$ at 2002, 1971, 1938 and 1886 cm^{-1} were observed.

The photochemistry of $(\eta^5\text{-}C_4H_4S)Cr(CO)_3$ was examined at both λ_{exc} = 355 nm and 266 nm using UV/vis detection. Excitation at both λ_{exc} = 355 nm and 266 nm, resulted in only one signal, the depletion and recovery of the parent at 420 nm. Due to the weakness of the signal, the k_{obs} could not be measured accurately. This signal was found to recover with a rate that was dependent on the concentration of CO. Comparing both signals at a particular concentration, they were both found to recover over a similar timescale. This would indicate that the signals recorded at 420 nm upon excitation at both λ_{exc} = 355 nm and 266 nm is due to recovery of the same photoproduct to $(\eta^5\text{-}C_4H_4S)Cr(CO)_3$.

TRIR studies had previously shown that formation of the dicarbonyl species takes place upon irradiation at both λ_{exc} = 355 nm and 266 nm. Therefore the signals recorded at 420 nm using UV/vis detection upon excitation at λ_{exc} = 355 nm and 266 nm is assigned to recovery of the parent from the solvated dicarbonyl species. However no signals were observed which could be assigned to either the $(\eta^4\text{-}C_4H_4S)Cr(CO)_3$(solvent) or $(\eta^4\text{-}C_4H_4S)Cr(CO)_4$, species.

The photochemistry of $(\eta^5\text{-}C_4H_4Se)Cr(CO)_3$ is somewhat different to that of the photochemistry of the $(\eta^5\text{-}C_4H_4S)Cr(CO)_3$. IR monitored photolysis at λ_{exc} = 355 nm of $(\eta^5\text{-}C_4H_4Se)Cr(CO)_3$ in a CO saturated cyclohexane resulted in formation of a ring slip species $(\eta^4\text{-}C_4H_4Se)Cr(CO)_4$ (2014, 1956 and 1914 cm^{-1}) and $Cr(CO)_6$ (1985 cm^{-1}) was observed. The assignment of the bands at 2014, 1956 and 1914 cm^{-1} to the $(\eta^4\text{-}C_4H_4Se)Cr(CO)_4$ species is by comparison of the bands to other tetracarbonyl species, $(\eta^4$-hexamethylbicyclo [2.2.0] hexadiene$)Cr(CO)_4$ 2025 (m), 1940 (s) and 1900 (m) cm^{-1} and $(\eta^4$-norboradiene$)Cr(CO)_4$ 2032 (m), 1960 (w), 1946 (s) and 1915 (m) cm^{-1}. Attempts to isolate the $(\eta^4\text{-}C_4H_4Se)Cr(CO)_4$ proved unsuccessful, due to the high reactivity of this species.

Photolysis at λ_{exc} = 355nm of $(\eta^5\text{-}C_4H_4Se)Cr(CO)_3$ in the presence of a trapping ligand (pyridine) resulted in the formation of the dicarbonyl species, $(\eta^5\text{-}C_4H_4Se)Cr(CO)_2(\eta^1\text{-}C_5H_5N)$ (1920 and 1859 cm^{-1}), Reaction 3.15.2. Two additional bands were also observed at 1969 and 1854 cm^{-1} and these bands were tentatively assigned to $(\eta^4\text{-}C_4H_4Se)Cr(CO)_3(\eta^1\text{-}C_5H_5N)$, Reaction 3.15.3.

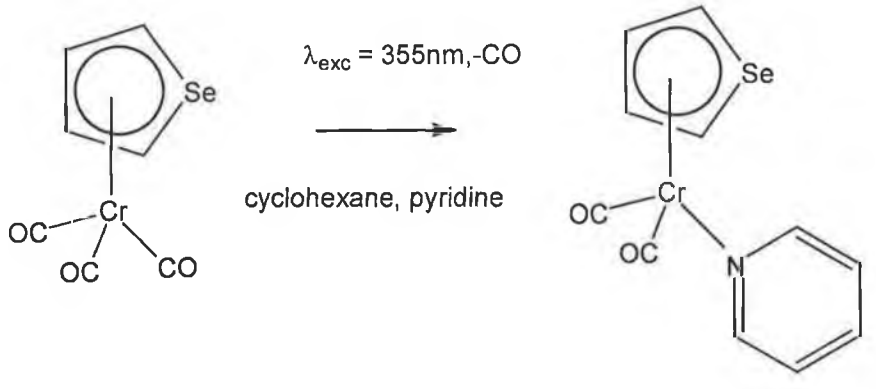

Reaction 3.15.2.

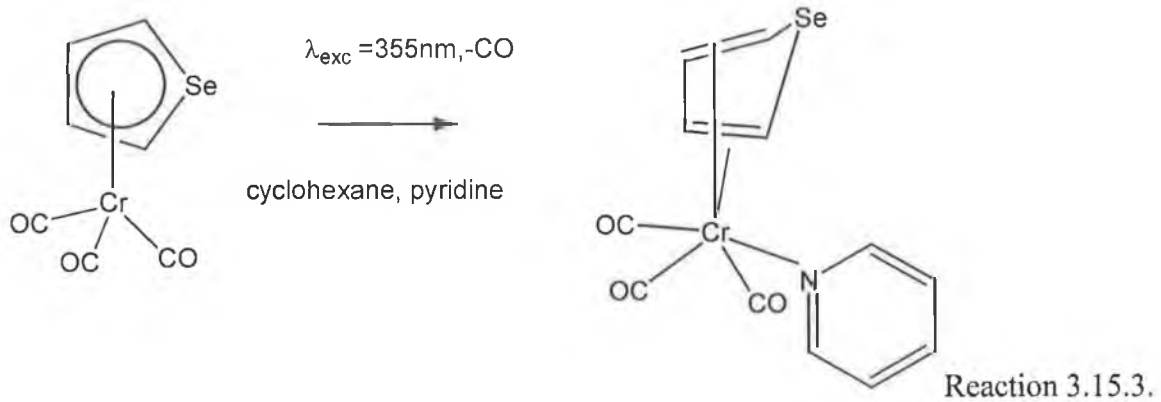

Reaction 3.15.3.

The photochemistry of $(\eta^5\text{-}C_4H_4Se)Cr(CO)_3$ was also examined using step scan and point by point TRIR at λ_{exc} = 355nm. Using step scan TRIR spectroscopy, photolysis λ_{exc} = 355 nm of $(\eta^5\text{-}C_4H_4Se)Cr(CO)_3$ in a CO saturated heptane solution resulted in the formation of bands at 1927 and 1859 cm^{-1} which were assigned to the dicarbonyl species $(\eta^5\text{-}C_4H_4Se)Cr(CO)_2$ and the IR bands at 2015,1959 and 1914 cm^{-1} are assigned to the ring slip species $(\eta^4\text{-}C_4H_4Se)Cr(CO)_4$. The IR bands at 2041, 2003 and 1953 cm^{-1} are assigned to the ring insertion species $(C,Se\text{-}C_4H_4Se)Cr(CO)_3$. The bands at 2015,1959 and 1914 cm^{-1} had previously been observed upon IR monitored photolysis of $(\eta^5\text{-}C_4H_4Se)Cr(CO)_3$ at λ_{exc} = 355 nm in CO saturated cyclohexane and assigned to the formation of $(\eta^4\text{-}C_4H_4Se)Cr(CO)_4$. However the bands at 2041, 2003 and 1953 cm^{-1} relating to $(C,Se\text{-}C_4H_4Se)Cr(CO)_3$ or endo $(\eta^4\text{-}C_4H_4Se)Cr(CO)_3$ were not observed. By comparison to the IR bands at 2046, 2001 and 1957 cm^{-1} observed in matrix isolation studies on $(\eta^5\text{-}C_4H_4Se)Cr(CO)_3$ in a CO doped argon matrix, an argon matrix and a nitrogen matrix at λ_{exc} = 406 nm irradiation, these bands were assigned to the $(C,Se\text{-}C_4H_4Se)Cr(CO)_3$ species or endo $(\eta^4\text{-}C_4H_4Se)Cr(CO)_3$. This would suggest that this species is extremely reactive, as it is only observed using time resolved techniques or by use of low temperature matrices.

Following deposition of $(\eta^5\text{-}C_4H_4Se)Cr(CO)_3$ in all matrices three carbonyl bands were observed at similar wavenumber. Irradiation was initially carried out at λ_{exc} = 500 nm and 436 nm with no changes observed. When the irradiation wavelength was changed to λ_{exc} = 406 nm depletion of the parent bands occurred with the formation of three new bands in

all matrices. In the argon matrix at 2046, 2001 and 1957 cm^{-1}, the CO doped argon matrix at 2044, 1997 and 1954 cm^{-1} and in the nitrogen matrix at 2001 and 1957 cm^{-1}. At this irradiation wavelength no evidence was observed for loss of CO in any of the matrices.

The bands observed following irradiation at λ_{exc} = 406 nm in all three matrices were also observed upon excitation at λ_{exc} = 355 nm in CO saturated hexane using step scan TRIR spectroscopy. In the TRIR spectroscopy experiments these bands were assigned to formation of a ring insertion species. As these three bands are only observed using time resolved techniques or by use of low temperature matrices its suggests that this species is extremely reactive.

The reaction of $(\eta^5\text{-}2,5(CH_3)_2C_4H_2S)Ir(C_5(CH_3)_5)^{2+}$ with the reducing agent $(\eta^5\text{-}C_5H_5)_2Co$, yields the neutral species, η^4-2,5 $(CH_3)_2C_4H_2S)Ir(C_5(CH_3)_5)$. Which rearranges in the presence of base to give the ring opened product system, $(C,S\text{-}2,5(CH_3)_2C_4H_2S)Ir(C_5(CH_3)_5)$. For the analogous selenophene complex, reaction of $(\eta^5\text{-}2,5(CH3)_2C_4H_2Se)Ir(C_5(CH3)_5)^{2+}$ with the reducing agent $Na[(CH_3OC_2H_4O)_2AlH_2]$ gave the ring opened $(C,Se\text{-}2,5\ (CH_3)_2C_4H_2Se)Ir(C_5(CH_3)_5)$ species.[16] The $(\eta^4\text{-}2,5(CH_3)_2C_4H_2Se)Ir(C_5(CH_3)_5)$ species, was not isolated, presumably the η^4 species rearranges to the more stable ring insertion product before it can be isolated.[16] In the case of the results obtained here, there are a number of possibilities for the species initially observed upon photolysis in the matrix experiments. One option is that $(\eta^4\text{-}C_4H_4Se)Cr(CO)_3$ is not observed as it quickly isomerises to form the ring insertion product, $(C,Se\text{-}C_4H_4Se)Cr(CO)_3$, and therefore the bands observed at 2046, 2001 and 1957 cm^{-1} (argon), 2001 and 1957 cm^{-1} (nitrogen) and 2044, 1997 and 1954 cm^{-1} (2% CO / 98% argon) could be assigned to this ring insertion product. Due to steric hindrance caused by the insertion of the $Cr(CO)_3$ moiety into the ring or by bending of the $Cr(CO)_3$ unit, this species does not further react with CO or complex dinitrogen. However, it is also possible that these bands may be due to the presence of a ring slip species, where the selenium atom bends towards the $Cr(CO)_3$ unit, *endo – Se* $(\eta^4\text{-}C_4H_4Se)Cr(CO)_3$.

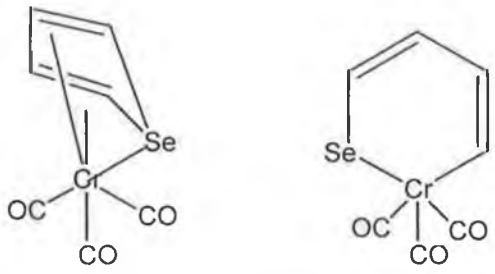

Figure 3.15.1 Proposed structures of (C,Se-C_4H_4Se)$Cr(CO)_3$ and endo – Se (η^4-C_4H_4Se)$Cr(CO)_3$.

At higher energy photolysis at $320 < \lambda_{exc} < 390$ nm in an argon matrix, the bands observed 2046, 2001 and 1957 cm^{-1} decayed with concomitant formation of two bands at 2032 and 1932 cm^{-1}, in addition to a further bands at 2138 cm^{-1}. These bands could belong to the formation of either the dicarbonyl species endo – Se (η^4-C_4H_4Se)$Cr(CO)_2$ or (C,Se-C_4H_4Se)$Cr(CO)_2$. The band at 2138 cm^{-1} is indicative of 'free' CO in the matrix. At higher energy photolysis at $320 > \lambda_{exc} < 390$ nm in an CO doped argon matrix formation of $Cr(CO)_6$ (1985 cm^{-1}) was also observed.

The photochemistry of (η^5-C_4H_4Se)$Cr(CO)_3$ was also investigated at $\lambda_{exc} = 355$ nm using UV/vis flash photolysis. Upon excitation at $\lambda_{exc} = 355$ nm in both CO saturated cyclohexane and pyridine doped cyclohexane, a transient signal at 480 nm was observed. Upon varying the concentration of CO and pyridine, the rate of grow in of the signal at 480 nm did not appear to change. This would indicate that this species was neither reacting with CO or pyridine. The signal can therefore be attributed to the formation of the ring insertion product, (C,Se-C_4H_4Se)$Cr(CO)_3$ species. Using steady state IR monitored photolysis at $\lambda_{exc} = 355$ nm, the bands assigned to the (η^4-C_4H_4Se)$Cr(CO)_4$ species and $Cr(CO)_6$, were observed upon photolysis in CO saturated cyclohexane. The bands observed using step scan TRIR at $\lambda_{exc} = 355$nm and matrix isolation experiments at $\lambda_{exc} = 406$ nm for the ring insertion species (C,Se-C_4H_4Se)$Cr(CO)_3$ or the ring slip species endo (η^4-C_4H_4Se)$Cr(CO)_3$, were not observed using steady state experiments at $\lambda_{exc} = 355$ nm in CO saturated cyclohexane. This would indicate that the ring insertion species or the ring slip species is a transient species. Upon excitation at $\lambda_{exc} = 355$ nm in CO saturated

cyclohexane a signal was also observed at 420 nm, which was thought to be recovery of the parent complex from the dicarbonyl.

3.16 Conclusions

A variety of techniques were used to investigate the photochemical pathways of both $(\eta^5\text{-}C_4H_4S)Cr(CO)_3$ and $(\eta^5\text{-}C_4H_4Se)Cr(CO)_3$. This study has demonstrated the importance of the ring slip process in the photochemistry of hydrodesulphurisation model complexes. Using a mixture of steady state, time resolved techniques and low temperature studies it was possible to show that irradiation of $(\eta^5\text{-}C_4H_4S)Cr(CO)_3$ at both high and low energy results in CO loss. High energy irradiation also results in formation of the η^4 ring slip species and eventual complete displacement of the ring.

The photochemistry of $(\eta^5\text{-}C_4H_4Se)Cr(CO)_3$, while similar does show some marked differences to that of the thiophene complex. The selenophene complex also shows a marked difference between the photochemistry observed in solution and matrix studies. Using a mixture of steady state techniques it was possible to observe formation of three species $(\eta^4\text{-}C_4H_4Se)Cr(CO)_4$, $(C,Se\text{-}C_4H_4Se)Cr(CO)_3$ or endo $(\eta^4\text{-}C_4H_4Se)Cr(CO)_3$ and $(\eta^5\text{-}C_4H_4Se)Cr(CO)_2$. Using matrix isolation studies it was only possible to observe the ring insertion species $(C,Se\text{-}C_4H_4Se)Cr(CO)_3$ or endo $(\eta^4\text{-}C_4H_4Se)Cr(CO)_3$, in addition to the CO loss photoproduct of this species.

3.17 References

1. Topsøe,H.; Clausen, B.S.; Massoth, F.E. *Hydrotreating Catalysis*, Springer-Verlag: Berlin, 1996.
2. Gates, B.C.; Katzer, J.R.; Schuit, G.C.A. *Chemistry of catalytic processes*, McGraw-Hill; New York, 1979.
3. Moffat, J.B. *Theoretical aspects of heterogeneous catalysis*, van Nostrand Reinhold Catalytic series; van Nostrand Rheinhold: New York, 1990, 206.
4. Angelici, R.J. *Bull. Soc. Chim. Belg.* 1995, **104**, 265.
5. Angelici, R.J. *Polyhedron*, 1997, **16**, 3073.
6. Chen, J.; Angelici, R.J. *Organometallics* 1989, **88**, 2277.
7. Chen, J.; Daniels, L.M.; Angelici, R.J. *J. Am. Chem. Soc.* 1990, **112**, 199.
8. Ogilivy, A.B.; Skaugest, A.E.; Rauchfauss, T.B. *Organometallics* 1989, **8**, 2739.
9. Choi. M.G.; Angelici, R.J. *J. Am. Chem. Soc.* 1989, **111**, 8753.
10. Muetterties, E.L.; Stein, *J. Chem. Rev.* 1979, **79**, 479.
11. Vivic, D.A.; Jones, W.D.; *Organometallics* 1997, **16**, 1912.
12. Zhang, X.; Dullaghan, C.A.; Watson E.J.; Carpenter G.B.; Sweigart D.A. *Organometallics* 1998, **17**, 2067.
13. Dullaghan, C.A.; Carpenter, G.B.; Sweigart D.A. *Organometallics* 1997, **16**, 5688.
14. Choi, M.G.; Angelici, R.J. *J. Am. Chem. Soc.* 1990, **112**, 7811.
15. Choi M.G.; Angelici R.J. *J. Am. Chem. Soc.* 1991, **113**, 5651.
16. White, C.J.; Angelici, R.J. *Organometallics* 1995, **14**, 332.
17. Harris, S. Organometallics 1994, **13**, 2628.
18. Crichton, O.; Rest, A.J.; Taylor, D.J.; *J. Chem. Soc., Dalton. Trans.* 1980, 167.
19. Mahmoud, K.A.; Rest, A.J.; Alt, H.G. *J. Chem. Soc., Dalton. Trans.* 1985, 1365.
20. Blaha, J.P.; Wrighton, M.S. *J. Am. Chem. Soc.* 1985, **107**, 2694.
21. Chetwynd-Talbot, J.; Grebenik, P.; Perutz, R.N.; Powell, M.H.A. Inorg. Chem. 1983, **2**, 1675.
22. Sanger, M.J.; Angelici, R.J.; *Organometallics* 1994, **13**, 1821.
23. Fischer, E.O.; Kreiter, C.G.; Berngruber, W. *Angew. Chem. Int. Ed. Engl.* 1967, **6**, 634.
24. Bennet, M.A.; Pratt, L; Wilkinson, G. *J. Chem. Soc.* 1961, 2037

25. Rest A.J.; Sodeau, J.R.; Taylor, D.J. *J. Chem. Soc., Dalton Trans.* 1978, 651.

26. Gilbert, A.; Kelly, J.M.; Budzweit, M.; Koerner von Gustorf E. *Z. Naturforsch.* 1976, **31b**, 1091.

27. Grevels, F.W.; Jacke, J.; Klotzbücher W.E.; Schaffner, K.; Hooker R.H. and Rest A.J. *J. Organomet. Chem*, 1990, **382**, 201.

Chapter 4

The photochemistry of $(\eta^6\text{-}C_8H_6S)Cr(CO)_3$ and $(\eta^6\text{-}C_{12}H_8S)Cr(CO)_3$

4.1 Introduction to the photochemistry of polyaromatic (η^6-arene)$Cr(CO)_3$ complexes

Initial photochemical studies on (η^6-arene)$Cr(CO)_3$ in solution indicated that the loss of CO is the primary photoprocess as shown in Reaction 4.1.1.[1] Strohmeier and Von Hobe subsequently studied the photochemistry of (η^6-C_6H_6)$Cr(CO)_3$ and they reported that photolysis of (η^6-C_6H_6)$Cr(CO)_3$ resulted in cleavage of the arene – metal bond ensuing in formation of free arene and $Cr(CO)_3$ in Reaction 4.1.2.[2]

$$(\eta^6\text{-}C_6H_6)Cr(CO)_3 \xrightarrow{h\nu} (\eta^6\text{-}C_6H_6)Cr(CO)_2 \qquad \text{Reaction 4.1.1}$$

$$(\eta^6\text{-}C_6H_6)Cr(CO)_3 \xrightarrow{h\nu} C_6H_6 + Cr(CO)_3 \qquad \text{Reaction 4.1.2}$$

These observations were later disputed, but in the light of experiments conducted on (η^6-$C_{10}H_8$)$Cr(CO)_3$, (η^6-C_6H_5N)$Cr(CO)_3$ or (η^6-XC_6H_5)$Cr(CO)_3$ where (X = -C(CO)H or -NH_2) (chapter 2), photolysis of the (η^6-arene)$Cr(CO)_3$ in CO saturated cyclohexane, has led to the formation of $Cr(CO)_6$ as the photoproduct.[3,4] Photolysis of (η^6-arene)$Cr(CO)_3$ in CO saturated cyclohexane initially leads to formation of $Cr(CO)_3$ and the free arene, the $Cr(CO)_3$ fragment being extremely reactive then reacts with CO in solution to form $Cr(CO)_6$. An alternative mechanism for the formation of $Cr(CO)_6$ implies a ring slip process (hapticity change) on the arene ring from η^6, η^4, η^2 with sequential addition of CO leading to eventual loss of the ring to yield $Cr(CO)_6$ as shown in Reaction 4.1.3.

$$(\eta^6\text{-arene})Cr(CO)_3 \xrightarrow[CO]{h\nu} (\eta^4\text{-arene})Cr(CO)_4 \xrightarrow[CO]{} (\eta^2\text{-arene})Cr(CO)_5 \xrightarrow[CO]{} Cr(CO)_6$$

Reaction 4.1.3

The (η^6-polyaromatic)$Cr(CO)_3$ complexes are known to undergo both thermal (Reaction 4.1.4) and photochemical (Reaction 4.1.5) arene exchange under an inert atmosphere.[5,6] The reaction is used as a convenient route to form many difficult to synthesise (η^6-arene)$Cr(CO)_3$ complexes.

$$(\eta^6\text{-arene})Cr(CO)_3 + \text{arene}^* \xrightarrow{\Delta} (\eta^6\text{-arene}^*)Cr(CO)_3 + \text{arene} \quad \text{Reaction 4.1.4}$$

$$(\eta^6\text{-arene})Cr(CO)_3 + \text{arene}^* \xrightarrow{h\nu} (\eta^6\text{-arene}^*)Cr(CO)_3 + \text{arene} \quad \text{Reaction 4.1.5}$$

The arene exchange reaction dominates the thermal chemistry of these compounds and has been studied in much detail. Activation of the arene-chromium bond was first noted when arene exchange of $(\eta^6\text{-arene})Cr(CO)_3$ was carried out in various arene solvents such as toluene and benzene. For the thermal reaction, the ease of displacement of the arene ring in a $(\eta^6\text{-arene})Cr(CO)_3$ complex, by another takes place in the following order hexamethylbenzene > mesitylene > xylene > toluene = benzene > chlorobenzene > fluorobenzene > naphthalene.[7,8] The driving force for the reaction is the greater thermodynamic stability of $(\eta^6\text{-arene}^*)Cr(CO)_3$ relative to $(\eta^6\text{-arene})Cr(CO)_3$, because of the increased electron donating capability of the arene*. The aim of this study is to investigate the photochemistry further of polyaromatic compounds using a mixture of UV/vis flash photolysis, TRIR spectroscopy and matrix isolation using IR spectroscopy.

4.2 Benzothiophene and dibenzothiophene complexes as model compounds for the hydrodesulphurisation process

For benzothiophene the most common coordination mode is the η^6 mode through the benzene ring. The η^1-S-bound coordination and η^2-C(2), C(3) olefinic -bond coordination and ring insertion modes are also possible.

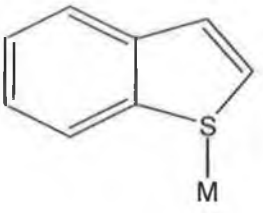

η^1-S- bound benzothiophene

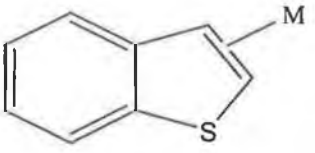

η^2-C(2),C(3) olefinic bond coordination

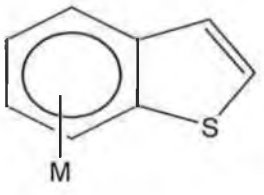

η^6- bound benzothiophene

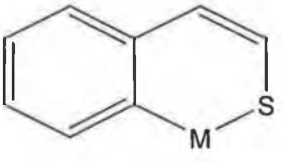

ring insertion coordination

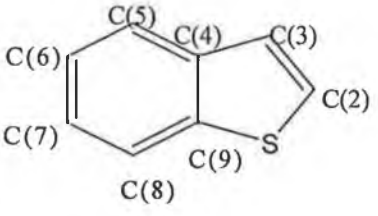

benzothiophene numbering scheme

Figure 4.2.1 η^1-S- bound benzothiophene, η^2-C(2),C(3) olefenic bound benzothiophene, η^6-bound benzothiophene and the ring insertion mode.

Reynolds *et al.* have synthesised a number of η^1-S-benzothiophene transition metal complexes.[9] These include $(\eta^1\text{-S-}C_8H_6S)W(CO)_5$, $(\eta^1\text{-S-}C_8H_6S)Mo(CO)_5$ and

(η^1-S-C_8H_6S)$Cr(CO)_5$. Angelici and co workers have observed complexation of benzothiophene through both the η^1-S-bound and η^2-2,3 coordinated of the C(2),C(3) olefenic bond. Angelici found that complexation of benzothiophene takes place through both the η^1-S- bound and η^2-C(2),(3) co-ordination of the C(2),C(3) olefenic bond to a (η^5-C_5R_5)$Re(CO)_2$ (R = H, CH_3) fragment.[10,11] When the C_5R_5 ligand is C_5H_5 the η^1-s bound coordination mode is favoured. However when the C_5R_5 ligand is $C_5(CH_3)_5$, the 2,3-η^2 isomer predominates. Thus, the higher electron density on the metal in the $C_5(CH_3)_5$ complex favours the 2,3-η^2 isomer as a result of the increased π backbonding to the olefin.

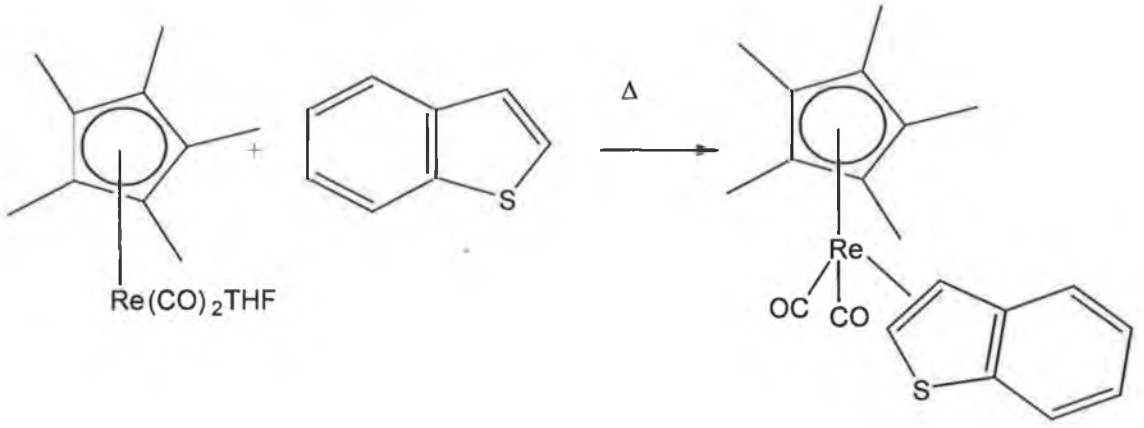

Reaction 4.2.1 Reaction of (η^5-C_5Me_5)$Re(CO)_2$(THF) with benzothiophene to give (η^5-$C_5(CH_3)_5$)$Re(CO)_2$(η^2-2(C),3(C) benzothiophene).

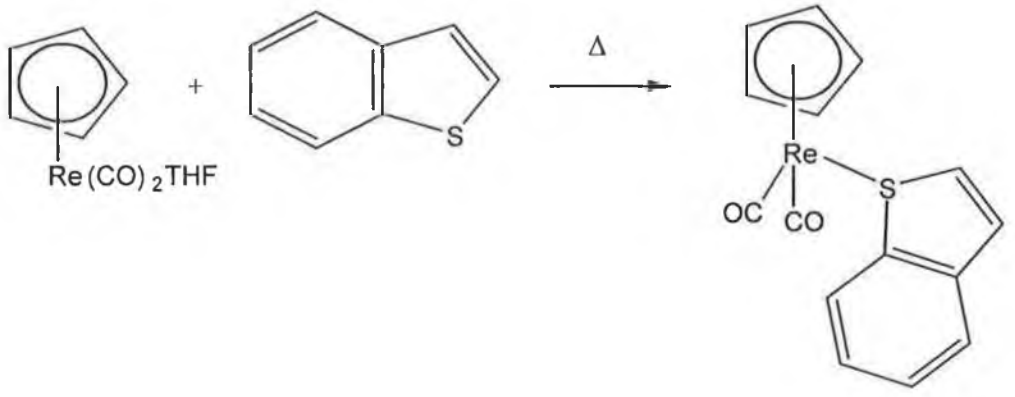

Reaction 4.2.2 Reaction of (η^5-C_5Me_5)$Re(CO)_2$(THF) with benzothiophene to give (η^5-C_5H_5)$Re(CO)_2$(η^1-s benzothiophene).

Angelici *et al.* also studied the thermal reaction of (η^6-C_8H_6S)$Cr(CO)_3$ with

(η^5-C_5H_5)Re(CO)$_2$(THF). When the benzothiophene ligand is complexed to the Cr(CO)$_3$ fragment the only observed coordination of the benzothiophene ligand is the 2,3 η^2-C(2),C(3) olefenic bond co-ordinated to a (η^5-C_5H_5)Re(CO)$_2$ fragment.[12] This observation was explained by the fact that the Cr(CO)$_3$ group on the benzothiophene effects the benzothiophene binding in two ways, the electron withdrawing effect of the Cr(CO)$_3$ unit could reduce the donor ability of the benzothiophene sulphur and increase the π accepting ability of the C(2)=C(3)bond.

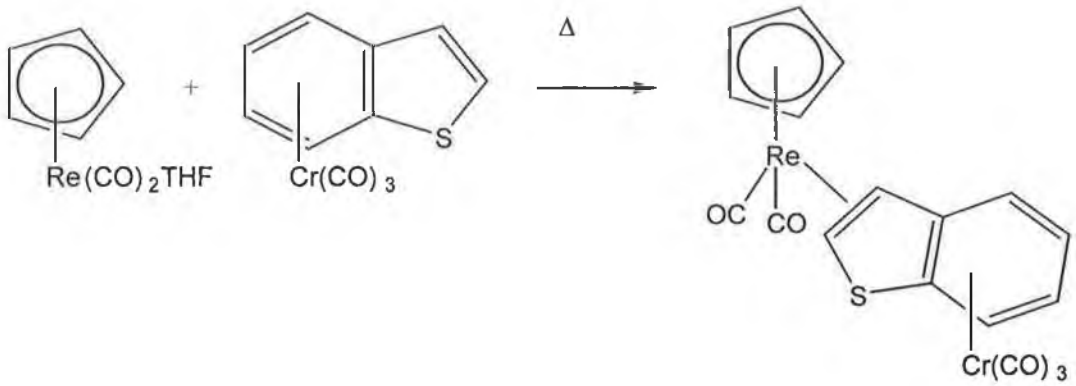

Reaction 4.2.3 Reaction of (η^5-C_5H_5)Re(CO)$_2$(THF) with (η^6-benzothiophene)Cr(CO)$_3$ to give (η^5-C_5H_5)Re(CO)$_2$(η^2-C(2),C(3) benzothiophene)((η^6-benzothiophene)Cr(CO)$_3$.

The bonding of the olefin to the metal involves σ donation from the C=C π orbital to a vacant orbital on the metal. π Back donation from a suitable filled d orbital on the metal into the C- C π^* antibonding orbital of the alkene serves to strengthen the bond.[13]

(a) (b)

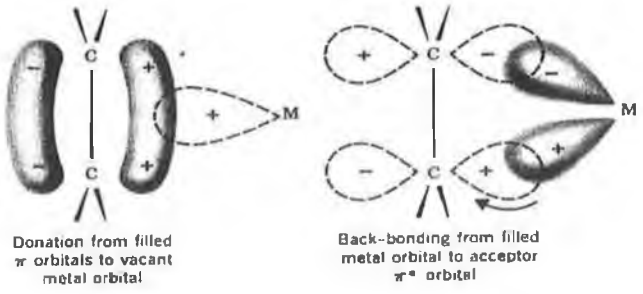

Figure 4.2.2 Diagrams showing the molecular orbital view of the alkene – metal bonding. (a) The donation of π electron density from the alkene to the metal. (b) The donation of π electron density from the metal to the alkene.

Zhang *et al.* have also shown the formation of a ring insertion species as an intermediate in the hydrodesulphurisation of benzothiophene using manganese based chemistry, Figure 4.2.3.[14]

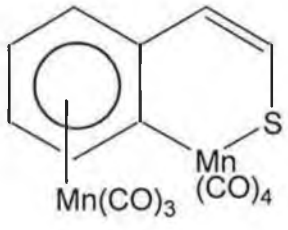

Figure 4.2.3

Dibenzothiophene has been found to have three coordination modes η^6, η^1-s bound coordination and the ring insertion species.

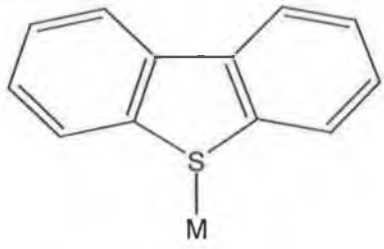

η^1-s bound dibenzothiophene

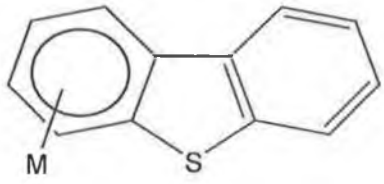

η^6- bound dibenzothiophene

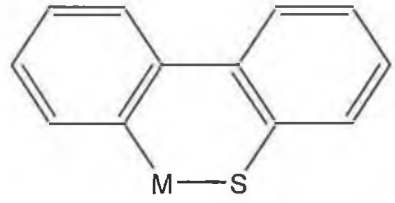

ring insertion coordination

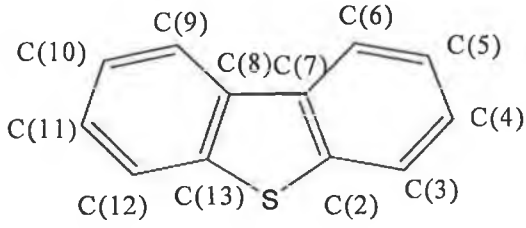

Figure 4.2.4 η^1-s bound benzothiophene, η^6-bound benzothiophene and ring opened coordination.

Reynolds *et al.* has synthesised a number of η^1-S dibenzothiophene transition metal complexes.[9] These include (η^1-S $C_{12}H_8S$)$W(CO)_5$, (η^1-S $C_{12}H_8S$)$Mo(CO)_5$ and (η^1-S $C_{12}H_8S$)$Cr(CO)_5$. Myers and Jones observed the insertion of (η^5-C_5H_5)$Rh(PMe_3)PhH$ into the sulfur–carbon bond of dibenzothiophene, Reaction 4.2.5, to give a six-membered metallacycle product.[15]

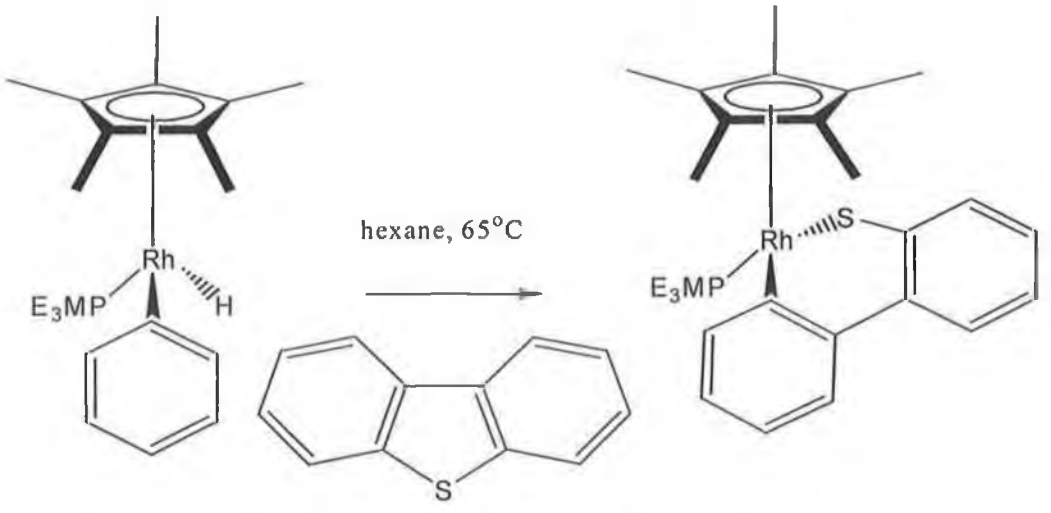

Reaction 4.2.5 Insertion of $(\eta^5\text{-}C_5H_5)Rh(PMe_3)PhH$ into the sulfur–carbon bond of dibenzothiophene.

Insertion of $Pt(PEt_3)_2$ into the sulfur –carbon bond in dibenzothiophene Reaction 4.2.6, has also been observed by Garcia *et al.*[16]

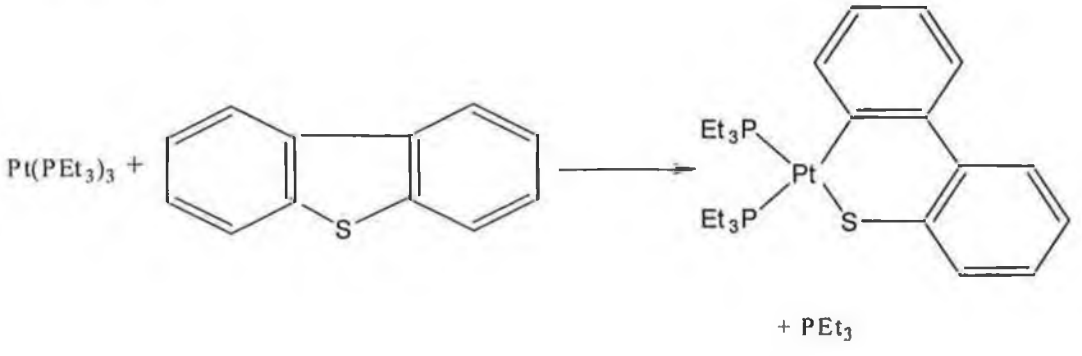

Reaction 4.2.6 Insertion of $Pt(PEt_3)_3$ into the sulfur –carbon bond in dibenzothiophene.

Bianchini *et al*, also showed the insertion of [(triphos)IrH] generated in situ by thermolysis of (triphos)Ir(H_2)(C_2H_8) in THF into dibenzothiophene.[17]

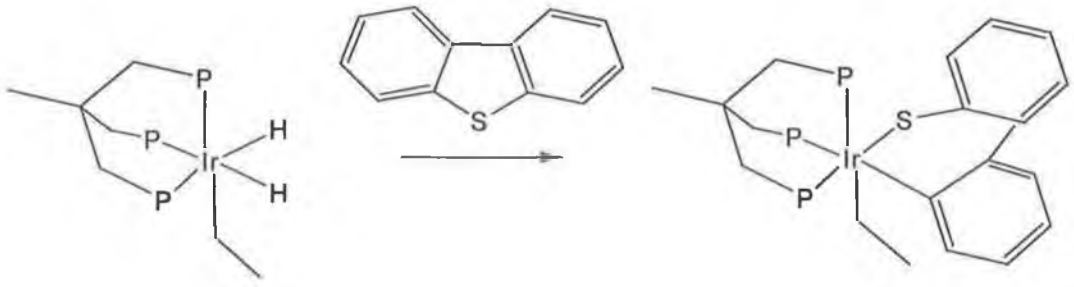

Reaction 4.2.7 Insertion of the [(triphos)IrH] into the sulfur –carbon bond in dibenzothiophene.

In this chapter the photochemistry of the chromium tricarbonyl complexes of both benzothiophene and dibenzothiophene are discussed.

4.3 TRIR experiments on $(\eta^6\text{-}C_8H_6S)Cr(CO)_3$

The photochemistry of $(\eta^6\text{-}C_8H_6S)Cr(CO)_3$ was investigated in CO saturated heptane at λ_{exc} = 355nm and was monitored using step-scan TRIR spectroscopy. Heptane was used as opposed to cyclohexane, as it does not absorb as much as cyclohexane in the carbonyl region of the IR spectrum. The negative peaks observed at 1977, 1915 and 1905 cm^{-1} in Figure 4.3.1 obtained 1.5 μs after excitation at λ_{exc} = 355 nm correspond to depletion of the parent. The positive peaks at 1921 and 1866 cm^{-1} are assigned to the photoproduct $(\eta^6\text{-}C_8H_6S)Cr(CO)_2$(solvated) as they occur at similar wavenumber to the bands previously reported for $(\eta^6\text{-}C_6H_6)Cr(CO)_2$ in both the argon and dinitrogen matrices. The bands observed by Creaven *et al.* for the $(\eta^6\text{-}C_6H_6)Cr(CO)_2$(heptane) complex at 1927 and 1877 cm^{-1} using point by point TRIR spectroscopy at λ_{exc} = 355 nm are at similar wavelength to those recorded for $(\eta^6\text{-}C_8H_6S)Cr(CO)_2$(heptane).[1]

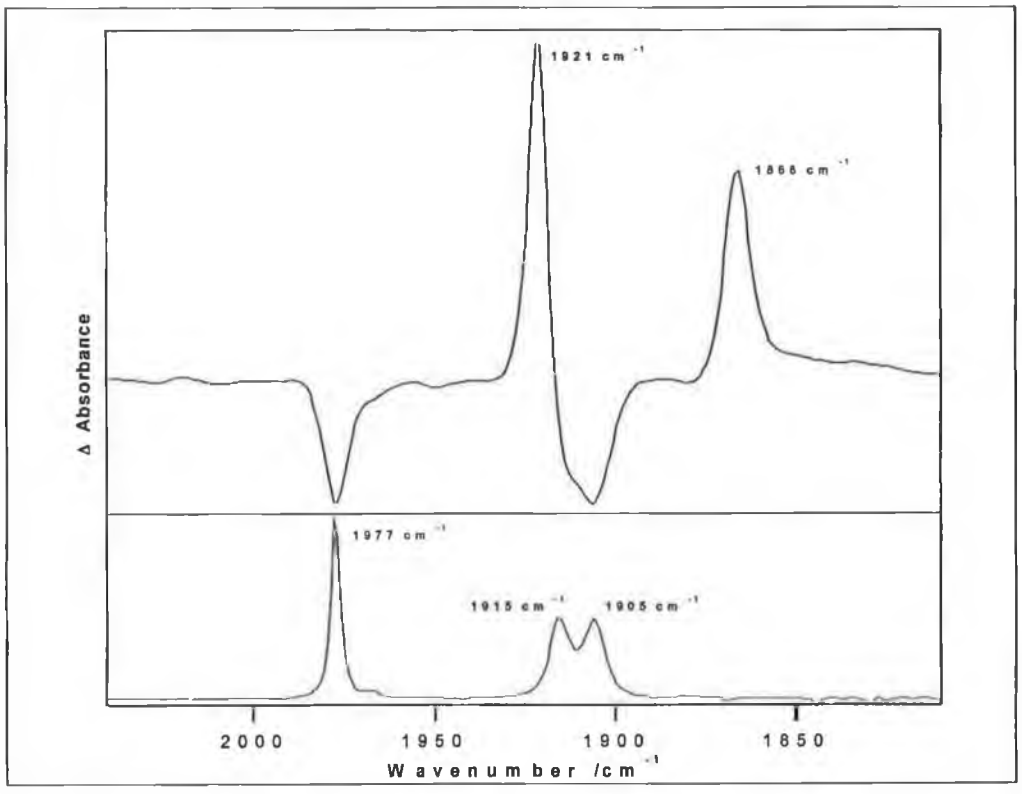

Figure 4.3.1 The step-scan TRIR difference spectrum of $(\eta^6\text{-}C_8H_6S)Cr(CO)_3$ recorded 1.5 μs after laser excitation at λ_{exc} = 355nm in CO saturated heptane (2 atmosphere).

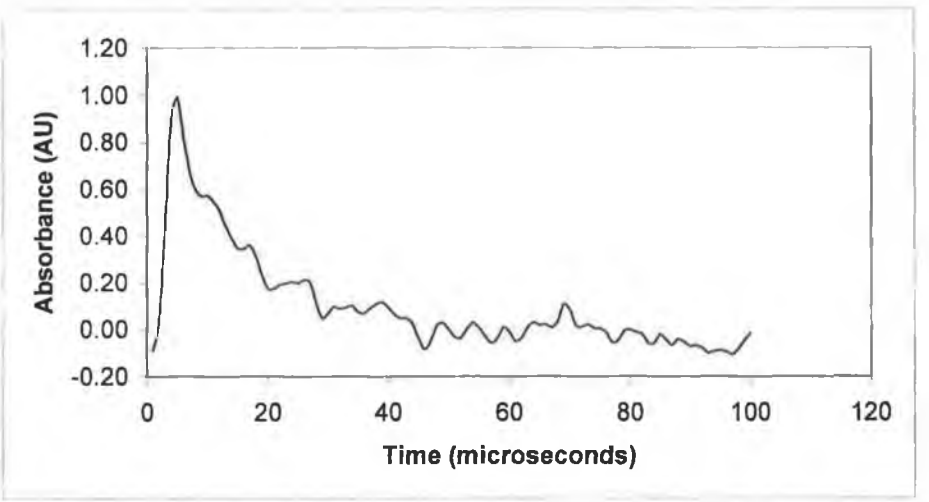

Figure 4.3.2 The kinetic trace obtained for $(\eta^6\text{-}C_8H_6S)Cr(CO)_3$ at 1921 cm^{-1} obtained using stepscan TRIR λ_{exc} = 355 nm in CO saturated (2 atmospheres) heptane.

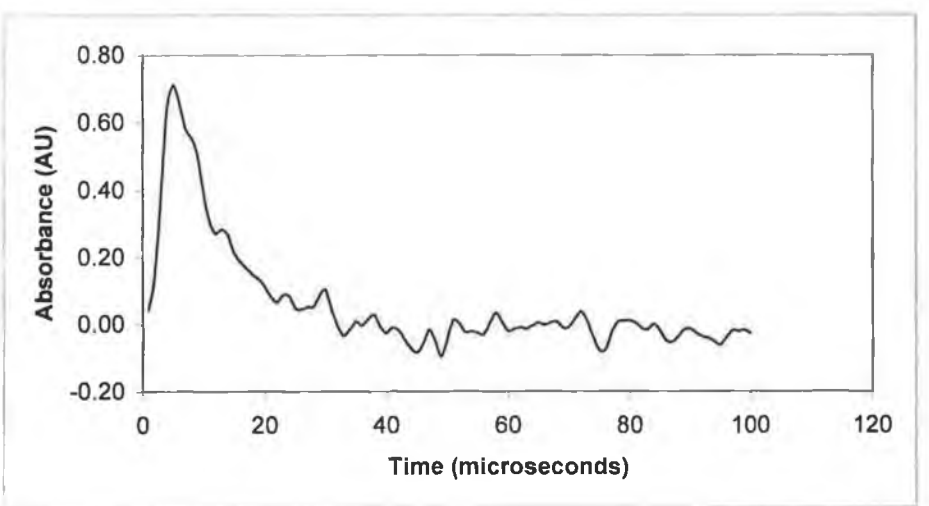

Figure 4.3.3 The kinetic trace obtained for $(\eta^6\text{-}C_8H_6S)Cr(CO)_3$ at 1921 cm^{-1} obtained using stepscan TRIR λ_{exc} = 355 nm in CO saturated (2 atmospheres) heptane.

The kinetic traces obtained by stepscan TRIR at λ_{exc} = 355 nm in CO (2 atmospheres) saturated heptane at 1921 and 1866 cm^{-1} are shown in Figures 4.3.2 and 4.3.3. From the two traces at 1921 and 1866 cm^{-1}, the rate constant for the reaction of $(\eta^6\text{-}C_8H_6S)Cr(CO)_2$(heptane) with CO was determined by subtracting k_{obs} (s^{-1}) in the absence of CO from that in the presence of 2.4×10^{-2} M CO and by dividing the result

by 2.4×10^{-2} M CO. The rate constant for this reaction was found to be 1×10^{7} $s^{-1}mol^{-1}dm^{3}$ at 298 K.

4.4 Matrix isolation studies of $(\eta^6\text{-}C_8H_6S)Cr(CO)_3$ in nitrogen and argon matrices

Nitrogen Matrix

The ν_{co} bands for the parent complex, $(\eta^6\text{-}C_8H_6S)Cr(CO)_3$ in a dinitrogen matrix are observed at 1979, 1917 and 1902 cm^{-1}. When a sample of $(\eta^6\text{-}C_8H_6S)Cr(CO)_3$ was irradiated at $\lambda_{exc} > 400$ nm, three new bands were observed to form at 1976, 1913 and 1906 cm^{-1}. This is illustrated in Figure 4.4.1. As the three bands at 1976, 1913 and 1902 cm^{-1} formed, no evidence for formation of free CO or a $\nu(N\equiv N)$ stretch was obtained. This would indicate that the species forming upon low energy photolysis is neither a ring slip species or a CO loss product, but rather a rotomer. On shifting to higher energy photolysis using a λ_{exc} >340 nm filter, in addition to a small increase in intensity of the bands at 1976, 1913 and 1906 cm^{-1}, two additional metal carbonyl bands were observed at 1934 and 1887 cm^{-1}. This is illustrated by Figure 4.4.2. The bands at 1934 and 1887 cm^{-1} have been assigned to the $(\eta^6\text{-}C_8H_6S)Cr(CO)_3(N_2)$ species. In addition there was a band at 2139 cm^{-1} which corresponds to free CO and another at 2151 cm^{-1} which corresponds to a $\nu(N\equiv N)$ stretch, Figure 4.4.3. This would indicate formation of the dicarbonyl species.

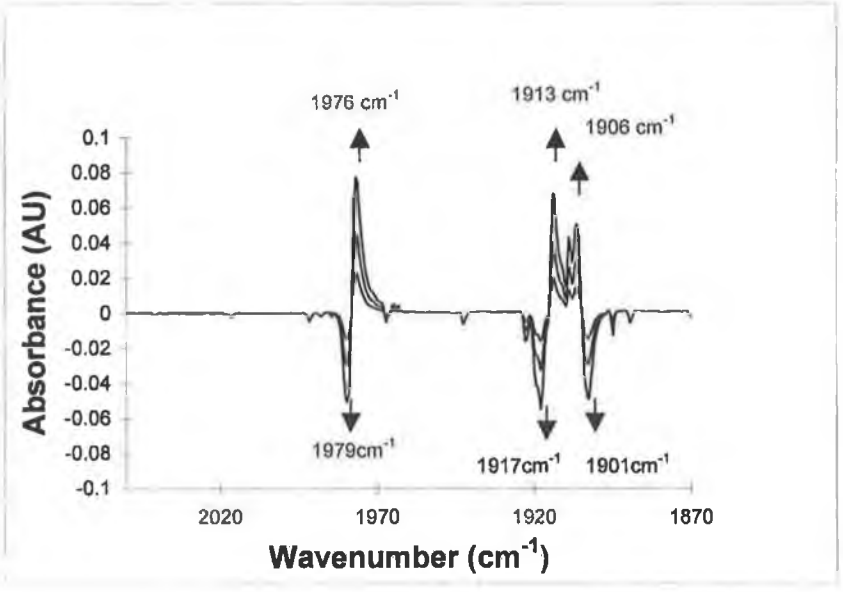

Figure 4.4.1 Spectral changes following photolysis of $(\eta^6\text{-}C_8H_6S)Cr(CO)_3$ at $\lambda_{exc} > 400$ nm for 35 minutes in a nitrogen matrix at 12K.

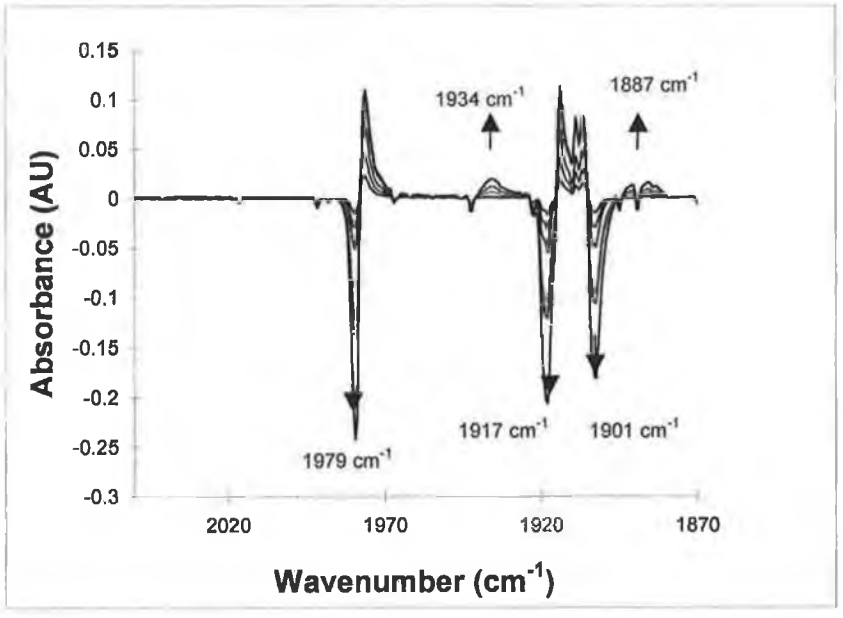

Figure 4.4.2 Spectral changes observed following photolysis of $(\eta^6\text{-}C_8H_6S)Cr(CO)_3$ at $\lambda_{exc} > 340$ nm for 90 minutes in a nitrogen matrix at 12K.

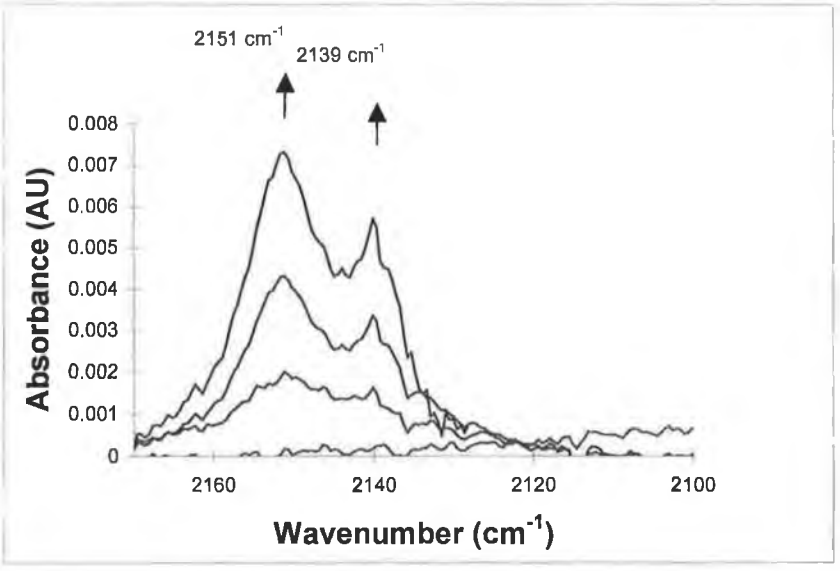

Figure 4.4.3 Spectral changes observed following photolysis of $(\eta^6\text{-}C_8H_6S)Cr(CO)_3$ at $\lambda_{exc} > 340$ nm for 90 minutes in a nitrogen matrix at 12K showing formation of a dinitrogen stretch (2151 cm^{-1}) and formation of free CO (2139 cm^{-1}).

Argon matrix

Photolysis at λ_{exc} >400nm of $(\eta^6\text{-}C_8H_6S)Cr(CO)_3$ in an argon matrix resulted in depletion of the parent bands at 1982, 1921 and 1908 cm^{-1} and formation of three new bands at 1979, 1917 and 1913 cm^{-1}. These bands are again assigned to a rotomer species. On irradiating the matrix with high energy irradiation at λ_{exc} >340nm, bands at 1937 and 1897 cm^{-1} were produced along with a small increase in the bands at 1979, 1917 and 1913 cm^{-1}. The bands at 1935 and 1898 cm^{-1} are assigned to the dicarbonyl species, $(\eta^6\text{-}C_8H_6S)Cr(CO)_2$. Evidence for formation of free CO (2137 cm^{-1}) was also observed.

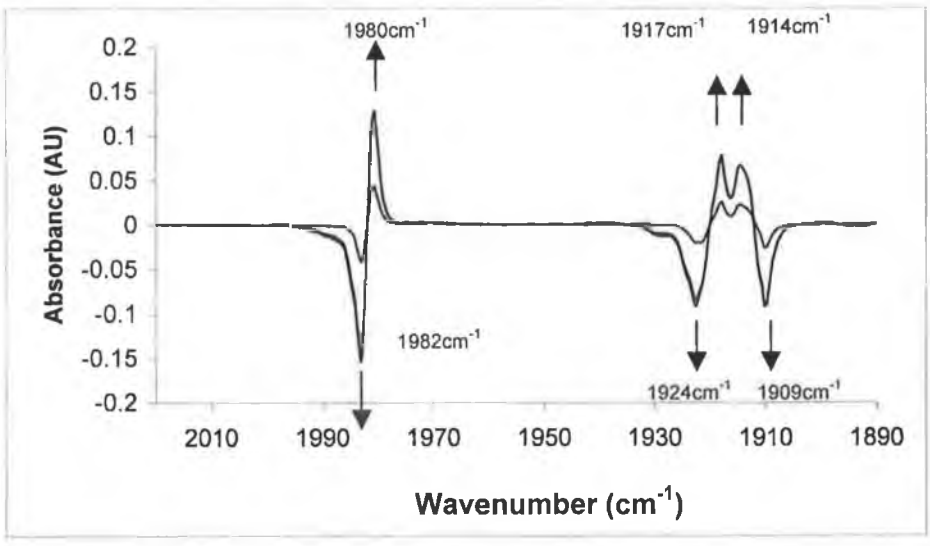

Figure 4.4.4 Spectral changes observed following photolysis of $(\eta^6\text{-}C_8H_6S)Cr(CO)_3$ at λ_{exc} >400 nm for 90 minutes in a argon matrix at 12K .

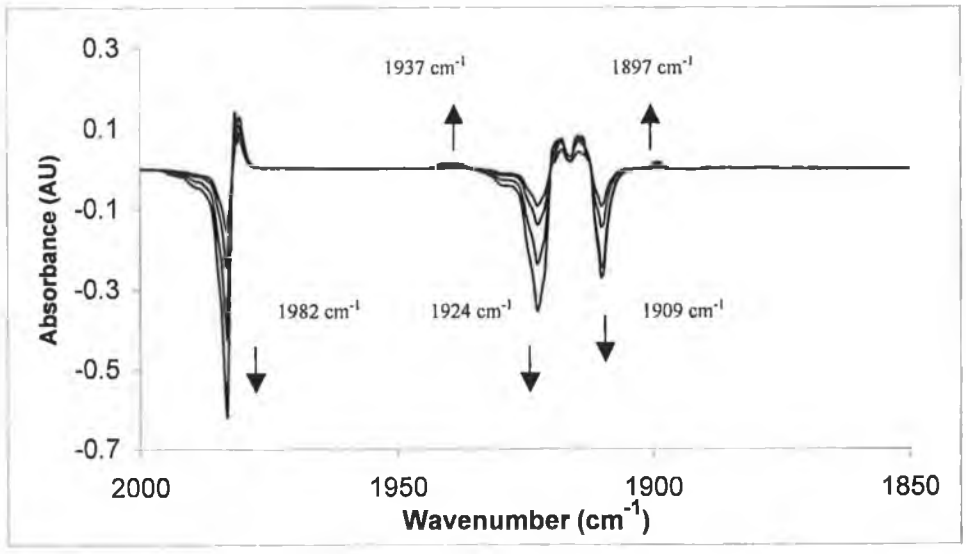

Figure 4.4.5 Spectral changes observed following photolysis of $(\eta^6\text{-}C_8H_6S)Cr(CO)_3$ at λ_{exc} >340 nm for 90 minutes in a argon matrix at 12K.

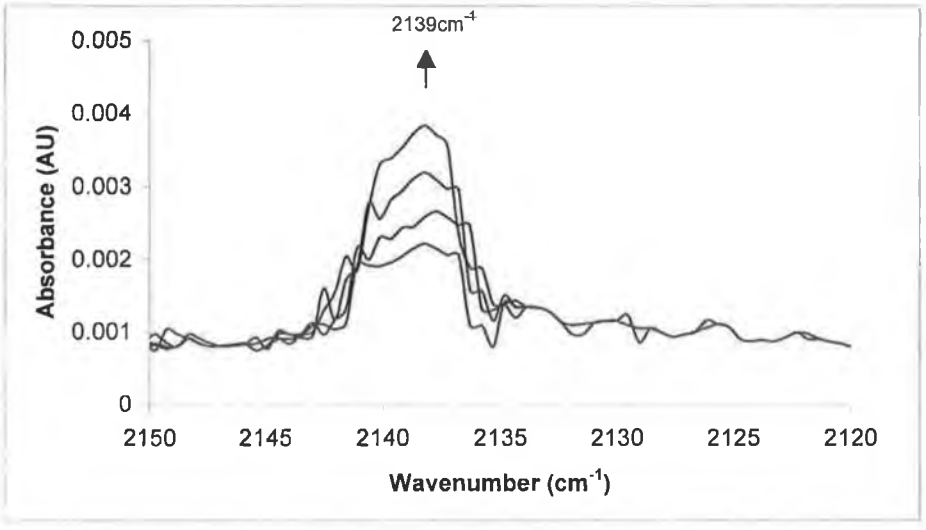

Figure 4.4.6 Spectral changes observed following photolysis of $(\eta^6\text{-}C_8H_6S)Cr(CO)_3$ at λ_{exc} >340 nm for 90 minutes in a argon matrix at 12K showing formation of free CO.

In both argon and dinitrogen matrix photolysis at λ_{exc} >340 nm resulted in depletion of the parent bands together with the formation of two bands in the carbonyl region, which are assigned to the formation of the dicarbonyl species. While irradiation at λ_{exc} >400 nm led depletion of the parent bands with simultaneous formation of a three band pattern, which was assigned to formation of a rotomer. The results of the matrix isolation experiments are summarised in Table 4.4.1.

Matrix	Bands (cm^{-1}) observed upon photolysis at high energy photolysis, λ_{exc} >340 nm	Bands (cm^{-1}) observed upon photolysis at low energy photolysis, λ_{exc} >400 nm
Argon matrix	1939 and 1898	1979, 1917 and 1913
Nitrogen matrix	1934 and 1887	1976, 1913 and 1906

Table 4.4.1 Bands observed in a nitrogen or argon matrix at 12K following photolysis at λ_{exc} > 400nm and >340 nm (xenon arc lamp).

When photolysis at λ_{exc} >340 nm carried out in the dinitrogen matrix formation of two bands at 1934 and 1887 cm^{-1} along with the formation of free CO was observed along with the formation of a band at assigned to a $\nu(N\equiv N)$ stretch. Rest *et al* have reported formation of $(\eta^6\text{-}C_6H_6)Cr(CO)_2$ upon photolysis of $(\eta^6\text{-}C_6H_6)Cr(CO)_3$ in argon, nitrogen and methane matrices.[21] In the argon matrix the $(\eta^6\text{-}C_6H_6)Cr(CO)_2$ bands were observed at 1937 and 1885 cm^{-1}. In the methane matrix these bands were observed at 1925 and 1870 cm^{-1} and in nitrogen, the bands were observed at 1939 and 1895 cm^{-1} with a $\nu(N\equiv N)$ stretch at 2148.4 cm^{-1}. On the basis of the results obtained by Rest *et al.* the bands at 1939 and 1898 cm^{-1} (argon matrix) were assigned to the formation of $(\eta^6\text{-}C_8H_6S)Cr(CO)_2$ and 1934 and 1887 cm^{-1} (nitrogen matrix) assigned to the formation of $(\eta^6\text{-}C_8H_6S)Cr(CO)_2(N_2)$.[21]

4.5 UV/vis monitored laser flash photolysis of $(\eta^6\text{-}C_8H_6S)Cr(CO)_3$ in CO saturated cyclohexane

Absorption spectra of $(\eta^6\text{-arene})Cr(CO)_3$ compounds are dominated by metal to ligand charge transfer absorptions.[18,19,20] On examination of the UV/vis spectra shown in Figure 4.5.1, it is obvious that $(\eta^6\text{-}C_8H_6S)Cr(CO)_3$ absorb at lower energy than $(\eta^6\text{-}C_6H_6)Cr(CO)_3$. Similar to the benzene analogue both of the compounds have a λ_{max} at $\approx$ 340 nm. This absorption band is thought to be a Cr $\rightarrow$ arene CT transition with some Cr $\rightarrow \pi^*$CO CT transition character.

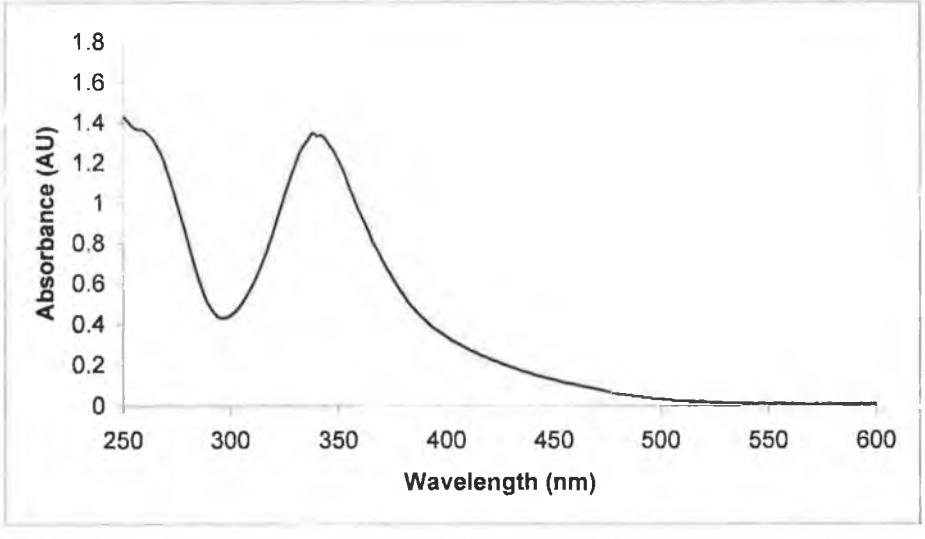

Figure 4.5.1 The UV/vis spectrum of $(\eta^6\text{-}C_8H_6S)Cr(CO)_3$ recorded in cyclohexane.

Following laser excitation at λ_{exc} = 355 nm of $(\eta^6\text{-}C_8H_6S)Cr(CO)_3$ in cyclohexane under 1 atmosphere of CO, a transient species was observed at 280 nm. In comparison to previous studies of other polyaromatic $(\eta^6\text{-arene})Cr(CO)_3$ complexes, this transient signal was thought to be the solvated dicarbonyl species, $(\eta^6\text{-arene})Cr(CO)_2(solvent)$. A typical transient species monitored at 280 nm is shown in Figure 4.5.3 for the $(\eta^6\text{-}C_8H_6S)Cr(CO)_3$ complex. The decay curve shown in Figure 4.5.3 represents the decay of the solvated complex with CO to yield the parent complex, Reaction 4.5.3. The dependence of the lifetime of the solvated dicarbonyl upon the concentration of CO, was investigated. The concentration of CO in solution was increased from 0.25

to 1 atmosphere and the lifetime of the solvated dicarbonyl species was found to decrease. A linear dependence between the k_{obs} (s^{-1}) of the transient signal at 280 nm and the concentration of CO and the second order rate constant for the reaction of the solvated dicarbonyl with CO was calculated from the slope of the graph. For the $(\eta^6\text{-}C_8H_6S)Cr(CO)_3$ complex, the second order rate constant for the reaction of the solvated dicarbonyl with CO was found to be 6×10^6 $s^{-1}mol^{-1}dm^3$. Therefore the primary photoreaction of this system can be stated by Reaction 4.5.1 and 4.5.2.

$$(\eta^6\text{-}C_8H_6S)Cr(CO)_3 \xrightarrow{h\nu} (\eta^6\text{-}C_8H_6S)Cr(CO)_2 + CO$$

Reaction 4.5.1.

$$(\eta^6\text{-}C_8H_6S)Cr(CO)_2 + s \longrightarrow (\eta^6\text{-}C_8H_6S)Cr(CO)_2(s)$$

s = cyclohexane

Reaction 4.5.2.

Under a under a CO atmosphere, this solvated intermediate recombines with CO to regenerate the parent tricarbonyl complex.

$$(\eta^6\text{-}C_8H_6S)Cr(CO)_2(s) + CO \longrightarrow (\eta^6\text{-}C_8H_6S)Cr(CO)_3$$

Reaction 4.5.3.

The UV/vis difference spectrum recorded 2 μs after laser excitation at λ_{exc} = 355 nm under 1 atmosphere of CO is given in Figure 4.5.1 for $(\eta^6\text{-}C_8H_6S)Cr(CO)_3$. For the $(\eta^6\text{-}C_8H_6S)Cr(CO)_3$ system, a maximum is observed at 280 nm and a depletion at 340 nm. The positive band at 280 nm $(\eta^6\text{-}C_8H_6S)Cr(CO)_3$ represents formation of the solvated dicarbonyl intermediate while the negative absorption at 340 nm signifies the depletion of the parent tricarbonyl.

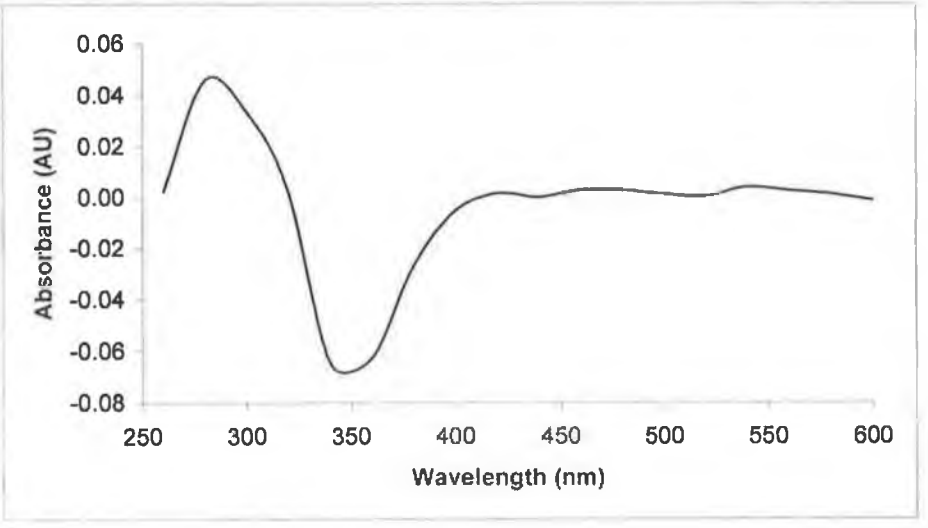

Figure 4.5.2 UV/vis difference spectrum obtained 2 μs after excitation of $(\eta^6\text{-}C_8H_6S)Cr(CO)_3$ at λ_{exc} = 355nm in CO saturated cyclohexane.

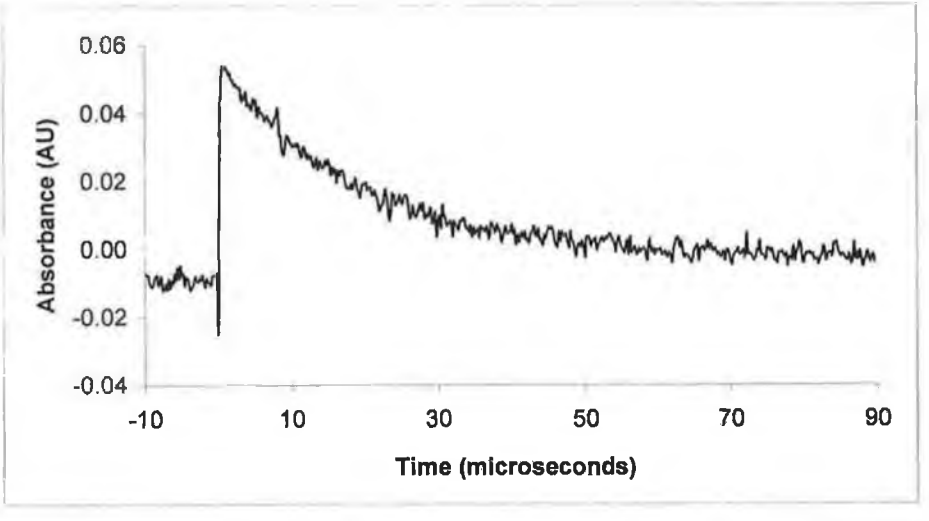

Figure 4.5.3 A typical transient obtained for the decay of $(\eta^6\text{-}C_8H_6S)Cr(CO)_2$(cyclohexane) upon flash photolysis of $(\eta^6\text{-}C_8H_6S)Cr(CO)_3$ at λ_{exc} = 355 nm in CO saturated cyclohexane.

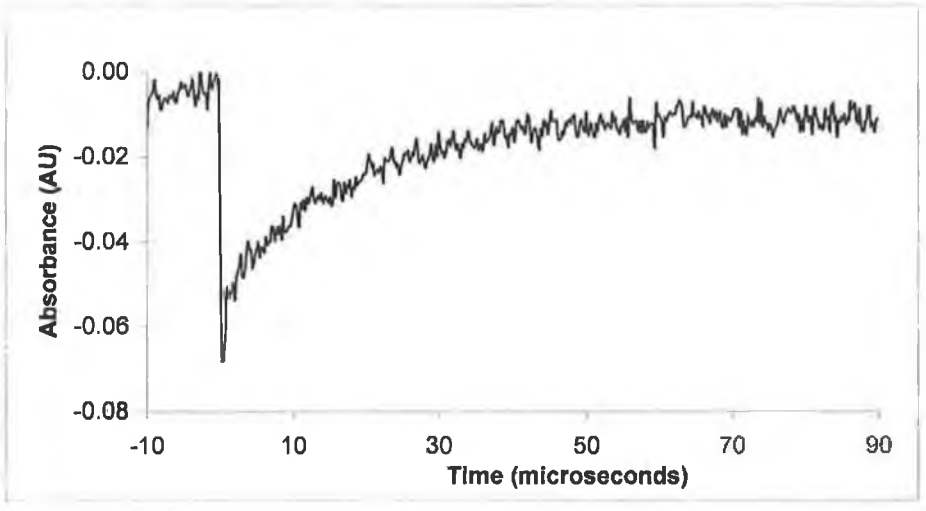

Figure 4.5.4 A typical signal obtained for the recovery of $(\eta^6\text{-}C_8H_6S)Cr(CO)_3$ upon flash photolysis of $(\eta^6\text{-}C_8H_6S)Cr(CO)_3$ at $\lambda_{exc} = 355$ nm in CO saturated cyclohexane.

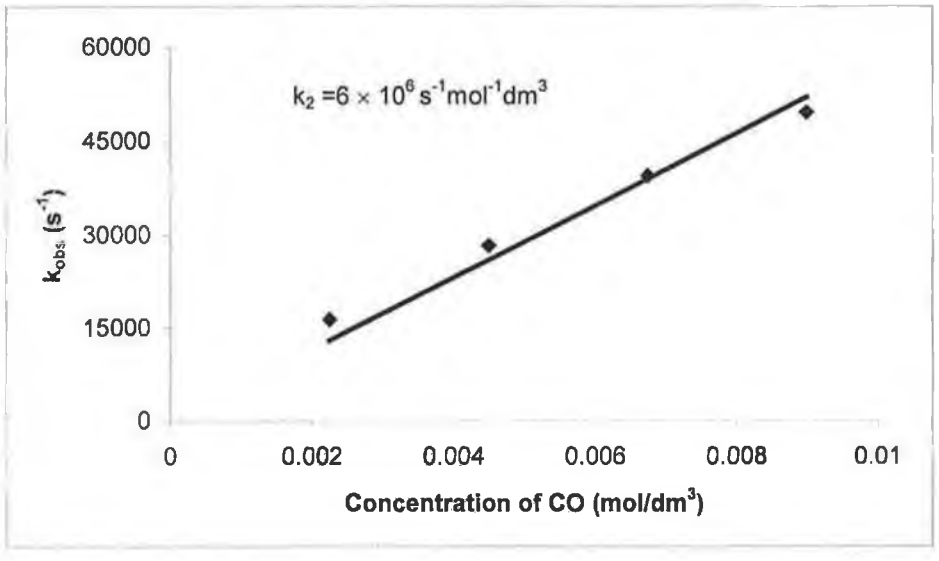

Figure 4.5.5 A plot of the observed rate constant at 280 nm against the concentration of CO (moles/litre) for the reaction of CO with $(\eta^6\text{-}C_8H_6S)Cr(CO)_2$(cyclohexane) at 298 K.

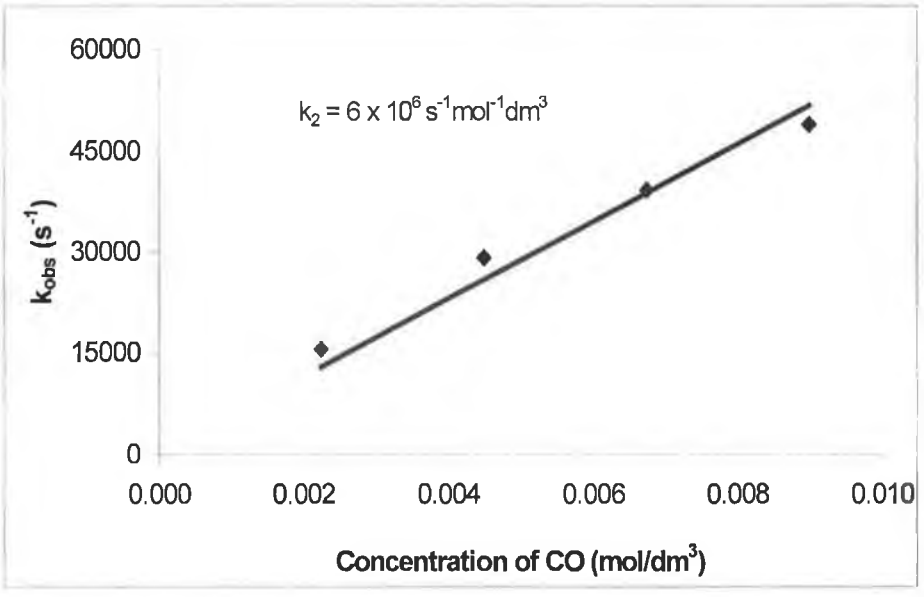

Figure 4.5.6 A plot of the observed rate constant at 340 nm against the concentration of CO (moles/litre) for the reaction of CO with $(\eta^6\text{-}C_8H_6S)Cr(CO)_2$(cyclohexane) at 298 K.

The UV/vis absorption spectrum of $(\eta^6\text{-}C_8H_6S)Cr(CO)_3$ was continuously recorded through out the flash photolysis experiment and the system was not fully reversible in a CO atmosphere. After prolonged photolysis at λ_{exc}= 355 nm, a decrease in the intensity of the absorption at the λ_{max} at 340 nm for $(\eta^6\text{-}C_8H_6S)Cr(CO)_3$ along with an increase in intensity of a band between 260 to 310 nm was recorded in the UV/vis spectrum. These changes are consistent with the formation of $Cr(CO)_6$ and free arene. An IR spectrum obtained on completion of the experiment revealed the presence of $Cr(CO)_6$. Repeating the experiment using long wavelength photolysis at $\lambda_{exc} > 400$ nm produced the same changes in the UV/vis spectrum. From these results it would suggest that CO loss is not the only photochemical pathway available to $(\eta^6\text{-}C_8H_6S)Cr(CO)_3$.

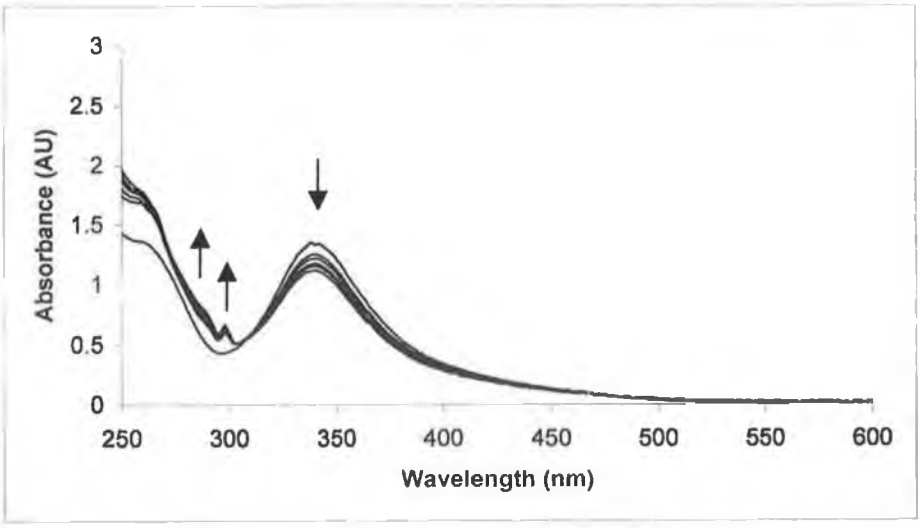

Figure 4.5.7 Changes in the UV/vis spectrum of $(\eta^6\text{-}C_8H_6S)Cr(CO)_3$ following photolysis at λ_{exc} = 355nm in CO saturated cyclohexane.

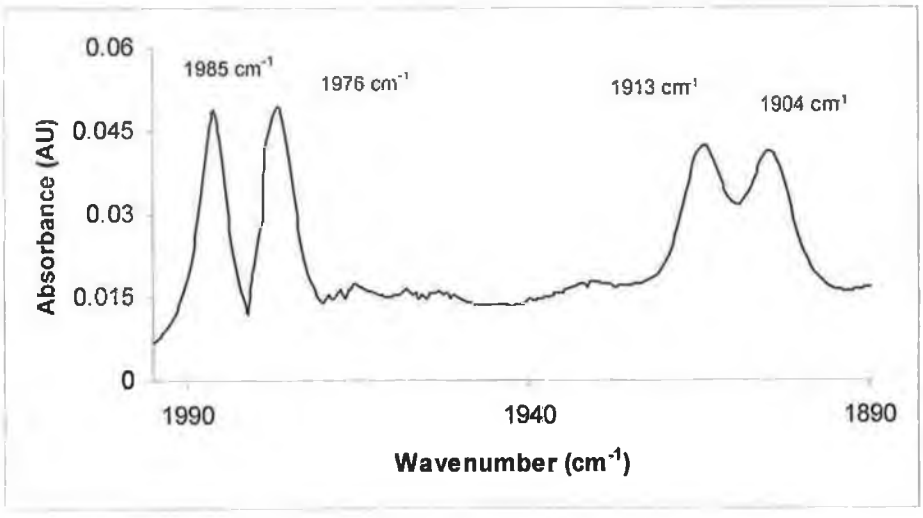

Figure 4.5.8 An IR spectrum recorded following photolysis at λ_{exc} = 355 nm of $(\eta^6\text{-}C_8H_6S)Cr(CO)_3$ in CO saturated cyclohexane. $(\eta^6\text{-}C_8H_6S)Cr(CO)_3$ ν_{co} : 1976,1913 and 1904 cm^{-1}, $Cr(CO)_6$, ν_{co} : 1985 cm^{-1}.

The k_{obs} for the decay of the transient signal at 290 nm using UV/vis flash photolysis at λ_{exc} = 355 nm was also recorded in heptane, from 0.25 - 1 atm CO in heptane, the second order rate constant for the reaction of the solvated dicarbonyl with CO in heptane could be calculated. The k_{obs} for the rate of decay of the signal at 290 nm was found to be dependent on the concentration of CO. By plotting the k_{obs} (s^{-1}) of the rate of decay of the signal recorded at 290 nm against the concentration of CO, the second order rate constant for the reaction was found to be 1×10^7 $s^{-1}mol^{-1}dm^3$. This is the same as the value calculated using TRIR for the reaction of solvated dicarbonyl with CO. Similarly by plotting the k_{obs} of the rate of recovery of the signal recorded at 340 nm thought to be the recovery of the parent against the concentration of CO, the second order rate constant for the reaction was found to be 1×10^7 $s^{-1}mol^{-1}dm^3$.

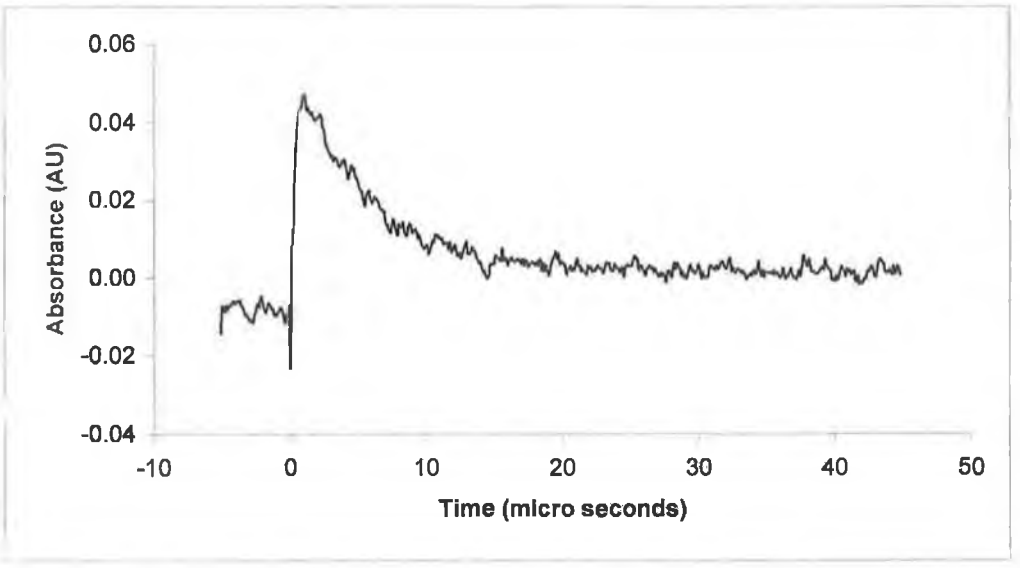

Figure 4.5.9 A typical transient obtained for the decay of $(\eta^6\text{-}C_8H_6S)Cr(CO)_2$(heptane) at 280 nm upon flash photolysis of $(\eta^6\text{-}C_8H_6S)Cr(CO)_3$ at λ_{exc} = 355 nm in CO saturated heptane.

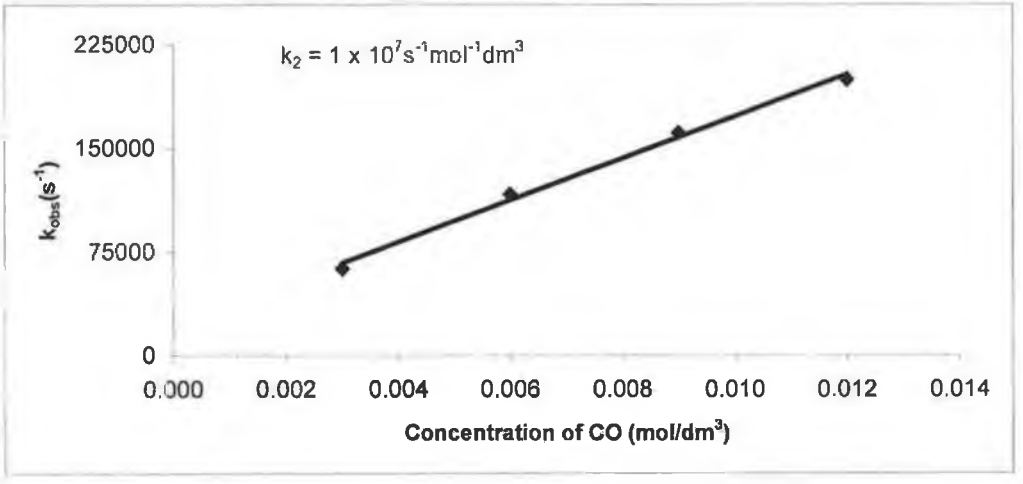

Figure 4.5.10 A plot of the observed rate constant at 280 nm against the concentration of CO (moles/litre) for the reaction of CO with $(\eta^6\text{-}C_8H_6S)Cr(CO)_2$(heptane) at 298 K.

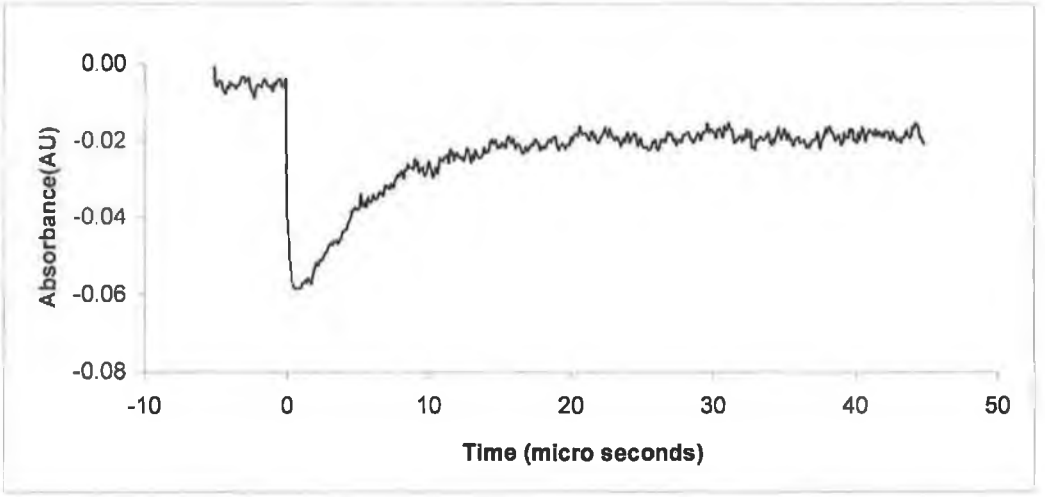

Figure 4.5.11 A typical signal obtained for the recovery of $(\eta^6\text{-}C_8H_6S)Cr(CO)_3$ upon flash photolysis of $(\eta^6\text{-}C_8H_6S)Cr(CO)_3$ at λ_{exc} = 355 nm in CO saturated heptane.

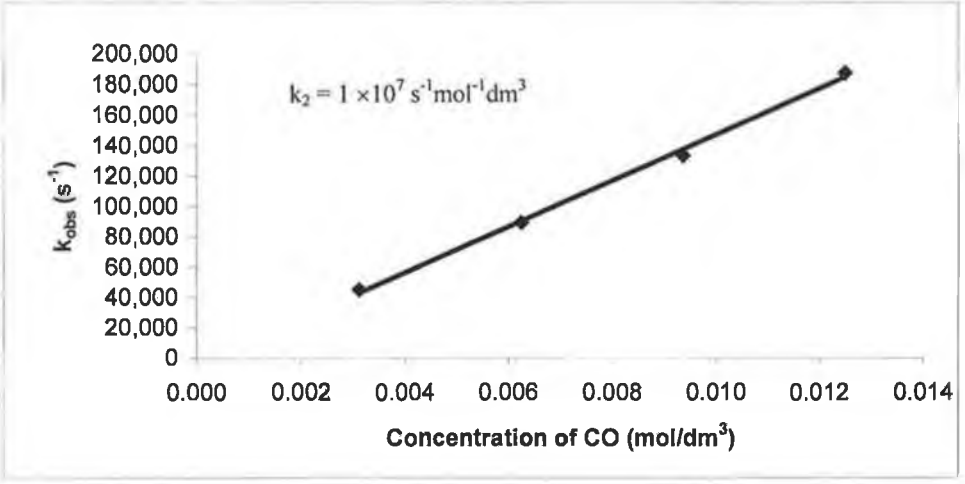

Figure 4.5.12 A plot of the observed rate constant at 340 nm against the concentration of CO (moles/litre) for the reaction of CO with $(\eta^6\text{-}C_8H_6S)Cr(CO)_2$(heptane) at 298 K.

4.5.1 UV/vis monitored laser flash photolysis of $(\eta^6\text{-}C_8H_6S)Cr(CO)_3$ in argon saturated cyclohexane

The photochemistry of the $(\eta^6\text{-}C_8H_6S)Cr(CO)_3$ was also investigated by UV/vis flash photolysis at λ_{exc} = 355 nm in argon (1 atmosphere) saturated cyclohexane. Figure 4.5.1.1 depicts the absorbance difference spectrum obtained 70 μs after laser flash photolysis. Examination of the absorbance difference spectra reveals a λ_{max} at 400 nm.

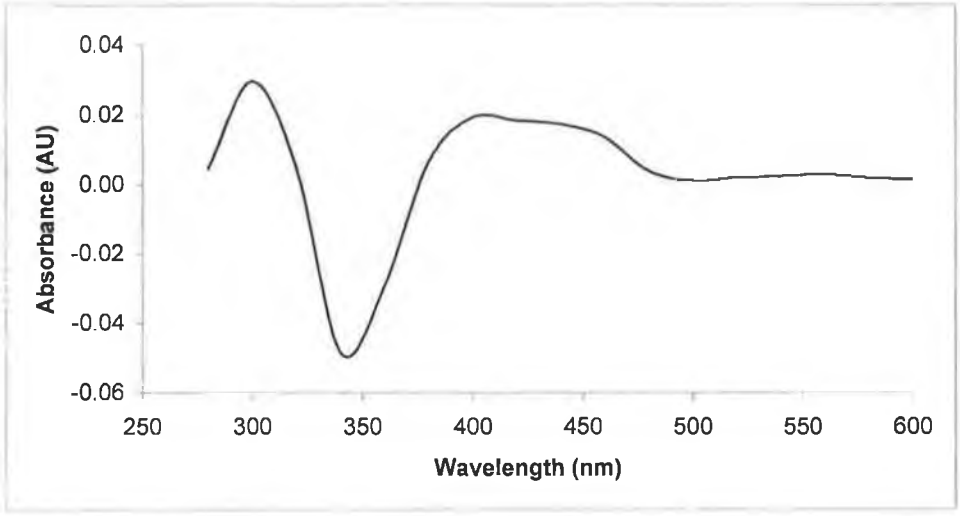

Figure 4.5.1.1 UV/vis difference spectrum obtained 70 μs after excitation of $(\eta^6\text{-}C_8H_6S)Cr(CO)_3$ at λ_{exc} = 355nm in argon saturated cyclohexane.

Comparison of the UV/vis spectrum obtained during the flash photolysis experiment with the difference spectra obtained by laser flash photolysis, discloses some information about the nature of the photoproduct. Examination of the UV/vis spectra, Figure 4.5.1.2 shows that a band grows in at ~ 400 nm for the $(\eta^6\text{-}C_8H_6S)Cr(CO)_3$ complex during the photolysis experiment. This is consistent with the signal recorded at 400 nm using laser flash photolysis, Figure 4.5.1.1.

The depletion of the band at 340 nm with no recovery using laser flash photolysis can also be observed, which is consistent with depletion of the band at 340 nm in the UV/vis spectrum. Formation of a band at 280 nm in the UV/vis spectrum is consistent

with the grow in observed at 280 nm using UV/vis laser flash photolysis. The signal recorded at 280 nm, is thought to be the reaction of $(\eta^6\text{-}C_8H_6S)Cr(CO)_2(s)$ species reacting with starting material to yield a dinuclear species. For the $(\eta^6\text{-}C_8H_6S)Cr(CO)_3$ complex a linear relationship exists between the k_{obs} (s^{-1}) for the rate of grow in at 400 nm and the concentration of $(\eta^6\text{-}C_8H_6S)Cr(CO)_3$, indicating a reaction of solvated dicarbonyl with unphotolysed starting material to yield a dinuclear species. The second order rate constant for formation of the dinuclear species was found to be 2 $\times 10^7$ $s^{-1}mol^{-1}dm^3$ at 298 K.

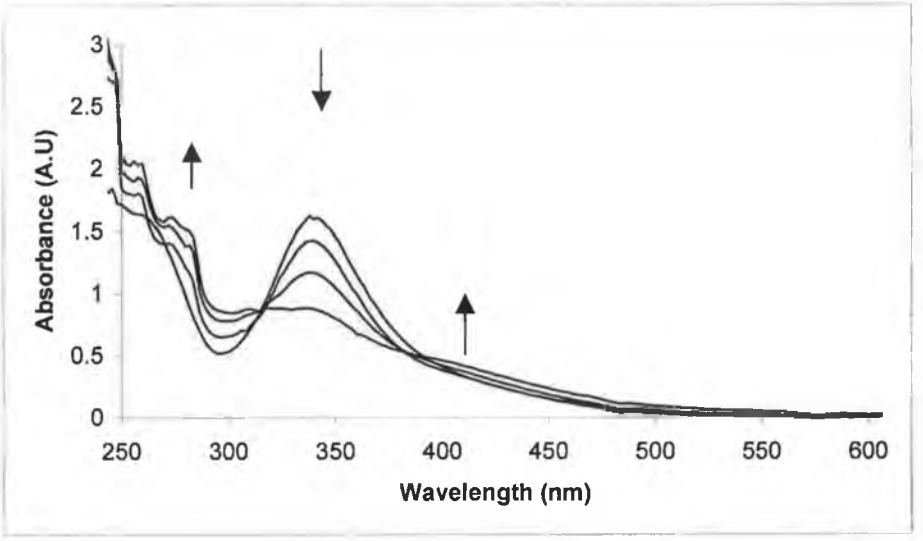

Figure 4.5.1.2 Changes in the UV/vis spectrum of $(\eta^6\text{-}C_8H_6S)Cr(CO)_3$ following photolysis at λ_{exc} = 355nm after 4 minutes in argon saturated cyclohexane.

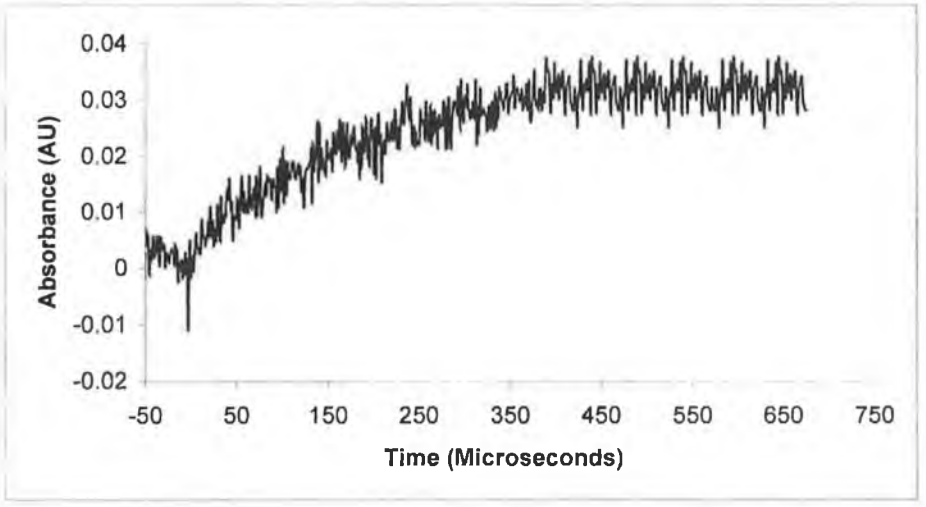

Figure 4.5.1.3 A typical grow in observed at 400 nm upon flash photolysis of $(\eta^6\text{-}C_8H_6S)Cr(CO)_3$ in argon saturated cyclohexane at λ_{exc} = 355nm.

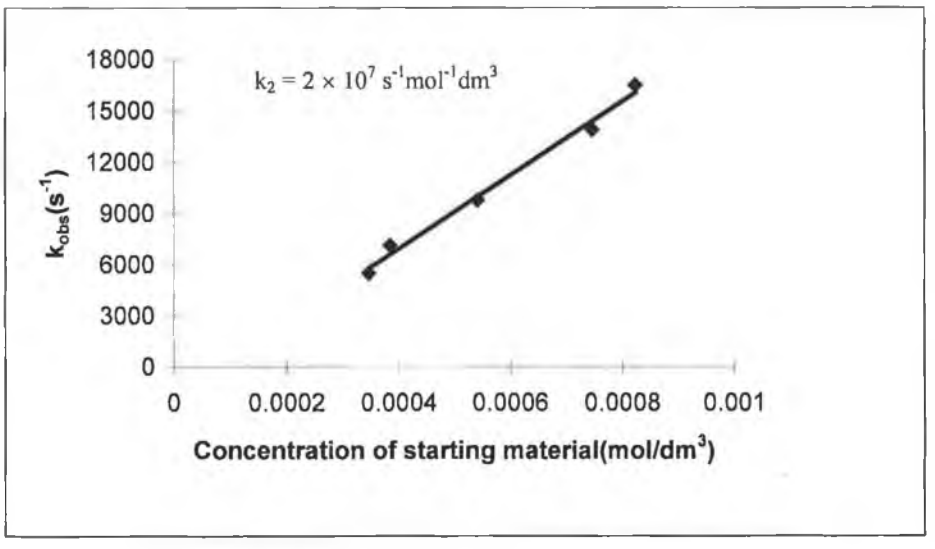

Figure 4.5.1.4 The plot of k_{obs} of the grow in at 400 nm versus concentration of starting material for $(\eta^6\text{-}C_8H_6S)Cr(CO)_3$ in argon saturated cyclohexane.

4.6 UV/vis monitored laser flash photolysis of $(\eta^6\text{-}C_{12}H_8S)Cr(CO)_3$ in CO saturated cyclohexane.

The absorption spectra of $(\eta^6\text{-arene})Cr(CO)_3$ compounds are dominated by metal to ligand charge transfer absorptions.[18,19,20] The main difference between the benzothiophene and dibenzothiophene analogues absorption spectra is that $(\eta^6\text{-}C_{12}H_8S)Cr(CO)_3$ absorbs further into the visible then $(\eta^6\text{-}C_{12}H_8S)Cr(CO)_3$. Similar to the $(\eta^6\text{-benzene})Cr(CO)_3$ both of the compounds have a λ_{max} at $\approx$ 340 nm. This absorption band is thought to be a Cr $\rightarrow$ arene charge transfer transition with some Cr $\rightarrow$ π^*CO charge transition character.

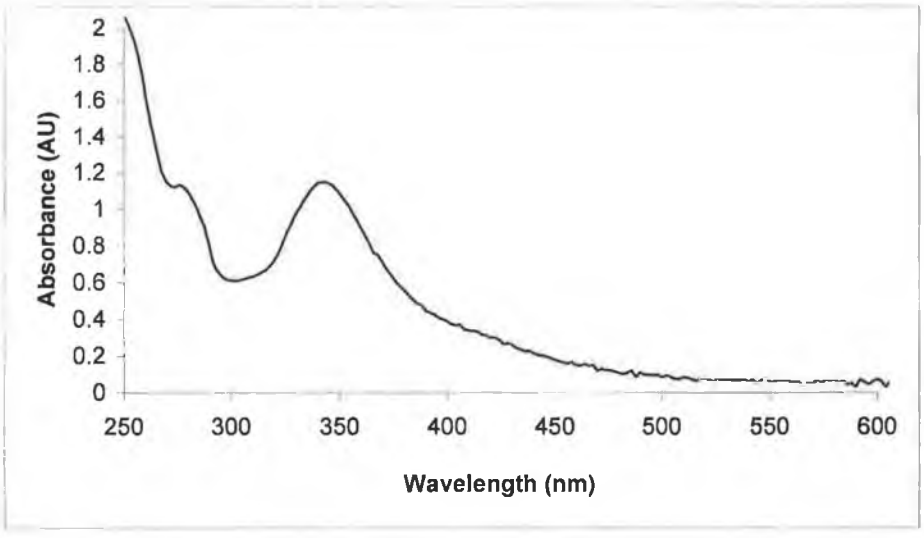

Figure 4.6.1 The UV/vis spectrum of $(\eta^6\text{-}C_{12}H_8S)Cr(CO)_3$ recorded in cyclohexane.

Following laser excitation at λ_{exc} = 355 nm of $(\eta^6\text{-}C_{12}H_8S)Cr(CO)_3$ in cyclohexane under 1 atmosphere of CO, a transient species was observed at 300 nm. Similarly to previous studies of other polyaromatic $(\eta^6\text{-arene})Cr(CO)_3$ complexes, this transient signal was thought to be the solvated dicarbonyl, $(\eta^6\text{-arene})Cr(CO)_2$(solvent) complex. A typical transient species monitored at 300 nm is shown in Figure 4.6.3 The decay curve shown in Figure 4.6.3 represents the reaction of the solvated complex with CO to yield the parent complex, Reaction 4.6.3. The dependence of the lifetime of the solvated dicarbonyl upon the concentration of CO, was investigated. The

concentration of CO in solution was increased from 0.25 atmospheres to 1 atmosphere and the life time of the solvated dicarbonyl species was found to decrease. A linear dependence between the k_{obs} of the transient signal at 300 nm and the concentration of CO was observed. The second order rate constant for the reaction of the solvated dicarbonyl with CO was calculated from the slope of the graph. For the $(\eta^6\text{-}C_{12}H_8S)Cr(CO)_3$ complex, the second order rate constant for the reaction of the solvated dicarbonyl with CO was found to be 7×10^6 $s^{-1}mol^{-1}dm^3$. Therefore the primary photoreaction of this system can be stated by Reaction 4.6.1 and 4.6.2.

$$(\eta^6\text{-}C_{12}H_8S)Cr(CO)_3 \xrightarrow{h\nu} (\eta^6\text{-}C_{12}H_8S)Cr(CO)_2 + CO \qquad \text{Reaction 4.6.1}$$

$$(\eta^6\text{-}C_{12}H_8S)Cr(CO)_2 + s \longrightarrow (\eta^6\text{-}C_{12}H_8S)Cr(CO)_2(s) \qquad \text{Reaction 4.6.2}$$

s = cyclohexane

When in the presence of a CO environment this solvated intermediate recombines with CO to regenerate the parent tricarbonyl complex.

$$(\eta^6\text{-}C_{12}H_8S)Cr(CO)_2(s) + CO \longrightarrow (\eta^6\text{-}C_{12}H_8S)Cr(CO)_3 + (s) \qquad \text{Reaction 4.6.3}$$

The UV/vis difference spectrum recorded 2 μs after laser excitation at λ_{exc} = 355 nm under 1 atmosphere of CO is given in Figure 4.6.1 for $(\eta^6\text{-}C_{12}H_8S)Cr(CO)_3$. For the $(\eta^6\text{-}C_{12}H_8S)Cr(CO)_3$ system, a maximum is observed at 300 nm and a depletion at 340 nm.

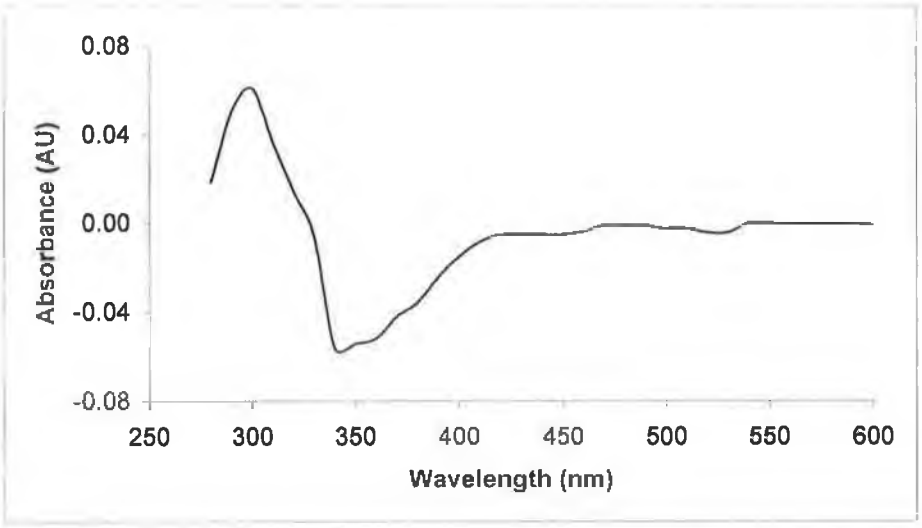

Figure 4.6.2 UV /vis difference spectrum obtained 2 μs after excitation of $(\eta^6\text{-}C_{12}H_8S)Cr(CO)_3$ at λ_{exc} = 355 nm in CO saturated cyclohexane.

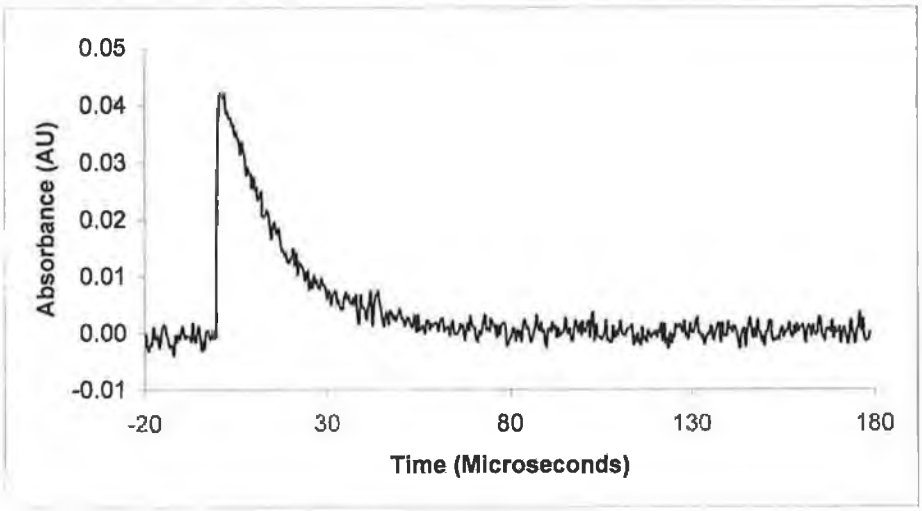

Figure 4.6.3 A typical transient signal obtained for the decay of $(\eta^6\text{-}C_{12}H_8S)Cr(CO)_2$(cyclohexane) upon flash photolysis of $(\eta^6\text{-}C_{12}H_8S)Cr(CO)_3$ at λ_{exc} = 355 nm in CO saturated cyclohexane.

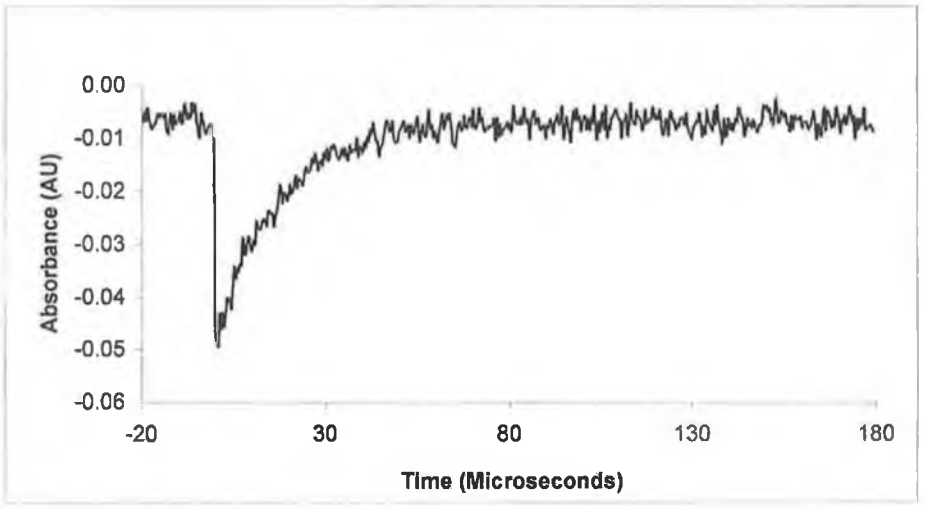

Figure 4.6.3 A typical transient signal obtained for the recovery of $(\eta^6\text{- } C_{12}H_8S)Cr(CO)_3$ upon flash photolysis of $(\eta^6\text{- } C_{12}H_8S)Cr(CO)_3$ at $\lambda_{exc} = 355$ nm in CO saturated cyclohexane.

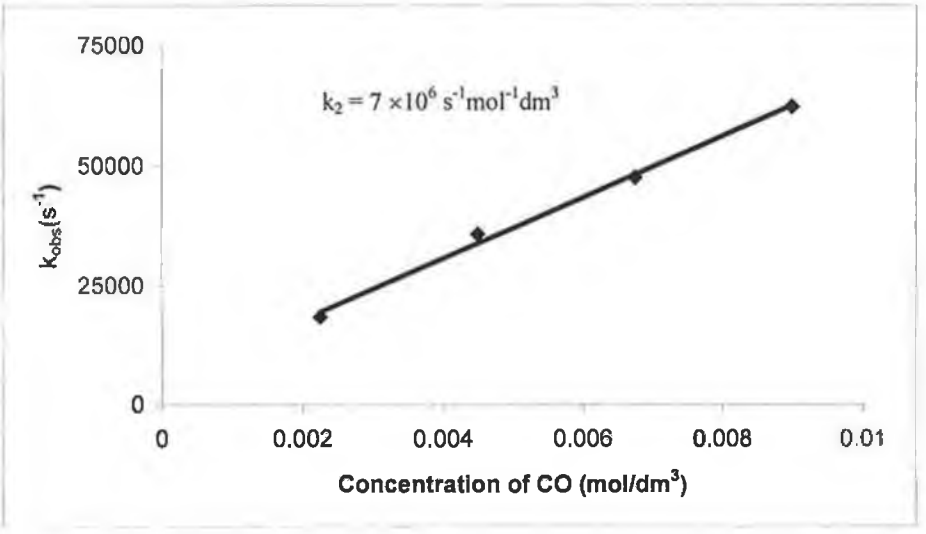

Figure 4.6.4 A plot of the observed rate constant recorded at 300 nm against the plot of concentration of CO (mol/litre) for the reaction of CO with $(\eta^6\text{- } C_{12}H_8S)Cr(CO)_2$(cyclohexane) at 298 K.

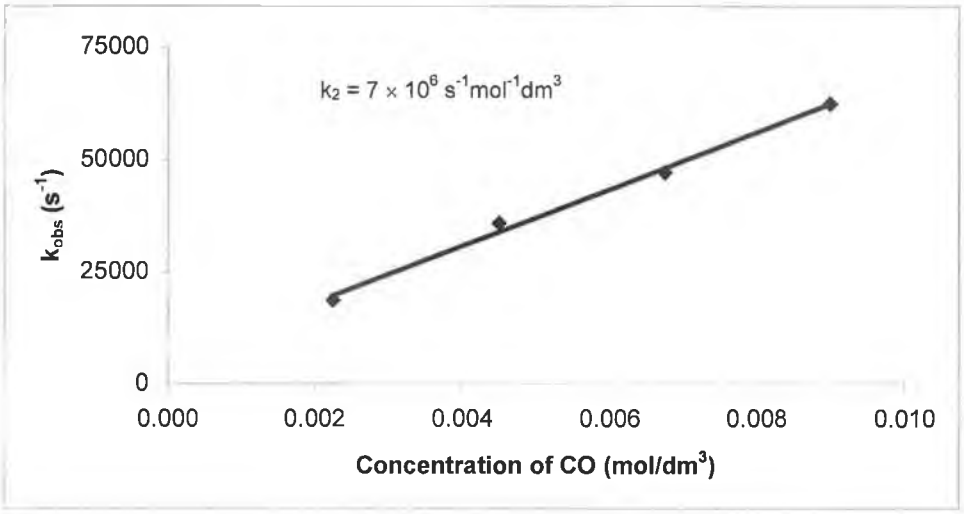

Figure 4.6.5 The plot of k_{obs} (s^{-1}) of the recovery at 340 nm versus concentration of CO (moles / litre) in CO saturated cyclohexane at 298 K.

The steady state UV/vis absorption spectrum of $(\eta^6\text{-}C_{12}H_8S)Cr(CO)_3$ was recorded through out the flash photolysis experiment. The system was not fully reversible under a CO atmosphere. After prolonged photolysis at λ_{exc}= 355 nm, a decrease in the intensity of the absorption at the λ_{max} at 340 nm for $(\eta^6\text{-}C_8H_6S)Cr(CO)_3$ along with an increase in intensity of a band at 260 to 310 nm was recorded in the UV/vis spectrum. These changes are consistent with the formation of $Cr(CO)_6$ and free arene. An IR spectrum obtained on completion of the experiment revealed the presence of $Cr(CO)_6$. Repeating the experiment using long wavelength photolysis at $\lambda_{exc} > 400$ nm produced the same changes in the UV/vis spectrum. From these results it would suggest that CO loss is not the only photochemical pathway open to this complex.

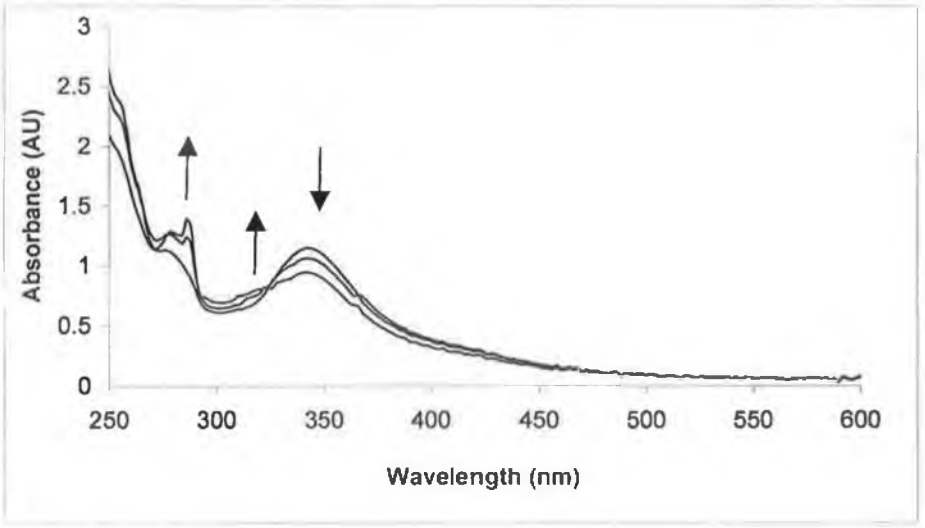

Figure 4.6.6 Changes in the UV/vis spectrum of $(\eta^6\text{-}C_{12}H_8S)Cr(CO)_3$ following photolysis at λ_{exc} = 355 nm for 5 minutes in CO saturated cyclohexane.

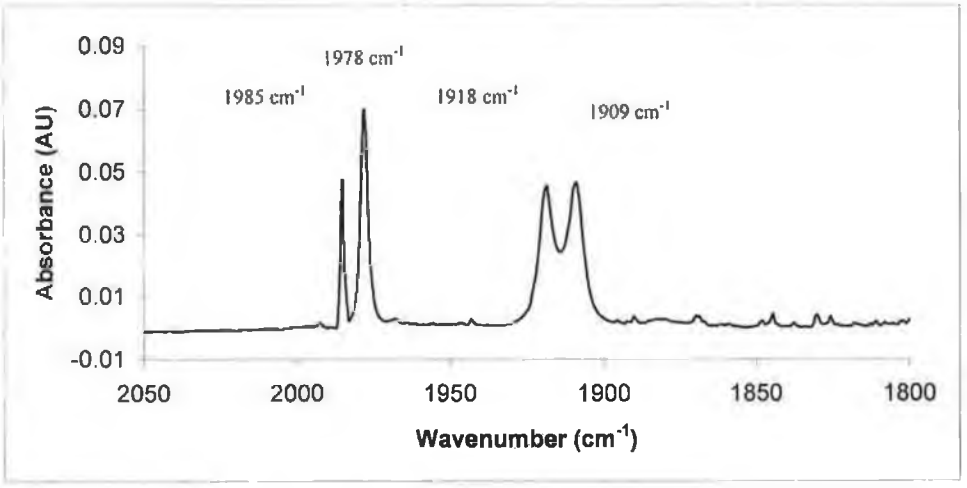

Figure 4.6.7 An IR spectrum recorded following photolysis at λ_{exc} = 355nm of $(\eta^6\text{-}C_{12}H_8S)Cr(CO)_3$ in CO saturated cyclohexane. $(\eta^6\text{-}C_{12}H_8S)Cr(CO)_3$ ν_{co} : 1978,1918 and 1909 cm^{-1}, $Cr(CO)_6$ ν_{co} : 1985 cm^{-1}.

4.6.1 UV/vis monitored laser flash photolysis of $(\eta^6\text{-}C_{12}H_8S)Cr(CO)_3$ in argon saturated cyclohexane.

The photochemistry of $(\eta^6\text{-}C_{12}H_8S)Cr(CO)_3$ was also investigated by UV/vis flash photolysis at λ_{exc} = 355 nm in argon (1 atmosphere) saturated cyclohexane. Figure 4.6.1.1 depicts the absorbance difference spectrum obtained 70 μs after the laser pulse for $(\eta^6\text{-}C_{12}H_8S)Cr(CO)_3$. Examination of the absorbance difference spectrum for both complexes reveals a λ_{max} at 300 nm and a broad absorption between 380 to 480 nm.

Comparison of the UV/vis spectrum obtained during the flash photolysis experiment with the difference spectra obtained by laser flash photolysis, reveals some information about the nature of the photoproduct. Examination of the UV/vis spectrum, Figure 4.6.1.2 shows that a feature is seen to grow in at ~ 400 nm for the $(\eta^6\text{-}C_{12}H_8S)Cr(CO)_3$ complex. This is consistent with the grow in recorded at 400 nm using laser flash photolysis, Figure 4.6.1.1. A negative absorption at 340 nm with no recovery using laser flash photolysis can also be observed, which is consistent with depletion of the band at 340 nm in the UV/vis spectrum. Formation of a band at 300 nm in the UV/vis spectrum is corresponds to the λ_{max} observed at 300 nm using UV/vis laser flash photolysis. The signal recorded at 300 nm, is thought to be the reaction of $(\eta^6\text{-}C_{12}H_8S)Cr(CO)_2$(s) species with starting material to yield a secondary photoproduct.

For the $(\eta^6\text{-}C_{12}H_8S)Cr(CO)_3$ complex the k_{obs} for the rate of grow in of the signal recorded at 400 nm did not appear to be dependent the concentration of starting material, indicating that a dimeric species was not being formed.

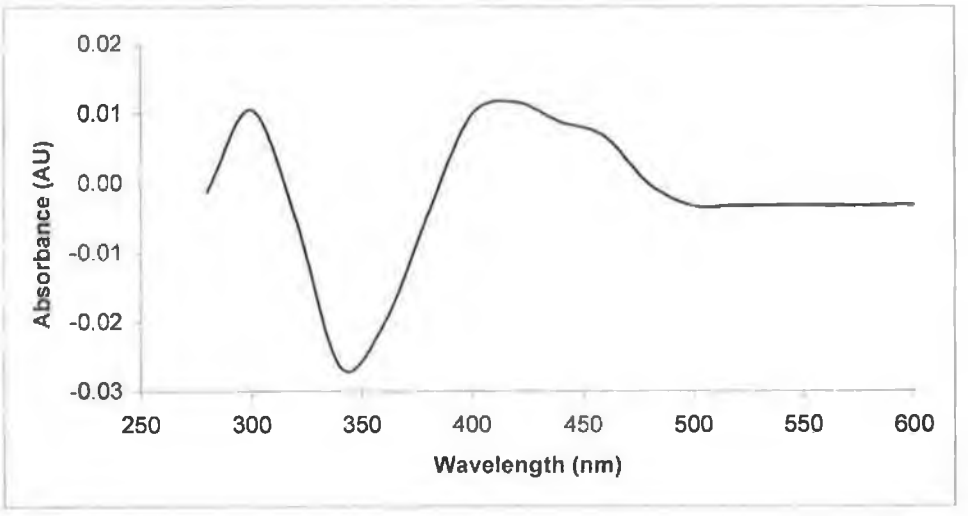

Figure 4.6.1.1 UV/vis difference spectrum obtained 70 μs after excitation of $(\eta^6\text{-}C_{12}H_8S)Cr(CO)_3$ at λ_{exc} = 355nm in argon saturated cyclohexane.

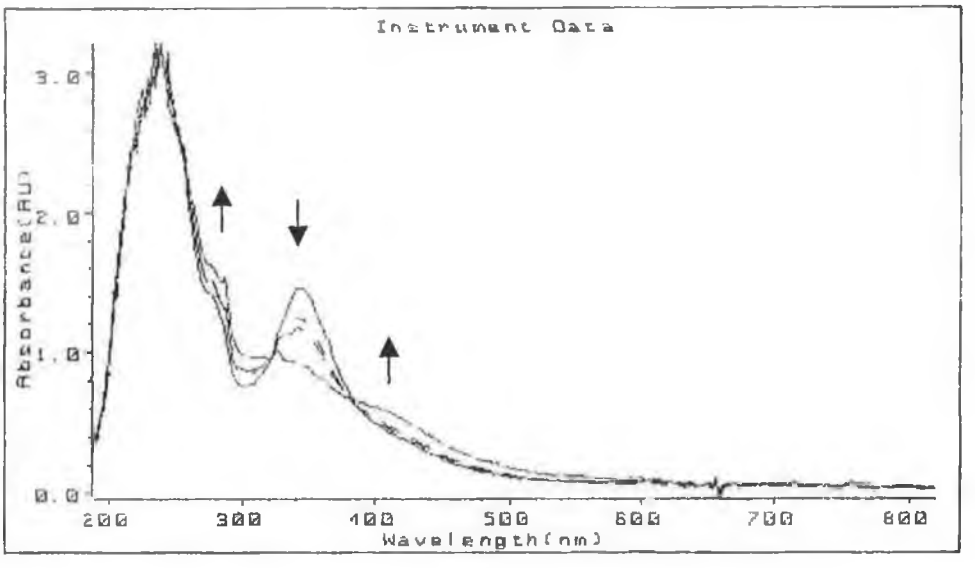

Figure 4.6.1.2 Changes in the UV/vis spectrum of $(\eta^6\text{-}C_{12}H_8S)Cr(CO)_3$ following photolysis at λ_{exc} = 355nm after 4 minutes in argon saturated cyclohexane.

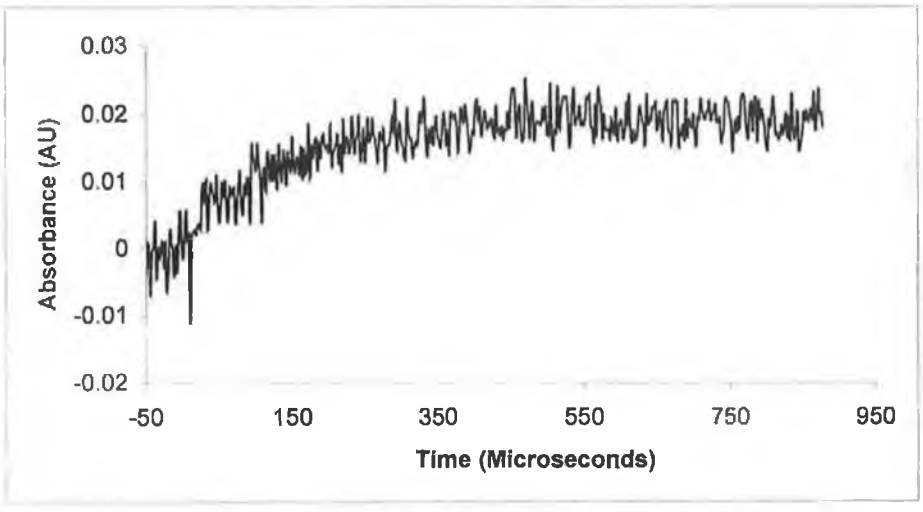

Figure 4.6.1.3 A typical grow in observed at 400 nm for $(\eta^6\text{-}C_{12}H_8S)Cr(CO)_3$ in argon saturated cyclohexane at λ_{exc} = 355 nm.

4.7 Discussion

The solution photochemistry (λ_{exc} = 355 nm) of (η^6-C_8H_6S)$Cr(CO)_3$ in CO saturated alkane solution is dominated by two processes, CO loss to form the dicarbonyl intermediate and arene loss, to form $Cr(CO)_6$. (Scheme 4.7.1).

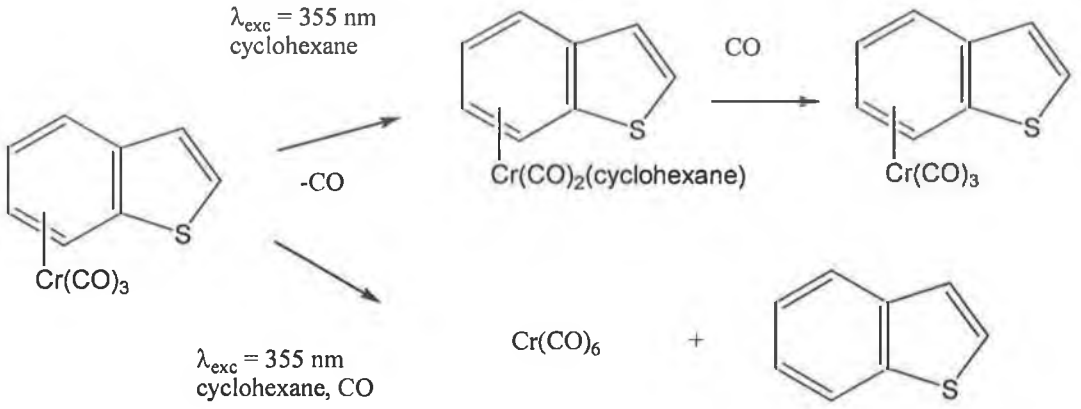

Scheme 4.7.1 The solution photochemistry of (η^6-C_8H_6S)$Cr(CO)_3$ upon excitation at λ_{exc} = 355nm in CO saturated cyclohexane.

Using UV/vis monitored laser flash photolysis at λ_{exc} = 355 nm, in CO saturated cyclohexane the transient decay at λ_{max} 280 nm was assigned to the solvated dicarbonyl species,(η^6-C_8H_6S)$Cr(CO)_2$(cyclohexane). In the presence of CO the parent tricarbonyl is found to reform. Recovery of the parent tricarbonyl species was noted at 340 nm for (η^6-C_8H_6S)$Cr(CO)_3$ in CO saturated cyclohexane following laser excitation at λ_{exc} = 355 nm. The 16 electron fragment is thought to coordinate the solvent molecule into a vacant site within 1 ps of formation. Simon *et al.* examined the dynamics of the formation of $Cr(CO)_5$(s) (s= cyclohexane or methanol) using picosecond time-resolved spectroscopy of $Cr(CO)_6$ and found that the cyclohexane analogue was formed within the time resolution of the equipment, 0.8 ps.[23] For (η^6-C_8H_6S)$Cr(CO)_3$, the second order rate constant for the reaction of (η^6-C_8H_6S)$Cr(CO)_2$(s) with CO was found to be 5×10^6 $s^{-1}mol^{-1}dm^3$ in cyclohexane using UV/vis laser flash photolysis at λ_{exc} 355nm and 1×10^7 s^{-1} $mol^{-1}dm^3$ in heptane using UV/vis laser flash photolysis and point by point TRIR detection at

λ_{exc} = 355 nm. The increase in the second order rate constant for the reaction of $(\eta^6\text{-}C_8H_6S)Cr(CO)_2(s)$ with CO in cyclohexane compared to heptane was similar to what Creaven *et al.* observed for $(\eta^6\text{-}C_6R_6)Cr(CO)_3$ systems, (where R = H, CH_3).[1] Creaven *et al.* measured the second order rate constant for the reaction of $(\eta^6\text{-}C_6H_6)Cr(CO)_2(s)$ with CO was found to be 9.8×10^6 $s^{-1}mol^{-1}$ dm^3 in cyclohexane and 2.3×10^7 $s^{-1}mol^{-1}dm^3$ in heptane.[24] For the hexamethyl analogue the second order rate constant for the reaction of $(\eta^6\text{-}C_6(C_2H_5)_6)Cr(CO)_2(s)$ with CO, was found to be 5.9×10^7 $s^{-1}mol^{-1}dm^3$ in cyclohexane and 1.1×10^8 $s^{-1}mol^{-1}dm^3$ in heptane.

$$(\eta^6\text{-}C_8H_6S)Cr(CO)_3 \xrightarrow{\lambda_{exc} = 355\ nm} (\eta^6\text{-}C_8H_6S)Cr(CO)_2 + CO$$

Reaction 4.7.2

$$(\eta^6\text{-}C_8H_6S)Cr(CO)_2 + solvent \longrightarrow (\eta^6\text{-}C_8H_6S)Cr(CO)_2(solvent)$$

Reaction 4.7.3

$$(\eta^6\text{-}C_8H_6S)Cr(CO)_2(solvent) + CO \longrightarrow (\eta^6\text{-}C_8H_6S)Cr(CO)_3 + solvent$$

solvent= cyclohexane or heptane

Reaction 4.7.4

A secondary species was observed using UV/vis monitored flash photolysis at λ_{exc} = 355 nm of $(\eta^6\text{-}C_8H_6S)Cr(CO)_3$ in argon saturated cyclohexane. A λ_{max} at 280 nm was observed and this band did not decay over the timescale of the experiment. By comparison to the UV/vis monitored flash photolysis experiments in CO, this signal was assigned to formation of the solvated dicarbonyl. The negative absorption at 340 nm assigned to the depletion/recovery of the parent was not found to recover. A feature with a λ_{max} at 400 nm showed a linear dependence between the rate of formation of the signal and the concentration of starting material. This would suggest that the photogenerated $(\eta^6\text{-}C_8H_6S)Cr(CO)_2(solvent)$ fragment was reacting with starting material to form a dinuclear species. Angelici *et al.* has studied the thermal reaction of $(\eta^6\text{-}C_8H_6S)Cr(CO)_3$ with $(\eta^5\text{-}C_5H_5)Re(CO)_2(THF)$.[12] When the benzothiophene ligand is complexed to the metal fragment $Cr(CO)_3$, the benzothiophene ligand was found to coordinate through the 2,3 η^2-C(2),C(3) olefenic bond to a $(\eta^5\text{-}C_5H_5)Re(CO)_2$ fragment. This observation was explained by the fact

that the $Cr(CO)_3$ group on the benzothiophene effects the benzothiophene binding in two ways, the electron withdrawing effect of the $Cr(CO)_3$ unit could reduce the donor ability of the benzothiophene sulphur and increase the π accepting ability of the C(2)=C(3)bond. Using the same rationale as Angelici it is plausible to propose the following reaction for the secondary photoproduct.

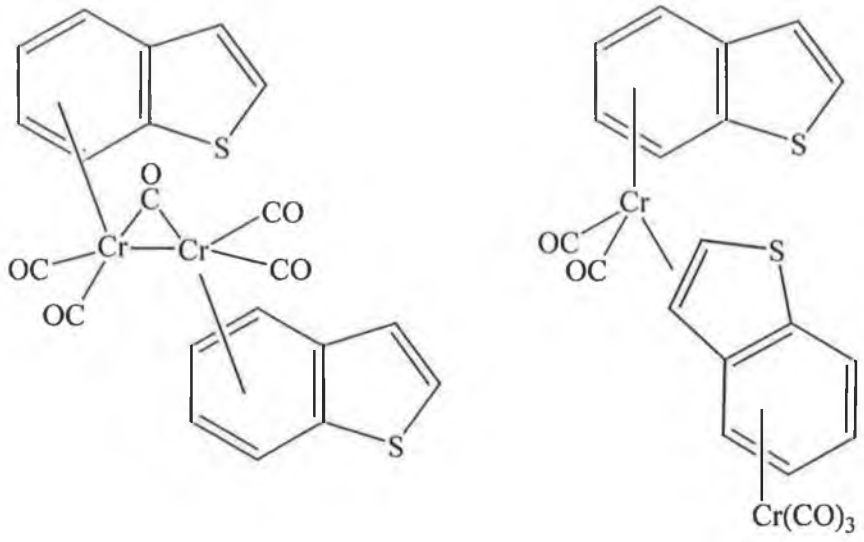

Figure 4.7.1 Possible structure of the secondary photoproduct $(\eta^6\text{-}C_8H_6S)_2Cr_2(CO)_5$.

$$(\eta^6\text{-}C_8H_6S)Cr(CO)_3 \xrightarrow{h\nu} (\eta^6\text{-}C_8H_6S)Cr(CO)_2 + CO \xrightarrow[solvent]{} (\eta^6\text{-}C_8H_6S)Cr(CO)_2(solvent)$$

$$(\eta^6\text{-}C_8H_6S)Cr(CO)_2(solvent) \longrightarrow (\eta^6\text{-}C_6H_8S)_2Cr(CO)_5$$
$$(\eta^6\text{-}C_8H_6S)Cr(CO)_3$$

Scheme 4.7.2

Alternatively, for $(\eta^6\text{-}C_6H_6)Cr(CO)_3$, $(\eta^5\text{-}C_5H_5)Mn(CO)_3$ and $(\eta^5\text{-}C_5H_5)V(CO)_4$ formation of a two metal centre species containing a bridging carbonyl has been observed.[1, 24, 25]

$$(\eta^6\text{-}C_6H_6)Cr(CO)_3 \xrightarrow[-CO]{h\nu} (\eta^6\text{-}C_6H_6)Cr(CO)_2 \xrightarrow[solvent]{} (\eta^6\text{-}C_6H_6)Cr(CO)_2(solvent) \rightarrow (\eta^6\text{-}C_6H_6)Cr(CO)_3$$

$$(\eta^6\text{-}C_6H_6)Cr(CO)_2(\mu\text{-}CO)(\eta^6\text{-}C_6H_6)Cr(CO)_2 .$$

Scheme 4.7.3

A similar type of complex could be proposed for the secondary species observed upon photolysis at λ_{exc} = 355 nm of $(\eta^6\text{-}C_8H_6S)Cr(CO)_3$ in argon saturated cyclohexane.

TRIR step scan spectroscopy experiments were carried out on $(\eta^6\text{-}C_8H_6S)Cr(CO)_3$ in CO saturated heptane. In TRIR experiments, the formation of two new bands were observed at 1921 and 1866 cm^{-1}. The lack of symmetry involved in these metal carbonyl fragments makes spectral interpretation easy, as the number of ν_{co} absorption bands exhibited by a particular photofragment equals the number of CO ligands present. From inspection of Figure 4.6.1, the parent bands due to $(\eta^6\text{-}C_8H_6S)Cr(CO)_3$ occur at 1977, 1915 and 1905 cm^{-1}, while the bands attributed to the formation of the dicarbonyl species occurs at 1921 and 1866 cm^{-1}.

Matrix isolation IR studies were carried out on $(\eta^6\text{-}C_8H_6S)Cr(CO)_3$ in both nitrogen and argon matrices. Photolysis of $(\eta^6\text{-}C_8H_6S)Cr(CO)_3$ in a nitrogen matix at λ_{exc} > 340 nm resulted in formation of bands at 1934 and 1887 cm^{-1}. These bands were found to be at similar wavenumber to those observed by Rest *et al.* at 1940 and 1896 cm^{-1} for $(\eta^6\text{-}C_6H_6)Cr(CO)_2(N_2)$.[21] The two bands at 1934 and 1887 cm^{-1} were assigned to $(\eta^6\text{-}C_8H_6S)Cr(CO)_2(N_2)$. Along with formation of the two bands at 1934 and 1887 cm^{-1}, two further bands were seen to simultaneously form at 2139 and 2151 cm^{-1}. The band at 2139 cm^{-1} was assigned to formation of free CO, while the band at 2151 cm^{-1} was assigned to formation of a dinitrogen stretch. On long wavelength photolysis at λ_{exc} >400 nm of $(\eta^6\text{-}C_8H_6S)Cr(CO)_3$ a three band pattern was produced at 1976,1913 and 1906 cm^{-1}. If after irradiation cleavage of the benzothiophene-chromium bond occurs resulting in the formation of a $Cr(CO)_3$ moiety only two bands would be observed in the carbonyl region of the IR at 1979 and 1889 cm^{-1}. Perutz and Turner's study of the photochemistry in low temperature noble gas matrices found that photolysis of $Cr(CO)_6$ resulted in formation of $Cr(CO)_3$.[22] Two carbonyl stretches

were observed for this species at 1979 and 1889 cm^{-1}. Therefore one can rule out the species that was produced on long wavelength photolysis (λ_{exc} >400 nm) being $Cr(CO)_3$. The nature of the species formed at long wavelength photolysis of $(\eta^6\text{-}C_8H_6S)Cr(CO)_3$ is more likely to be a rotomer.

Photolysis of $(\eta^6\text{-}C_8H_6S)Cr(CO)_3$ in a argon matrix at λ_{exc} > 340 nm resulted in formation of a two band pattern at 1937 and 1897 cm^{-1}. The two bands at 1937 and 1897 cm^{-1} were assigned to formation of $(\eta^6\text{-}C_8H_6S)Cr(CO)_2$.[21] Along with the two bands at 1937 and 1870 cm^{-1} a band was also seen to simultaneously form at 2137 cm^{-1} which was assigned to the formation of free CO. Upon photolysis at lower energy λ_{exc} > 400 nm, a three band pattern was observed at 1980, 1917 and 1914 cm^{-1}. By comparison to the results obtained in the nitrogen matrix, the three bands at 1980, 1917 and 1914 cm^{-1} are assigned to formation of a rotomer.

It has been reported that the NMR spectrum of $(\eta^6$-isopropylbenzene$)Cr(CO)_3$ complex is temperature dependent.[26] At 30°C the five aromatic protons of $(\eta^6$-isopropylbenzene$)Cr(CO)_3$ in the ^1H spectrum give rise to a singlet at τ 4.92 which reversibly broaden into a multiplet at - 40°C. Similarly variable temperature nuclear magnetic resonance studies of $(\eta^6$-2,4, –trideuteroisopropylbenzene$)Cr(CO)_3$ have been carried out in three different solvents carbon disulfide, deuterochloroform and decalin.[27] At low temperatures,the H-3 and H-6 were clearly resolved and gave 2 singlets. Upon increasing the temperature the signals coalesced to a single resonance. This temperature effect was found to be totally reversible. Also the meta proton H-3 was relatively deshielded at lower temperatures compared to the ortho H-6. It then follows that the $(\eta^6$-2,4,5–trideuteroisopropylbenzene$)Cr(CO)_3$ complex eclipsed form related to the more deshielded signal since protons lying under a superimposed metal carbonyl bond are more deshielded. Black et al. has also observed the formation of a rotomer species on cooling mixed alcohol and ether solutions of both $(\eta^5\text{-}C_5H_5)Mn(CO)_3$ and $(\eta^6\text{-}C_6H_6)Cr(CO)_3$ form 293 K to 77 K.[29]

These experiments provide evidence for the existence of different rotomers at low temperatures. On can therefore assign the formation of the three band pattern at low energy photolysis at λ_{exc} > 400nm to the formation of a rotomer of the $(\eta^6\text{-}C_8H_6S)Cr(CO)_3$. X–ray crystallography studies of $(\eta^6\text{-}C_8H_6S)Cr(CO)_3$ reveal that the CO ligands in the $Cr(CO)_3$ group are staggered with respect to the benzene carbons of the benzothiophene ligand.[28]. Then it is plausible that upon photolysis the $Cr(CO)_3$ moiety rotates from a staggered to an eclipsed form.

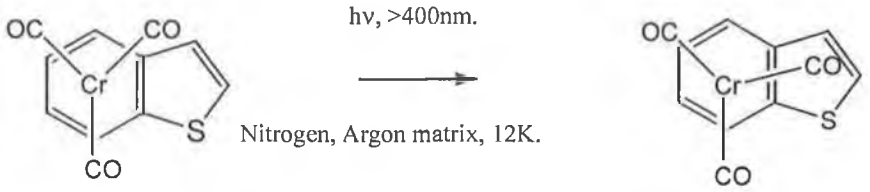

Staggered *Eclipsed*

Figure 4.7.2 The proposed photochemical pathway upon low energy photolysis at λ_{exc} >400nm of $(\eta^6\text{-}C_8H_6S)Cr(CO)_3$ complex in a nitrogen and argon matrix at 12K.

The solution photochemistry λ_{exc} = 355 nm of $(\eta^6\text{-}C_{12}H_8S)Cr(CO)_3$ in CO saturated alkane solution is dominated by two processes, CO loss to form the dicarbonyl intermediate and arene loss, to form $Cr(CO)_6$.

Using UV/vis laser flash photolysis at λ_{exc} = 355 nm of $(\eta^6\text{-}C_{12}H_8S)Cr(CO)_3$, in CO saturated cyclohexane, it was possible to observe the solvated dicarbonyl species at λ_{max} 300 nm. Recovery of the parent tricarbonyl species was noted at 340 nm. The maxima at 300 nm was assigned as the primary photoproduct of the appropriate $(\eta^6\text{-}C_{12}H_8S)Cr(CO)_2(s)$ species, by analogy to the difference spectra obtained by UV/vis flash photolysis of $(\eta^6\text{-}C_6H_6)Cr(CO)_3$, at λ_{exc} = 355 nm.[1] As the rate of decay of the signal recorded in CO saturated cyclohexane at 300 nm was found to be dependent on the concentration of CO, this transient signal was assigned to the reaction of the solvated dicarbonyl with CO to regenerate the parent, Reaction 4.7.7.

$$(\eta^6\text{-}C_{12}H_8S)Cr(CO)_3 \xrightarrow{\lambda_{exc} = 355nm} (\eta^6\text{-}C_{12}H_8S)Cr(CO)_2 + CO \quad \text{Reaction 4.7.5}$$

$$(\eta^6\text{-}C_{12}H_8S)Cr(CO)_2 + \text{cyclohexane} \longrightarrow (\eta^6\text{-}C_{12}H_8S)Cr(CO)_2(\text{cyclohexane})$$

Reaction 4.7.6

$$(\eta^6\text{-}C_{12}H_8S)Cr(CO)_2(\text{cyclohexane}) + CO \longrightarrow (\eta^6\text{-}C_{12}H_8S)Cr(CO)_3$$

Reaction 4.7.7

Following Uv/vis monitored laser flash photolysis at λ_{exc} = 355 nm of $(\eta^6\text{-}C_{12}H_8S)Cr(CO)_3$ in argon saturated cyclohexane, a secondary species was observed. The λ_{max} at 400 nm was not found to decay over the timescale of the experiment, indicating that the photogenerated $(\eta^6\text{-}C_{12}H_8S)Cr(CO)_2$(solvent) reacted further. The negative absorption at 340 nm assigned to the recovery of the parent in the presence of CO, did not recover in an argon atmosphere. A feature with a λ_{max} at ~ 400 nm was found to show a linear dependence between the k_{obs} and the concentration of starting material. For the $(\eta^6\text{-}C_{12}H_8S)Cr(CO)_3$ complex the k_{obs} for the rate of grow in of the signal recorded at 400 nm was found to be independent to the concentration of starting material, indicating that a dimeric species was not being formed, therefore a more complex reaction must be considered.

4.8 Conclusion

Solution photochemistry of both $(\eta^6\text{-}C_8H_6S)Cr(CO)_3$ and $(\eta^6\text{-}C_{12}H_8S)Cr(CO)_3$ results in the formation of $Cr(CO)_6$ upon photolysis at $\lambda_{exc} = 355$ nm. Laser flash photolysis and step scan TRIR spectroscopy experiments carried out at $\lambda_{exc} = 355$nm, provided evidence for the formation of dicarbonyl intermediate. Matrix isolation studies on the $(\eta^6\text{-}C_8H_6S)Cr(CO)_3$ system showed formation of the dicarbonyl intermediate on high energy photolysis.

On long wavelength photolysis of $(\eta^6\text{-}C_8H_6S)Cr(CO)_3$ in either an argon or nitrogen matrix a further photoproduct was observed. This photoproduct is thought to be a rotomer. It had been thought that for $(\eta^6\text{-arene})Cr(CO)_3$ complexes, CO loss was the only photochemical pathway open to these systems. The quantum yield (Φ) for this process is thought to be relatively high at 0.72.[6] However experiments carried out on a series of functionalised $(\eta^6\text{-arene})Cr(CO)_3$ complexes and the polyaromatic systems $(\eta^6\text{-}C_{10}H_8)Cr(CO)_3$, $(\eta^6\text{-}C_{14}H_{10})Cr(CO)_3$ and $(\eta^6\text{-}C_{20}H_{12})Cr(CO)_3$ showed that CO loss was not the only photochemical pathway open to these species. Photolysis of these systems in CO saturated alkane solution resulted in formation of $Cr(CO)_6$.[2] Likewise photolysis of $(\eta^6\text{-}C_8H_6S)Cr(CO)_3$ and $(\eta^6\text{-}C_{12}H_8S)Cr(CO)_3$ resulted in the formation of $Cr(CO)_6$ upon photolysis at $\lambda_{exc} = 355$ nm. Unlike $(\eta^5\text{-}C_4H_4S)Cr(CO)_3$ and $(\eta^5\text{-}C_4H_4Se)Cr(CO)_3$, for both $(\eta^6\text{-}C_8H_6S)Cr(CO)_3$ and $(\eta^6\text{-}C_{12}H_8S)Cr(CO)_3$ no evidence for a ring slip or ring insertion species was observed. Hoeever both $(\eta^6\text{-}C_8H_6S)Cr(CO)_3$ and $(\eta^6\text{-}C_{12}H_8S)Cr(CO)_3$ underwent arene displacement when photolysed at $\lambda_{exc} = 355$ nm in CO saturated cyclohexane solution.

4.8 References

1. Creaven, B.S.; George, M.W.; Ginzburg, A.G.; Hughes, C.; Kelly J.M.; Long, C.; McGrath, I.M.; Pryce, M.T. *Organometallics* 1993, **12**, 3127.
2. Strohmeier, W.; van Hobe D. *Z.Naturforsch.* 1963, **18b**, 770.
3. Pryce, M.T. *Ph.D Thesis,* Dublin City University, 1993.
4. Breheny, K. *Ph.D Thesis,* Dublin City University, 1996.
5. Natta, G.; Ercoli, R.;Calderazzo, S.; Santambrozio, E.; *Chim Ind. (Milan)*; 1959, **41**, 975.
6. Wrighton, M.S.; Haverty, J.L. *Z.Naturforsch.* 1975, **254**, 806. Gilbert, A.; Kelly, J.M.; Budzwait, M.; Koernet von Gustoff, E. *Z.Naturforsch.* 1976, **311**, 1091.
7. Mahaffy, C.A.L.; Pauson, P.L. *J. Chem. Res.(S).* 1979, 126.
8. Mahaffy C.A.L.; Pauson, P.L. *J. Chem. Res.(M).* 1979, 1972.
9. Reynolds, M.A.; Guzei, I.A.; Logsdon, B.C.; Thomas, L.M.; Jacobson, R.A.; Angelici, R.J. *Organometallics* 1999, **18**, 4075.
10. Choi, M.G.; Angelici R.J. *Organometallics* 1992, **11**, 3328.
11. Choi M.G.; Robertson, M.J.: Angelici R.J. *J. Am. Chem. Soc.* 1991, **113**, 4005.
12. Angelici, R.J.; Rudd II, J.A. *Inorganica Chimica. Acta* 1995, **240**, 393.
13. Cotton F.A.; Wilkinson, G.; Gaus P.L. *Basic Inorganic Chemistry. Second edition.* Wiley. New York. 1993.
14. Zhang, X.; Dullaghan, C.A.;Watson, E.J.; Carpenter, G.B.; Swiegart, D.A. *Organometallics* 1998, **17**, 2067.
15. Myers, A.W.; Jones W.D. *Organometallics* 1996, **15**, 2905.
16. Garcia, J.J.; Arevalo, A.; Monitiel, V. Del Rio, F.; Quiroz, B. Adams, H.; Maitlia, P.M. *Organometallics* 1997, **16**, 3216.
17. Bianchini, C.; Masi, D.; Meli, A.; Peruzzini, M.; Vizza, F. Zanobini, F. *Organometallics* 1998, **17**, 2495.
18. Carroll, D.G.; McGlynn, S.P. *Inorg. Chem.* 1968, **7**, 1285.
19. Ercoli, R.; Mangini, A. *Ric. Sci. Suppl.* 1958, **84**, 1167.
20. Yamada, S.; Nakamura, H.; Tsuchida, R. *Bull. Chem. Soc. Jap.* 1957, **30**, 647.
21. Rest, A.J.; Sodeau, J.R.; Taylor, D.J. *J. Chem. Soc., Dalton Trans.* 1978, 651.
22. Perutz, R.R; Turner, J.J.; *J. Am. Chem. Soc.* 1975, **97**, 4800.

23. Simon, J.D.; Xie, X. *J. Phys. Chem.* 1986, **90**, 6751.

24. Creaven, B.S.; Dixon, A.J.; Kelly J.M.; Long, C.; Poliakoff, M. *Organometallics* 1987, **6**, 2600.

25. George, M.W. *Ph.D. Thesis*, University of Nottingham 1990.

26. Gracey, D.E.F.; Jackson, W.R.; Jennings, W.B.; Rennison, S.C.; Spratt, R. *J. Chem.* Soc., *Chem. Comm.* 1966, 231.

27. Jackson, W.R.; Jennings W.B.; Reninson S.C.; Spratt, R. *Phys. Org . Chem. Soc. (B).* 1969, 1214.

28. Das P.K. ; Mukhopadhyay, A., M.; Ray, S.; Bhattacharya, S.; Datta, S.; De, A. *Acta. Cryst.(C).* 1992, **48**, 266.

29. Black, J.D.; Boylan, M.J. and Braterman, P.S. *J. Chem. Soc., Dalton Trans.* 1981, 673.

Chapter 5

The photochemistry of $(\eta^5\text{-}C_4H_4N)Mn(CO)_3$

5.1 Introduction

Strohmeier and co workers showed that photolysis of $(\eta^5\text{-}C_5H_5)Mn(CO)_3$ in solution results in loss of CO, Reaction 5.1.1.[1]

$$(\eta^5\text{-}C_5H_5)Mn(CO)_3 \xrightarrow{h\nu} (\eta^5\text{-}C_5H_5)Mn(CO)_2 + CO \qquad \text{Reaction 5.1.1.}$$

In addition $(\eta^5\text{-}C_5H_5)Mn(CO)_2$ has also been generated by UV photolysis of $(\eta^5\text{-}C_5H_5)Mn(CO)_3$ in CH_4 matrices at 20 K.[2] UV photolysis of $(\eta^5\text{-}C_5H_5)Mn(CO)_3$ in hydrocarbon glasses at 77 K also yielded $(\eta^5\text{-}C_5H_5)Mn(CO)_2$.[3,4] Prolonged UV irradiation in both the CH_4 matrix at 20 K and the hydrocarbon glass at 77 K yielded the monocarbonyl species, $(\eta^5\text{-}C_5H_5)Mn(CO)$. Laser photolysis at λ_{exc} = 308 nm, with UV/vis monitoring and point by point time resolved IR spectroscopy was used to characterise two transient species formed by the photolysis of $(\eta^5\text{-}C_5H_5)Mn(CO)_3$ in alkane solution.[5] The first species was identified as $(\eta^5\text{-}C_5H_5)Mn(CO)_2$(solvent) where solvent = cyclohexane or *n*-heptane. Under a CO atmosphere, the $(\eta^5\text{-}C_5H_5)Mn(CO)_2$(solvent) species reacts with CO to regenerate the parent, $(\eta^5\text{-}C_5H_5)Mn(CO)_3$. The second transient species $(\eta^5\text{-}C_5H_5)_2Mn_2(CO)_5$ is formed by the reaction of $(\eta^5\text{-}C_5H_5)Mn(CO)_2$(solvent) with unphotolysed $(\eta^5\text{-}C_5H_5)Mn(CO)_3$.

5.2 Bonding in $(\eta^5\text{-}C_5H_5)Mn(CO)_3$ complexes

The bonding between the cyclopentadienyl ring and the metal is based on three interactions, one σ and two π.[6] The σ component is a three orbital interaction and results from the combination of metal p_z and d_z^2 orbitals, empty and filled respectively with the ligands symmetrical π orbitals. Three molecular orbitals arise from the interaction, a filled bonding orbital, σ, is composed of the ligands $1\pi_s$ orbital. Its antibonding equivalent counterpart σ^*, is empty and has mainly metal p_z character. The two π components of the bonding results from the combination of the empty metal d_{xz} and d_{yz} as they have the correct symmetry to overlap with the orbital with the ligands π orbitals, the C_5H_5 e_1" set, $2\pi_s$ and $1\pi_a$. From these interactions, result the complex frontier orbitals, the two highest occupied molecular orbitals (HOMO), π_s and π_a, and the two lowest unoccupied molecular orbitals (LUMO), π_s^* and π_a^*. The

result of this is the establishment of three (η^5-C_5H_5)-Metal bonds, which correspond to three cyclopentadienyl → Metal donations.

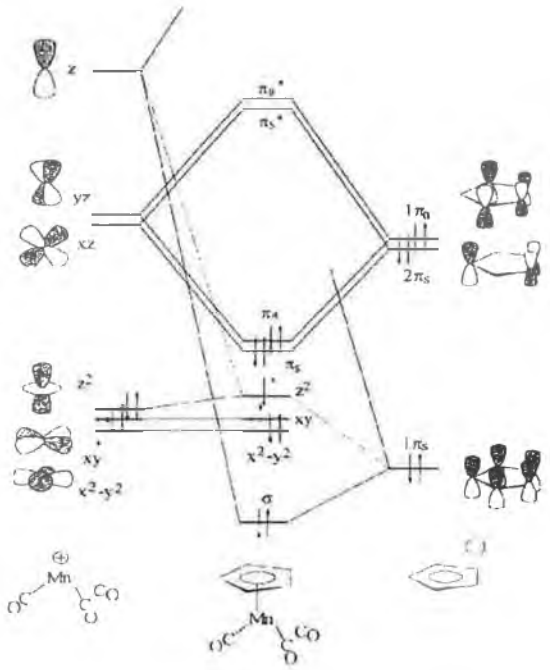

Figure 5.2.1 Simplified molecular orbital diagram of the bonding interactions in (η^5-C_5H_5)$Mn(CO)_3$.

5.3 Haptotropic shifts in (η^5-C_5H_5)$Mn(CO)_3$ complexes

Although the (η^3-C_5H_5) species have been implicated in the chemistry of (η^5-C_5H_5) metal carbonyl complexes, examples of well characterised complexes with shifted cyclopentadienyl (η^3-C_5H_5) coordination are relatively scarce. There have been some reports of photo-induced ring slip in (η^5-C_5H_5)$Mn(CO)_3$ complexes. Crichton, Rest and Taylor have reported that photolysis of (η^5-C_5H_5)$Co(CO)_2$ in a pure CO matrix monitored by IR spectroscopy yielded depletion of the parent bands at 2032 and 1972 cm^{-1} and the appearance of bands at 2075 and 2018 cm^{-1}.[7] The two bands at 2075 and 2018 cm^{-1} were assigned to (η^3-C_5H_5)$Co(CO)_3$ because of the similarity in frequency to the bands observed for (η^3-C_3H_5)$Co(CO)_3$, (2076 and 2025 cm^{-1}).

Rest *et al.* carried out a related study on $(\eta^5\text{-}C_5H_5)Fe(CO)_2CH_3$ and again observed a shift of the ν_{co} bands to higher wavenumber as expected for an increase in the number of CO bands to yield the $(\eta^3\text{-}C_5H_5)Fe(CO)_3CH_3$.[8] Blaha and Wrighton also observed a similar behaviour for the related species of $(\eta^5\text{-}C_5H_5)Fe(CO)_2CH_2Ph$ in the presence of added ligand (L = CO or PPh_3) and observed the formation of the η^4-ring slip product $(\eta^4\text{-}C_5H_4CH_2Ph)Fe(CO)_2L$.[9]

More recently haptotropic shifts of $(\eta^5\text{-}C_5H_5)Mn(CO)_3$ complexes induced by a two electron reduction or by phosphine addition have been observed.[6,10] The geometries of the cyclopentadienyl ligand in is found to be nearly planar in the $(\eta^1\text{-}C_5H_5)Mn(CO)_3^{2-}$ and $(\eta^2\text{-}C_5H_5)Mn(CO)_3PH_3$ complexes.

The only characterised complexes in which the $(\eta^3\text{-}C_5H_5)$ ring folded coordination is observed, is Brintzingers bent metallocenes, $(\eta^3\text{-}C_5H_5)(\eta^5\text{-}C_5H_5)W(CO)_2$ and its chromium-pentamethyl-cyclopentadienyl analogue.[11,12] Therefore the two extreme possibilities exist for the coordination geometry of the shifted C_5H_5 ring. In one case the haptotropic shift corresponds to a folding of the C_5 ring with the two carbons atoms C_4 and C_5 being pushed away from the metal. On the other hand the haptotropic shift may be accompanied by a ring slippage where the cyclopentadienyl ring keeps its planarity. The two different types of ring slippage are shown in Figure 5.3.1.

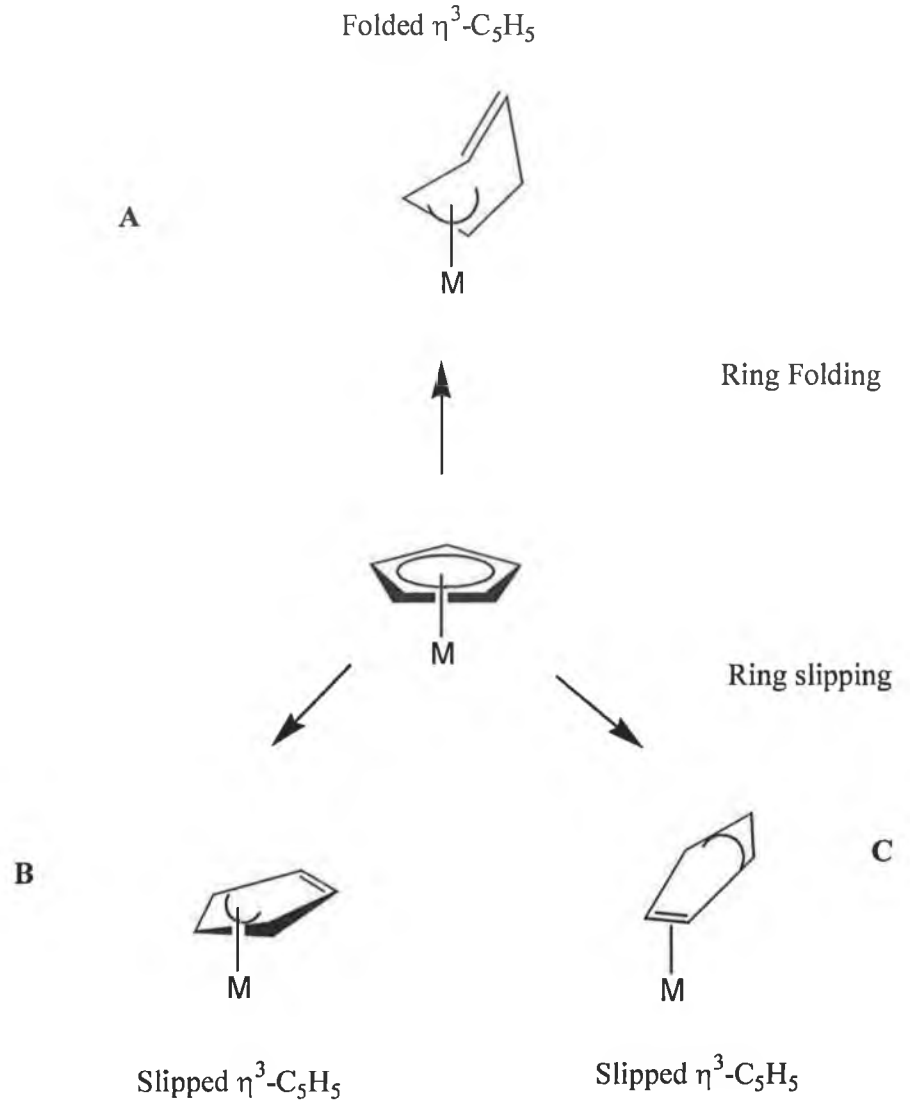

Figure 5.3.1 The different coordination modes of the cyclopentadienyl ligand.

Veiros carried out a number of studies of haptotropic shifts in cyclopentadienyl organometallic complexes.[13] The coordination geometry of shifted cyclopentadienyl ligands in organometallic complexes resulting from a two electron reduction of the $(\eta^5\text{-}C_5H_5)Mn(CO)_3$ species was investigated by means of molecular orbital calculations performed with the B3LYP HF/ density functional theory hybrid functional. In these geometric rearrangements, an increase of two electrons at the metal centre is seen as a consequence of ligand addition or simple reduction of the $(\eta^5\text{-}C_5H_5)$ metal complex. The two electrons occupy the LUMO of the reactant , which, in the case of an electronic saturated complex is a metal - $(\eta^5\text{-}C_5H_5)$

antibonding orbital, π_s* or π_a*, Figure 5.3.2. The relief of the antibonding character of this orbital is the driving force for the haptotropic shift geometrical distortion.

Figure 5.3.2 shows a simplified schematic view of the frontier orbitals of the model complex $(\eta^5\text{-}C_5H_5)Mn(CO)_3^{2-}$, resulting from a two electron reduction of the parent $(\eta^5\text{-}C_5H_5)Mn(CO)_3$, neutral piano-stool complex. Three coordination geometries are considered: folded η^3-cyclopentadienyl, planar $\eta^{1\text{-}3}$-cyclopentadienyl and planar η^2-cyclopentadienyl.

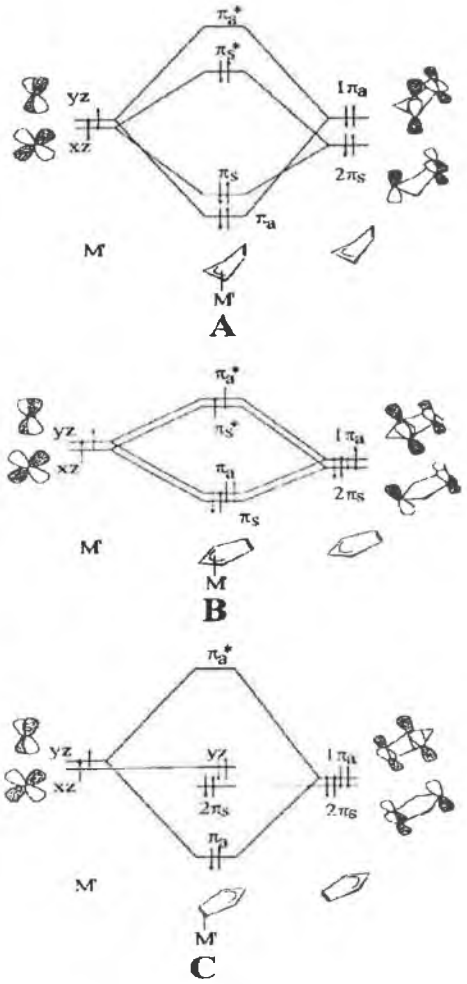

Figure 5.3.2 Schematic representations of the $(\eta^X\text{-}C_5H_5)$-M π interactions (π_s and π_a), for the different shifted C_5H_5 coordinations (X = 1-5).

In the case of the ring folding haptotropic shift a stabilisation of π_s* is achieved as two of the cyclopentadienyl carbon atoms are pushed away from the metal diminishing that orbitals antibonding character. Some energetic costs are however associated with this type of rearrangement. On one hand, the folding of the ligand implies the breaking of its π system aromaticity and on the other, the folding of the ligand implies there is a weakening of the Mn-cyclopentadienyl bonding interaction with the augmentation of two M – C distances, which is reflected by a stabilisation of the π_s bonding orbital. In the case of the ring slippage yielding (η^3-C_5H_5) coordination, the fragments local symmetry is maintained. This results in nearly degenerate π_s and π_a orbitals and their antibonding counterparts. Therefore a weakening of the metal – C_5H_5 bond is achieved by the stabilisation of the π_s* and π_a* orbitals, which is paralleled by a destabilisation of the corresponding bonding orbitals. The ligands aromaticity is kept and the short energy gap between the π_s* and π_a* orbitals can lead to paramagnetic species with a spin triplet ground state. An increased slippage degree towards an η^1 coordination will further destabilise the metal – C_5H_5 bond, leading to a smaller band gap between the bonding and the antibonding π orbitals. In the limit of an ideal η^1-cyclopentadienyl, the overall metal – C_5H_5 bond will be based on the σ interaction.

5.4 Haptotropic shifts in (η^5-C_4H_4N)$Mn(CO)_3$ complexes

Veiros studied the electronic structure and bonding of (η^5-C_4H_4N)$Mn(CO)_3$ by means of *ab initio* calculations using the B3LYP hybrid functional with a LANL2DZ basis set.[6] Two electron reduction of (η^5-C_4H_4N)$Mn(CO)_3$ the C_4H_4N ligand was shown to adopt a σ rather than a η^3 coordination geometry.

5.5 Thermal CO substitution reactions of $(\eta^5\text{-}C_4H_4N)Mn(CO)_3$ complex

Kinetic studies carried out on the thermal CO substitution reaction with P(*n*-Bu)$_3$ in decalin at 130°C of $(\eta^5\text{-}C_4H_4N)Mn(CO)_3$ found that the pyrrolyl complex reacted considerably faster (10^8 times faster) than the $(\eta^5\text{-}C_5H_5)Mn(CO)_3$ complex.[14] The large rate enhancement was attributed to the more electronegative N atom then C, resulting in a greater tendency for electron withdrawl from the metal by the N heterocycle relative to the carbocycle. Alternatively if CO substitution takes place through a low energy associative reaction pathway involving an 18 electron active intermediate the increase in rate can be explained in terms of the azaallyl intermediate (Scheme 5.5.1), being lower in energy then the allyl intermediate. The increase in rate of reaction of $(\eta^5\text{-}C_4H_4N)Mn(CO)_3$ could therefore be explained as a result of CO substitution taking place through a low energy associative pathway. In the case of the $(\eta^5\text{-}C_5H_5)Mn(CO)_3$ complex, due to the prohibitively high energy of the allyl intermediate, CO substitution takes place through a dissociative or interchange mechanism.

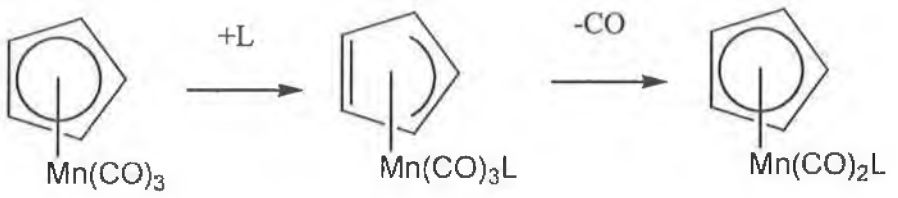

18 electrons

18 electrons
high energy allyl intermediate

18 electrons

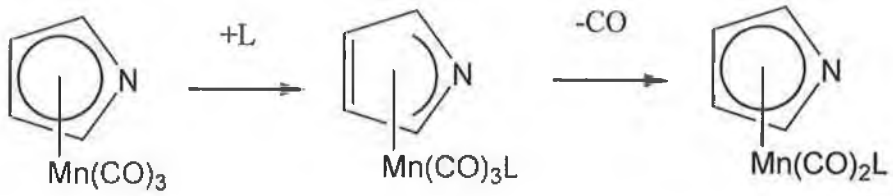

18 electrons

18 electrons
low energy 2 aza-allyl intermediate

18 electrons

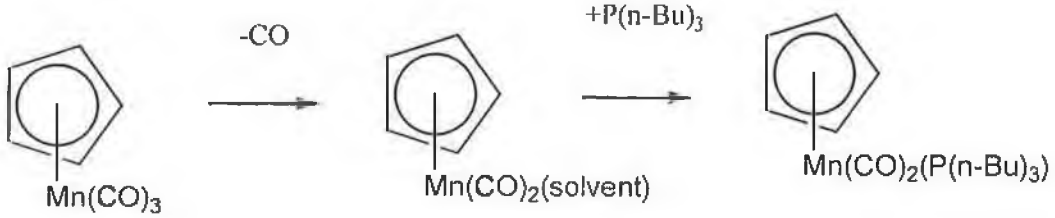

Scheme 5.5.1.

5.6 Spectroscopic properties of $(\eta^5\text{-}C_4H_4N)Mn(CO)_3$

The absorption spectrum of $(\eta^5\text{-}C_4H_4N)Mn(CO)_3$ is shown in Figure 5.6.1. Assignment of the absorption bands is made by comparison to the absorption bands of the UV/vis spectrum of $(\eta^5\text{-}C_5H_5)Mn(CO)_3$ spectrum. The absorption band with a λ_{max} 340nm is probably charge transfer in character with considerable M $\rightarrow$ η^5 C_5H_4N CT character, but the ligand field transitions are very likely to be in the same region.[15,16] This absorption also has some M $\rightarrow$ CO π^* CT character. The absorption in the region of 250 - 270 nm is thought to be ligand field in character. These ligand field transitions are obscured by more intense charge transfer bands.

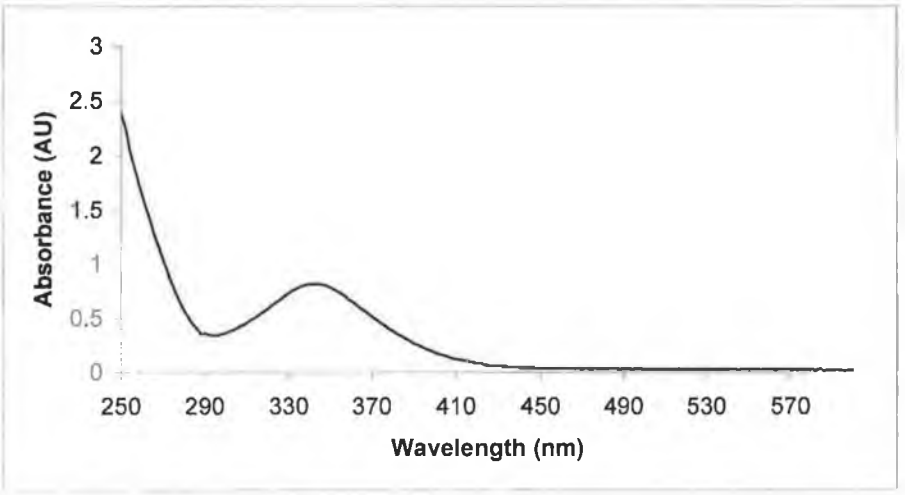

Figure 5.6.1 The UV/vis spectrum of $(\eta^5\text{-}C_4H_4N)Mn(CO)_3$ recorded in cyclohexane.

The three carbonyl bands $(\eta^5\text{-}C_4H_4N)Mn(CO)_3$ at 2040, 1963 and 1953 cm^{-1} of almost equal intensity are observed in the IR spectrum as the complex has C_s symmetry. The lack of symmetry makes spectral interpretation easy, as the number of ν_{co} absorption bands exhibited by a particular photofragment equals the number of CO ligands

5.7 IR and UV/vis steady state monitored photolysis of $(\eta^5\text{-}C_4H_4N)Mn(CO)_3$

Both IR and UV/vis steady state spectroscopy monitored steady state photolysis of $(\eta^5\text{-}C_4H_4N)Mn(CO)_3$ at λ_{exc} = 355nm in CO saturated cyclohexane resulted in the formation of $Mn_2(CO)_{10}$. IR monitored photolysis of $(\eta^5\text{-}C_4H_4N)Mn(CO)_3$ in CO saturated cyclohexane, showed depletion of the parent bands at 2040, 1963 and 1953 cm^{-1} and a grow in at 2014 cm^{-1}.

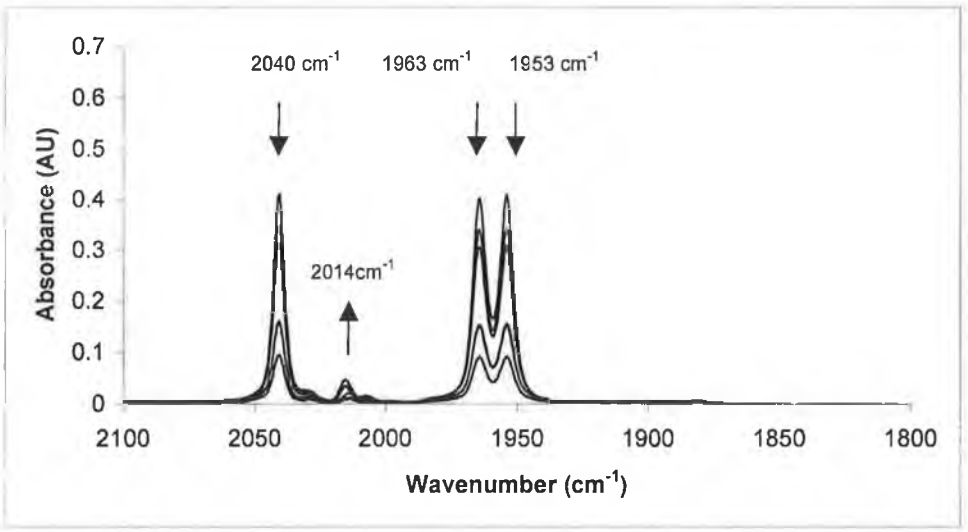

Figure 5.7.1 IR monitored steady state photolysis of $(\eta^5\text{-}C_4H_4N)Mn(CO)_3$ at λ_{exc} = 355nm in CO saturated (1 atmosphere) cyclohexane for 6 minutes. $(\eta^5\text{-}C_4H_4N)Mn(CO)_3$ ν_{co} bands : 2040,1963 and 1953 cm^{-1}. $Mn_2(CO)_{10}$ ν_{co} bands : 2014 cm^{-1}.

UV/vis monitored steady state photolysis at λ_{exc} = 355nm of $(\eta^5\text{-}C_4H_4N)Mn(CO)_3$ in CO saturated cyclohexane is shown in Figure 5.7.2. There is a grow in from 250 – 330 nm. These changes are consistent with formation of $Mn_2(CO)_{10}$. An IR spectrum recorded on completion of the experiment confirmed the presence of $Mn_2(CO)_{10}$, (2043 (v.weak), 2014 (strong) and 1983 cm^{-1} (v.weak)) Figure 5.7.3. The bands at 2043 and 1983 cm^{-1} are not observed due to the relative weakness of the bands compared to the band at 2014 cm^{-1}.

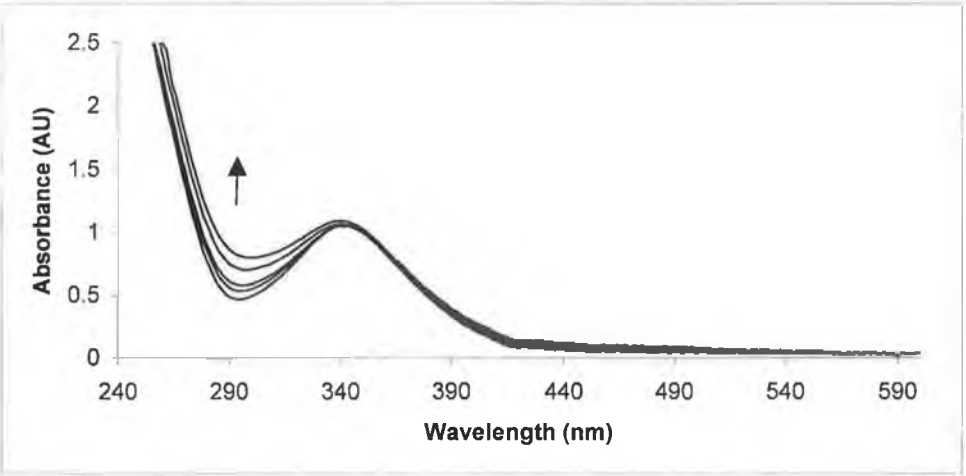

Figure 5.7.2 UV/vis spectrum of $(\eta^5\text{-}C_4H_4N)Mn(CO)_3$ showing the spectral changes observed following photolysis at λ_{exc} = 355nm in CO saturated (1 atmosphere) cyclohexane for 4 minutes.

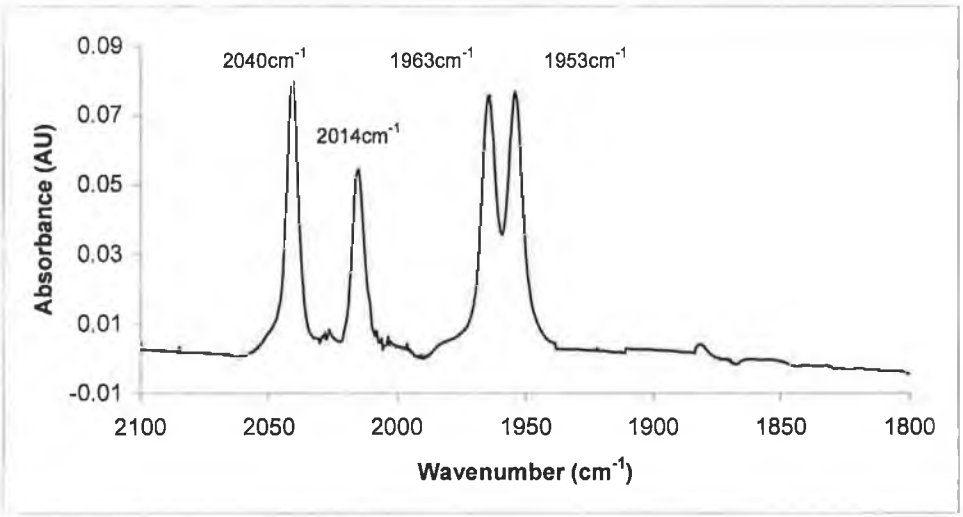

Figure 5.7.3 IR spectrum of $(\eta^5\text{-}C_4H_4N)Mn(CO)_3$ showing the spectral changes observed following photolysis at λ_{exc} = 355nm in CO saturated (1 atmosphere) cyclohexane for 4 minutes. $(\eta^5\text{-}C_4H_4N)Mn(CO)_3$ ν_{co} bands : 2040,1963 and 1953 cm^{-1}. $Mn_2(CO)_{10}$ ν_{co} bands : 2014 cm^{-1}.

IR monitored photolysis at λ_{exc} = 355nm of $(\eta^5\text{-}C_4H_4N)Mn(CO)_3$ was carried out in cyclohexane containing a five times molar excess of PPh_3. Photolysis at λ_{exc} = 355

nm, resulted in depletion of the parent bands and formation of a band at 1895 cm^{-1}. However all three parent bands did not decrease at the same rate which suggests, there is a further band at 1953 cm^{-1}. The two bands at 1953 and 1895cm^{-1} are assigned to the formation of $(\eta^5\text{-}C_4H_4N)Mn(CO)_2(PPh_3)$.

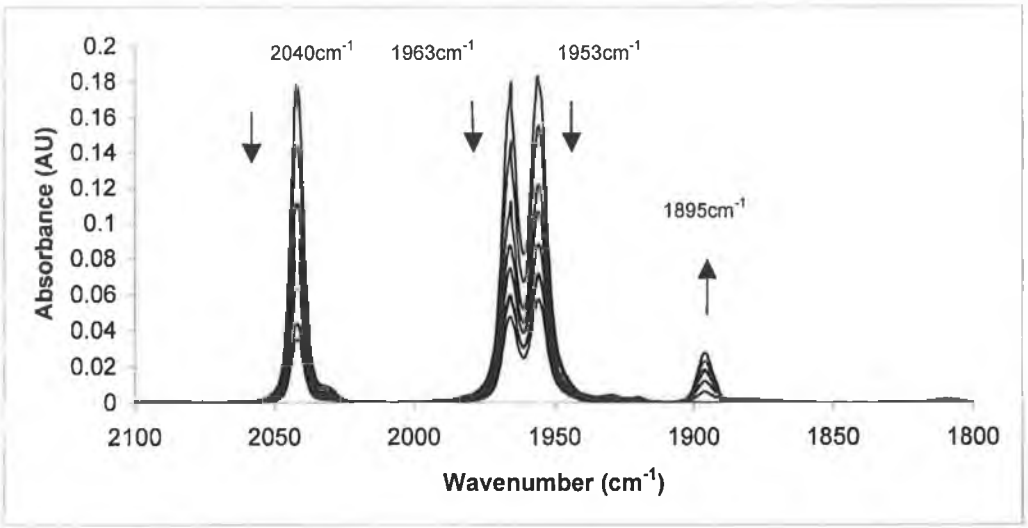

Figure 5.7.4 IR monitored steady state photolysis at λ_{exc} = 355nm of $(\eta^5\text{-}C_4H_4N)Mn(CO)_3$ 0.0011 M in cyclohexane containing a five times molar excess of PPh_3 0.0055 M for 3 minutes. $(\eta^5\text{-}C_4H_4N)Mn(CO)_3$ ν_{co} bands : 2040,1963 and 1953 cm^{-1}. $(\eta^5\text{-}C_4H_4N)Mn(CO)_3$ ν_{co} bands : 2040,1963 and 1953 cm^{-1}. $(\eta^5\text{-}C_4H_4N)Mn(CO)_2(PPh_3)$ ν_{co} bands : 1953 and 1895 cm^{-1}.

5.8 TRIR spectroscopy of $(\eta^5\text{-}C_4H_4N)Mn(CO)_3$

The photochemistry of $(\eta^5\text{-}C_4H_4N)Mn(CO)_3$ was investigated in CO saturated heptane at λ_{exc} = 355 nm and was monitored using step scan TRIR spectroscopy. Heptane was used as opposed to cyclohexane, as cyclohexane absorbs more strongly in the carbonyl region of the IR spectrum then heptane. Following flash photolysis the parent bands are represented as the negative bands which absorb at 2041 1964 and 1955 cm^{-1}. The positive peaks at 1972 and 1905 cm^{-1} are assigned to the photoproduct $(\eta^5\text{-}C_4H_4N)Mn(CO)_2$(heptane). Creaven *et al.* carried out point by point TRIR on photolysis at λ_{exc} = 355 nm of $(\eta^5\text{-}C_5H_5)Mn(CO)_3$ in CO saturated heptane and identified the $(\eta^5\text{-}C_5H_5)Mn(CO)_2$(heptane) species with bands at 1964 and 1892 cm^{-1}. The two bands at 1964 and 1892 cm^{-1} are similar in wavenumber to those for $(\eta^5\text{-}C_4H_4N)Mn(CO)_2$(heptane), 1972 and 1905 cm^{-1}.[5]

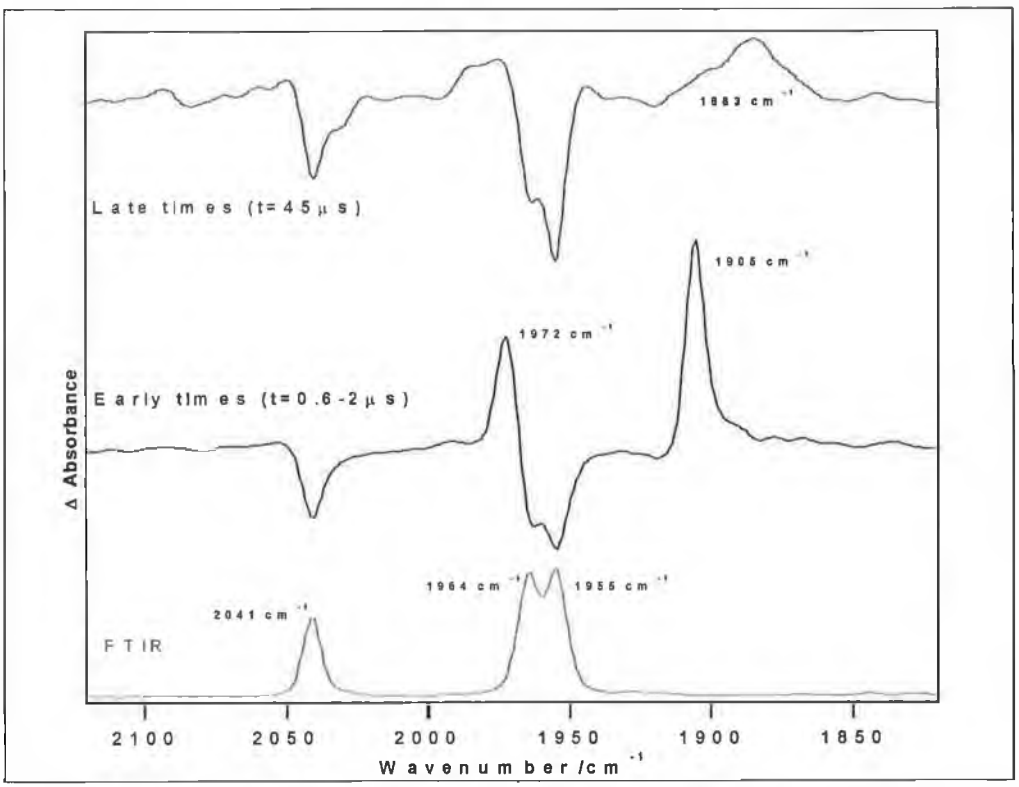

Figure 5.8.1 Step scan TRIR spectrum of $(\eta^5\text{-}C_4H_4N)Mn(CO)_3$ at λ_{exc} = 355nm, 0.6 μs and 45 μs after excitation in CO (2 atmosphere) saturated heptane.

The kinetic traces obtained by stepscan TRIR at λ_{exc} = 355nm in CO (2 atmospheres) saturated heptane at 1972, 1955, 1905 and 1884 cm^{-1} are shown in Figure 5.9.2. From the two traces at 1905 and 1884 cm^{-1}, the rate constant for this reaction was determined by subtracting the k_{obs} in the absence of CO from that in the presence of 2.4×10^{-2} mol dm^3 CO and by dividing the result by 2.4×10^{-2} mol dm^{-3} CO. The rate constant for this reaction was found to be 5.6×10^6 $mol^{-1}s^{-1}$ dm^3 at 298 K.

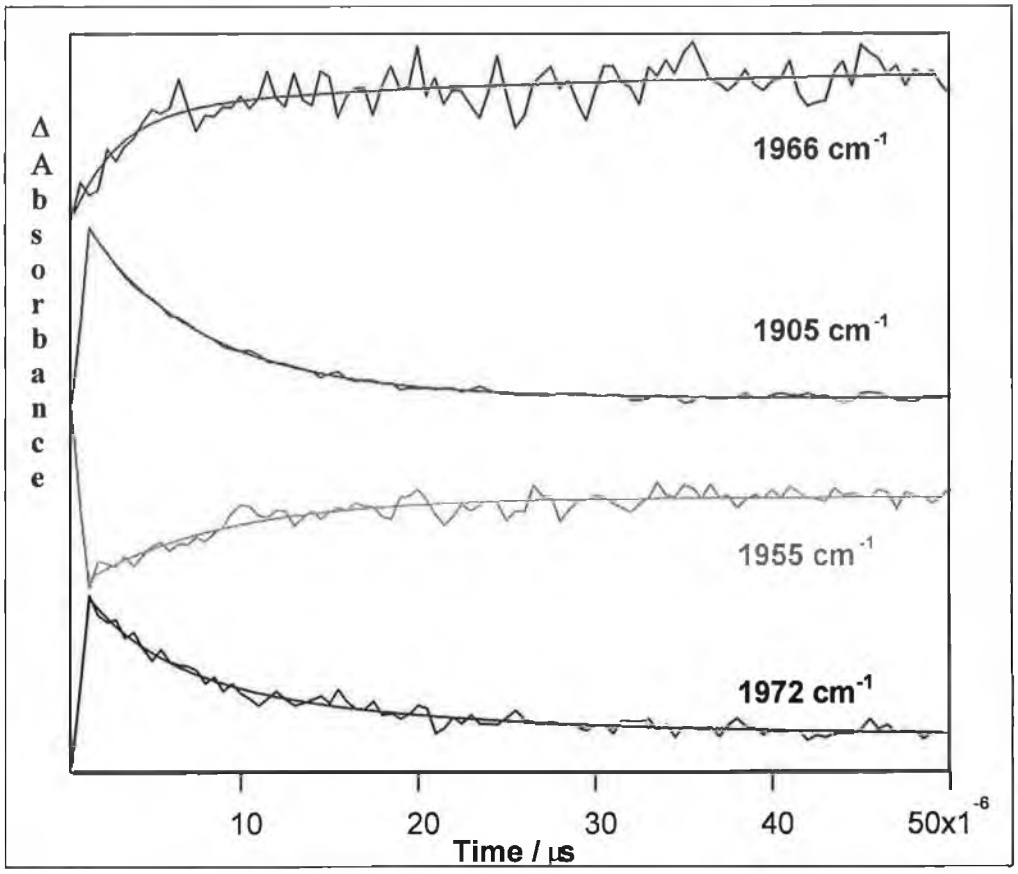

Figure 5.9.2 Kinetic traces from step scan TRIR spectrum of $(\eta^5\text{-}C_4H_4N)Mn(CO)_3$ at λ_{exc} = 355nm in CO (2 atmospheres) saturated heptane at 298 K.

5.9 Matrix isolation studies of $(\eta^5\text{-}C_4H_4N)Mn(CO)_3$

Matrix isolation on $(\eta^5\text{-}C_4H_4N)Mn(CO)_3$ was carried out in both a nitrogen and CO matrix at 20 K. Previous studies on $(\eta^5\text{-}C_5H_5)Mn(CO)_3$ in both noble gas matrices and frozen hydrocarbon glass matrices showed that upon photolysis in all media the dominant process is CO loss.[2,3]

$$(\eta^5\text{-}C_5H_5)Mn(CO)_3 \xrightarrow{h\nu} (\eta^5\text{-}C_5H_5)Mn(CO)_2 + CO.$$

Reaction 5.9.1

The table below gives the reported values for the bands for the dicarbonyl species $(\eta^5\text{-}C_5H_5)Mn(CO)_2$ in the different media.

Medium	Bands cm^{-1}	Assignment
CH_4 Matrix @ 12 K[2]	1961, 1892	$(\eta^5\text{-}C_5H_5)Mn(CO)_2$
Hydrocarbon glasses @ 77 K[3]	1955, 1886	$(\eta^5\text{-}C_5H_5)Mn(CO)_2$
Argon Matrix @ 12 K[2]	1972, 1903	$(\eta^5\text{-}C_5H_5)Mn(CO)_2$
Nitrogen Matrix @ 12 K[2]	1978, 1927 2175	$(\eta^5\text{-}C_5H_5)Mn(CO)_2(N_2)$ $\nu(N\equiv N)$

Table 5.9.1 Observed wavenumbers (cm^{-1}) of IR bands of $(\eta^5\text{-}C_5H_5)Mn(CO)_2$ fragment in different low temperature media.

Nitrogen matrix

Photolysis of $(\eta^5\text{-}C_4H_4N)Mn(CO)_3$ was carried out in a nitrogen matrix at 20 K. Following deposition of $(\eta^5\text{-}C_4H_4N)Mn(CO)_3$,, parent bands are observed at 2045, 1964 and 1956 cm^{-1}. $(\eta^5\text{-}C_4H_4N)Mn(CO)_3$ was initially photolysed at $\lambda_{exc} > 400$ nm, > 375 nm, and subsequently at > 320 nm (Xenon arc lamp). Upon photolysis at $\lambda_{exc} > 400$ nm only very minor changes were recorded. However when the irradiation wavelength was changed to $\lambda_{exc} > 375$ nm, and subsequently > 320 nm depletion of the parent bands at 2045, 1964 and 1956 cm^{-1} were observed and three bands are seen to grow in at 1991, 1936 and 1926 cm^{-1}. The three bands at 1991, 1936 and 1926 cm^{-1}, are assigned to the formation of $(\eta^1\text{-}C_4H_4N)Mn(CO)_3(N_2)_2$. Three additional bands at 2139, 2148 and 2196 cm^{-1} also are seen to form. The formation of the band at 2139 cm^{-1} is thought to be free CO, while the two bands at 2148 and 2196 cm^{-1} are assigned to dinitrogen stretches. As can be seen from Figure 5.9.1, the rate of grow in of the band does not appear to be the same as for the dinitrogen stretches at 2148 and 2196 cm^{-1}. The band at 2139 cm^{-1} assigned to the formation of free CO is therefore more likely to result from decomposition of the parent compound then as a by product of formation of a photoproduct. As the bands for the dicarbonyl species occur in the same region as the bands assigned to the $(\eta^1\text{-}C_4H_4N)Mn(CO)_3(N_2)_2$, one cannot rule this species being formed. As broad band photolysis was used the dicarbonyl species could have back reacted to reform the parent.

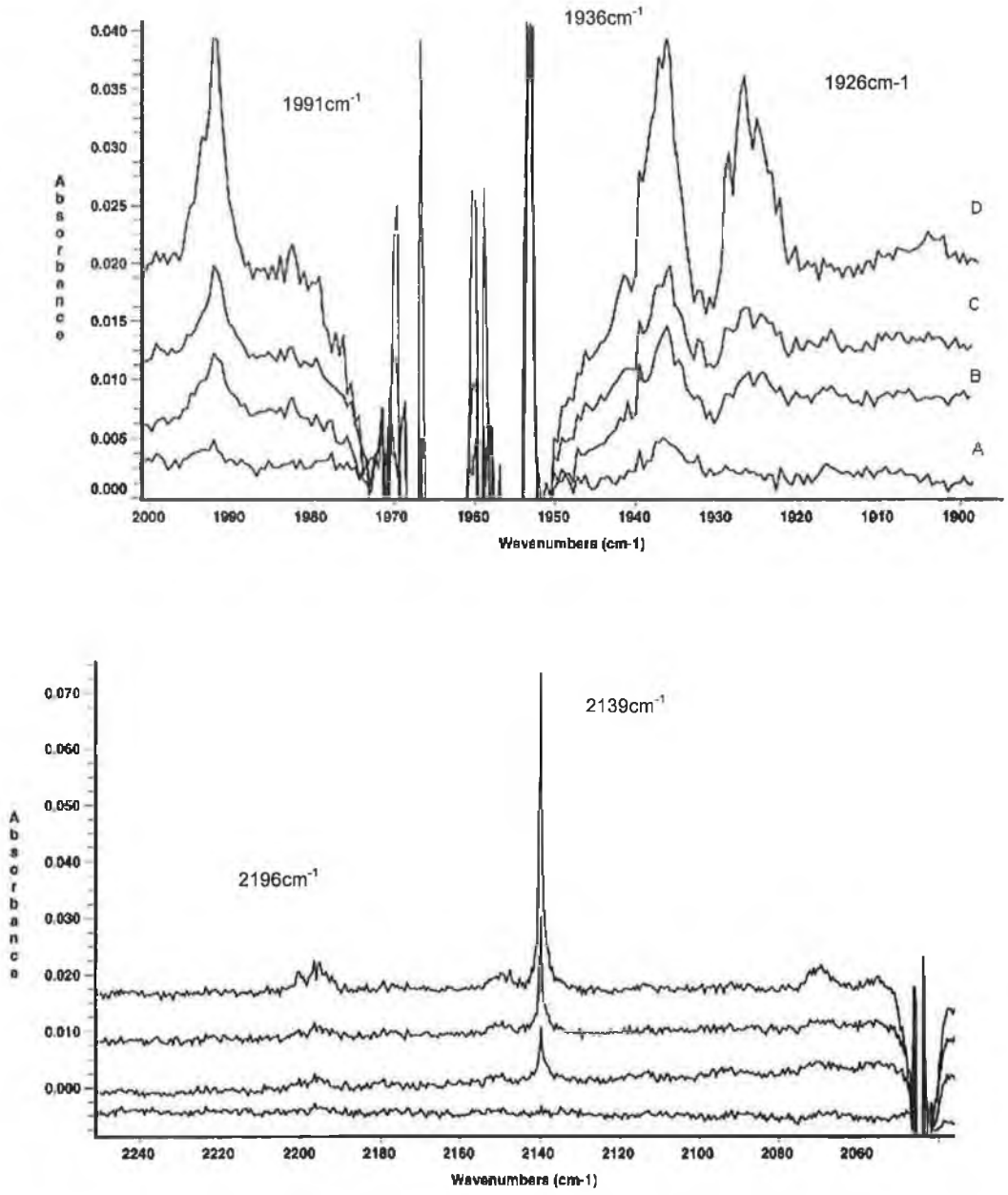

Figure 5.9.1 Photochemical changes observed upon photolysis of $(\eta^5\text{-}C_4H_4N)Mn(CO)_3$ in a nitrogen matrix at 20 K under the following conditions: (a) 1 hour, > 400 nm. (b) 1 hour, > 400 nm, + 50 minutes >375 nm. (c), > 400 nm, + 50 minutes, >375nm, + 3 hours 35 minutes, >375nm. (d) 1 hour, > 400 nm, + 50 minutes >375nm, + 3 hours 35 minutes >375nm, + 2hours >320nm (xenon arc lamp).

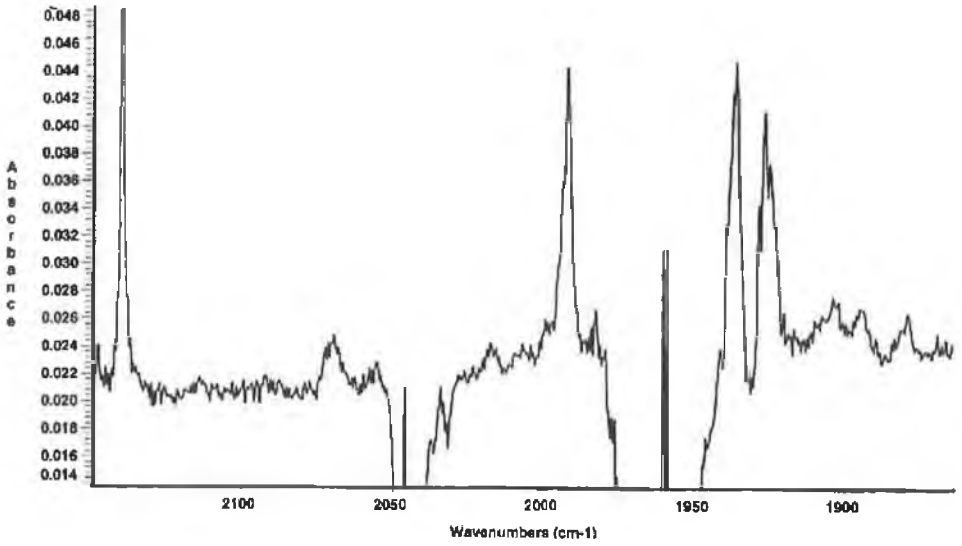

Figure 5.10.2 Photochemical changes observed upon photolysis of $(\eta^5\text{-}C_4H_4N)Mn(CO)_3$ in a nitrogen matrix at 20 K under the following conditions: (d) 1 hour, > 400 nm, + 3 hours 35 minutes >375nm, + 2hours >320nm (xenon arc lamp).

CO matrix

The photochemistry of the $(\eta^5\text{-}C_4H_4N)Mn(CO)_3$ complex was also investigated in a 5% CO matrix at 20 K. As can be seen from Figure 5.9.5, bands were seen to grow in at 2068, 2031, 2025 1997and 1993 cm^{-1}. Upon photolysis at λ_{exc} = 295 nm depletion of the three parent bands was observed along with formation of bands at 2068, 2031, 2025, 1997 and 1993 cm^{-1}. All of the bands were seen to grow in at the same rate. Figure 5.10.5 shows the final difference after photolysis for 1 hour λ_{exc} >375 nm, + 2 hours 40 minutes λ_{exc} >295nm. The bands at 2025 (strong) and 1993 (strong) cm^{-1} are thought to belong to the $(\eta^1\text{-}N\text{-}C_4H_4N)Mn(CO)_5$ species. This assignment is based upon comparison to the $(\eta^1\text{-}C_5H_7)Mn(CO)_5$ species which has bands at 2105 (v.v.weak), 2011 (strong) and 1991 (strong) cm^{-1}. This is further backed up by the fact that the relative intensities of the bands assigned to the formation of the $(\eta^1\text{-}N\text{–}C_4H_4N)Mn(CO)_5$ species are of the same relative intensities of those of

(η^1-C_5H_7)$Mn(CO)_5$.[18,19] The band at 2105 cm^{-1} was not observed because of the relative weakness of the band.

The bands at 2068 (weak) and 1999.7 cm^{-1} (strong) are thought to belong to the (η^3-C_4H_4N)$Mn(CO)_4$. This assignment is based upon comparison to the (η^3-C_5H_7)$Mn(CO)_4$ which has bands at 2068 (weak), 1994 (strong), 1976 (medium) and 1965 cm^{-1} (v.weak).[18,19] For the (η^3-C_4H_4N)$Mn(CO)_4$ species the bands at 1965 cm^{-1} was not observed as one of the parent IR bands occurs at this wavenumber, no band was observed at 1976 cm^{-1}.

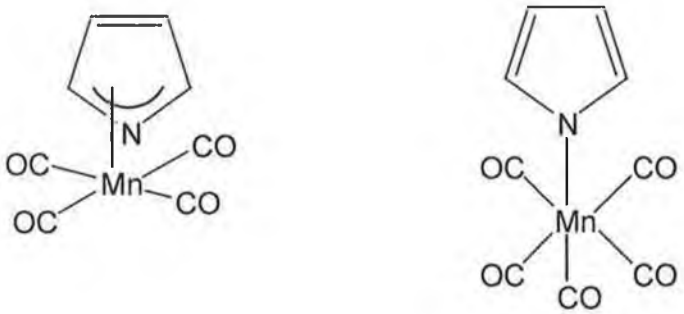

Figure 5.9.3 The proposed ring slip intermediates observed upon photolysis at λ_{exc} >375nm (xenon arc lamp) in 5% CO doped matrix.

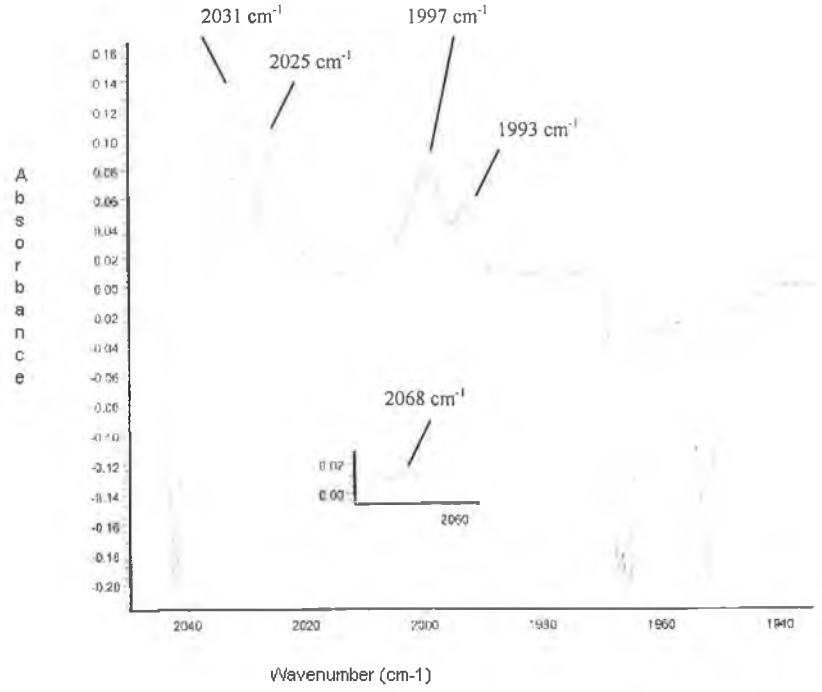

Figure 5.9.4 IR monitored photolysis of $(\eta^5\text{-}C_4H_4N)Mn(CO)_3$ in 5% CO matrix at 20K 1 hour >375 nm, + 2 hours 40 minutes >295nm (xenon arc lamp).

5.10 UV/vis monitored laser flash photolysis of $(\eta^5\text{-}C_4H_4N)Mn(CO)_3$, the primary photoproduct

The absorption spectrum of $(\eta^5\text{-}C_4H_4N)Mn(CO)_3$ is dominated by two features. These are an absorption band with a λ_{max} at 340 nm which is probably charge transfer in character with considerable M $\rightarrow$ η^5 C_5H_4N CT character, but the ligand field transitions are very likely to be in the same region.[15,16] This absorption also has some a M $\rightarrow$ CO π^* CT character. Secondly an absorption with in the region of 250 - 270 nm is thought to be ligand field in character.

Following laser excitation at λ_{exc} = 355 nm of $(\eta^5\text{-}C_4H_4N)Mn(CO)_3$ in cyclohexane under 1 atmosphere of CO, a transient species was observed at 290 nm. This transient decay was assigned to the reaction of the solvated dicarbonyl with CO to yield the parent complex. The effect of CO concentration on the lifetime of the species was investigated. Upon increasing the concentration of CO the lifetime of the solvated

dicarbonyl was found to decrease. A linear relationship was found to exist between k_{obs} from the rate of decay of the solvated dicarbonyl and the concentration of CO. The second order rate constant for the reaction of CO with the solvated dicarbonyl species, was found to be 3×10^6 $s^{-1}mol^{-1}dm^3$. The rate of recovery of the parent species which absorbed at 370 nm was found to be the same as that of the rate of decay of the solvated dicarbonyl. The overall reaction scheme can be represented as below (Reaction 5.10.1-5.10.2):

$$(\eta^5\text{- } C_4H_4N)Mn(CO)_3 \xrightarrow{h\nu} (\eta^5\text{- } C_4H_4N)Mn(CO)_2 + CO$$

Reaction 5.10.1

$$(\eta^5\text{- } C_4H_4N)Mn(CO)_2 + s \longrightarrow (\eta^5\text{- } C_4H_4N)Mn(CO)_2(s)$$

Reaction 5.10.2

When in a CO environment this solvated intermediate recombines with CO to regenerate the parent tricarbonyl complex.

$$(\eta^5\text{-}C_4H_4N)Mn(CO)_2(s) + CO \longrightarrow (\eta^5\text{-}C_4H_4N)Mn(CO)_3$$

Reaction 5.10.3

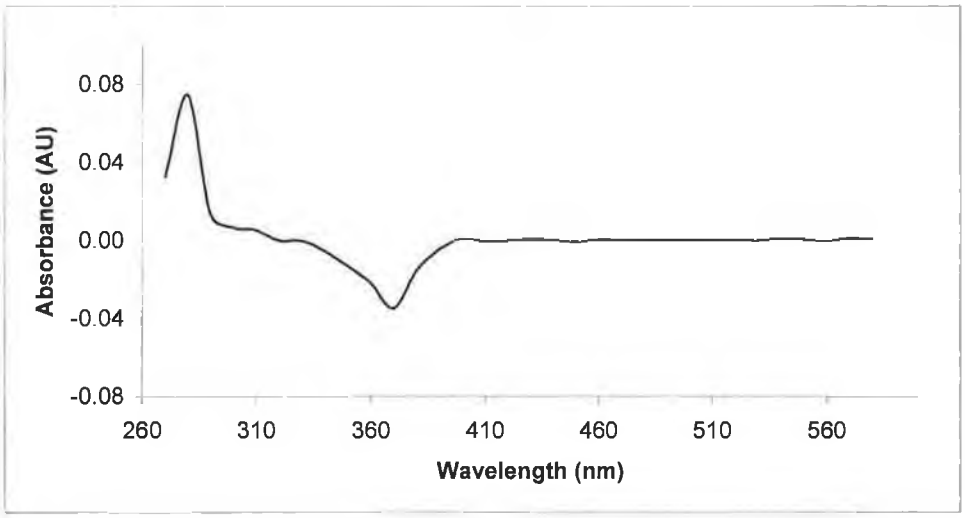

Figure 5.10.1 UV/vis difference spectrum obtained 2 μs after excitation of $(\eta^5\text{-}C_4H_4N)Mn(CO)_3$ at λ_{exc} = 355nm in CO saturated cyclohexane.

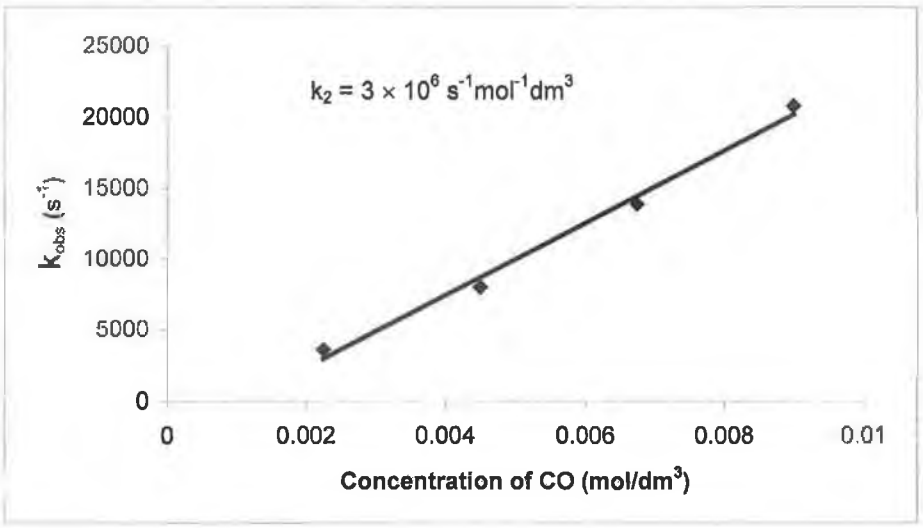

Figure 5.10.2 Plot of concentration of k_{obs} for rate of decay of the transient signal recorded at 290 nm upon photolysis at λ_{exc} = 355 nm in cyclohexane against the concentration of CO.

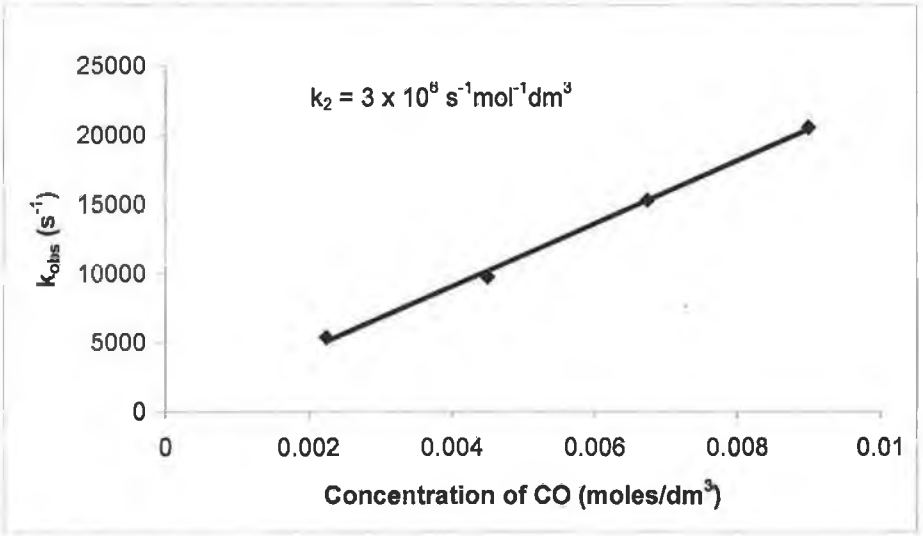

Figure 5.10.3 Plot of concentration of k_{obs} for rate of decay of the transient signal recorded at 370 nm upon photolysis at λ_{exc} = 355 nm in cyclohexane against the concentration of CO.

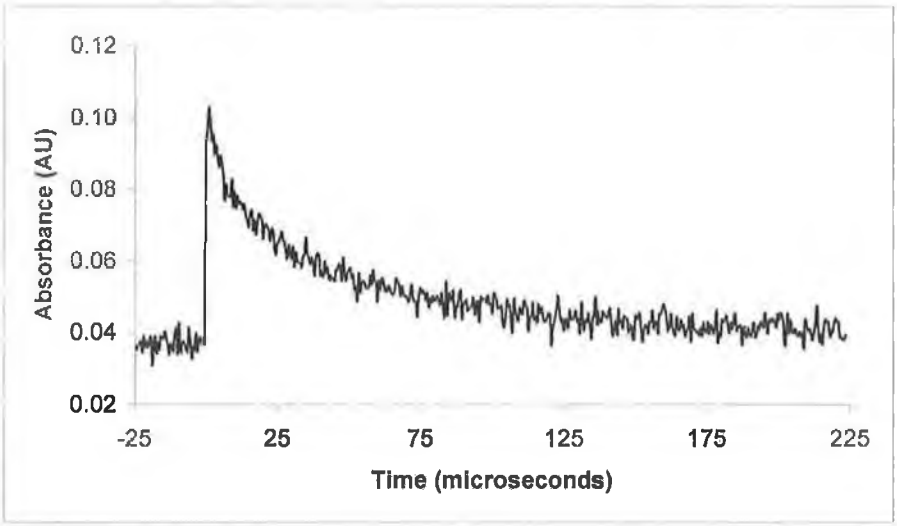

Figure 5.10.4 Transient signal observed for $(\eta^5\text{-}C_4H_4N)Mn(CO)_3$ at 290 nm following flash photolysis at λ_{exc} = 355 nm in CO saturated (1 atmosphere) cyclohexane.

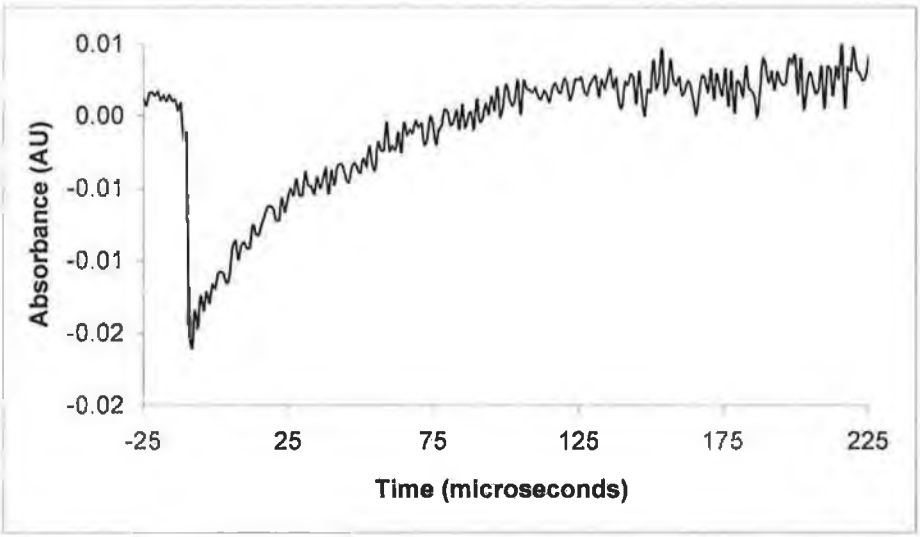

Figure 5.10.5 Transient signal observed for $(\eta^5\text{-}C_4H_4N)Mn(CO)_3$ at 370 nm following flash photolysis at λ_{exc} = 355nm in CO saturated (1 atmosphere) cyclohexane.

The kinetic traces at 280 nm and 370 nm obtained using UV/vis flash photolysis in CO saturated (1 atmosphere) heptane at λ_{exc} = 355 nm are shown in Figure 5.9.4 and 5.9.5. The k_{obs} for the rate of decay of the signal of the signal at 290 nm was found to be dependent on the concentration of CO. By plotting the k_{obs} of the rate of decay of the signal recorded at 290 nm against the concentration of CO, the second order rate constant for the reaction was found to be 5×10^6 $^1s^{-1}mol^{-1}dm^3$. Similarly by plotting the k_{obs} of the rate of decay of the signal recorded at 370 nm against the concentration of CO, the second order rate constant for the reaction was found to be 5×10^6 $s^{-1}mol^{-1}dm^3$.

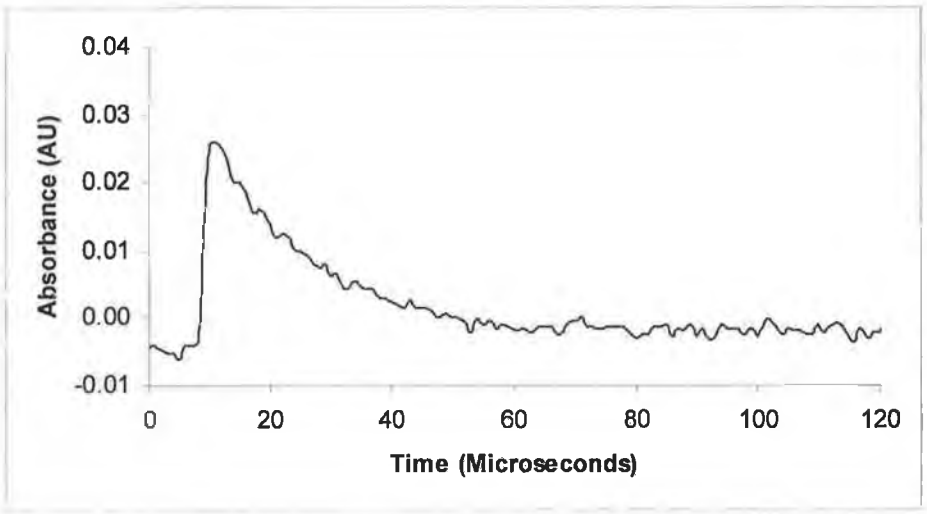

Figure 5.10.6 Transient signal observed for $(\eta^5\text{-}C_4H_4N)Mn(CO)_3$ at 290nm following laser excitation at 355nm in CO saturated (1 atmosphere) heptane.

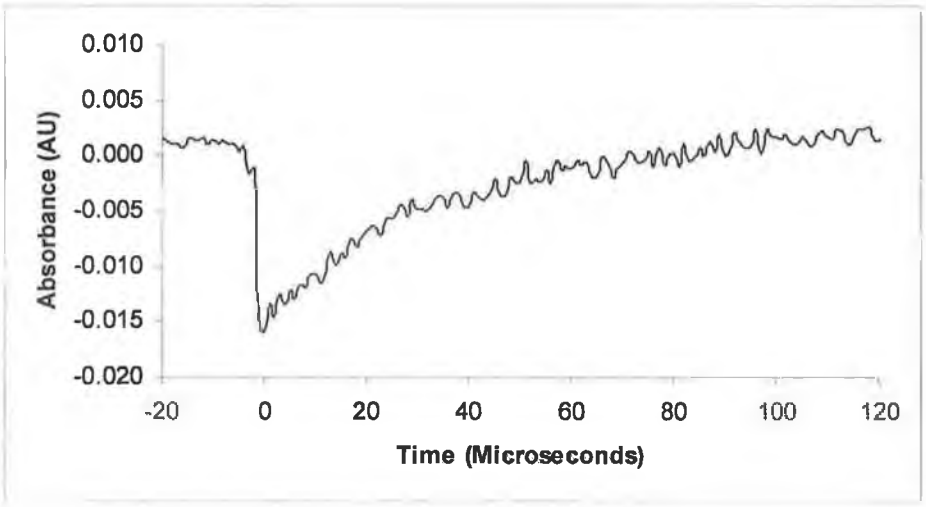

Figure 5.10.7 Transient signal observed for $(\eta^5\text{-}C_4H_4N)Mn(CO)_3$ at 370nm following laser excitation at 355nm in CO saturated (1 atmosphere) heptane.

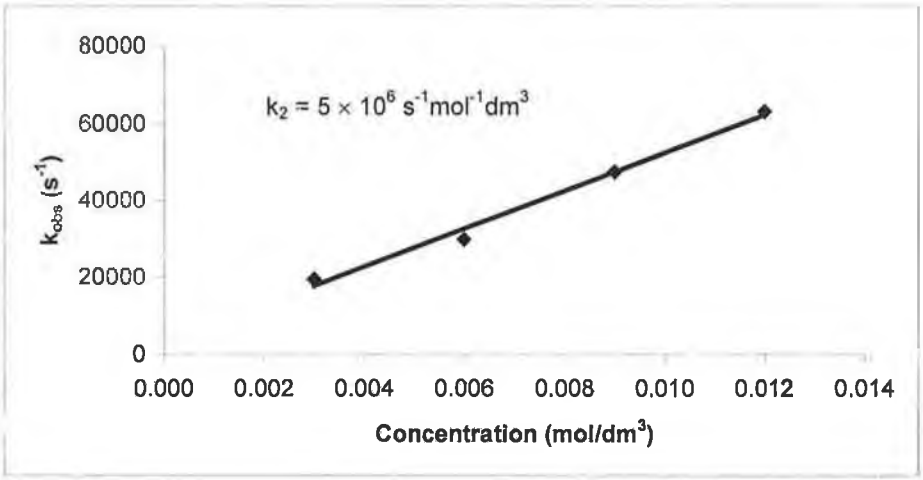

Figure 5.10.8 Plot of concentration of k_{obs} for rate of decay of the transient signal recorded at 290nm upon photolysis at λ_{exc} = 355 nm in heptane against the concentration of CO.

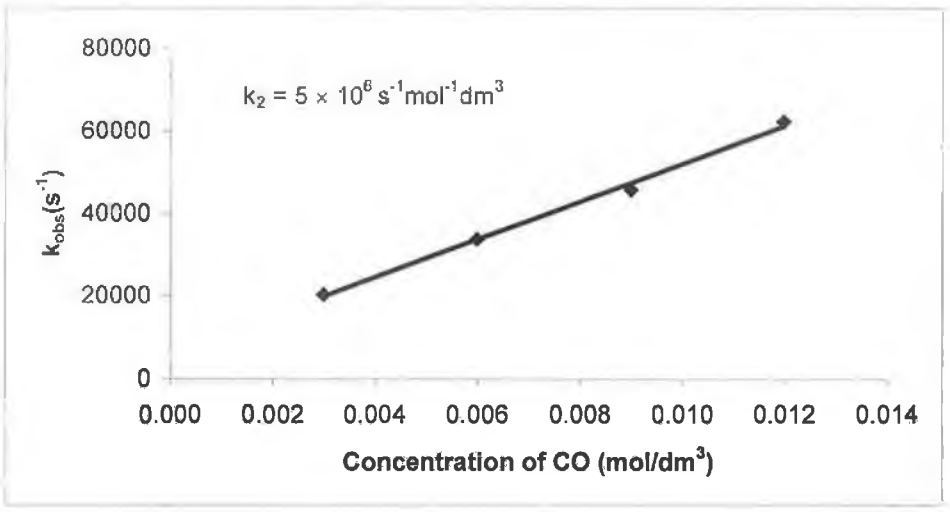

Figure 5.10.9 Plot of concentration of k_{obs} for rate of recovery of the signal recorded at 370nm upon photolysis at λ_{exc} = 355 nm in heptane against the concentration of CO.

5.10.1 UV/vis monitored laser flash photolysis of $(\eta^5\text{-}C_4H_4N)Mn(CO)_3$ in argon saturated cyclohexane, the secondary photoproduct

The photochemistry of $(\eta^5\text{-}C_4H_4N)Mn(CO)_3$ was also investigated by UV/vis flash photolysis with λ_{exc}= 355nm in argon saturatred cyclohexane. Figures 5.10.1.2. depicts the difference spectrum obtained 70 μs after the laser pulse. Examination of the difference spectrum reveals a λ_{max} at 400 nm.

Comparison of the UV/vis difference spectrum recorded during flash photolysis at λ_{exc} = 355 nm in argon saturated cyclohexane experiments with the difference spectrum, reveals some information about the nature of the photoproduct. Examination of the ground state spectrum reveals that a band is produced at ~ 400 nm. This is consistent with the grow in recorded at 405 nm using laser flash photolysis. Formation of a feature that absorbs in the region of 250 - 330 nm in the UV/vis spectrum is consistent with the grow in of the band at 290 nm observed using UV/vis laser flash photolysis. The band at 290 nm was not found to decay over the timescale of the experiment. The band at 290nm is thought relate to the reaction of $(\eta^5\text{-}C_4H_4N)Mn(CO)_2$(cyclohexane) species with starting material to yield a multi metal centre species. The k_{obs} for the rate of grow in of the signal with a λ_{max} at 405 nm was found to be linearly dependent on the concentration of starting material indicating a reaction of solvated dicarbonyl with unphotolysed starting material to yield $(\eta^5\text{-}C_4H_4N)_2Mn_2(CO)_5$. The second order rate constant was found to be 9×10^7 $s^{-1}mol^{-1}dm^3$. The reaction is thought to proceed as shown below.

$$(\eta^5\text{-}C_4H_4N)Mn(CO)_3 \xrightarrow{h\nu} (\eta^5\text{-}C_4H_4N)Mn(CO)_2 + CO$$

Reaction 5.10.1.1

$$(\eta^5\text{-}C_4H_4N)Mn(CO)_2 + s \longrightarrow (\eta^5\text{-}C_4H_4N)Mn(CO)_2(s)$$

Reaction 5.10.1.2

$$(\eta^5\text{-}C_4H_4N)Mn(CO)_2(s) + (\eta^5\text{-}C_4H_4N)Mn(CO)_3 \longrightarrow (\eta^5\text{-}C_4H_4N)_2Mn_2(CO)_5$$

Reaction 5.10.1.3

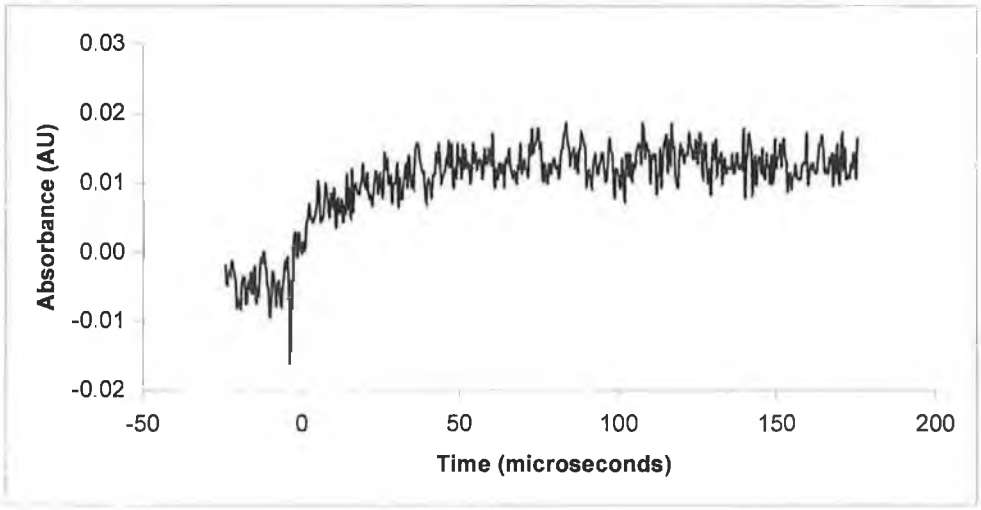

Figure 5.10.1.1 Signal observed at 405 nm following laser flash photolysis at λ_{exc} = 355nm in argon saturated cyclohexane.

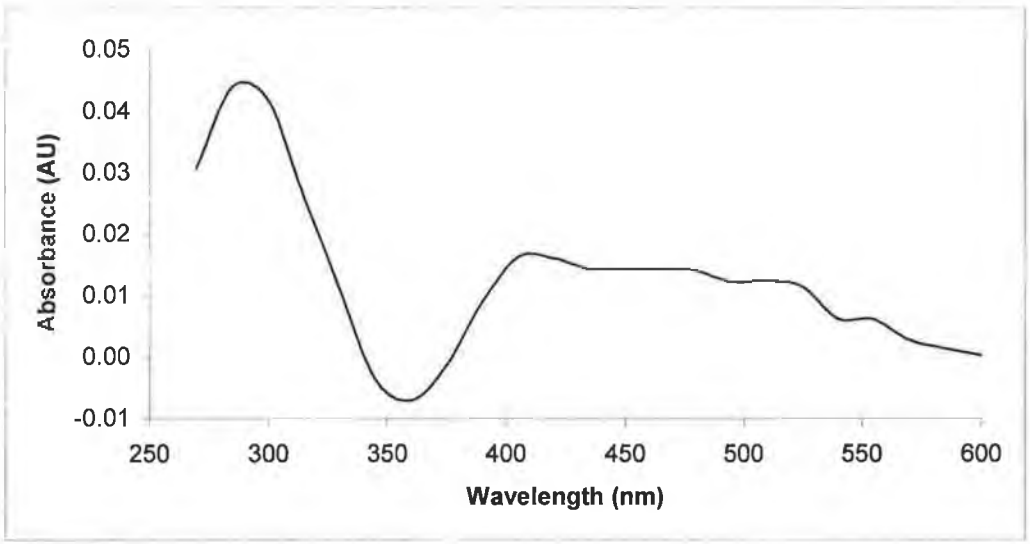

Figure 5.10.1.2 UV/vis difference spectrum obtained 50 μs after excitation of $(\eta^5\text{-}C_4H_4N)Mn(CO)_3$ at λ_{exc} = 355 nm in argon saturated cyclohexane.

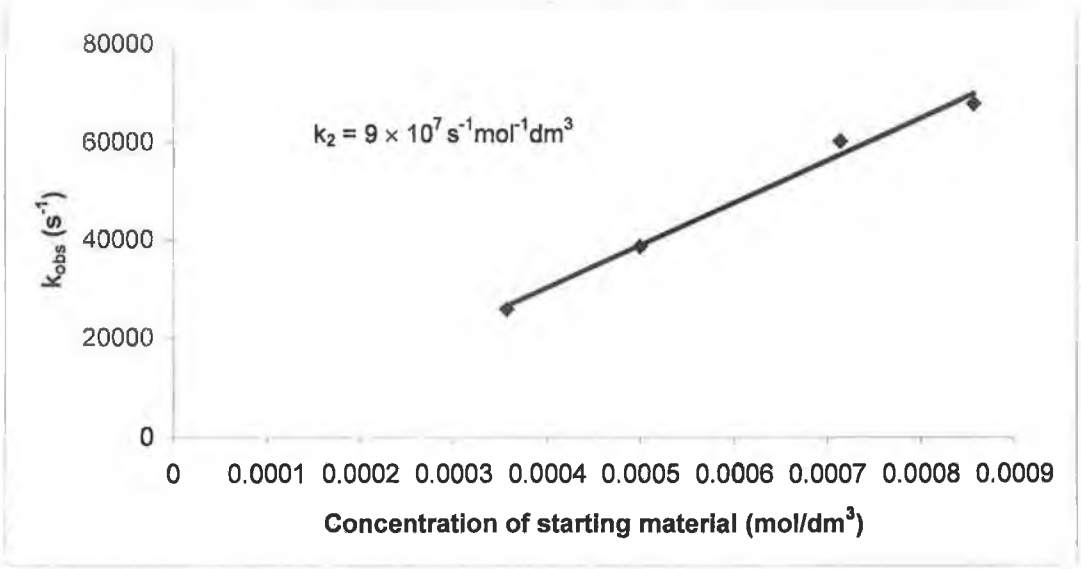

Figure 5.10.1.3 The k_{obs} for the rate of formation of the signal recorded at 405 nm versus the concentration of starting material.

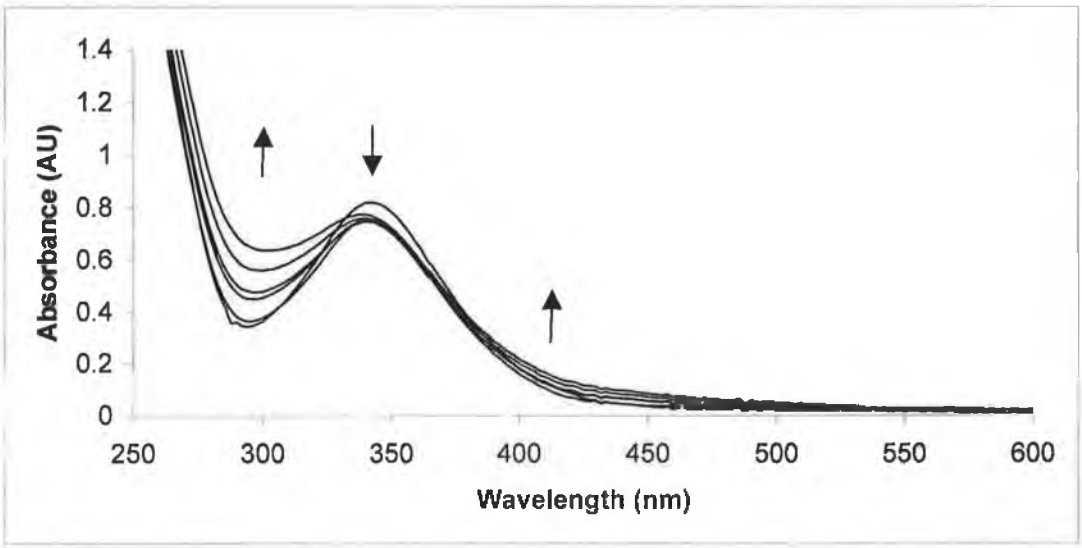

Figure 5.10.1.4 UV/vis spectrum of $(\eta^5\text{-}C_4H_4N)Mn(CO)_3$ showing the spectral changes observed following photolysis at $\lambda_{exc} = 355nm$ in argon saturated cyclohexane for 6 minutes.

The structure of the dinuclear $(\eta^5\text{-}C_4H_4N)_2Mn_2(CO)_5$ species is thought to be similar to that of $(\eta^5\text{-}C_5H_5)_2Mn_2(CO)_5$.[5] The TRIR spectrum for the latter species revealed that the dinuclear species contained a bridging CO ligand and had the structure $(\eta^5\text{-}C_5H_5)Mn(CO)_2(\mu\text{-}CO)(\eta^5\text{-}C_5H_5)Mn(CO)_2$. By analogy to this system, the $(\eta^5\text{-}C_4H_4N)_2Mn_2(CO)_5$ species is thought to have a similar structure.

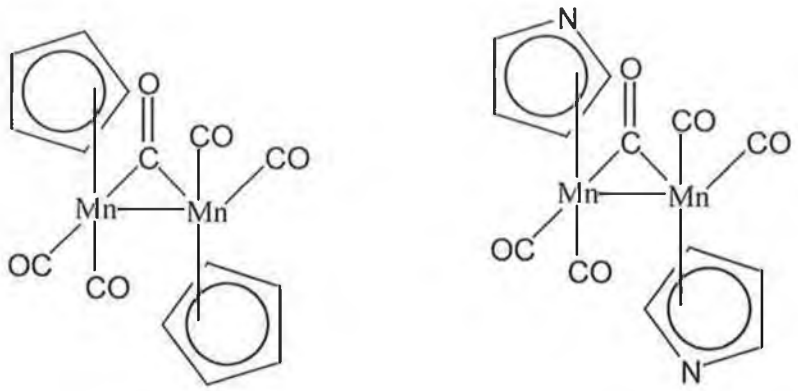

Figure 5.10.1.5 The structure of $(\eta^5\text{-}C_5H_5)Mn(CO)_2(\mu\text{-}CO)(\eta^5\text{-}C_5H_5)Mn(CO)_2$ and the proposed structure of $(\eta^5\text{-}C_4H_4N)_2Mn_2(CO)_5$ species.

5.11 Discussion

Following steady state IR and UV/vis monitored photolysis at λ_{exc} = 355 nm of $(\eta^5\text{-}C_4H_4N)Mn(CO)_3$ in CO saturated cyclohexane, formation of $Mn_2(CO)_{10}$ was observed. Steady state IR monitored photolysis at λ_{exc} = 355 nm of $(\eta^5\text{-}C_4H_4N)Mn(CO)_3$ in cyclohexane doped with PPh_3 gave evidence for formation of $(\eta^5\text{-}C_4H_4N)\ Mn(CO)_2PPh_3$.

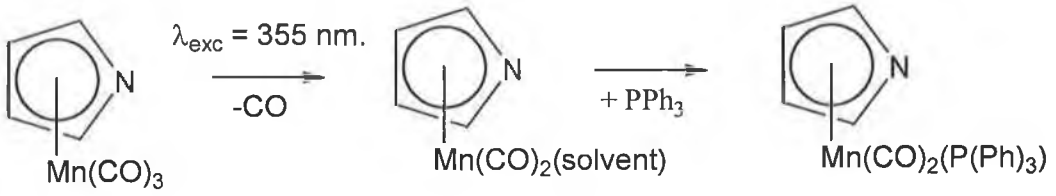

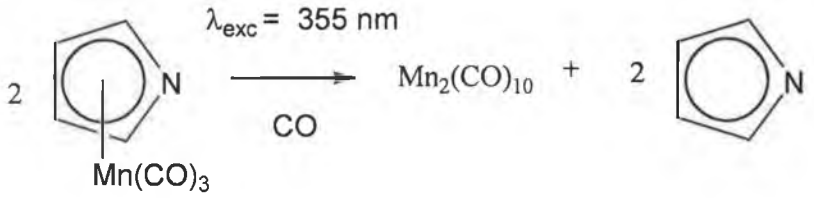

Scheme 5.11.1.

UV/vis flash photolysis of $(\eta^5\text{-}C_4H_4N)Mn(CO)_3$ at λ_{exc} = 355 nm, showed the primary photoprocess to be formation of the solvated dicarbonyl species, $(\eta^5\text{-}C_4H_4N)Mn(CO)_2(s)$. Under a CO atmosphere this species was found to react with CO to reform the parent.

The rate constant for the reaction of $(\eta^5\text{-}C_4H_4N)Mn(CO)_2(s)$ species with CO to regenerate the $(\eta^5\text{-}C_4H_4N)Mn(CO)_3$ was found to be 3×10^6 $s^{-1}mol^{-1}dm^3$ in cyclohexane and 5.8×10^6 $s^{-1}mol^{-1}dm^3$ in heptane. For the $(\eta^5\text{-}C_5H_5)Mn(CO)_3$ system Creaven *et al.* recorded the rate constant for the reaction of $(\eta^5\text{-}C_5H_5)Mn(CO)_2(s)$ species with CO to regenerate $(\eta^5\text{-}C_5H_5)Mn(CO)_3$ being 3×10^5 $s^{-1}mol^{-1}dm^3$ in cyclohexane and 1.1×10^6 $s^{-1}mol^{-1}dm^3$ in heptane.[5] Basolo *et al.* carried out kinetic studies on the thermal CO substitution reaction with P*n*-Bu_3 in decalin at 130°C of $(\eta^5\text{-}C_4H_4N)Mn(CO)_3$ and found that the pyrrolyl complex reacted considerably faster

(10^8 times faster) than the $(\eta^5\text{-}C_5H_5)Mn(CO)_3$ complex.[14] The large rate enhancement was attributed to N being more electronegative then C. Or alternatively CO substitution takes place through a low energy associative reaction pathway involving an 18 electron active intermediate. The increase in rate of reaction of $(\eta^5\text{-}C_4H_4N)Mn(CO)_3$ could therefore be explained as a result of CO substitution taking place through a low energy associative pathway. In the case of the $(\eta^5\text{-}C_5H_5)Mn(CO)_3$ complex, due to the prohibitively high energy of the allyl intermediate, CO substitution takes place through a dissociative or interchange mechanism.

Under low concentrations of CO a secondary photoprocess is observed. This is thought to be reaction of the solvated dicarbonyl species with starting material to yield a dimeric species. By comparison to $(\eta^5\text{-}C_5H_5)_2Mn_2(CO)_5$,the structure of the dinuclear $(\eta^5\text{-}C_4H_4N)_2Mn_2(CO)_5$ species is thought to be similar to that of $(\eta^5\text{-}C_5H_5)_2Mn_2(CO)_5$, which contains a bridging CO ligand and had the structure $(\eta^5\text{-}C_5H_5)Mn(CO)_2(\mu\text{-}CO)(\eta^5\text{-}C_5H_5)Mn(CO)_2$.[5] The rate constant for the reaction of $(\eta^5\text{-}C_4H_4N)Mn(CO)_2(s)$ species with starting material to yield the $(\eta^5\text{-}C_4H_4N)_2Mn_2(CO)_5$ was found to be 9×10^7 $s^{-1}mol^{-1}dm^3$ in cyclohexane, its formation is indicative of the photochemical synthesis of $(\eta^5\text{-}C_5H_5)Co(CO)(\mu\text{-}CO)(\eta^5\text{-}C_5H_5)Co(CO)$, which presumably involves a reaction similar to that shown in Reaction 5.11.1.[17]

$$(\eta^5\text{-}C_5H_5)Co(CO)(s) + (\eta^5\text{-}C_5H_5)Co(CO)_2 \longrightarrow (\eta^5\text{-}C_5H_5)Co(CO)(\mu\text{-}CO)\,(\eta^5\text{-}C_5H_5)Co(CO).$$

Reaction 5.11.1

Step scan TRIR spectroscopy at λ_{exc} = 355 nm showed depletion of the parent bands and formation of a two bands at 1972 and 1905 cm^{-1}. These two bands were assigned to the formation of the solvated dicarbonyl species, $(\eta^5\text{-}C_4H_4N)Mn(CO)_2(s)$. The second order rate constant was found to be 5.4×10^6 $s^{-1}mol^{-1}dm^3$ in heptane when measured using step scan TRIR. This value differs slightly from the value recorded using UV/vis laser flash photolysis. Although the values are similar, the discrepancy

maybe due to the fact that the traces recorded using step scan TRIR spectroscopy are weaker and the signal to noise ratio is lower.

Matrix isolation studies were carried out on $(\eta^5\text{-}C_4H_4N)Mn(CO)_3$ in a dinitrogen matrix at 20 K upon photolysis at $\lambda_{exc} > 375$ nm and > 325 nm, formation of a three band pattern is consistent with formation of $(\eta^1\text{-}C_4H_4N)Mn(CO)_3(N_2)_2$. However one can not rule out formation of the dicarbonyl complex. Photolysis in a CO matrix, resulted in formation of the ring slip species, $(\eta^1\text{-}N\text{-}C_4H_4N)Mn(CO)_5$. Though broad band photlysis was employed, additional bands were also observed and one cannot rule out that the η^3 intermediate is formed. This is then photolysed further to form the η^1 intermediate, as shown in the scheme below, Scheme 5.11.2.

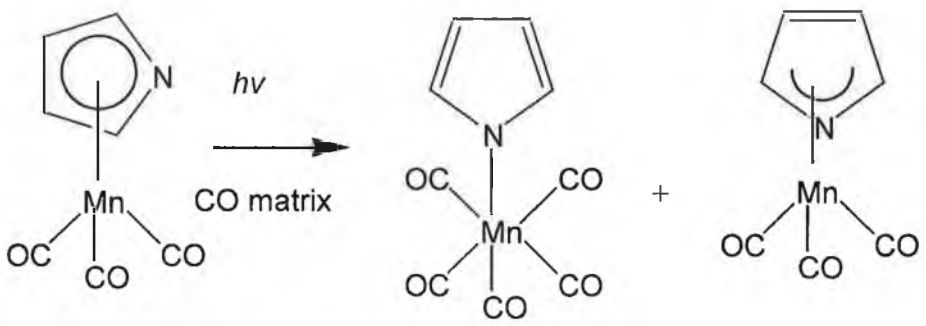

Scheme 5.11.2

The reaction observed in the matrix is reminiscent of the thermal reaction observed by Ji, Rerek and Basolo have also reported the reaction for $(\eta^5\text{-}C_{13}H_{19})Mn(CO)_3$ (with L = PBu_3 where Bu = n butyl).[20] At low PBu_3 concentrations the reaction proceeded cleanly to the monosubstituted complex $(\eta^5\text{-}C_{13}H_9)Mn(CO)_2L$ presumably through an unobserved η^3-fluorenyl intermediate $(\eta^3\text{-}C_{13}H_9)Mn(CO)_3L$. Biagioni *et al.* reinvestigated the reaction of $(\eta^5\text{-}C_{13}H_{19})Mn(CO)_3$ with alkyl phosphines at higher concentrations, producing the η^1-fluorenyl complex.[21] Also Heenan *et al.* have shown that $(\eta^5\text{-}C_5H_5)(\eta^5\text{-}C_4H_4N)Fe$ undergoes a η^5 to η^1 haptotropic shift of the pyrrolyl ligand to give $(\eta^5\text{-}C_5H_5)(\eta^1\text{-}C_4H_4N)Fe(CO)_2$ upon long-wavelength photolysis at ($\lambda_{exc} > 495$ nm) in CO saturated cyclohexane and in frozen matrices at 12 K.[22] Irradiation at $\lambda_{exc} = 532$ nm of $(\eta^5\text{-}C_5H_5)(\eta^5\text{-}C_4H_4N)Fe$ led to formation of

exo-(η^5-C_5H_5)(η^3-C_4H_4N)Fe(CO).[22] Breheny *et al.* have also shown that irradiation of (η^6-C_5H_5N)$Cr(CO)_3$ at λ_{exc} = 308 nm in a N_2 and CO matrices, produced the η^6 to η^1 ring slip product (η^1-C_5H_5N)$Cr(CO)_3(N_2)_2$ and (η^1-C_5H_5N)$Cr(CO)_5$ respectively.[23] The CO loss species (η^6-C_5H_5N)$Cr(CO)_2$, was also noted to form upon irradiation at λ_{exc} = 308 nm.

5.12 Conclusions

Solution photochemistry of (η^5-C_4H_4N)$Mn(CO)_3$ results in the formation of $Mn_2(CO)_{10}$ upon photolysis at λ_{exc} = 355 nm. Laser flash photolysis and step scan time resolved infrared spectroscopy experiments carried out at λ_{exc} = 355nm, provided evidence for the formation of a dicarbonyl intermediate. Matrix isolation studies on the (η^5-C_4H_4N)$Mn(CO)_3$ system showed formation of the dicarbonyl intermediate on high energy photolysis.

Following short wavelength irradiation at λ_{exc} >295 nm photolysis of (η^5-C_4H_4N)$Mn(CO)_3$ in a 5% CO matrix, two ring slip intermediates were observed to form, (η^1- *N*-C_4H_4N)$Mn(CO)_5$ and the (η^3-C_4H_4N)$Mn(CO)_4$ species . In solution the (η^1- *N*-C_4H_4N)$Mn(CO)_5$ species is further photolysed to form the $Mn_2(CO)_{10}$ species. For (η^5-C_5H_5)$Mn(CO)_3$ complexes, CO loss was thought to be the only photochemical pathway open to these systems. The quantum yield for this process is thought to be high, approaching 1. However the solution and low temperature matrices experiments carried out in this study prove this to be not the case as photochemical ring slip and eventual ring loss is observed.

5.13 References

1. Strohmeier, W.V.; Gerlach, K. *Z. Naturforsch.,B. Anorg. Chem., Org. Chem., Biochem., Biophys., Biol.* 1960, **15B,** 675.
2. Rest, A.J.; Sodeau, J.R.; Taylor, D.J. *J. Chem. Soc., Dalton Trans.* 1978, 651.
3. Black, D.J.; Boylan, M.J.; Braterman, P.S. *J. Chem. Soc., Dalton Trans.* 1981, 673.
4. Hill, R.S.; Wrighton, M.S. *Organometallics* 1987, **6**, 632.
5. Creaven, B.S.; Dixon A.J.; Kellly J.M.; Long, C.; Poliakoff, M. *Organometallics* 1987, **6**, 2605.
6. Veiros, L.F. *J. Organomet. Chem.* 1999, **587**, 221.
7. Crichton, O.; Rest, A.J.; Taylor, D.J. *J. Chem. Soc., Dalton Trans.* 1980, 167.
8. Mahmoud, K.A.; Rest, A.J.; Alt, H.G. *J. Chem. Soc., Dalton Trans.* 1985, 1365.
9. Blaha, J.P.; Wrighton, M.S. *J. Am. Chem. Soc.* 1985, **107**, 2694.
10. Veiros, L.F. *Organometallics* 2000, **19**, 3127.
11. Huttner, G.; Brintzinger, H.H.; Bell, L.C.; Friedrich, P.; Bejenke, V.; Neugebauer, D. *J. Organomet. Chem.* 1978, **141**, 329.
12. Van Raaij, E.U. Brintzinger, H.H. Zsolnai, L. Huttner, G. *Z. Anorg. Allg. Chem.* 1989, **577**, 277.
13. Veiros, L.F. *Organometallics* 2000, **19**, 5549.
14. Ji, L.N.; Kershner, D.L.; Basolo, F. *J. Organomet. Chem.* 1985, **296**, 83.
15. Giordano, P.L.; Wrighton, M.S. *Inorg. Chem.* 1977, **16**, 160.
16. Lichtenberger, D.L.; Fenske, R.F. *J. Am. Chem. Soc.* 1976, **98**, 50.
17. Volhardt, K.P.C.; Bercaw, J.E.; Bergman, R.G. *J. Organomet. Chem.* 1975, **97**, 283.
18. Pryce, M.T. *Ph.D Thesis.* Dublin City University. 1993.
19. Kaesz, H.D.; King, R.B.; Stone F.G.A. *Z. Naturforsch.* 1960, **15B**, 682.
20. Ji L.N.; Rerek M.E.; Basolo F. *Organometallics* 1984, **3**, 740.
21. Biagioni, R.N.; Lokovic, I.M.; Sketton, J.; Hartuny, J.B. *Organometallics* 1990, **9**, 547.
22. Heenan, D.P.; Long, C.; Montiel-Palma, V.; Perutz, R.N.;Pryce, M.T. *Organometallics* . 2000, **19**, 3867.

23. Breheny C.J.; Draper, S.M.; Grevels, F.W.; Klotzbucher, W.E.; Long, C.; Pryce M.T.; Russell, G. *Organometallics* 1996, **15**, 3679-3687.

Chapter 6

Experimental

6.1 Materials

The following solvents were of spectroscopic grade and used without purification ; cyclohexane, heptane and 1,1,2 triflourotrichloroethane (Aldrich chemicals). Argon and carbon monoxide were supplied by Air Products and BOC. $(\eta^6\text{-}C_6H_5CO_2CH_3)Cr(CO)_3$ (Aldrich chemicals) was used without further purification and $(\eta^6\text{-}C_6H_5CO_2CH_3)Cr(CO)_3$ was supplied as a gift by Prof Stefano Maiorana.

6.2 Equipment

IR spectra were recorded on a Perkin Elmer 983-G FTIR spectrometer using a sodium chloride solution cell. UV/vis spectra were recorded on a Hewlet Packard 8452A PDA spectrometer using a quartz cell of 1 cm^3. NMR measurements were recorded on a Bruker 400 MHz spectrometer.

6.3 The synthesis of $(\eta^6\text{-arene})Cr(CO)_3$

The synthesis of $(\eta^6\text{-arene})Cr(CO)_3$ was achieved by means of two methods. The first was the reaction of chromium hexacarbonyl with the arene of choice in a high boiling point solvent such as decalin. The second method was by using the thermal exchange reaction.

6.3.1 The reaction of chromium hexacarbonyl with arene, for the synthesis of $(\eta^6\text{-arene})Cr(CO)_3$

The scope of this reaction is quite wide and involves the preparation of numerous arene-metal carbonyls by simple heating of an aromatic ligand with chromium hexacarbonyl in a suitable solvent either in an open system or an autoclave. Excess aromatic compound may sometimes be used, as in the case of the synthesis of $(\eta^6\text{-}C_6H_5NH_2)Cr(CO)_3$. In other instances inert organic solvents such as decalin or high boiling point ethers (such as dibutyl ether or high boiling point pet ether) are used. The overall reaction can therefore be displayed as (Reaction 6.3.1.1).

$Cr(CO)_6$ + arene $\xrightarrow{\Delta}$ (η^6-arene)$Cr(CO)_3$ + 3CO↑. Reaction 6.3.1.1

This very useful reaction was developed independently by three different groups, Fischer *et al.* in Germany,[1] Nicholls and Whiting in England and Natta *et al.* in Italy.[2,3] The synthesis that was chosen to synthesise the following compounds was based on the procedure developed by P.L.Pauson and C.A.L Mahaffy.[4]

6.3.2 The synthesis of (η^6-$C_6H_5OCH_3$)$Cr(CO)_3$

To a 25 ml round bottomed flask fitted with a simple reflux condenser, (not spiral or similar type as to avoid $Cr(CO)_6$ being washed back less efficiently) was added $Cr(CO)_6$ (0.4 g, 1.8 mmol), $C_6H_5OCH_3$ (2.8 g, 25.9 mmol) dibutyl ether (12 ml) and freshly distilled THF (1 ml). The flask and condenser were then thoroughly outgassed with nitrogen. After degassing the reaction flask, a reflux condenser was fitted with a nitrogen bubbler so as to carry out the reaction under an inert atmosphere. The mixture was then heated with stirring for 24 hours in the dark. On completion of the reaction a yellow-orange solution was observed. This was cooled and filtered through celite. The solvent was then removed by vacuum at a pressure of 10^{-1} Torr at room temperature leaving a dark yellow oil. On the addition of cold pentane, a fine yellow powder was formed. This was then recrystallised from a toluene-pentane mixture giving 360 mg of product. The percentage yield of (η^6-$C_6H_5OCH_3$)$Cr(CO)_3$ based on the number of moles of chromium hexacarbonyl is 82%. ν_{co} bands (cyclohexane) : 1978 , 1908 cm^{-1}. NMR ($CDCl_3$) : 5.56 (d, 2H), 5.10 (dd, 3H), 4.87 (s, 1H) and 3.81(s, 3H) ppm.

6.3.3 The synthesis of (η^6-$C_6H_5NH_2$)$Cr(CO)_3$

To a 25 ml round bottomed flask fitted with a simple reflux condenser, (not spiral or similar type as to avoid $Cr(CO)_6$ being washed back less efficiently) was added $Cr(CO)_6$ (0.4 g, 1.8 mmol), $C_6H_5NH_2$ (2.4 g, 24.73 mmol) dibutyl ether (12 ml) and freshly distilled THF (1ml). The flask and condenser were then thoroughly outgassed with nitrogen. After degassing the reaction flask, a reflux condenser was fitted with a nitrogen bubbler so as to carry out the reaction under an inert atmosphere. The mixture

was then heated with stirring for 24 hours in the dark. On completion of the reaction a yellow-orange solution was observed. This was cooled and filtered through celite. The solvent was then removed by vacuum at a pressure of 10^{-1} Torr, at room temperature leaving a dark yellow oil. On the addition of cold pentane, a fine yellow powder was formed. This was then recrystallised from a toluene-pentane mixture giving 288 mg of product. The percentage yield of $(\eta^6\text{-}C_6H_5NH_2)Cr(CO)_3$ based on the number of moles of chromium hexacarbonyl is 70%. ν_{co} bands (cyclohexane) :1967, 1893 and 1888 cm^{-1}. . NMR ($CDCl_3$) : 5.56 (dd, 2H) and 4.79 (m, 3H) ppm.

6.3.4 The synthesis of $(\eta^6\text{-}C_8H_6S)Cr(CO)_3$

To a 25 ml round bottomed flask fitted with a simple reflux condenser, (not spiral or similar type as to avoid $Cr(CO)_6$ being washed back less efficiently) was added $Cr(CO)_6$ (0.4 g 1.8 mmol) C_8H_6S (2.5 g, 18.65 mmol) dibutyl ether (12 ml) and freshly distilled THF (1ml). The flask and condenser were then thoroughly outgassed with nitrogen. After degassing the reaction flask, a reflux condenser was fitted with a nitrogen bubbler so as to carry out the reaction under an inert atmosphere. The mixture was then heated with stirring for 48 hours in the dark. On completion of the reaction a red solution was observed, this was cooled and filtered through celite. This was then chromatographed on a silica column using a mobile phase of a 2:1 petroleum ether 40°C- 60°C : dichloromethane solvent mixture. Free arene and $Cr(CO)_6$ were eluted with the solvent front. The $(\eta^6\text{-}C_8H_6S)Cr(CO)_3$ was eluted as a orange band and collected. The solvent was then removed under vacuum at a pressure of 10^{-1} Torr. The $(\eta^6\text{-}C_8H_6S)Cr(CO)_3$ was recrystallised from a toluene-pentane mixture giving 223.56 mg of product. The percentage yield of $(\eta^6\text{-}C_8H_6S)Cr(CO)_3$ based on the number of moles of chromium hexacarbonyl is 46%. ν_{co} cyclohexane : 1976, 1913 and 1904 cm^{-1}. . NMR ($CDCl_3$) : 7.45 (d, 1H), 7.10 (d, 1H), 6.27 (d 1H), 6.22 (d, 1H), 5.45 (dd, 1H) and 5.22 (dd, 1H) ppm.

6.3.5 The synthesis of $(\eta^6\text{-}C_{12}H_8S)Cr(CO)_3$

To a 25 ml round bottomed flask fitted with a simple reflux condenser, (not spiral or similar type as to avoid $Cr(CO)_6$ being washed back less efficiently) was added $Cr(CO)_6$ (0.4 g, 1.8 mmol) $C_{12}H_8S$ (3 g, 16 mmol) dibutyl ether (12 ml) and freshly distilled THF (1 ml). The flask and condenser were then thoroughly outgassed with nitrogen. After degassing the reaction flask, a reflux condenser was fitted with a nitrogen bubbler so as to carry out the reaction under an inert atmosphere. The mixture was then heated for 48 hours in the dark while stirring. On completion of the reaction a red solution was observed. This was cooled and filtered through celite. It was chromatographed on a silica column using a mobile phase of a 2:1 petroleum ether 40°C-60°C : dichloromethane solvent mixture. The $(\eta^6\text{-}C_{12}H_8S)Cr(CO)_3$ was eluted as a orange band. The solvent was then removed under vacuum at a pressure of 10^{-1} Torr. The $(\eta^6\text{-}C_{12}H_8S)Cr(CO)_3$ was then recrystallised using a toluene-pentane mixture giving 242 mg of product. The percentage yield of $(\eta^6\text{-}C_{12}H_8S)Cr(CO)_3$ based on the number of moles of $Cr(CO)_6$ is 42%. ν_{co} (cyclohexane) : 1978, 1918 and 1909 cm^{-1}. NMR ($CDCl_3$) : 7.98 (dd, 1H), 7.76 (dd 1H), 7.50 (m, 2H), 6.43 (d, 1H), 6.18 (d, 1H), 5.57 (dd, 1H) 5.32 ppm (dd, 1H).

6.3.6 The synthesis of $(\eta^6\text{-}C_{14}H_{10})Cr(CO)_3$

To a 25 ml round bottomed flask fitted with a simple reflux condenser, (not spiral or similar type as to avoid $Cr(CO)_6$ being washed back less efficiently) was added $Cr(CO)_6$ (0.4 g, 1.8 mmol) $C_{14}H_{10}$ (3.4 g, 18.47 mmol) dibutyl ether (12 ml) and freshly distilled THF (1 ml). The flask and condenser were then thoroughly outgassed with nitrogen. After degassing the reaction flask, a reflux condenser was fitted with a nitrogen bubbler so as to carry out the reaction under an inert atmosphere. The mixture was then heated for 4-6 hours in the dark while stirring. On completion of the reaction a dark red solution was observed. This was cooled and filtered through celite. It was then chromatographed on a silica column using a mobile phase of a 2:1 petroleum ether 40°C-60°C : dichloromethane solvent mixture. The $(\eta^6\text{-}C_{14}H_{10})Cr(CO)_3$ was

eluted as a red band and collected before the solvent was then removed under vacuum at a pressure of 10^{-1} Torr. The $(\eta^6\text{-}C_{14}H_{10})Cr(CO)_3$ was then recrystallised using a toluene-pentane mixture giving 141 mg of product. ν_{co} (cyclohexane) : 1975, 1904 and 1899 cm^{-1}. NMR ($CDCl_3$) : 8.29 (d, 1H),7.76 (d, 1H), 7.63 (d, 3H), , 7.28 (dd 1H), 6.61 (m 1H), 5.95 (m 1H), 5.50 (m 2H).

6.3.7 The synthesis of $(\eta^5\text{-}C_4H_4N)Mn(CO)_3$

The method used for the synthesis of $(\eta^5\text{-}C_4H_4N)Mn(CO)_3$ was based on that described by Joshi and Pauson.[5] To a 25 ml round bottom flask, 7 mls of high boiling point pet ether (100°C-140°C), 1.75 mls (20 mmol) of C_4H_4N and 0.6 g (1.54 mmol) of $Mn_2(CO)_{10}$ were added . The solution was then degassed, by purging the solution with a steady stream of argon through the solution for 15 minutes. The solution was then refluxed for 17 hours after which time, the solution was orange – brown in colour. The solution was allowed to cool before it was chromatographed on a silica column using pentane. The solvent was then removed under vacuum at a pressure of 10^{-1} Torr giving 220 mg (1.073 mmol) of $(\eta^5\text{-}C_4H_4N)Mn(CO)_3$. The percentage yield based on the number of moles of $Mn_2(CO)_{10}$ was 69.75 %. ν_{co} bands cyclohexane : 2040, 1963 and 1953 cm^{-1}. NMR ($CDCl_3$) : 6.11 (s, 2H) and 5.25 (s, 2H) ppm.

6.4 The arene exchange reaction

Arene exchange reactions are an established method for the synthesis of arene metal tricarbonyl's, that are not available via the reaction of chromium hexacarbonyl with the arene of choice. This method has the most obvious and valuable advantage over other methods in that it precludes the use of extremely sensitive intermediates. This may cause the reaction to proceed with a low yield if even small traces of impurites such as water or oxygen are present. The reaction consists of two steps, the first being the synthesis of $(\eta^6\text{-}C_{14}H_{10})Cr(CO)_3$ and the second being the displacement of the phenanthrene by the desired arene to give the $(\eta^6\text{-arene})Cr(CO)_3$, Reaction 6.4.1.

6.4.1 The arene exchange reaction of $(\eta^6\text{-}C_{14}H_{10})Cr(CO)_3$ with C_4H_4S to yield $(\eta^5\text{-}C_4H_4S)Cr(CO)_3$

The procedure used to carry out the exchange reaction was adopted from that of Loft, Mowlem and Widdowson.[6] To a 10 ml flask, 400 mg, of $(\eta^6\text{-}C_{14}H_{10})Cr(CO)_3$, C_4H_4S (2.2 g, 26.2 mmol)and 2.5 ml of freshly dried THF were added. The solution was then outgassed, by passing a strong argon stream through the solution for 15 minutes. A reflux condenser fitted with a nitrogen bubbler was placed on the flask and the solution was refluxed for 75 minute after which time no further reaction could be observed by using thin layer chromatography. The red solution was then cooled and the solvent and excess ligand where removed by vacuum at a pressure of 10^{-1} Torr, at room temperature.

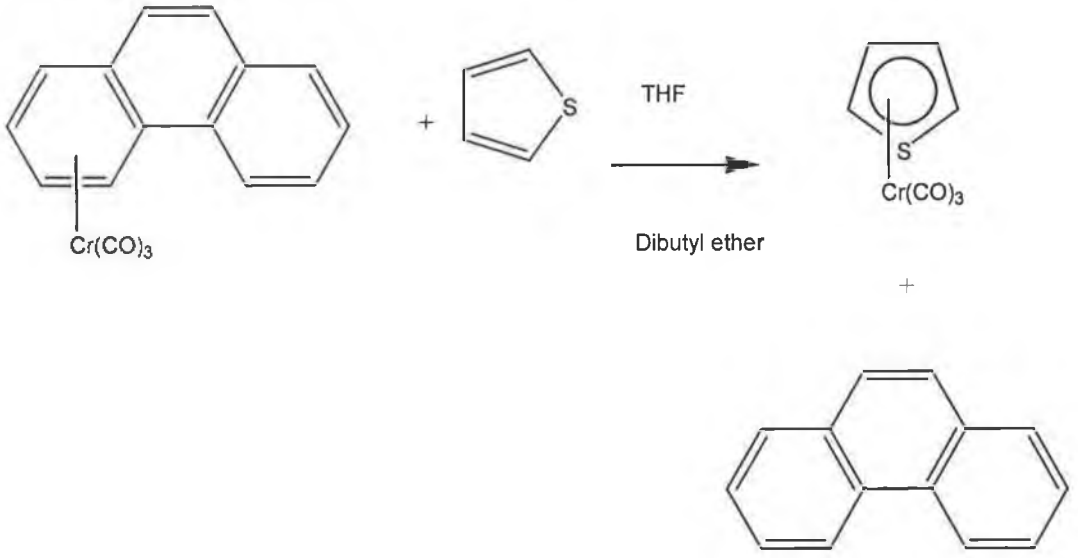

Reaction 6.4.1. The arene exchange reaction of $(\eta^6\text{-}C_{14}H_{10})Cr(CO)_3$ with C_4H_4S.

The orange powder collected was then flash chromatographed using first 3:1 solvent mixture of pet ether : dichloromethane on neutral silica to separate any unreacted materials from the $(\eta^5\text{-}C_4H_4S)Cr(CO)_3$. Two distinct bands were observed, the first being $(\eta^6\text{-}C_{14}H_{10})Cr(CO)_3$, the second being the $(\eta^5\text{-}C_4H_4S)Cr(CO)_3$. After elution of the first band the mobile phase of the column was changed to dichloromethane to remove the second band. After removal of the second red band, $(\eta^5\text{-}C_4H_4S)Cr(CO)_3$

the solvent was removed under vacuum, at room temperature leaving a fine red powder. The $(\eta^5\text{-}C_4H_4S)Cr(CO)_3$ was then recrystallised from cold pentane giving 140 mg of product. Based on the number of moles of $(\eta^6\text{-}C_{14}H_{10})Cr(CO)_3$, the percentage yield of $(\eta^5\text{-}C_4H_4S)Cr(CO)_3$ was 50%. ν_{co} bands (cyclohexane) : 1981, 1912 and 1892 cm^{-1}. . NMR ($CDCl_3$) : 5.59 (s, 2H) and 5.37 (s, 2H) ppm.

6.4.2 The arene exchange reaction of $(\eta^6\text{-}C_{14}H_{10})Cr(CO)_3$ with C_4H_4Se to yield $(\eta^5\text{-}C_4H_4Se)Cr(CO)_3$

The procedure used to carry out the exchange reaction was again adopted from that of Loft, Mowlem and Widdowson.[6] To a 10 ml flask, 400 mg of $(\eta^6\text{-}C_{14}H_{10})Cr(CO)_3$, C_4H_4Se (3 g, 22.9 mmol)and 2.5 ml of freshly dried THF were added. The solution was then outgassed, by passing a strong argon stream through the solution for 15 minutes. A reflux condenser fitted with a nitrogen bubbler was placed on the flask and the solution was refluxed for 75 minute after which time no further reaction could be observed by means of thin layer chromatography. The red solution was then cooled and the solvent and excess ligand where removed by vacuum at a pressure of 10^{-1} Torr, at room temperature. To separate any unreacted materials from the $(\eta^5\text{-}C_4H_4Se)Cr(CO)_3$ the orange powder collected was then flash chromatographed using first 3:1 solvent mixture of pet ether : dichloromethane on neutral silica. Two distinct bands were observed, the first being the $(\eta^6\text{-}C_{14}H_{10})Cr(CO)_3$ the second being the $(\eta^5\text{-}C_4H_4Se)Cr(CO)_3$. After elution of the first band the mobile phase of the column was changed to dichloromethane to remove the second band. After removal of the second red $(\eta^5\text{-}C_4H_4Se)Cr(CO)_3$ band the solvent was removed under vacuum at room temperature leaving a dark red fine powder. The $(\eta^5\text{-}C_4H_4Se)Cr(CO)_3$ was then recrystallized from a toluene pentane mixture giving 197 mg of product. Based on the number of moles of $(\eta^6\text{-}C_{14}H_{10})Cr(CO)_3$, the percentage yield of $(\eta^5\text{-}C_4H_4Se)Cr(CO)_3$ was 57%. ν_{co} (cyclohexane) : 1983, 1914 and 1896 cm^{-1}. . NMR ($CDCl_3$) : 5.95 (s, 2H) and 5.79 (s, 2H) ppm.

6.5 Attempted preparative photochemical synthesis of $(\eta^4\text{-}C_4H_4Se)Cr(CO)_4$

TRIR monitored flash photolysis at λ_{exc} = 355 nm and steady state photolysis at λ_{exc} = 355 nm of $(\eta^5\text{-}C_4H_4Se)Cr(CO)_3$ showed the presence of IR bands that were assigned to the formation of the $(\eta^4\text{-}C_4H_4Se)Cr(CO)_4$ species. An attempt was made to synthesize this complex by preparative photolysis. Preparative photochemistry is usually carried out in one of two ways. The first being the immersion well method. This is where the reaction solution surrounds the lamp. The second the external irradiation method, where the reaction solution is surrounded by a battery of lamps. The immersion well set-up is very effective in capturing the lamps output and therefore is very economical. A typical example of immersion well apparatus is shown in Figure 6.5.1. The lamps used in this method are contained in a double walled immersion well structure of either quartz or high grade boro silicate glass which is transparent to UV light. The wall is fitted with a standard taper joint which allows it to be used with a variety of reactor sizes. The well is usually made of pyrex or quartz. Pyrex is less expensive then quartz but only transmits light of wavelengths above 300 nm, whilst quartz is transparent down to 200 nm. The quartz immersion well used came with a Pyrex sleeve which fitted around the lamp to allow the cut off of short wavelength UV irradiation. The double walled structure of the wells allows the reaction solution to be insulated from the heat of the medium or high pressure mercury arc lamp by the circulation of cooling solution usually water. However a low temperature circulator permitting photolysis at low temperatures to prevent thermal degradation of any products formed can be connected. The outer vessel of the reactor is usually made of Pyrex.

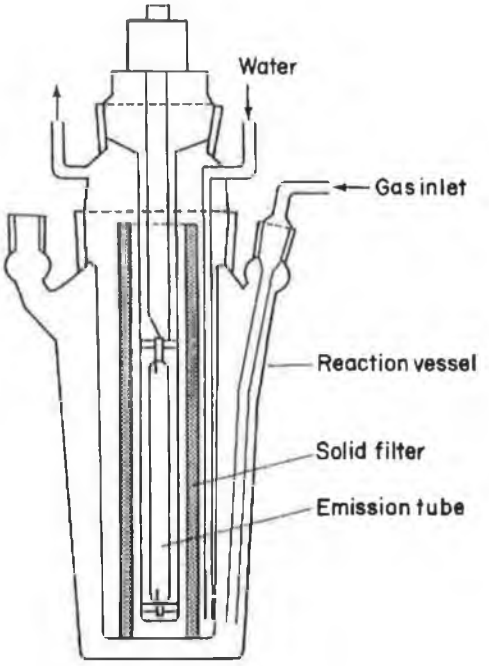

Figure 6.5.1 A typical immersion well apparatus for preparative photochemistry.

6.5.1 Procedure for the synthesis of $(\eta^4\text{-}C_4H_4Se)Cr(CO)_3$

To 80 ml of degassed hexane was added 200 mg of $(\eta^5\text{-}C_4H_4Se)Cr(CO)_3$. A steady stream of CO was then allowed to bubble through the solution with stirring. The solution was photolysed with a mercury arc lamp fitted with a Pyrex sleeve and the reaction was monitored by IR spectroscopy. After 20 minutes no trace of starting complex was observed and new bands attributed to the formation of $(\eta^4\text{-}C_4H_4Se)Cr(CO)_4$ and $Cr(CO)_6$ were noted. The solution was transferred to a 100 ml round bottom flask and the solvent was removed at room temperature by vacuum and a red leaving a orange-red powder. An IR spectrum of the solution was recorded and it was found that the IR bands corresponded to the starting material and $Cr(CO)_6$. This would suggest that the η^4 intermediate thermally back reacted under vacuum to starting material (Reaction 6.5.1.1).

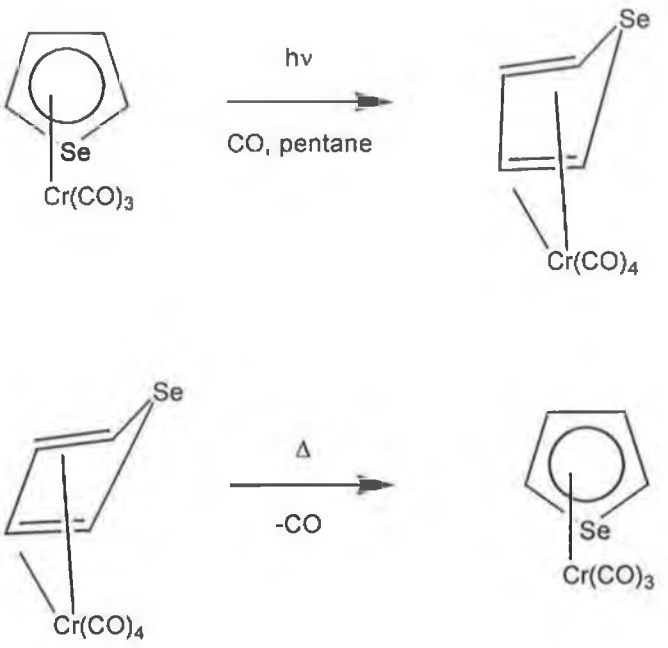

Reaction 6.5.1.1 The photochemical and thermal chemistry of $(\eta^5\text{-}C_4H_4Se)Cr(CO)_3$ and $(\eta^4\text{-}C_4H_4Se)Cr(CO)_4$.

6.6 Determination of molar absorbtivity values

Molar absorbtivity values were determined at the wavelength of excitation for all compounds in order to calculate the concentration of the sample. By knowing the absorbance and using the Beer-Lambert law the concentration of the sample was calculated. The Beer –lambert law is given by the following equation.

$$A = \varepsilon cl$$

Where A = absorbance at specific wavelength.

c = concentration of sample (moles dm^{-3}).

l = pathlength of cell (1 cm).

ε = molar absorbtivity (dm^3 moles cm^{-1}).

6.7 Determination of solubility of CO in alkane solution

The solubility of CO in hydrocarbons solvents was determined by using the mole fraction data determined by Makanczy *et al.*[8] The calculations for cyclohexane are given as a representive example.

Solubility of CO @ 298 K expressed in mole fraction = 9.94×10^{-4} $moles^{-1}$

1 litre of cyclohexane = 779 grams.

1 mole of cyclohexane = 84 grams.

$\Rightarrow$ moles / litre = $1/84 \times 779$

= 9.274 moles / litre

9.94×10^{-4} moles-1 = $\frac{\#[CO]}{9.274}$

$[CO] = 9.1 \times 10^{-3}$ moles at 1 atmosphere.

6.8 Determination of quantum yields for the photo displacement of the arene ring in the (η^6-C_6H_5X)$Cr(CO)_3$ systems (X = NH_2, OCH_3, $C(O)OCH_3$ and C(O)H).

The quantum yield for a photochemical reaction is given by ;

$$\Phi = \frac{\text{number of moles of product formed}}{\text{number of quanta absorbed}}$$

The number of quanta absorbed was determined using potassium ferioxalate actinometry.[9,10] When a solution of $K_2(FeC_2O_4)$ in aqueous sulphuric acids is irradiated with light in the range 253 nm to 577 nm the Fe^{3+} are reduced to Fe^{2+} ions. The yield of Fe^{2+} ions can then be experimentally determined. A red complex is formed with 1,10 phenanthroline which can be monitored at 510 nm. The advantages of using this system are :

- It is easy and fast to use.
- Quantum yields are relatively insensitive to wavelength, concentration, temperature and light intensity.
- Oxygen does not have to be excluded.

6.8.1 Preperation of the actinometry solution

5 ml of 0.2 moles /litre $Fe_2(SO_4)_3$ and 5 ml of 1.2 moles / litre $K_2C_2O_4$ were pipetted to a 100 ml volumtric flask. This solution was then made up to the mark.

6.8.2 Determination of the light intensity of the source

A volume of the $K_3Fe(C_2O_4)_3$ solution equal to that of the sample irradiated was placed in the reaction vessel. The $K_3Fe(C_2O_4)_3$ solution was then irradiated for an appropriate time. 1 ml of the irradiated solution was transferred by pipet to a 10 ml volumetric flask. To this 2 mls of a 0.2% 1,10 phenanthroline solution along with 0.5

ml of buffer solution and made up to the mark. The solution was then left in the dark for an hour to develop. A blank was prepared with a nonirradiated volume of actinometer equal to the aliquot of irradiated sample withdrawn.

6.8.3 Calculation of light intensity of source.

Using the absorbance obtained along with the selected the appropriate quantum yield for ferrous production at the wavelength of interest (λ_{exc} = 355 nm the quantum yield was 1.25) the light intensity of the source was :

$$N_{Fe^{2+}} = \frac{6.023 \times 10^{20} \times V_1 \times V_3 \times A}{V_2 \times l \times \varepsilon}$$

Where :

V_1 = Volume of actinometer irradiated (dm^3).
V_2 = Volume of actinometer transferred into volumetric flask (dm^3).
V_3 = Final volume (dm^3).
A = Absorbance at 510 nm.
L = cell path length (cm).
ε = Molar absorbtivity of Fe^{2+} / phenanthroline complex at 510 nm (mol^{-1} $cm^{-1}dm^3$).

The number of quanta absorbed is then determined from the following equation:

$$n_a = \frac{n_{Fe^{2+}}}{\Phi}$$

n_a = The number of quanta absorbed.

Φ = The quantum yield of Fe^{2+} at λ_{max} of interest.

6.9 Laser flash photolysis with UV/vis monitoring

All solutions were prepared for laser flash photolysis experiments in a degassing bulb attached to a fluorescense cell and protected from light by surrounding the degassing bulb with aluminium foil. Samples were prepared in the dark by dissolution in cyclohexane. The concentration of solute was adjusted so that the absorbance at λ_{exc} (266, 355 or 532nm) was between 0.8 or 1.2 AU. The solutions were subjected to

degassing by three cycles of a freeze-thaw procedure to 10^{-2} Torr and then liquid pumped to remove any traces of water.

The required atmosphere of interest is then placed over the sample. The steady state spectral changes before and after were recorded as well as periodic monitoring of spectra through out.

6.10 TRIR spectroscopy

All solutions were prepared for experiments in a schlenk tube and protected from light by surrounding the tube with aluminium foil. The hexane had been previously dried and was then transferred to the schlenk tube by canula under an inert atmosphere. The solutions were subjected to degassing by pumping the sample to a pressure of 10^{-1} Torr and then liquid pumped to remove any traces of water, CO_2. The required atmosphere of interest is then placed over the sample.

6.11 References

1. Fischer, E.; Ofele, K.; Essler, H.; Frolich, W.; Mortensen, W.D.; Semmlinger, W.; *Z. Natturforsch.* 1958, **91**, 2763.
2. Nicholls and Whiting.; *J. Chem. Soc.* 1959. 551.*
3. Natta, G.;Ercoli, R.; Calderazzo, F.; Santambrogia, S.; *Chim. Ind.(Milan).* 1958, **40**, 1003.
4. Mahaffy, C.A.L.; Pauson, P.L.; *Inorg. Synth.*; 1974, **19**, 154.
5. Joshi, K.K.; Pauson, P.L.; *Proc. Chem. Soc.*; 1963, 326.
6. Loft, M.S.; Mowlem, T.J.; Widdowson, D.A.; *J. Chem. Soc. Perkin.Trans.*; 1995. 93.
7. Willard, H.H.; Merritt, L.L..; Dean, J.A.; Settle F.A.; *Instrumental methods of analysis.* Wadsworth. Belmont, California.; 7th ed. 1988.
8. Makranczy, J.; Megyery- Balog, K.; Rosz, L.; Patyt, D.; *Hungarian J. Indust. Chem.*; 1976, **4**, 269.
9. Rabek, J.F.; *Experimental methods in photochemistry and photophysics.* Wiley. New York. 1982.
10. (a) Murov, R.; *Hand Book of photochemistry,* New York.; 1973. (b) O'Keeffe, S. *Ph.D thesis*, Dublin City University, 1997.

Appendix A

Data for determination of quantum yields for arene displacement of the substituted (η^6-C_6H_5X)$Cr(CO)_3$ systems (X = NH_2, OCH_3, $C(CO)OCH_3$, C(O)H) at 298K

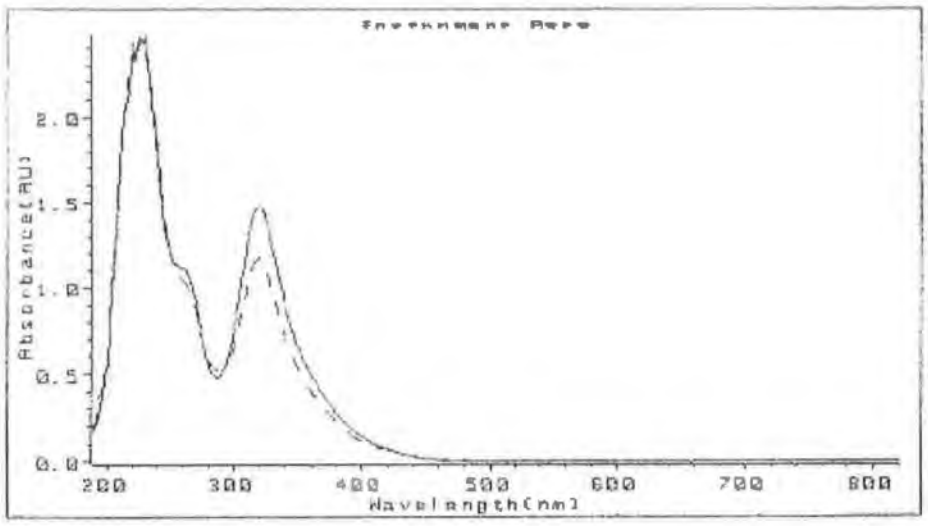

Figure 7.1.1 UV/vis spectrum recorded upon photolysis of $(\eta^6\text{-}C_6H_5NH_2)Cr(CO)_3$ in CO saturated cylohexane (1 atmosphere of CO), at 355nm.

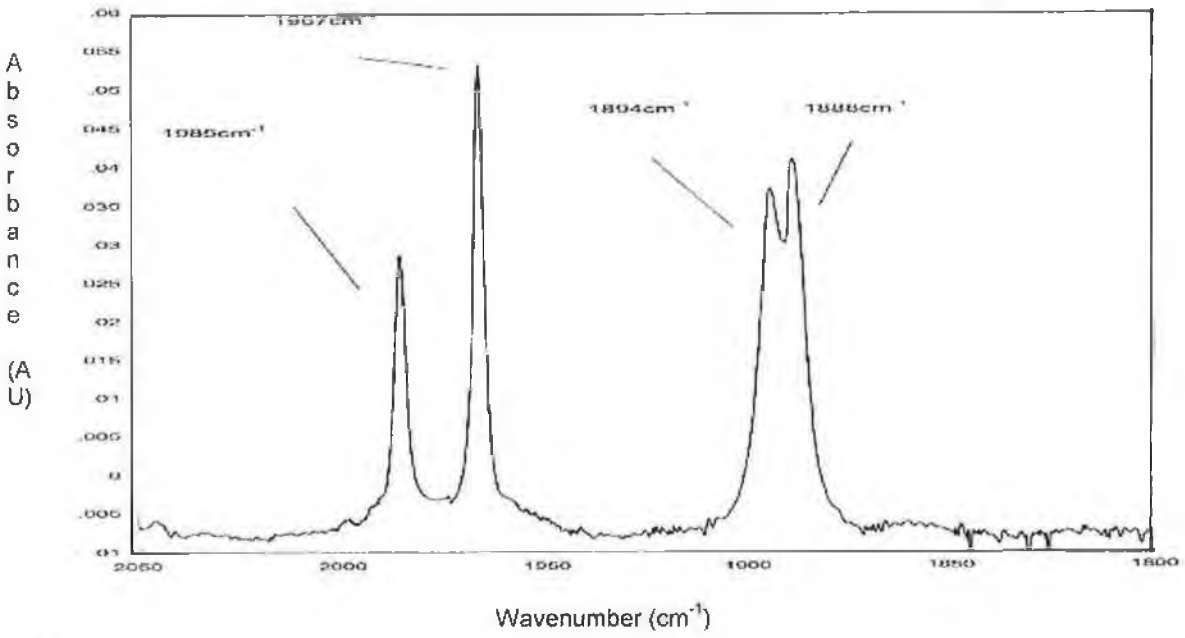

Figure 7.1.2 IR spectrum recorded upon photolysis of $(\eta^6\text{-}C_6H_5NH_2)Cr(CO)_3$ in CO saturated cylohexane (1 atmosphere of CO), at 355nm (NdYAG laser).

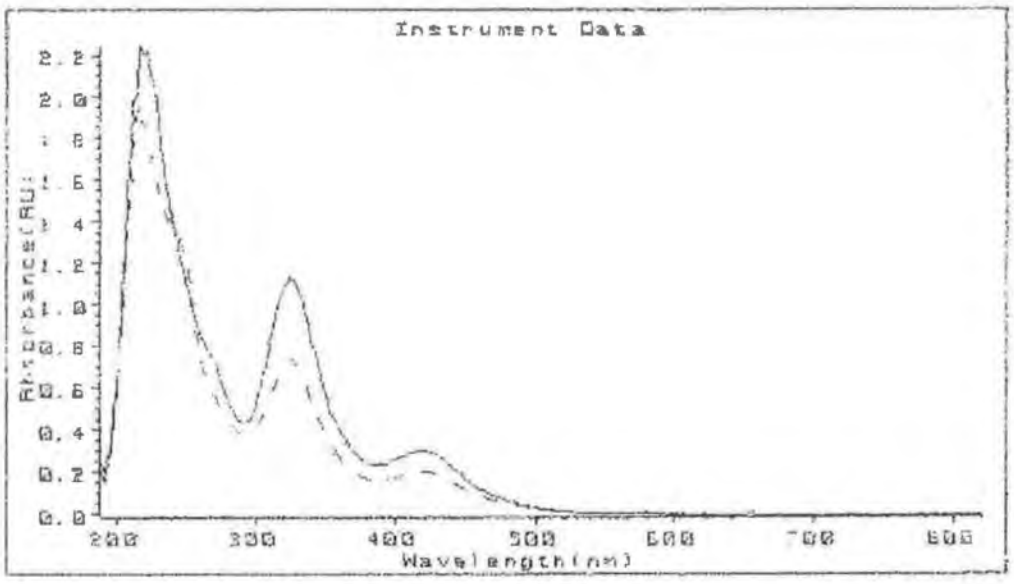

Figure 7.1.3 UV/vis spectrum recorded upon photolysis of (η^6-C_6H_5COH)$Cr(CO)_3$ in CO saturated cylohexane (1 atmosphere of CO), at 355nm .

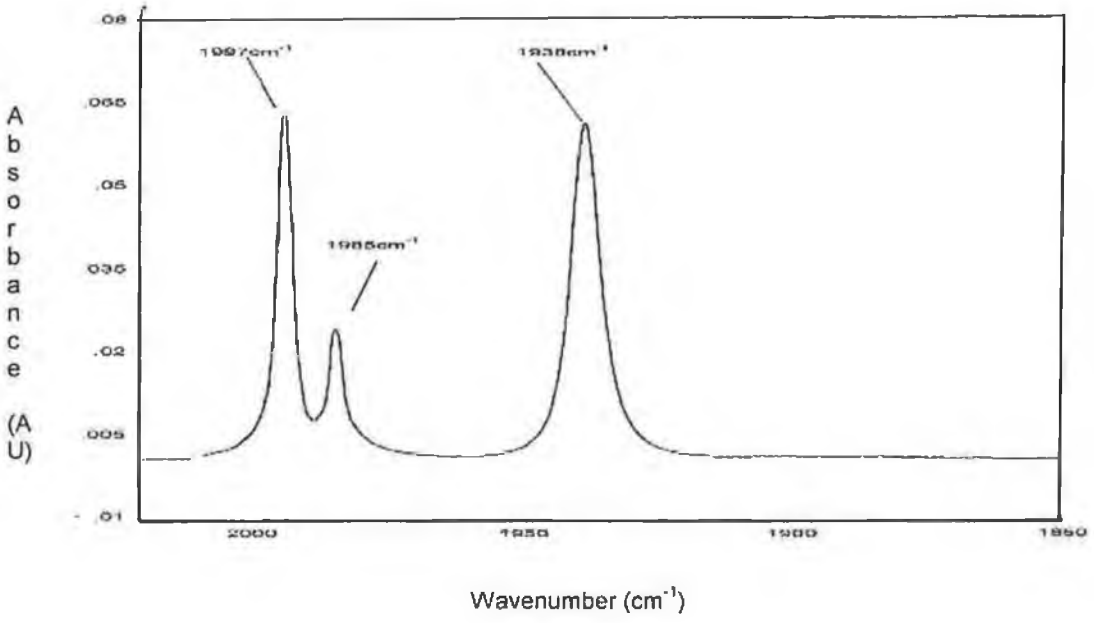

Figure 7.1.4 IR spectrum recorded upon photolysis of (η^6-C_6H_5COH)$Cr(CO)_3$ in CO saturated cylohexane (1 atmosphere of CO), at 355nm (NdYAG laser).

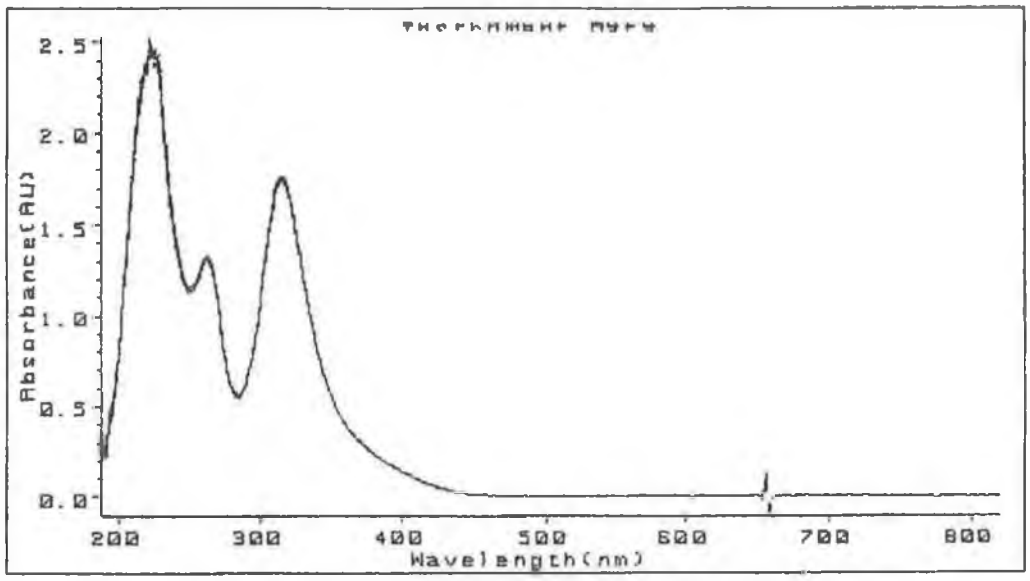

Figure 7.1.5 UV/vis spectrum recorded upon photolysis of $(\eta^6\text{-}C_6H_6)Cr(CO)_3$ in CO saturated cylohexane (1 atmosphere of CO), at 355nm.

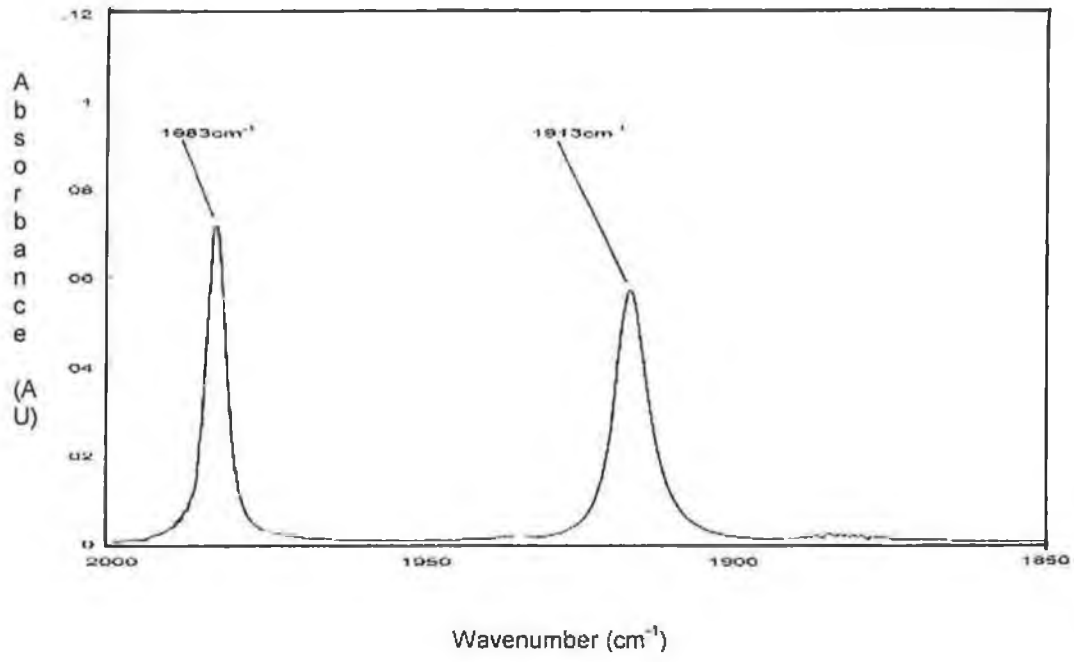

Figure 7.1.6 IR spectrum recorded upon photolysis of $(\eta^6\text{-}C_6H_6)Cr(CO)_3$ in CO saturated cylohexane (1 atmosphere of CO), at 355nm.

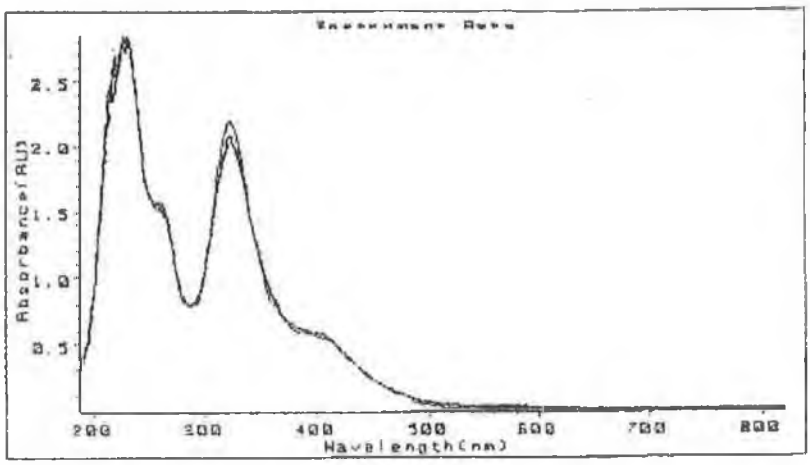

Figure 7.1.7. UV/vis spectrum recorded upon photolysis of $(\eta^6\text{-}C_6H_5CO_2CH_3)Cr(CO)_3$ in CO saturated cylohexane (1 atmosphere of CO), at 355nm.

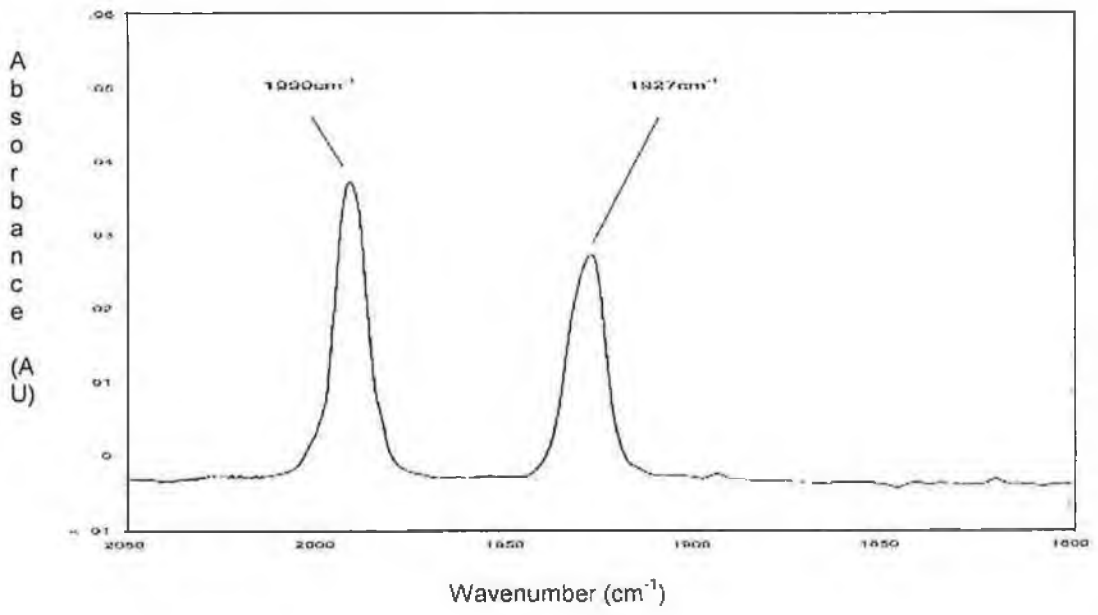

Figure 7.1.8. IR spectrum recorded upon photolysis of $(\eta^6\text{-}C_6H_5CO_2CH_3)Cr(CO)_3$ in CO saturated cylohexane (1 atmosphere of CO), at 355nm (NdYAG laser).

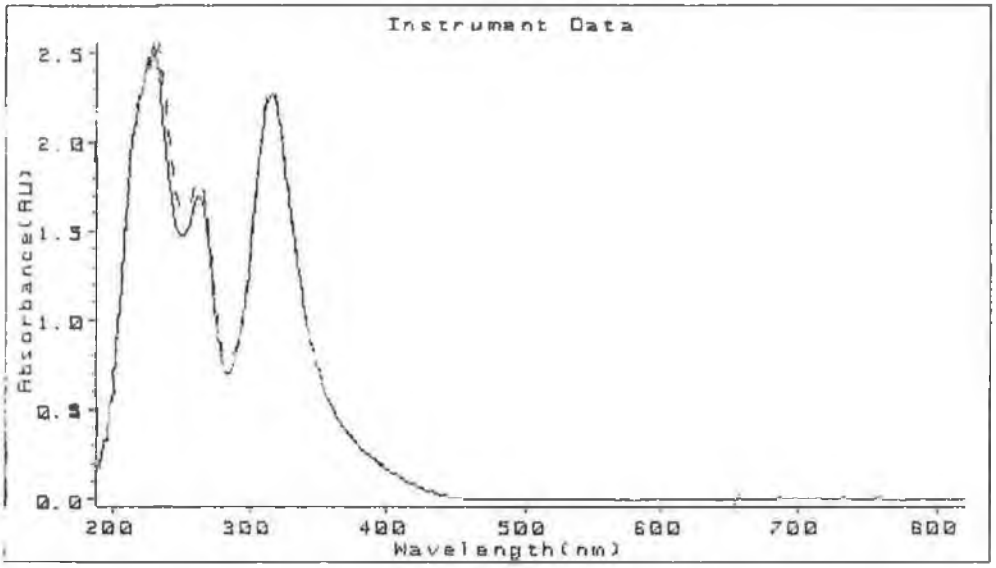

Figure 7.1.9 UV/vis spectrum recorded upon photolysis of $(\eta^6\text{-}C_6H_5OCH_3)Cr(CO)_3$ in CO saturated cylohexane (1 atmosphere of CO), at 355nm.

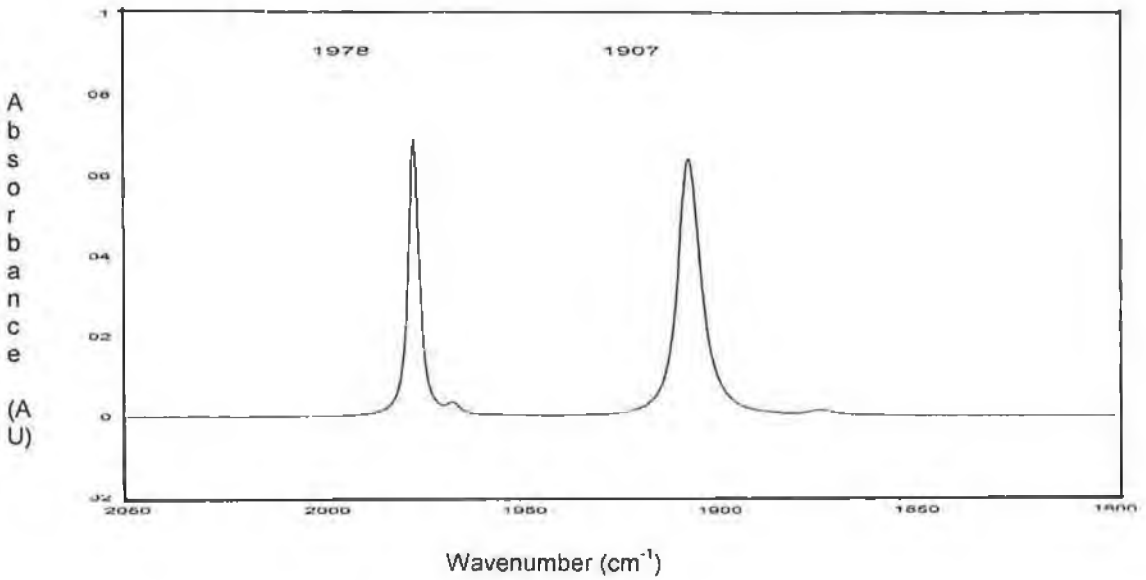

Figure 7.1.10 IR spectrum recorded upon photolysis of $(\eta^6\text{-}C_6H_5OCH_3)Cr(CO)_3$ in CO saturated cylohexane (1 atmosphere of CO), at 355nm.

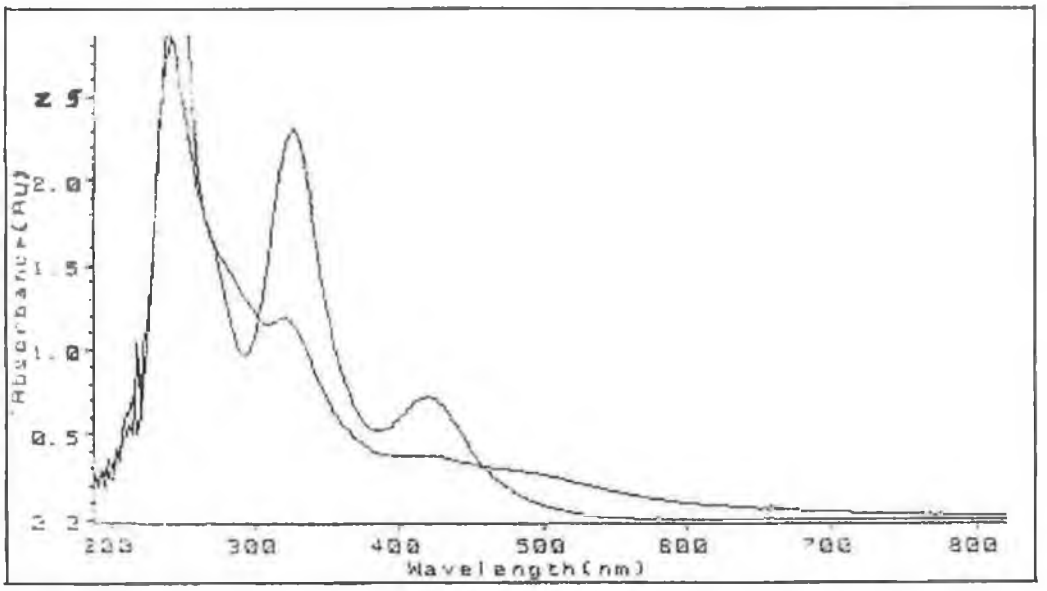

Figure 7.1.11 UV/vis spectrum recorded upon photolysis of $(\eta^6\text{-}C_6H_5COH)Cr(CO)_3$ in CO saturated 1,1,2 trifluorotrichloroethane (1 atmosphere of CO), at 355nm.

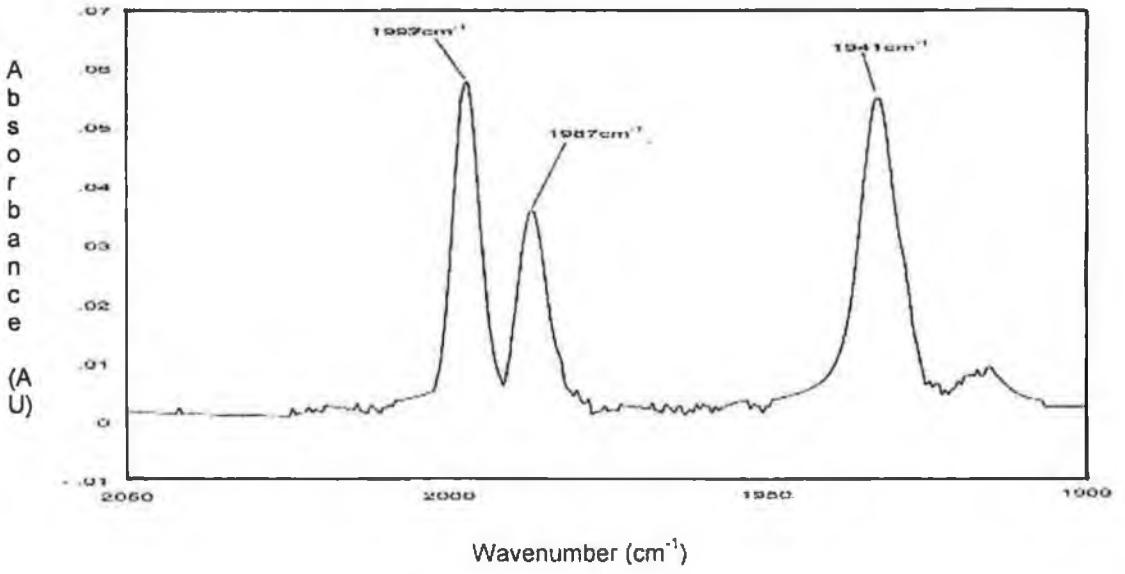

Figure 7.1.12 IR spectrum recorded upon photolysis of $(\eta^6\text{-}C_6H_5COH)Cr(CO)_3$ in CO saturated 1,1,2 trifluorotrichloroethane (1 atmosphere of CO), at 355nm.

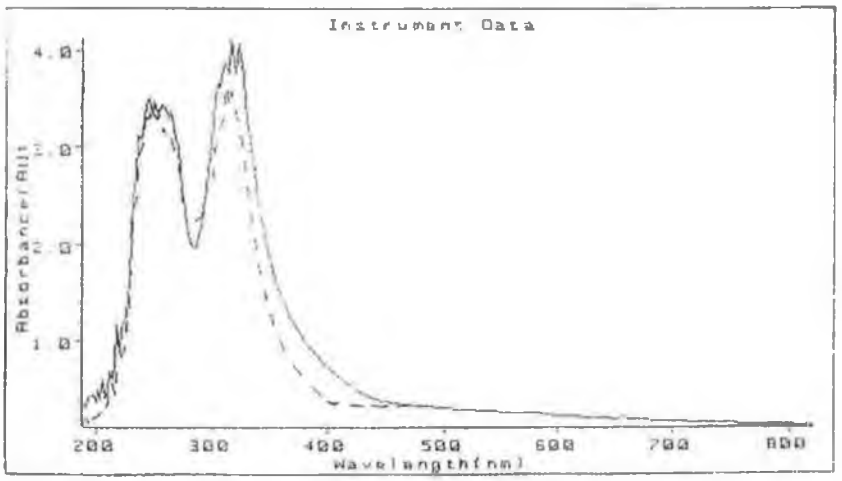

Figure 7.1.15 UV/vis spectrum recorded upon photolysis of $(\eta^6\text{-}C_6H_5OCH_3)Cr(CO)_3$ in CO saturated 1,1,2 trifluorotrichloroethane (1 atmosphere of CO), at 355nm.

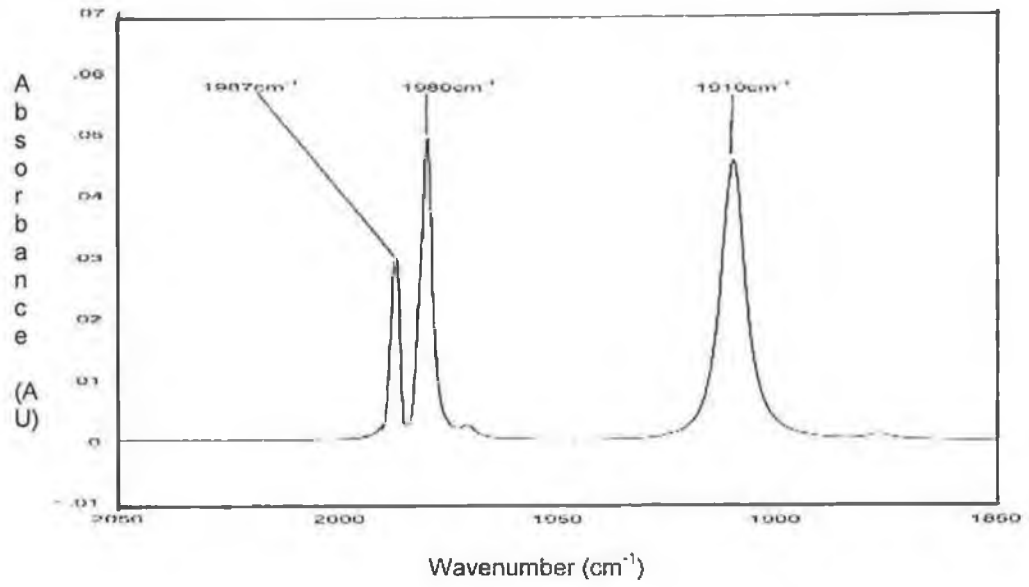

Figure 7.1.16 IR spectrum recorded upon photolysis of $(\eta^6\text{-}C_6H_5OCH_3)Cr(CO)_3$ in CO saturated 1,1,2 trifluorotrichloroethane (1 atmosphere of CO) at 355nm.

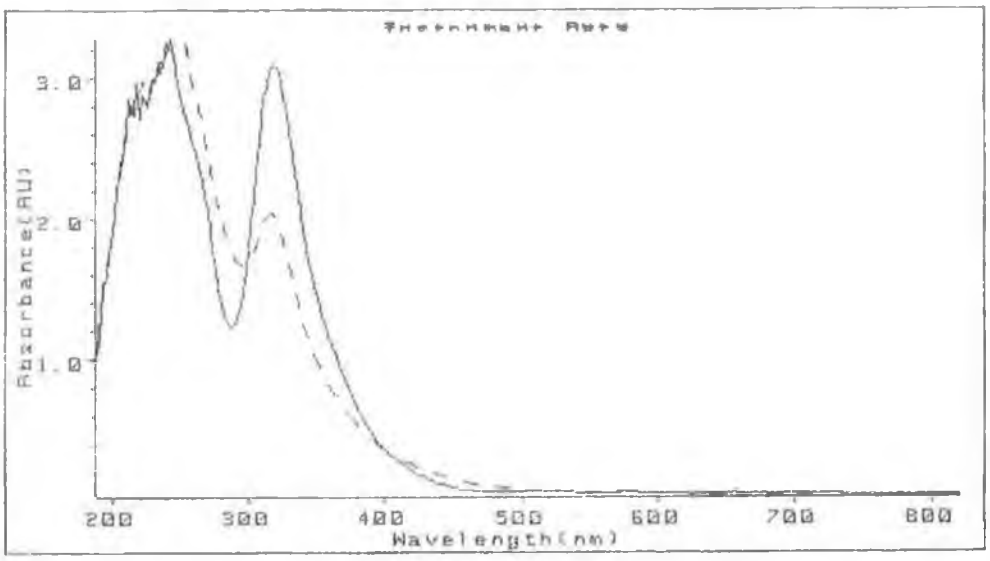

Figure 7.1.17 UV/vis spectrum recorded upon photolysis of $(\eta^6\text{-}C_6H_5NH_2)Cr(CO)_3$ in CO saturated 1,1,2 trifluorotrichloroethane (1 atmosphere of CO), at 355nm.

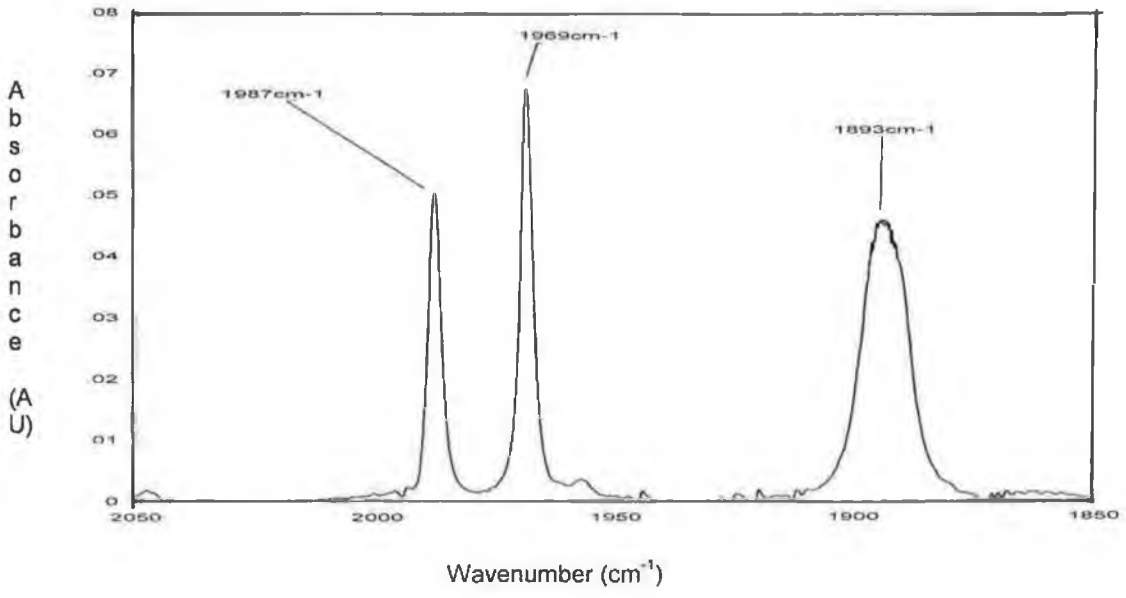

Figure 7.1.18 UV/vis spectrum recorded upon photolysis of $(\eta^6\text{-}C_6H_5NH_2)Cr(CO)_3$ in CO saturated 1,1,2 trifluorotrichloroethane (1 atmosphere of CO), at 355nm.

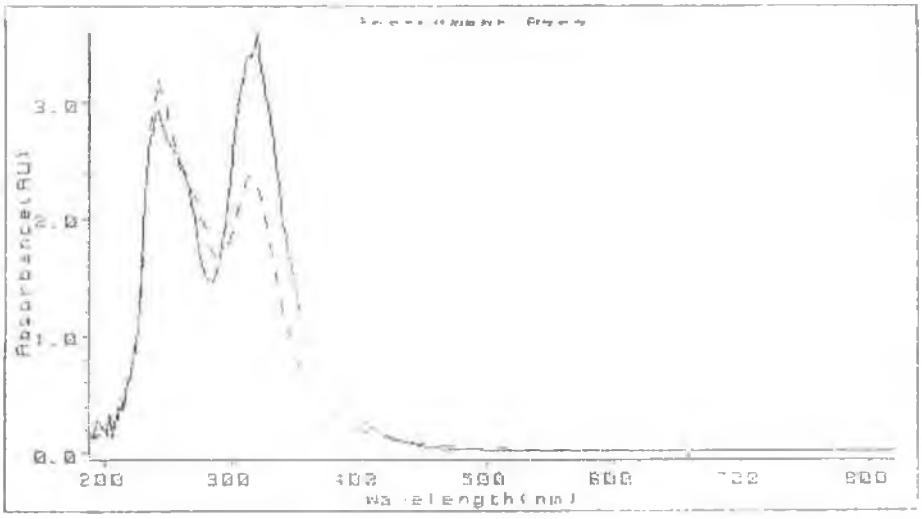

Figure 7.1.19 UV/vis spectrum recorded upon photolysis of $(\eta^6\text{-}C_6H_6)Cr(CO)_3$ in CO saturated 1,1,2 trifluorotrichloroethane (1 atmosphere of CO), at 355nm (NdYAG laser).

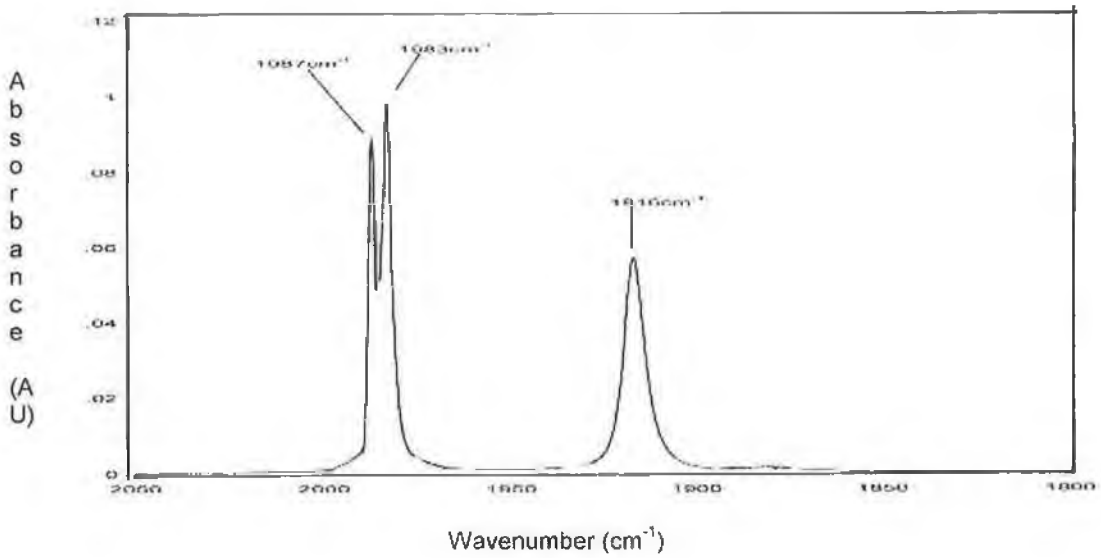

Figure 7.1.20 UV/vis spectrum recorded upon photolysis of $(\eta^6\text{-}C_6H_6)Cr(CO)_3$ in CO saturated 1,1,2 trifluorotrichloroethane (1 atmosphere of CO), at 355nm.

(η^6-arene)$Cr(CO)_3$ complex.	Cyclohexane	1,1,2trifluorotrichloro ethane
(η^6-aniline)$Cr(CO)_3$	2719	2436
(η^6-anisole)$Cr(CO)_3$	2913	2776
(η^6-benzene)$Cr(CO)_3$	3060	2396
(η^6-methylbenzoate)$Cr(CO)_3$	3712	3344
(η^6-benzenecarboxaldehyde)$Cr(CO)_3$	3732	3302

Table 7.1.1 Extinction coefficients measured @ 355nm for (η^6-arene)$Cr(CO)_3$ in 1,1,2 trifluorotrichloroethane and cyclohexane.

(η^6-arene)$Cr(CO)_3$ complex.	Cyclohexane	1,1,2trifluorotrichloro ethane
(η^6-aniline)$Cr(CO)_3$	0.08	0.24
(η^6-anisole)$Cr(CO)_3$	0.000432	0.27
(η^6-benzene)$Cr(CO)_3$	0	0.15
(η^6-methylbenzoate)$Cr(CO)_3$	0.0000236	0.18
(η^6-benzenecarboxaldehyde)$Cr(CO)_3$	0.048	0.17

Table 7.1.2 Quantum yields measured @ 355nm for (η^6-arene)$Cr(CO)_3$ in 1,1,2 trifluorotrichloroethane and cyclohexane.

The quantum yield for a photochemical reaction is given by ;

$$\Phi = \frac{\text{number of moles of product formed}}{\text{number of quanta absorbed}}$$

$$N_{Fe2+} = \frac{6.023 \times 10^{20} \times V_1 \times V_3 \times A}{V_2 \times l \times \varepsilon}$$

Where :

V_1 = Volume of actinometer irradiated (cm^3).
V_2 = Volume of actinometer transferred into volumetric flask (cm^3).
V_3 = Final volume (cm^3).
A = Absorbance at 510 nm.
L = cell path length (cm).
ε = extinction of coefficient of Fe^{2+} / phenanthroline complex at 510 nm (dm^3 mol^{-1} cm^{-1}).

The number of quanta absorbed is then determined from the following equation ;

$$n_a = \frac{n_{Fe2+}}{\Phi}$$

n_a = The number of quanta absorbed.

Φ = The quantum yield of Fe^{2+} at λ_{max} of interest.

Appendix B

Data for determination of molar absorbtivity values at 298K

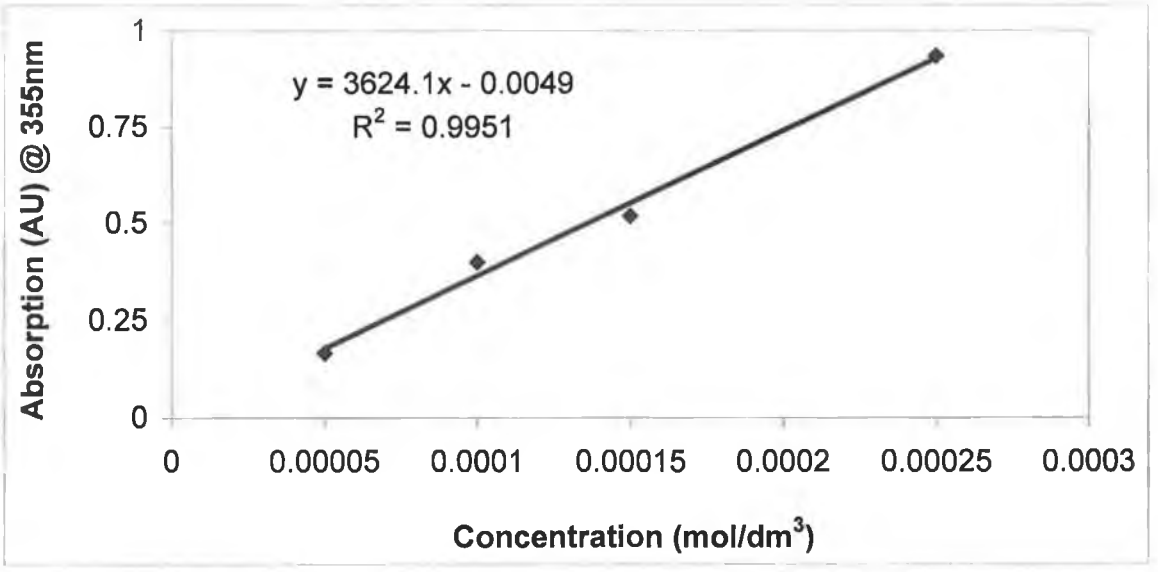

Figure 8.1.1 Beer lambert plot of absorbance (AU) versus concentration of $(\eta^6\text{-}C_8H_6S)Cr(CO)_3$ (mol/dm^3) in cyclohexane.

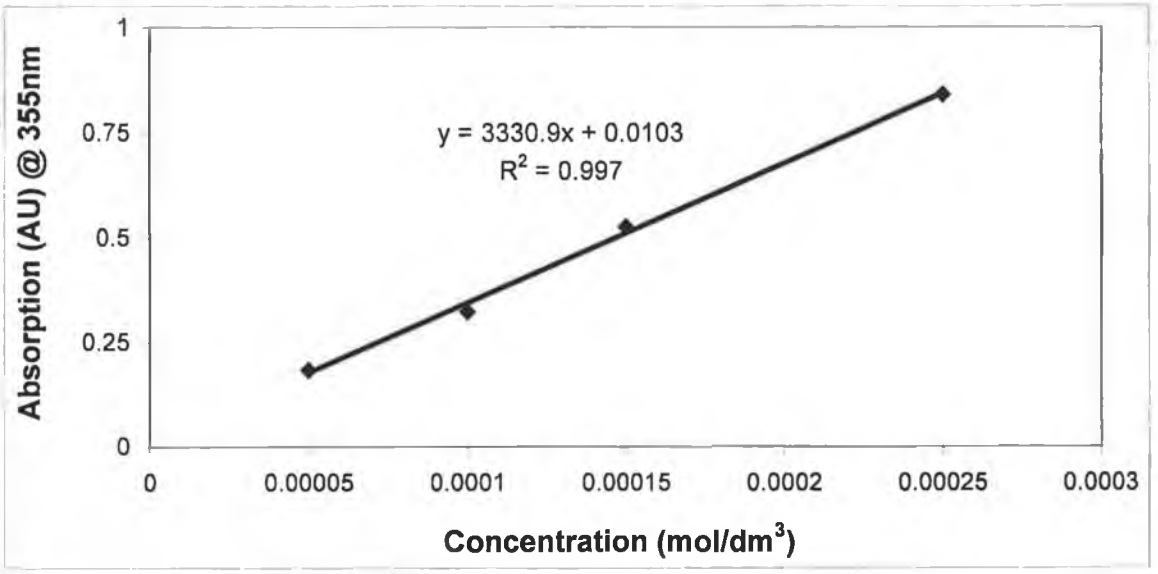

Figure 8.1.2 Beer lambert plot of absorbance (AU) versus concentration of $(\eta^6\text{-}C_{12}H_8S)Cr(CO)_3$ (mol/dm^3) in cyclohexane.

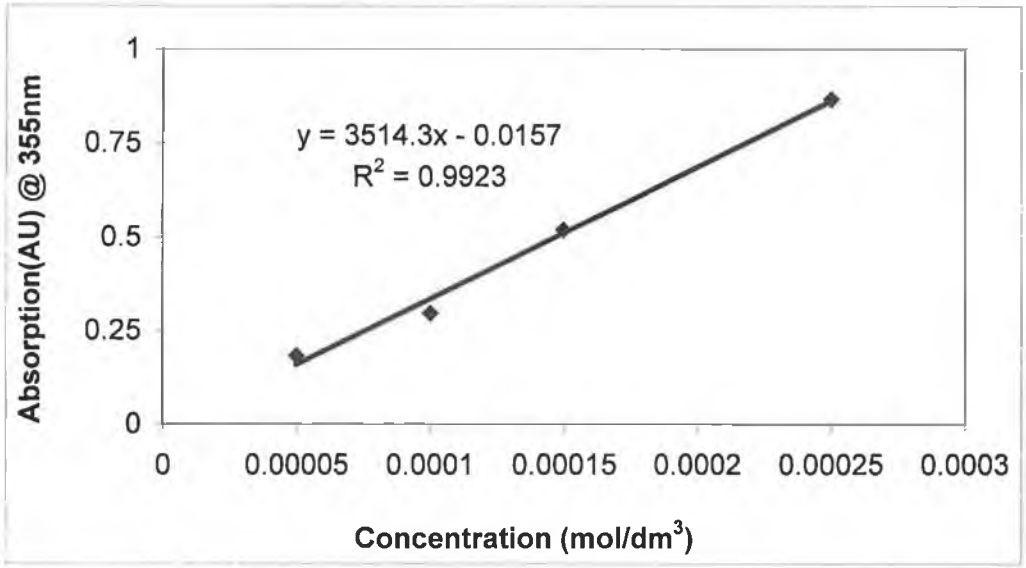

Figure 8.1.3 Beer lambert plot of absorbance (AU) versus concentration of $(\eta^5\text{-}C_4H_4S)Cr(CO)_3$ (mol/dm^3) in cyclohexane.

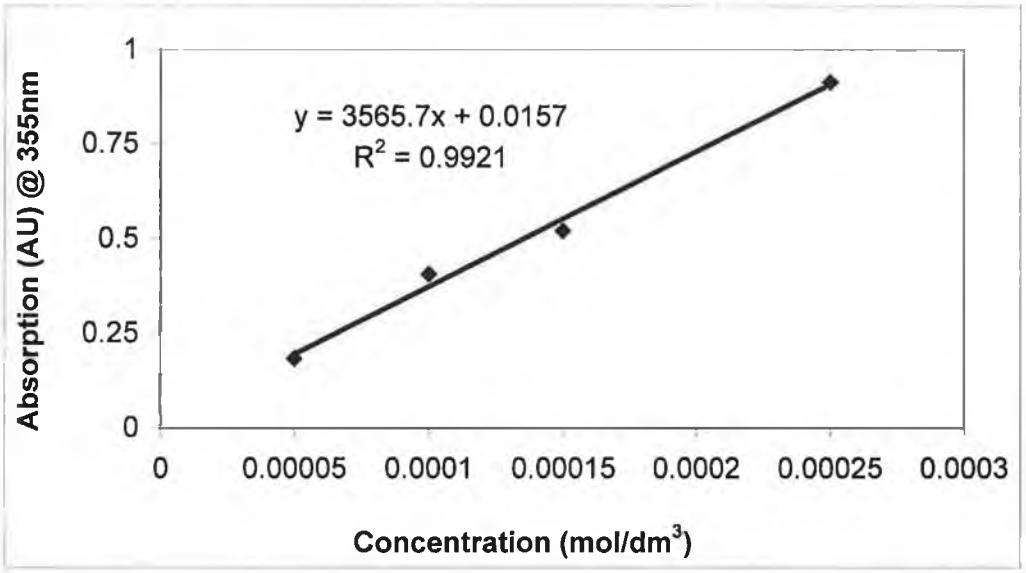

Figure 8.1.4 Beer lambert plot of absorbance (AU) versus concentration of $(\eta^5\text{-}C_4H_4Se)Cr(CO)_3$ (mol/dm^3) in cyclohexane.

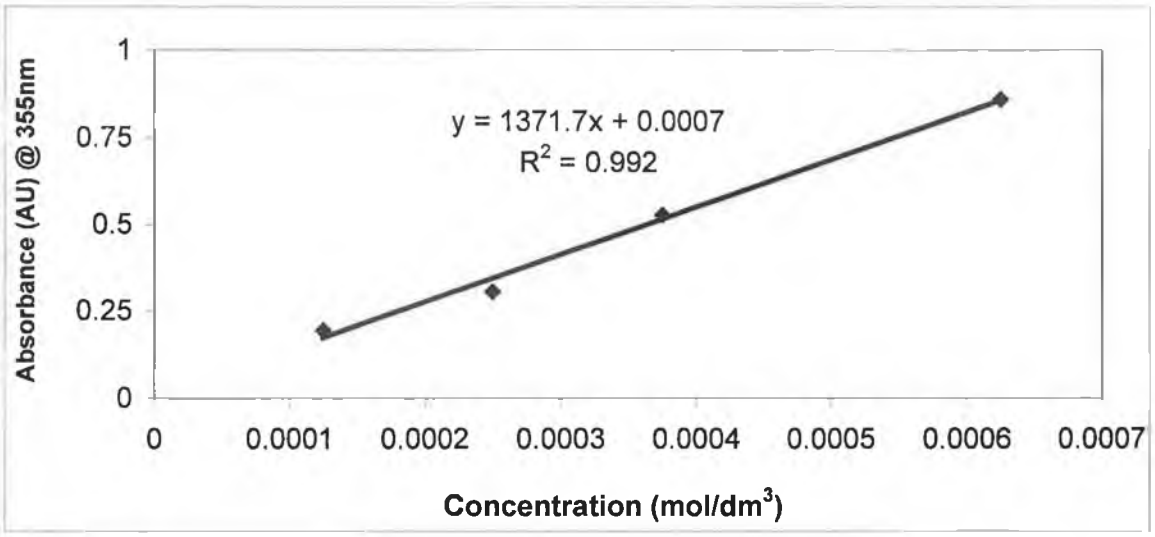

Figure 8.1.5 Beer lambert plot of absorbance (AU) versus concentration of $(\eta^5\text{-}C_4H_4N)Mn(CO)_3$ (mol/dm^3) in cyclohexane.

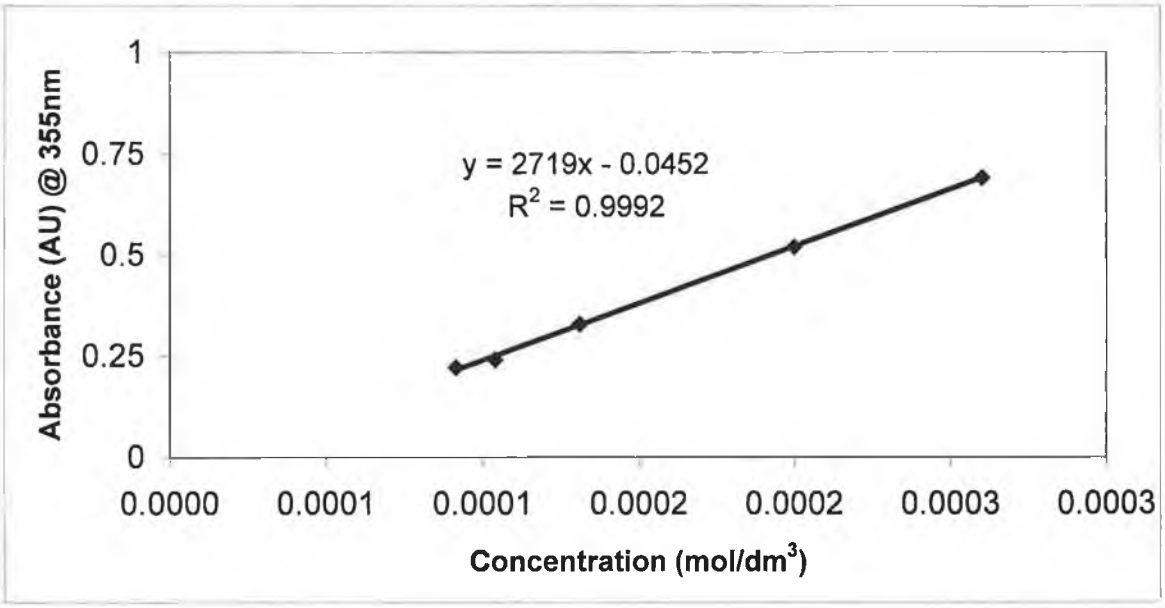

Figure 8.1.6 The plot of the absorbance @ 355nm (AU) versus the concentration (mol/dm^3) of $(\eta^6\text{-}C_6H_5NH_2)Cr(CO)_3$, recorded in cyclohexane.

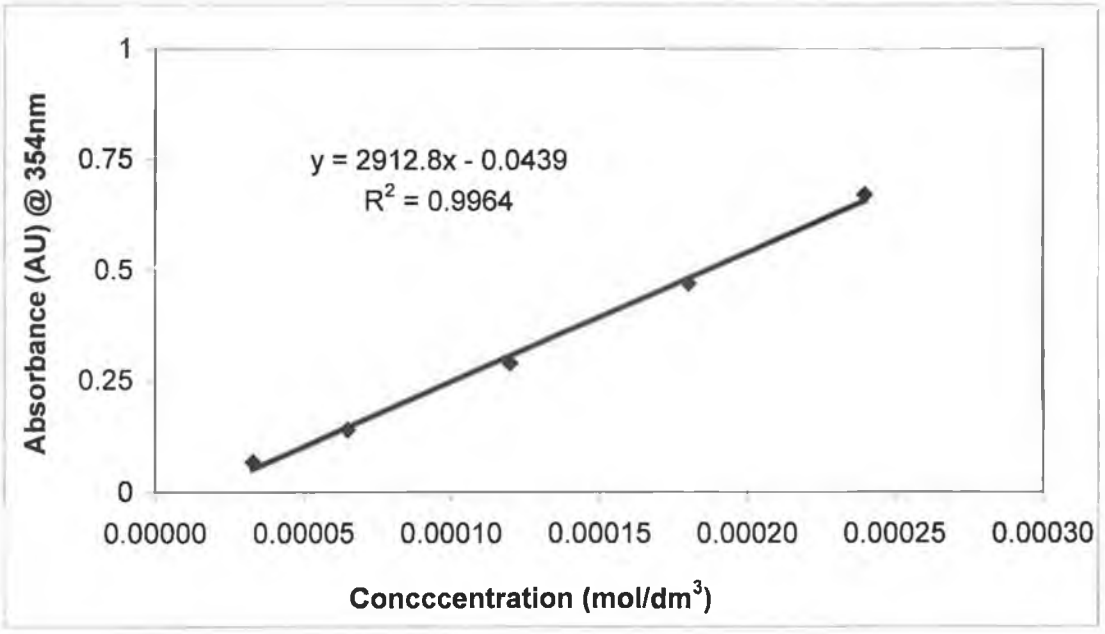

Figure 8.1.7 The plot of the absorbance @ 355nm (AU) versus the concentration (mol/dm^3) of $(\eta^6\text{-}C_6H_5OCH_3)Cr(CO)_3$, recorded in cyclohexane.

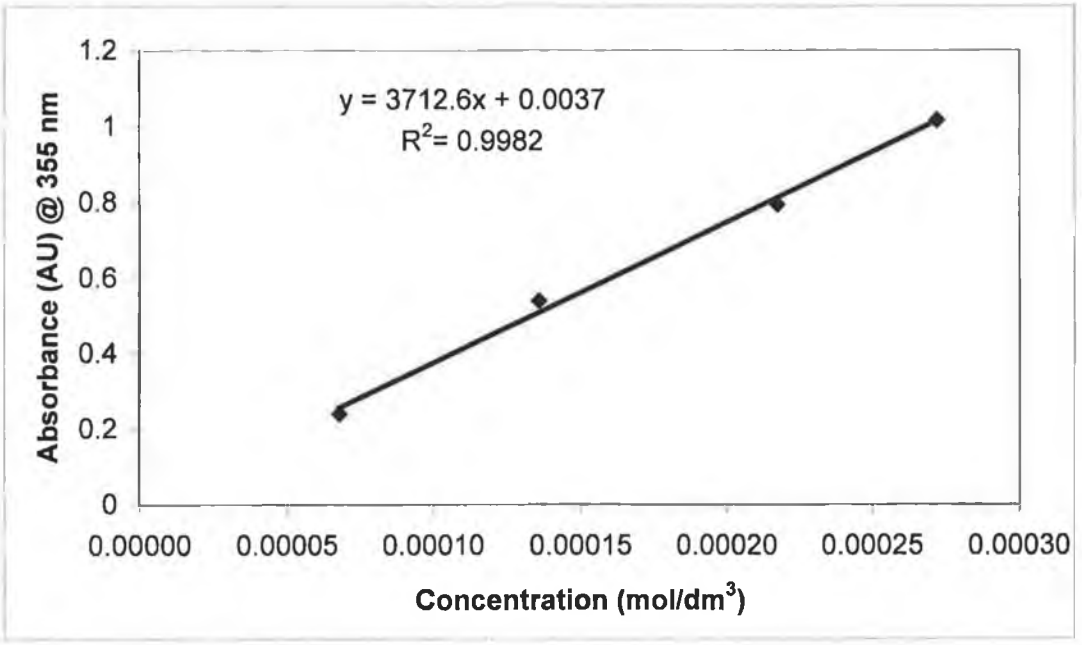

Figure 8.1.8 The plot of the absorbance @ 355nm (AU) versus the concentration (mol/dm^3) of $(\eta^6\text{-}C_6H_5CO_2CH_3)Cr(CO)_3$, recorded in cyclohexane.

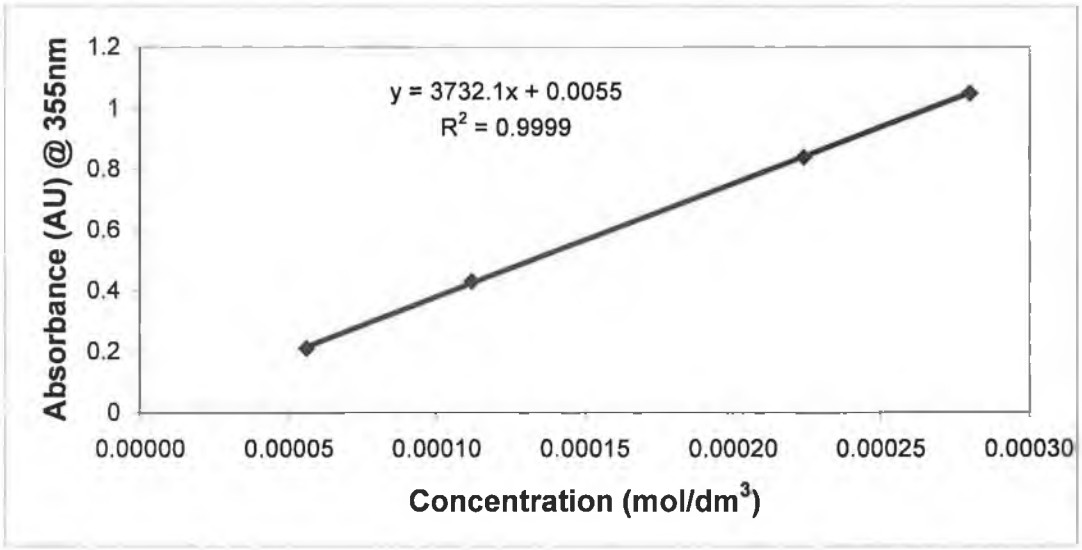

Figure 8.1.9 The plot of the absorbance @ 355nm (AU) versus the concentration (mol/dm^3) of $(\eta^6\text{-}C_6H_5COH)Cr(CO)_3$, recorded in cyclohexane.

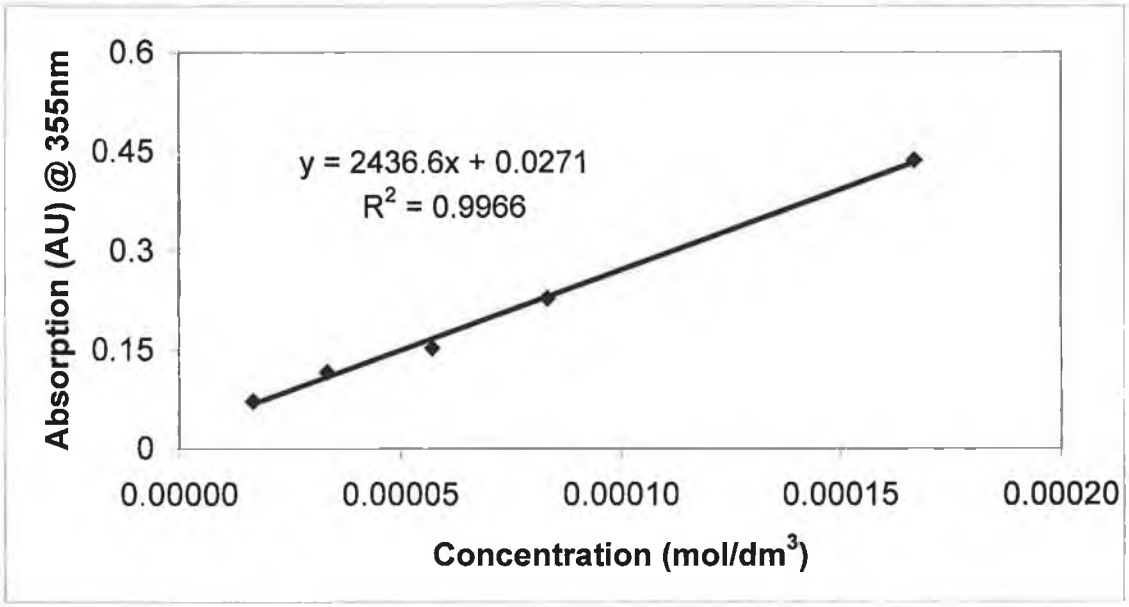

Figure 8.1.10 The plot of the absorbance @ 355nm (AU) versus the concentration (mol/dm^3) of $(\eta^6\text{-}C_6H_5NH_2)Cr(CO)_3$, recorded in 1,1,2 trifluorotrichloroethane.

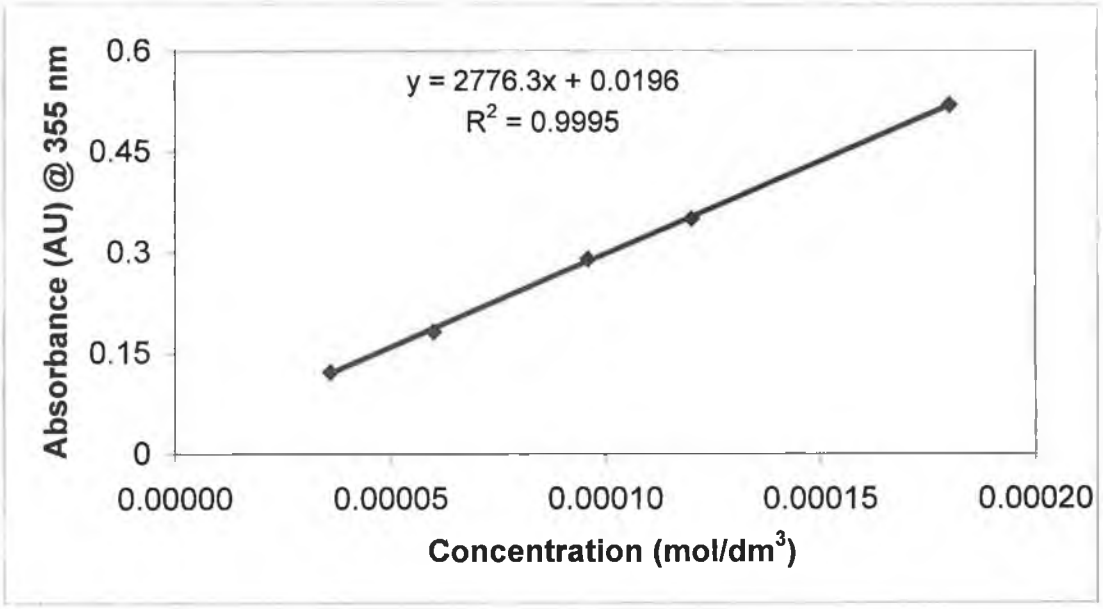

Figure 8.1.11 The plot of the absorbance @ 355nm (AU) versus the concentration (mol/dm^3) of (η^6-$C_6H_5OCH_3$)$Cr(CO)_3$, recorded in 1,1,2 trifluorotrichloroethane.

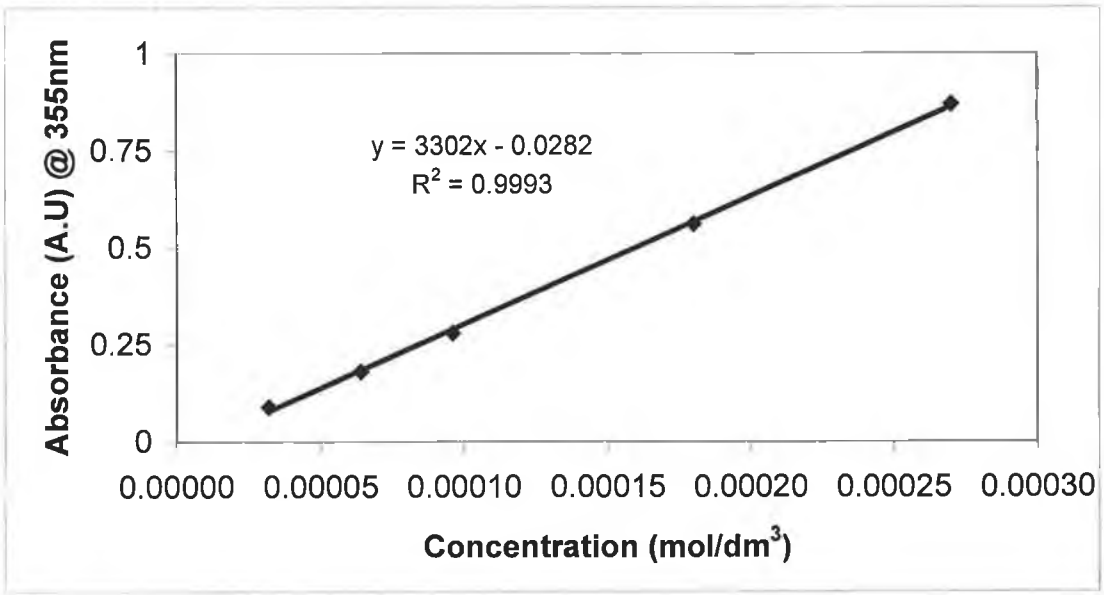

Figure 8.1.12 The plot of the absorbance @ 355nm (AU) versus the concentration (mol/dm^3) of (η^6-C_6H_5COH)$Cr(CO)_3$, recorded in 1,1,2 trifluorotrichloroethane.

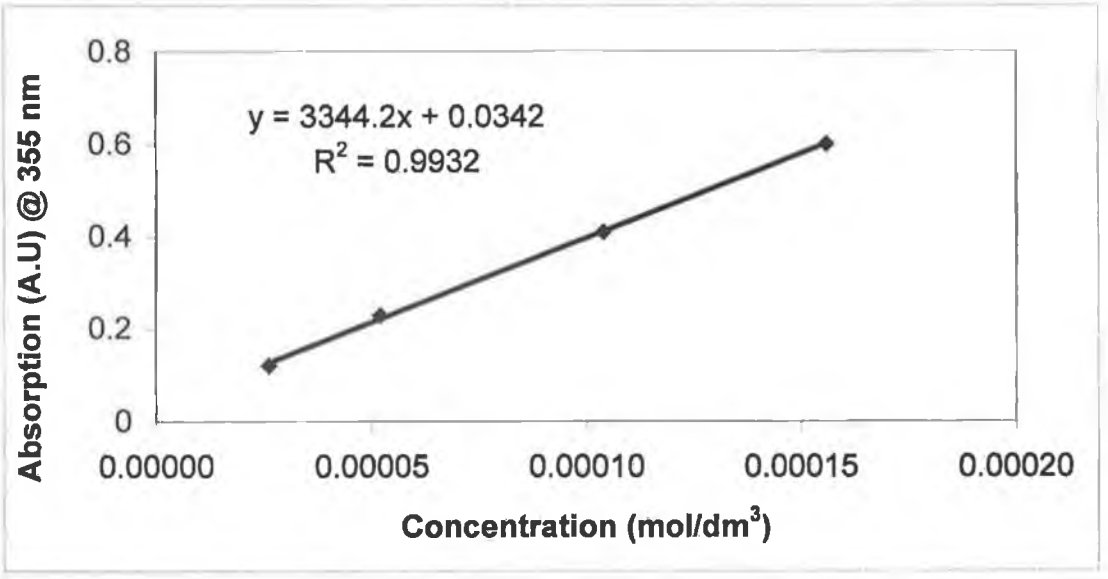

Figure 8.1.13 The plot of the absorbance @ 355nm (AU) versus the concentration (mol/dm^3) of (η^6-$C_6H_5CO_2CH_3$)$Cr(CO)_3$, recorded in 1,1,2 trifluorotrichloroethane.

$mol/dm^3 \times 10^4$	Absorption (AU)
0	0
0.5	0.167
1	0.4
1.5	0.52
2.5	0.935

Table 8.1.1 Data for determination of the molar absorbtivity @ 355nm for $(\eta^6\text{-}C_8H_6S)Cr(CO)_3$ in cyclohexane.

$mol/dm^3 \times 10^4$	Absorption (AU)
0	0
0.5	0.184
1	0.323
1.5	0.526
2.5	0.84

Table 8.1.2 Data for determination of the molar absorbtivity @ 355nm for $(\eta^6\text{-}C_{12}H_8S)Cr(CO)_3$ in cyclohexane.

$mol/dm^3 \times 10^4$	Absorption (AU)
0	0
0.5	0.182
1	0.298
1.5	0.52
2.5	0.868

Table 8.1.3 Data for determination of the molar absorbtivity @ 355nm for $(\eta^5\text{-}C_4H_4S)Cr(CO)_3$ in cyclohexane.

$mol/dm^3 \times 10^4$	Absorption (AU)
0	0
0.5	0.17
1	0.34
1.5	0.51
2.5	0.85

Table 8.1.4 Data for determination of the molar absorbtivity @ 355nm for $(\eta^5\text{-}C_4H_4Se)Cr(CO)_3$ in cyclohexane.

$mol/dm^3 \times 10^4$	Absorption (AU)
0	0
1.25	0.19
2.5	0.30
3.75	0.53
6.25	0.86

Table 8.1.5 Data for determination of the molar absorbtivity @ 355nm for $(\eta^5\text{-}C_4H_4N)Mn(CO)_3$ in cyclohexane.

$mol/dm^3 \times 10^{-4}$	Absorption (AU)
0	0
0.917	0.202
1.04	0.265
1.31	0.358
2	0.562
2.6	0.724

Table 8.1.6 Data for determination of the molar absorbtivity @ 355nm for $(\eta^6\text{-}C_6H_5NH_2)Cr(CO)_3$ in cyclohexane.

$mol/dm^3 \times 10^{-4}$	Absorption (AU)
0	0
0.327	0.068
0.65	0.142
1.2	0.294
1.80	0.473
2.4	0.672

Table 8.1.7 Data for determination of the molar absorbtivity @ 355nm for $(\eta^6\text{-}C_6H_5OCH_3)Cr(CO)_3$ in cyclohexane.

$mol/dm^3 \times 10^{-4}$	Absorption (AU)
0	0
0.68	0.244
1.36	0.542
2.18	0.794
2.72	1.016

Table 8.1.8 Data for determination of the molar absorbtivity @ 355nm for $(\eta^6\text{-}C_6H_5CO_2CH_3)Cr(CO)_3$ in cyclohexane.

$mol/dm^3 \times 10^{-4}$	Absorption (AU)
0	0
0.56	0.213
1.12	0.435
2.24	0.837
2.82	1.052

Table 8.1.9 Data for determination of the molar absorbtivity @ 355nm for $(\eta^6\text{-}C_6H_5COH)Cr(CO)_3$ in cyclohexane.

$mol/dm^3 \times 10^{-4}$	Absorption (AU)
0	0
0.167	0.0702
0.333	0.116
0.567	0.153
0.833	0.228
1.67	0.439

Table 8.1.10 Data for determination of the molar absorbtivity @ 355nm for $(\eta^6\text{-}C_6H_5NH_2)Cr(CO)_3$ in 1,1,2 trifluorotrichloro ethane.

$mol/dm^3 \times 10^{-4}$	Absorption (AU)
0	0
0.36	0.122
0.62	0.182
0.96	0.292
1.22	0.354
1.81	0.522

Table 8.1.11 Data for determination of the molar absorbtivity @ 355nm for $(\eta^6\text{-}C_6H_5OCH_3)Cr(CO)_3$ in 1,1,2 trifluorotrichloroethane.

$mol/dm^3 \times 10^{-4}$	Absorption (AU)
0	0
0.26	0.152
0.52	0.27
1.04	0.41
1.56	0.62

Table 8.1.12 Data for determination of the molar absorbtivity @ 355nm for $(\eta^6\text{-}C_6H_5CO_2CH_3)Cr(CO)_3$ in 1,1,2 trifluorotrichloro ethane.

$mol/dm^3 \times 10^{-4}$	Absorption (AU)
0	0
0.32	0.089
0.64	0.182
0.96	0.28
1.82	0.568
2.72	0.874

Table 8.1.13 Data for determination of the molar absorbtivity @ 355nm for $(\eta^6\text{-}C_6H_5COH)Cr(CO)_3$ in 1,1,2 trifluorotrichloroethane.

Appendix C

Data for determination of second order rate constants at 298 K

Concentration of CO (mol dm^{-3})	k_{obs} (s^{-1})
0.00225	23583
0.0045	41478
0.00675	59121
0.009	77502

Table 9.1 The observed rate constant (k_{obs}) at various concentration of CO, for the reaction of CO with (η^6-$C_6H_5NH_2$)$Cr(CO)_2$(cyclohexane) recorded at 280 nm at 298 K upon photolysis at 355 nm.

Concentration of CO (mol dm^{-3})	k_{obs} (s^{-1})
0.00225	23597
0.0045	41502
0.00675	59195
0.009	77562

Table 9.2 The observed rate constant (k_{obs}) at various concentration of CO, for the reaction of CO with (η^6-$C_6H_5NH_2$)$Cr(CO)_2$(cyclohexane) to regenerate the parent recorded at 340 nm at 298 K upon photolysis at 355 nm.

Concentration of CO (mol dm^{-3})	k_{obs} (s^{-1})
0.00225	22915
0.0045	38669
0.00675	54410
0.009	70162

Table 9.3 The observed rate constant (k_{obs}) at various concentration of CO, for the reaction of CO with (η^6-$C_6H_5OCH_3$)$Cr(CO)_2$(cyclohexane) recorded at 280 nm at 298 K upon photolysis at 355 nm.

Concentration of CO (mol dm^{-3})	k_{obs} (s^{-1})
0.00225	22908
0.0045	38702
0.00675	54380
0.009	70157

Table 9.4 The observed rate constant (k_{obs}) at various concentration of CO, for the reaction of CO with (η^6-$C_6H_5OCH_3$)$Cr(CO)_2$(cyclohexane) to regenerate the parent recorded at 320 nm at 298 K upon photolysis at 355 nm.

Concentration of CO (mol dm^{-3})	k_{obs} (s^{-1})
0.00225	20777
0.0045	29769
0.00675	38801
0.009	47742

Table 9.5 The observed rate constant (k_{obs}) at various concentration of CO, for the reaction of CO with (η^6-$C_6H_5CO_2CH_3$)$Cr(CO)_2$(cyclohexane) recorded at 280 nm at 298 K upon photolysis at 355 nm.

Concentration of CO (mol dm^{-3})	k_{obs} (s^{-1})
0.00225	20802
0.0045	29781
0.00675	38795
0.009	47751

Table 9.6 The observed rate constant (k_{obs}) at various concentration of CO, for the reaction of CO with (η^6-$C_6H_5CO_2CH_3$)$Cr(CO)_2$(cyclohexane) at 298K to regenerate the parent recorded at 340 nm at 298 K upon photolysis at 355 nm.

Concentration of CO (mol dm^{-3})	k_{obs} (s^{-1})
0.00225	4487
0.0045	8898
0.00675	15721
0.009	22503

Table 9.7 The observed rate constant (k_{obs}) at various concentration of CO, for the reaction of CO with (η^6-C_6H_5COH)$Cr(CO)_2$(cyclohexane) recorded at 280 nm at 298 K upon photolysis at 355 nm.

Concentration of CO (mol dm^{-3})	k_{obs} (s^{-1})
0.00225	4487
0.0045	8898
0.00675	15721
0.009	22503

Table 9.8 The observed rate constant (k_{obs}) at various concentration of CO, for the reaction of CO with (η^6-C_6H_5COH)$Cr(CO)_2$(cyclohexane) to regenerate the parent recorded at 340 nm at 298 K upon photolysis at 355 nm.

Concentration of CO (mol dm^{-3})	k_{obs} (s^{-1})
0.00225	16398
0.0045	29302
0.00675	39508
0.009	49612

Table 9.9 The observed rate constant (k_{obs}) at various concentration of CO, for the reaction of CO with (η^6-C_8H_6S)$Cr(CO)_2$(cyclohexane) recorded at 280 nm at 298 K upon photolysis at 355 nm.

Concentration of CO (mol dm^{-3})	k_{obs} (s^{-1})
0.00225	15987
0.0045	29157
0.00675	39246
0.009	49975

Table 9.10 The observed rate constant (k_{obs}) at various concentration of CO, for the reaction of CO with (η^6-C_8H_6S)$Cr(CO)_2$(cyclohexane) to regenerate the parent recorded at 340 nm at 298 K upon photolysis at 355 nm.

Concentration of CO (mol dm^{-3})	k_{obs} (s^{-1})
0.000313	62983
0.000625	116523
0.000938	160984
0.00125	199342

Table 9.11 The observed rate constant (k_{obs}) at various concentration of CO, for the reaction of CO with (η^6-C_8H_6S)$Cr(CO)_2$(heptane) recorded at 280 nm at 298 K upon photolysis at 355 nm.

Concentration of CO (mol dm^{-3})	k_{obs} (s^{-1})
0.000313	59875
0.000625	102113
0.000938	158754
0.00125	199432

Table 9.12 The observed rate constant (k_{obs}) at various concentration of CO, for the reaction of CO with (η^6-C_8H_6S)$Cr(CO)_2$(heptane) at 298K to regenerate the parent recorded at 340 nm at 298 K upon photolysis at 355 nm.

Concentration of CO (mol dm^{-3})	k_{obs} (s^{-1})
0.00225	18493
0.0045	25813
0.00675	47654
0.009	62316

Table 9.13 The observed rate constant (k_{obs}) at various concentration of CO, for the reaction of CO with (η^6-$C_{12}H_8S$)$Cr(CO)_2$(cyclohexane) recorded at 300 nm at 298 K upon photolysis at 355 nm.

Concentration of CO (mol dm^{-3})	kobs (s^{-1})
0.00225	17219
0.0045	27157
0.00675	47654
0.009	62003

Table 9.13 The observed rate constant (k_{obs}) at various concentration of CO, for the reaction of CO with (η^6-$C_{12}H_8S$)$Cr(CO)_2$(cyclohexane) to regenerate the parent recorded at 340 nm at 298 K upon photolysis at 355 nm.

Concentration of CO (mol dm^{-3})	kobs (s^{-1})
0.00225	5378
0.0045	9745
0.00675	15321
0.009	20569

Table 9.14 The observed rate constant (k_{obs}) at various concentration of CO, for the reaction of CO with (η^6-C_4H_4N)$Mn(CO)_2$(cyclohexane) at 298 K recorded at 290 nm at 298 K upon photolysis at 355 nm.

Concentration of CO (mol dm^{-3})	kobs (s^{-1})
0.00225	4582
0.0045	8032
0.00675	13902
0.009	20794

Table 9.15 The observed rate constant (k_{obs}) at various concentration of CO, for the reaction of CO with (η^6-C_4H_4N)$Mn(CO)_2$(cyclohexane) to regenerate the parent recorded at 370 nm at 298 K upon photolysis at 355 nm.

Concentration of CO (mol dm^{-3})	kobs (s^{-1})
0.00313	19428
0.00625	29856
0.00938	47488
0.0125	63258

Table 9.16 The observed rate constant (k_{obs}) at various concentration of CO, for the reaction of CO with (η^6-C_4H_4N)$Mn(CO)_2$(heptane) recorded at 290 nm at 298 K upon photolysis at 355 nm.

Concentration of CO (mol dm^{-3})	kobs (s^{-1})
0.00313	20316
0.00625	33704
0.00938	45824
0.0125	62418

Table 9.17 The observed rate constant (k_{obs}) at various concentration of CO, for the reaction of CO with (η^6-C_4H_4N)$Mn(CO)_2$(heptane) to regenerate the parent recorded at 370 nm at 298 K upon photolysis at 355 nm.

Concentration of starting material (mol dm^3)	kobs (s^{-1})
0.00018	103405
0.000287	158976
0.000375	220416
0.000427	285003

Table 9.18 The observed rate constant (k_{obs}) at various concentration of starting material, for the reaction of starting material with (η^6-$C_6H_5NH_2$)$Cr(CO)_2$(cyclohexane) to generate the dimer recorded at 400 nm at 298 K upon photolysis at 355 nm.

Concentration of starting material (mol dm^3)	kobs (s^{-1})
0.000347	5500
0.00385	7137
0.00542	9765
0.000747	13880
0.000824	16500

Table 9.19 The observed rate constant (k_{obs}) at various concentration of starting material, for the reaction of starting material with (η^6-C_8H_6S)$Cr(CO)_2$(cyclohexane) to generate the dimer recorded at 400 nm at 298 K upon photolysis at 355 nm.

Concentration of starting material (mol dm^3)	kobs (s^{-1})
0.000357	25876
0.0005	38652
0.000714	60238
0.000857	67891

Table 9.20 The observed rate constant (k_{obs}) at various concentration of starting material, for the reaction of starting material with (η^6-C_4H_4N)$Mn(CO)_2$(cyclohexane) to generate the dimer recorded at 405 nm at 298 K upon photolysis at 355 nm.